Exploration of Chemical Complexity

Edited by:
Hari Shankar Biswas
Dilip Kumar Maiti
Sandeep Poddar
Amiya Bhaumik

Published by:
Lincoln University College, Malaysia
www.lucp.net

Exploration of Chemical Complexity

Dr. Hari Shankar Biswas
Assistant Professor, Department of Chemistry
Surendranath College
Kolkata, West Bengal, India

Dr. Dilip Kumar Maiti
Professor, Department of Chemistry
University of Calcutta
Kolkata, West Bengal, India

Dr. Sandeep Poddar
Deputy Vice Chancellor (Research & Innovation)
Lincoln University College
Malaysia

Dr. Amiya Bhaumik
President
Lincoln University College
Malaysia

Published by:

Lincoln University College, Malaysia

www.lucp.net

Published on: 3rd July, 2024

Published by:

Lincoln University College
Wisma Lincoln
No. 12-18, Off Jalan, Perbandaran SS 6/12
47301 Petaling Jaya
Selangor Darul Ehsan
Malaysia
Tel.: +603-7806 3478
Fax: +603-7806 3479
Toll Free: 1-300-880-111
E-mail: lucp@lincoln.edu.my
Web.: www.lucp.net

ISBN: 978-967-2819-30-1

e ISBN: 978-967-2819-29-5

Price : 175 MYR

Prof. Pabitra Chattopadhyay
Vice-Chancellor
University of Gour Banga, Malda,
West Bengal, India

Foreword

It is with great pleasure I present this book "Exploration of Chemical Complexity". The field of chemistry is fundamental to numerous scientific disciplines and industries, driving advancements that shape our modern world. From the development of new materials and pharmaceuticals to the understanding of biological processes and environmental systems, chemistry lies at the heart of innovation. This book delves into these diverse facets, offering insights and perspectives that highlight the dynamic and intricate the nature of this essential science.

The authors of this volume have crafted this text that not only captures the fundamental principles but also explores the radical developments in the field. Their approach is both rigorous and accessible, offering a bridge between theoretical concepts and practical applications. The book is structured to cater to a diverse audience, from students, early-career researchers to professionals eager to advance their understanding of chemical complexity.

In the book, one can find a treasure trove of knowledge that not only illuminates fundamental principles but also explores cutting-edge advancements in chemical research. “Exploration of Chemical Complexity” stands as a testament to the dynamic and ever evolving field of chemistry. It is my hope that this work will inspire curiosity and will drive us towards further exploration into the profound complexity that defines our material world.

I would also like to extend my gratitude towards Lincoln University College, Malaysia, for acknowledging the significance of this work and facilitating the release of this edited volume. I extend my heartfelt congratulations to the authors for their remarkable contributions to this volume.This book "Exploration of Chemical Complexity" will inspire continued research and progress in chemistry, encouraging a deeper understanding with greater appreciation of the chemical world. Finally, I would like to give a hearty round of applause to the editors of this edited volume. Their tireless efforts and persuasive academic ideas have given this edited volume its final form.

Prof. Pabitra Chattopadhyay
Vice-Chancellor
University of Gour Banga, Malda, West Bengal, India

Preface

The field of chemical sciences is vast, complex, and ever evolving. As researchers consistently uncover new insights into the molecular mechanisms that shape the material world, this book entitled "Exploration of Chemical Complexity," offers a compilation of groundbreaking essay that showcases the latest advancements and discoveries in the field of chemistry related subfields.

The first chapter of this book discusses the Chromogenic Sensor for Cu^{2+} detection. Colorimetric sensors for Cu^{2+} ion detection is in high demand because of their simple visualization with the naked eye and rapid implementation. An azo-phenol moiety-based Cu^{2+} ion chemosensor was synthesized and different spectroscopic techniques have been used for its characterization. The chemosensor showed a significant colour change from faint yellow to purple while making a complex compound with Cu^{2+} ions.

Barun Kumar Mondal and Soumendu Bisoi delve into the promising domain of SAPO-34 Zeolites and Polyamide (PA) in their discussion, particularly focussing on the construction of Mixed Matrix Membranes (MMMs) for the efficient separation of CO_2 and CH_4 gases. According to their results, adding more SAPO-34 as a filler material and polyamide (PY-PA) as the base polymer makes the permeance go up by a noticeable amount. This innovative approach paves the way for the development of advanced membranes, potentially revolutionizing sustainable gas separation applications.

Rupankar Paira's chapter "A Brief Review on Recent Rh-Catalyzed C-H Bond Activation in Pyridines and Quinolines" attempts to highlight the latest developments in Rh-catalysis for C-H bond activation. The author has mainly explored the developments based on pyridine and quinoline substrates, due to their diversified biological importance. This chapter mostly talks about changes that have happened in the last ten years. The author hopes that using these changes on other pyridine, oxazole, and aza-heterocycle derivatives will lead to more research and teamwork, which will help people learn more about the endless possibilities of chemistry of rhodium.

According to Piyali Mitra's chapter, nanoconjugates are more relevant than ever in the realm of innovative photo-based nanodevices for drug administration and photocatalysis. Furthermore, it elucidates the fact that nanostructured materials fabricate the electronic excited states, or excitons, during light-matter interactions. The photophysical properties of semiconductor nanocrystals are also very different from those of bulk materials. This is due to the quantum confinement effect and the higher surface-to-volume ratio. The primary objective of this chapter is to emphasize that nanoconjugates are ushering in a new era for the upcoming generation.

Suranjan Chatterjee explores the quantitative oxidation of nitrous acid and its conjugate base nitrite to N(V) species in aqueous acidic media (pH 2.0-6.0) facilitated by a tetranuclear higher valent manganese complex, $[Mn_4(\mu\text{-}O)_6(bipy)_6]^{4+}$ (1, bipy = 2,2′-bipyridine), and its conjugate acid $[Mn_4(\mu\text{-}O)_5(\mu\text{-}OH)(bipy)_6]^{5+}$ ($1H^+$). The study reveals that the protonated metal oxidant $1H^+$ reacts faster than 1, with an unusual kinetic predominance of HNO_2 over its conjugate base NO_2^-. Additionally, the reaction exhibits a remarkable kinetic isotope effect, with an increased reaction rate in D_2O media.

The article by Chhandasi Guha Roy Sarkar explores the anticancer properties of 1,3-diaryltriazene-based compounds, emphasizing their significance in cancer treatment. It offers a comprehensive overview of recent advancements and potential therapeutic applications in the ongoing fight against cancer.

The chapter "Redefining Chemical Practices for a Low Carbon Future through Sustainability with Eco Chemistry" explores the cutting-edge strategies supported by Eco-Chem in the pursuit of a sustainable future. Eco-Chem aims to minimise environmental effect and maximise chemical process efficiency by following low-carbon chemistry concepts. This book chapter highlights the Eco-Chem's tactics to improve sustainability and drastically reduce carbon footprints using green solvents, renewable feedstocks, and energy-efficient techniques. This comprehensive approach facilitates industries' transition to a low-carbon economy and a sustainable future by providing scalable and cost-effective alternatives to conventional methods.

Traditional solvents and reaction conditions often pose significant challenges due to their toxicity, volatility, and adverse effects on human health. Aniruddha Mondal, Amit Kumar Kundu and Prasenjit Mandal in their article, provide an overview of the environmental challenges associated with traditional solvents and reaction media and discuss the principles of green chemistry and their significance in sustainable development. Additionally, it explores the classification, properties, and examples of commonly used green solvents, highlighting their role in promoting environmentally friendly practices in the field of chemistry.

In recent years, pyrazolines have emerged as a crucial heterocycle due to their diverse biological activities. The 2-pyrazoline scaffold is part of a lot of important drug molecules, including antipyrine, phenylbutazone, oxyphenbutazone, ibipinabant, and ramiphenazone. This chapter, written by Attreyee Mukherjee, delves into the biological significance of compounds containing the pharmacologically active 2-pyrazoline moiety in medicinal chemistry. It also explores Structure-Activity Relationship (SAR) studies aimed at enhancing their therapeutic implications, providing a comprehensive overview of their role and potential in drug development.

Food ingredients are labeled differently on the packaging of processed foods. It is necessary to comprehend and be aware of these substances' impacts on health. In this chapter, Subhrajit Banerjee makes an effort to enumerate some of these important substances along with recent health effects associated with their use. Apurba Biswas's article gives a full and up-to-date summary on the synthesis of polynuclear complexes of first transition metals and their magnetic properties. It also briefly talks about the working of magneto-structural correlations.

In his chapter, Amit Kumar Dutta aims to provide an overview of various low-cost, large-scale hydrogen fuel production systems using limitless water supplies and infinitely free solar energy. The goal is to produce commercially zero-emission hydrogen fuel. Therefore, researchers have developed solar-energy-driven water-splitting technology using a heterogeneous photocatalyst, utilizing nano-sized semiconducting catalyst materials. This technology aims to enhance the efficiency of solar-to-hydrogen conversion, boost the rate of hydrogen production, and commercialize it for the benefit of society.

This chapter, written by Biswajit Panda, talks about the latest progress made in understanding how gold helps the cycloisomerization of ortho-nitro-alkynylbenzene. It provides detailed mechanistic insights, shedding light on the key intermediates and transition states that govern this transformation. The discussion extends to the implications of these mechanistic findings for optimizing reaction conditions and expanding the scope of this synthetic strategy. Through this exploration, the chapter aims to enhance the efficiency and applicability of gold-catalyzed cycloisomerization in organic synthesis.

The last chapter, written by Sugata Samanta, examines the behaviour of lactic acid and propionic acid based on the pKa values with respect to temperature and finds a parabolic relationship between the two. The study also calculates the equivalent conductance at infinite dilution for these acids, yielding values of 451.60 and 445.86 $Ohm^{-1}cm^{2}eqv^{-1}$, respectively. These findings are supported by Python program analyses, providing a comprehensive understanding of the acids' thermodynamic properties and contributing valuable insights to the field of physical chemistry.

This book sheds light on the intricacy of chemical processes through several in-depth investigations and state-of-the-art studies, offering invaluable insights into theoretical frameworks and real-world applications. By deciphering these complexities, it seeks to foster creativity and advance the science of chemistry, ultimately driving scientific research and technological innovation. In this way, "*Exploration of Chemical Complexity*" serves as a profound journey through the multifaceted world of chemical systems. The diverse perspectives and innovative research presented not only illuminate the profound complexity inherent in chemical phenomena but also highlight the importance of interdisciplinary approaches in unraveling these mysteries. As we stand at the forefront of this constantly evolving field, the insights and discoveries shared in this volume are believed to inspire future research and deepen our appreciation of the chemical sciences. Consequently, this book will serve as a valuable resource for scholars, practitioners, and students alike, propelling continued exploration and understanding in the dynamic landscape of chemical complexity.

Hari Shankar Biswas
Dilip Kumar Maiti
Sandeep Poddar
Amiya Bhaumik

Content Pages

doi: 10.31674/book.2024ecc.001

A New Ratiometric Highly Selective Chromogenic Sensor for Cu^{2+} Detection

Puspendu Roy

Department of Chemistry, Netaji Nagar Day College, Kolkata, West Bengal, India

Corresponding Author's Email: roypuspendu1991@gmail.com

Abstract:

An azo-phenol moiety-based chemosensor is synthesized and different spectroscopic techniques have been used to confirm its structure. A significant colour change from pale yellow to purple was noticed while the chemosensor made a complex with Cu^{2+} ion but it did not show any significant colour change while studied with other competitive metal ions. Job's plot and mass spectroscopic analysis have been used to predict the 1:1 chemosensor-Cu^{2+} complex formation. DFT studies have been performed to explain the binding mechanism between the HL and Cu^{2+}.Association constant (Ka, $8.94x10^4$ M^{-1}) confirms that the probe has very high affinity for Cu^{2+} complex formation. Thus, the probe is highly effective in comparison to other reported probes for selective colorimetric and ratiometric detection of Cu^{2+}.

Keywords: *Azo Phenol Moiety Based Chemosensor; Colorimetric and Ratiometric Cu^{2+} Sensor; DFT Computational Studies*

Introduction:

As copper is required in almost every living organism (Kim, Nevitt & Thiele, 2008), it is employed as a catalyst in several biological methods such as hormone maturation, oxygen transportation and signal transduction (Robinson & Winge, 2010). In human body, Cu^{2+} is the third most abundant essential trace element and it has an important role in many physiological methods (Chang, 2023; Linder & Hazegh-Azam, 1996). The concentration of Cu^{2+} ion in environmental sample has to be monitored to prevent the effect of disorder in Cu (II) metabolism by severe neurodegenerative diseases, such as Alzheimer's and Wilson's diseases (Finkel, Serrano & Blasco, 2007; Zou *et al*., 2012; Guo, Chen & Duan, 2010; Dalapati *et al*., 2011, Vulpe *et al*., 1993; Hahn *et al*., 1995).

Colorimetric sensors are in high demand due to the simple visualization of color by the naked eye and also for its simple and rapid implementation (Veedu *et al*., 2024; Elmagbari *et al*., 2024; Trevino *et al*., 2023; Cao *et al*., 2022; Chen *et al*., 2010; Shang, Zhang & Dong, 2009; Ajayakumar *et al*., 2010). So, the synthesis of chemosensor for the detection of Cu^{2+}, especially selective ratiometric detection, is in high demand.

In this present work, the synthetic method and photo-physical properties of ONS linkage containing azo phenol moiety-based ligand has been described, which shows a significant colour change from light yellow to pink upon complexation with Cu^{2+} because of the increase in ICT (internal charge transfer). Several spectroscopic studies prove that the chemosensor exhibits a very good affinity for Cu^{2+} in acetonitrile solvent.

Synthesis of azo phenol moiety based ligand (HL)

3.06 g of 2-(ethylthio)benzenamine was dissolved in 10 mL of 1:1 HCl solution and then the solution was cooled by keeping it in an ice bath. 2.0 g $NaNO_2$ in 10 mL water was poured into it in ice cold condition under stirring. Then the mixture of solution was added to 25 mL of 6 g solution of Na_2CO_3 under ice cold condition and 2.56 g of 4-chlorophenol was added under vigorous stirring codition. An orange-red precipitate was filtered off and the precipitate was washed with cold water and then dried. Column chromatography technique was used for the further purification of the product by using 35% (v/v) ethyl acetate-petroleum ether mixture.

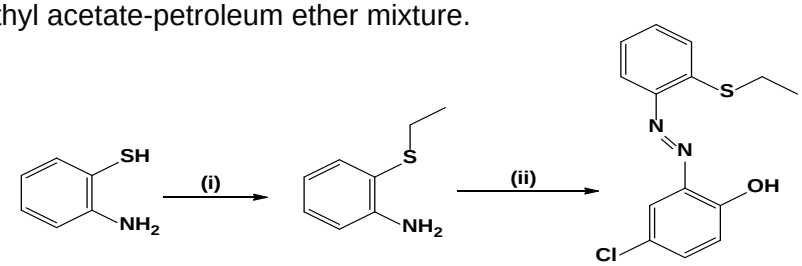

Scheme 1: Synthetic route of ligand ((i) Na in dry MeOH, (ii) $NaNO_2$, dil. HCl, 4-chloro phenol in Na_2CO_3 (0-5^{0}C)

Synthesis of Cu^{2+} complex

Ligand (HL) was dissolved in acetonitrile solvent and $CuCl_2.H_2O$ was added to it under stirring condition for 3 hours. The residue was filtered and washed with hexane. The obtained yield was 0.094 g (78.2%).

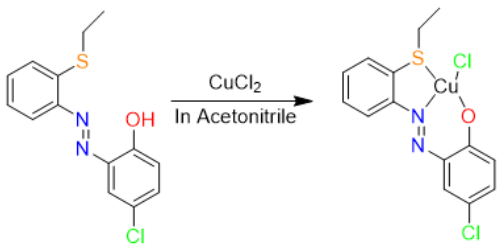

UV-Vis titration method

10 μM stock solution of the chemosensor ligand (HL) was prepared in CH_3CN. 10 μM of Chloride salts of the each guest cations were also prepared in CH_3CN. Various

concentrations of chemosensor ligand (host) were also taken and increasing concentrations of guest cations were used separately. The sharp changes in UV-Vis spectra of chemosensor ligand (host) upon gradual addition of the guest cations solutions were studied.

Job's plot (absorbance method)

A series of 10 μM solutions of HL and $CuCl_2$ were prepared for the Job's plot by maintaining the total volume of the metal ion and HL remained constant (4 ml) in CH_3CN. In the Job's plots ΔA versus mole fraction of Cu^{2+} was plotted. (ΔA = intensity change of the absorption spectrum at 515 nm).

DFT Computational method

Gaussian09 program has been used for DFT computations (Frisch, 2009). B3LYP was used for the geometrical optimization of the Cu complex (Beck, 1993; Lee, Yang & Parr, 1988). For C, H, N and O atoms 6-31+G(d) basis set was employed. The LANL2DZ basis set with effective core potential has been assigned for the Cu atom (Hay & Wadt, 1985; Wadt & Hay, 1985; Furche & Ahlrichs, 2002; Scalmani *et al*., 2006). The calculations based on vibrational frequency predict that the optimized structures represent the local minima of potential energy surface with only positive eigen-values. The time-dependent density functional theory (TDDFT) (Bauernschmitt & Ahlrichs, 1996; Stratmann, Scuseria & Frisch, 1998) in DMSO solvent has been used to predict singlet-singlet vertical electronic excitations. Conductor-like polarizable continuum model (CPCM) (Barone & Cossi, 1998; Cossi *et al*., 2003) has been employed for B3LYP optimized geometries.

Cation sensing studies of HL by UV-Vis titration

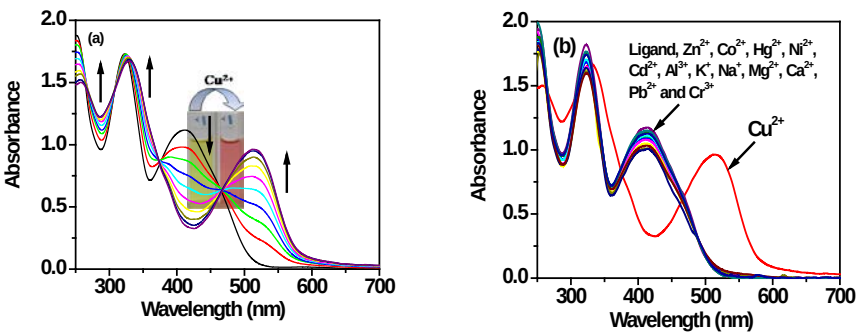

Figure 1: UV-vis titrimetric spectra of HL in presence of (i) Cu^{2+} (0–1.5 equivalents) and (ii) different cations (3 equivalents). *(Source: Roy et al., 2017)*

An absorption spectra of the chemosensor ligand upon gradual addition of increasing concentrations of Cu^{2+} (0–1.5 equiv) is shown in Figure 1. The spectra of ligand (Probe) shows two prominent absorbance peak at 323 nm and 410 nm in absence of any guest cation analytes. The absence of peak at 515 nm denotes that the probe is stable in this situation. A significant change in the absorbance spectra was observed after addition of Cu^{2+}. To obtain clear colorimetric change the solution of HL (10 µM) and the solution of Cu^{2+} in acetonitrile have been prepared. The absorption band gradually decreases at 410 nm and a new band appears at 515 nm which gradually increases while incremental concentrations of Cu^{2+} were used and a prominent isobestic point at 466 nm was observed.

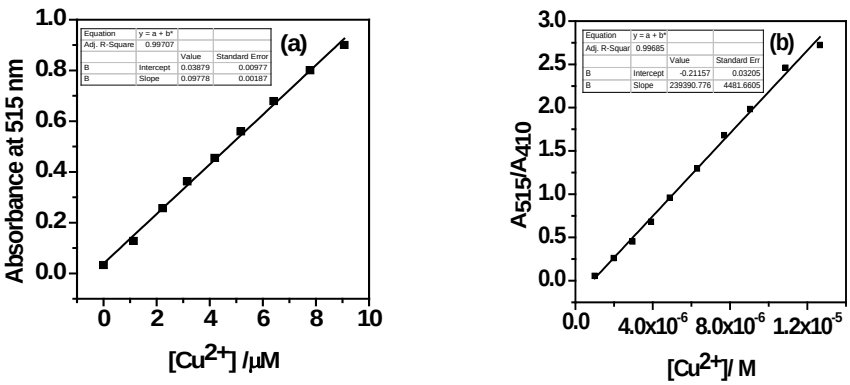

Figure 2: (a) Linear absorbance curve at 515 nm and (b) absorbance intensity ratio at A_{515}/A_{410} nm of HL depending on the Cu^{2+} concentration *(Source: Roy et al., 2017)*

A significant and clear color change of the stock solution from faint yellow to purple was observed by the photophysical changes. The large red shift (105 nm) of the absorption spectra of chemosensor receptor was noticed as ICT mechanism enhanced while the receptor made a complex with Cu^{2+} ion. The absorbance profile of HL maintains a beautiful linear relationship with added Cu^{2+} concentration (SI). The absorbance profile at 515 nm also maintains very good linearity when plotted against Cu^{2+} concentration, as R^2 value is closer to 1. The limit of detection of the chemosensor for Cu^{2+} is calculated from the absorption spectral change by taking the Cu^{2+} concentration of 6.26×10^{-8} M and by using the equation DL = K Sb1/S, where the value of K is taken as 3, Sb1 denotes the standard deviation of the blank solution, and S denotes the slope of the calibration curve. Absorption intensity band at 410 nm decreases and a ratiometric increase in the absorption intensity band at 515 nm is observed after gradual incremental addition of Cu^{2+} solution. Saturation of intensity band is observed after the addition of a 1.0 equivalent of 10 µM solution of Cu^{2+} ions shown in Fig. 1.

The novelty of any chemosensor probe can be determined by two very important parameters called interference and selectivity. The selectivity and sensitivity of the chemosensor towards Cu^{2+} were examined by employing several guest cations (Cd^{2+}, Co^{2+}, Cr^{3+}, Fe^{3+}, Hg^{2+}, K^{+} , Mg^{2+}, Na^{+} , Mn^{2+}, Ni^{2+}, Al^{3+}, Pb^{2+}, In^{3+} and Zn^{2+}). No significant change was observed in the absorbance spectra while other guest ions (except Cu^{2+}) were added. After the addition of Cu^{2+}, the absorbance of the chemosensor at 515 nm was increased by 27-fold. This phenomenon proves that the chemosensor can conveniently detect Cu^{2+} ion by simple naked-eye inspection.

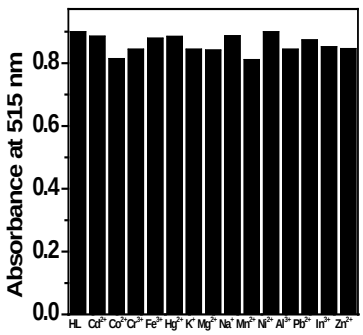

Figure 3: Competition study of several guest analytes(30 μM) using UV-vis method in the solution of probe(10 μM) in presence of Cu^{2+} (20 μM). *(Source: Roy et al., 2017)*

Job's plot

By using same concentration (in the order of 10 μM in CH_3CN at 25 °C) of chemosensor ligand and Cu^{2+}, the stock solution was prepared. Different sets of equal volume of chemosenor ligand-guest cations solution was prepared and the emission spectrum in each case was recorded. In the Job's plot ΔI.Xhost was taken as Y axis and Xhost was taken as X axis (ΔI = change in intensity of the absorbance spectrum at 515 nm and Xhost = the mole fraction of the ligand). It is evident from the Job's plot titration that the stoichiometry between probe and Cu^{2+} is 1:1.

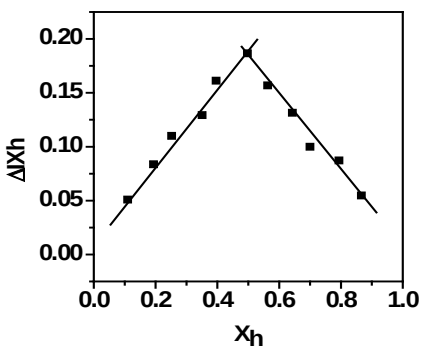

Figure 4: Job's plot of the prober for Cu^{2+} Study of complexation mode (*Source: Roy et al., 2017)*

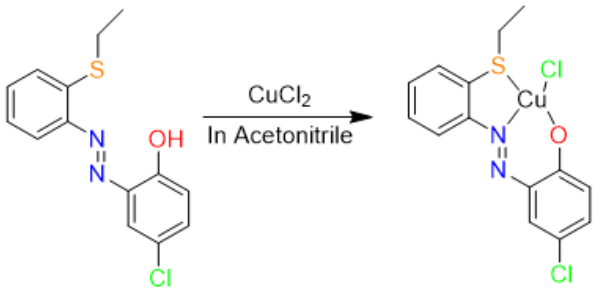

Scheme 2: Probable HL with Cu^{2+} complexation mode

The binding mechanism of HL is given in Scheme 2. The stoichiometry of the chemosensor probe and Cu^{2+} is 1 : 1 and it is further confirmed by the Job's plot shown in Fig. 4 and it is further confirmed by HRMS spectra. The HL – Cu^{2+} complex shows a signal at m/z 413.523 in the HRMS spectra. Both the experiments confirm that a strong association occurs between the radii of Cu^{2+} and the cavity space of the chemosensor which results in strong interaction between Cu^{2+} and the coordinating sites of the ligand.

pH study

The Cu^{2+} sensing by the probe was studied at different pH levels to achieve more extensive results. HEPES buffer solution was used, and the UV-absorption spectra of the chemosensor probe (HL) were examined both in the absence and presence of Cu^{2+} ions. Aqueous solutions of 1 M HCl or 1 M NaOH were employed to adjust the pH.

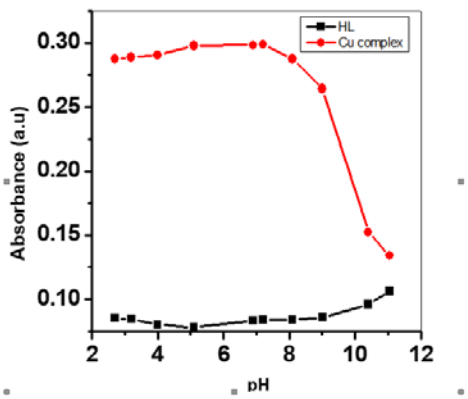

Figure 5: Absorbance vs pH plot of chemosensor and chemosensor-Cu^{2+} at 515 nm (10 µM) in CH_3CN *(Source: Roy et al., 2017)*

Spectra shows, the absorption intensity of the chemosensor probe is almost unaffected at different pH condition but it shows a large change of absorption intensity between pH 8- 11 in presence of Cu^{2+} ion. Between the pH 5-8, the probe can form a stable complex with Cu^{2+} ion. The probe has a tendency to combine with proton At very low pH (< 3) and so the probe is less effective in sensing the Cu^{2+} at very low pH. Hence, it is evident that the synthesized probe can sense Cu^{2+} ions within the pH range of 5-8.

DFT Computational studies for HL-Cu^{2+} complex

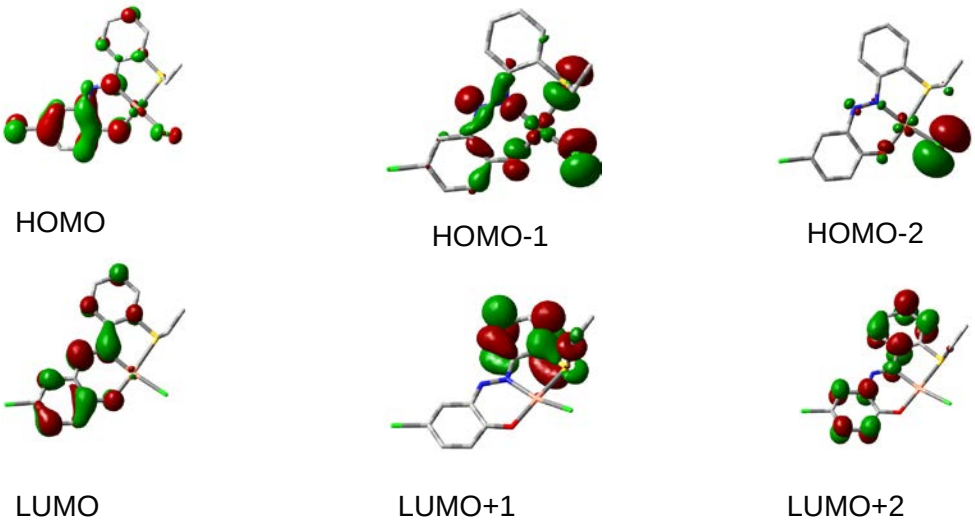

Figure 6: Some selected α-spin molecular orbitals of chemosensor Cu^{2+}Complex
(Source: Roy et al., 2017)

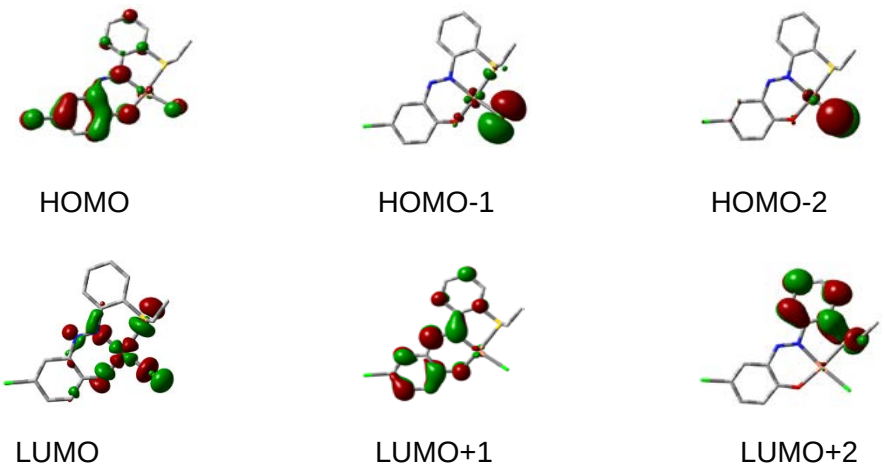

Figure 7: Some selected *β*-spin molecular orbitals of chemosensor-Cu^{2+}Complex
(Source: Roy et al., 2017)

Table 1: *Energy and percentage compositions of some selected α-spin molecular orbitals of chemosensor-Cu^{2+}Complex*

Molecular Orbitals	Energy	Percentage Composition		
		Cu	Ligand	Cl
LUMO+5	0.36	50	50	0
LUMO+4	-0.04	42	57	01
LUMO+3	-0.24	01	99	0
LUMO+2	-0.63	01	99	0
LUMO+1	-1.35	03	97	0
LUMO	-3.12	01	99	0
HOMO	-6.03	03	93	04
HOMO-1	-6.43	12	61	26
HOMO-2	-6.73	05	09	87
HOMO-3	-6.84	06	09	85
HOMO-4	-7.12	01	96	03
HOMO-5	-7.49	06	57	38
HOMO-6	-7.67	01	97	02
HOMO-7	-8.21	01	98	01
HOMO-8	-8.48	06	81	13
HOMO-9	-8.68	07	93	01
HOMO-10	-8.72	0	100	0

Table 2: *Energy and percentage compositions of some selected β-spin molecular orbitals of chemosensor-Cu^{2+}Complex*

Molecular Orbitals	Energy	Percentage Composition		
		Cu	Ligand	Cl
LUMO+5	-0.03	43	57	01
LUMO+4	-0.22	01	99	0
LUMO+3	-0.62	01	99	0
LUMO+2	-1.34	03	97	0
LUMO+1	-3.08	01	99	0
LUMO	-3.66	47	40	13
HOMO	-6.02	03	92	05
HOMO-1	-6.02	04	07	89
HOMO-2	-6.75	06	06	88
HOMO-3	-7.04	03	78	19
HOMO-4	-7.16	03	83	14
HOMO-5	-7.64	01	98	01
HOMO-6	-8.14	06	85	10

HOMO-7	-8.22	03	96	01
HOMO-8	-8.49	32	52	17
HOMO-9	-8.67	15	77	08
HOMO-10	-8.71	02	98	0

HOMO of (α-spin) have a reduced contribution of dπ(Cu) along with a major contribution of π(L). The LUMO (α-spin) has 99% π * (L) character, with a major contribution of π * (N=N). LUMO+1 to LUMO+3 have π * (L) character. The HOMOs of β-spin again have π(L) character, but significant contributions of the dπ(Cu) orbitals have been found in HOMO-8 in comparison with the α-spin occupied molecular orbitals. The LUMO (*β*-spin) has 47% dπ(Cu) character. The LUMO+1 (*β*-spin) to LUMO+4 (*β*-spin) have π * (L) character. In the UV-Vis spectra of the Cu^{2+}complex shoulder peak at 410 and 323 nm corresponds to π(L) → π * (L). For the copper (II) complex, the weak bands at 515 nm corresponds to mixed intra-ligand charge transfer (ILCT), π(L) → π * (L), and ligand to metal charge transfer (LMCT), π(L) → dπ(Cu), transitions.

Conclusion

An azo-phenol moiety-based chemosensor is synthesized and different spectroscopic techniques have been used to confirm its structure. The chemosensor showed a significant colour change from faint yellow to purple, while the chemosensor made a complex with Cu^{2+} but it did not show any significant colour change while studied with other competitive metal ions. Job's plot and mass spectroscopic analysis have been used to predict the 1:1 chemosensor-Cu^{2+} complex formation. pH study shows that the synthesized probe can sense Cu^{2+} ion between the pH range 5-8 . DFT studies have been performed to explain the binding mechanism between the HL and Cu^{2+}. Association constant (Ka, 8.94×10^4 M^{-1}) indicates that the synthesized probe has a very high affinity for binding to the Cu^{2+} ion.

Acknowledgement

The author is grateful to Netaji Nagar Day College and Jadavpur University, India for their encouragement, support and constant help.

References

Ajayakumar, M. R., Mukhopadhyay, P., Yadav, S., & Ghosh, S. (2010). Single-electron transfer driven cyanide sensing: a new multimodal approach. *Organic Letters*, *12*(11), 2646-2649.

Barone, V., & Cossi, M. (1998). Quantum calculation of molecular energies and energy gradients in solution by a conductor solvent model. *The Journal of Physical Chemistry A*, *102*(11), 1995-2001. https://doi.org/10.1021/jp9716997

Bauernschmitt, R., & Ahlrichs, R. (1996). Treatment of electronic excitations within the adiabatic approximation of time dependent density functional theory. *Chemical Physics Letters*, *256*(4-5), 454-464. https://doi.org/10.1016/0009-2614(96)00440-X

Beck, A. D. (1993). Density-functional thermochemistry. III. The role of exact exchange. *J. Chem. Phys*, *98*(7), 5648-5652. https://doi.org/10.1063/1.464913

Cao, F., Jiao, F., Ma, S., & Dong, D. (2022). Laser-induced breakdown spectroscopy mediated amplification sensor for copper (Ⅱ) ions detection using click chemistry. *Sensors and Actuators B: Chemical*, *371*, 132594. https://doi.org/10.1016/j.snb.2022.132594

Chang, L. W. (Ed.). (2023). *Toxicology of Metals, volume I*. CRC press, USA.

Chen, X., Nam, S. W., Kim, G. H., Song, N., Jeong, Y., Shin, I., ... & Yoon, J. (2010). A near-infrared fluorescent sensor for detection of cyanide in aqueous solution and its application for bioimaging. *Chemical Communications*, *46*(47), 8953-8955. https://doi.org/10.1039/C0CC03398G

Cossi, M., Rega, N., Scalmani, G., & Barone, V. (2003). Energies, structures, and electronic properties of molecules in solution with the C-PCM solvation model. *Journal of Computational Chemistry*, *24*(6), 669-681. https://doi.org/10.1002/jcc.10189

Dalapati, S., Jana, S., Alam, M. A., & Guchhait, N. (2011). Multifunctional fluorescent probe selective for Cu (II) and Fe (III) with dual-mode of binding approach. *Sensors and Actuators B: Chemical*, *160*(1), 1106-1111. https://doi.org/10.1016/j.snb.2011.09.034

Elmagbari, F. M., Hammouda, A. N., Soliman, S. M., EL-Ferjani, R. M., Elagili, F. A., Amer, Y. O. B., ... & Bonomo, R. P. (2024). Solution structure, crystal structure, Hirshfeld surface analysis of copper (II) diamide species as an optical chemical sensor. *Polyhedron*, *256*, 116996. https://doi.org/10.1016/j.poly.2024.116996

Finkel, T., Serrano, M., & Blasco, M. A. (2007). The common biology of cancer and ageing. *Nature*, *448*(7155), 767-774. https://doi.org/10.1038/nature05985

Frisch, M. J. E. A. (2009). gaussian 09, Revision d. 01, Gaussian. *Inc, Wallingford CT*, *201*.

Furche, F., & Ahlrichs, R. (2002). Adiabatic time-dependent density functional methods for excited state properties. *The Journal of Chemical Physics*, *117*(16), 7433-7447. https://doi.org/10.1063/1.1508368

Guo, Z. Q., Chen, W. Q., & Duan, X. M. (2010). Highly selective visual detection of Cu (II) utilizing intramolecular hydrogen bond-stabilized merocyanine in aqueous buffer solution. *Organic Letters*, *12*(10), 2202-2205. https://doi.org/10.1021/ol100381g

Hahn, S. H., Tanner, M. S., Danke, D. M., & Gahl, W. A. (1995). Normal metallothionein synthesis in fibroblasts obtained from children with Indian childhood cirrhosis or copper-associated childhood cirrhosis. *Biochemical and Molecular Medicine*, *54*(2), 142-145. https://doi.org/10.1006/bmme.1995.1021

Hay, P. J., & Wadt, W. R. (1985). An initio effective core potentials for molecular calculations. Potentials for the transition metal Sc to Hg. *The Journal of Chemical Physics*, *82*(1), 270-283.

https://doi.org/10.1016/j.surfin.2024.104301

Kim, B. E., Nevitt, T., & Thiele, D. J. (2008). Mechanisms for copper acquisition, distribution and regulation. *Nature Chemical Biology*, *4*(3), 176-185.

Lee, C., Yang, W., & Parr, R. G. (1988). Development of the Colle-Salvetti correlation-energy formula into a functional of the electron density. *Physical Review B*, *37*(2), 785. https://doi.org/10.1103/PhysRevB.37.785

Linder, M. C., & Hazegh-Azam, M. (1996). Copper biochemistry and molecular biology. *The American Journal of Clinical Nutrition*, *63*(5), 797S-811S. https://doi.org/10.1093/ajcn/63.5.797

Robinson, N. J., & Winge, D. R. (2010). Copper metallochaperones. *Annual Review of Biochemistry*, *79*, 537-562. https://doi.org/10.1146/annurev-biochem-030409-143539

Roy, P., Das, S., Aich, K., Gharami, S., Patra, L., & Mondal, T. K. (2017). A new highly selective and ratiometric chromogenic sensor for Cu^{2+} detection. *Journal of the Indian Chemical Society, 94*, 755-760.

Scalmani, G., Frisch, M. J., Mennucci, B., Tomasi, J., Cammi, R., & Barone, V. (2006). Geometries and properties of excited states in the gas phase and in solution: Theory and application of a time-dependent density functional theory polarizable continuum model. *The Journal of Chemical Physics*, *124*(9). https://doi.org/10.1063/1.2173258

Shang, L., Zhang, L., & Dong, S. (2009). Turn-on fluorescent cyanide sensor based on copper ion-modified CdTe quantum dots. *Analyst*, *134*(1), 107-113. https://doi.org/10.1039/B812458B

Stratmann, R. E., Scuseria, G. E., & Frisch, M. J. (1998). An efficient implementation of time-dependent density-functional theory for the calculation of excitation energies of large molecules. *The Journal of Chemical Physics*, *109*(19), 8218-8224. https://doi.org/10.1063/1.477483

Trevino, K. M., Wagner, C. R., Tamura, E. K., Garcia, J., & Louie, A. Y. (2023). Small molecule sensors for the colorimetric detection of Copper (II): A review of the literature from 2010 to 2022. *Dyes and Pigments*, *214*, 110881. https://doi.org/10.1016/j.dyepig.2022.110881

Veedu, A. P., Kumar, S. K., Kuppusamy, S., Mohan, A. M., & Deivasigamani, P. (2024). Solid-state real-time colorimetric sensing of ultra-trace copper ions using aqueous compatible chromatic probe imbued porous polymer monolithic sensor. *Surfaces and Interfaces*, *48*, 104301. https://doi.org/10.1016/j.surfin.2024.104301

Vulpe, C., Levinson, B., Whitney, S., Packman, S., & Gitschier, J. (1993). Isolation of a candidate gene for Menkes disease and evidence that it encodes a copper–transporting ATPase. *Nature Genetics*, *3*(1), 7-13. https://doi.org/10.1038/ng0193-7

Wadt, W. R., & Hay, P. J. (1985). Ab initio effective core potentials for molecular calculations. Potentials for main group elements Na to Bi. *The Journal of Chemical Physics*, *82*(1), 284-298.

Zou, Q., Li, X., Zhang, J., Zhou, J., Sun, B., & Tian, H. (2012). Unsymmetrical diarylethenes as molecular keypad locks with tunable photochromism and fluorescence via Cu^{2+} and CN^- coordinations. *Chemical Communications*, *48*(15), 2095-2097. https://doi.org/10.1039/C2CC16942H

doi: 10.31674/book.2024ecc.002

SAPO-34 Zeolites/Polyamide (PA) Mixed-Matrix Membranes with Enhanced CO_2/CH_4 Separation Performance

Barun Kumar Mondal, Soumendu Bisoi*

Department of Chemistry, Narajole Raj College, Paschim Medinipur, West Bengal, India

**Corresponding Author's Email: soumendubisoi@gmail.com*

Abstract

A novel mixed-matrix membrane (MMM) comprising semi-fluorinated aromatic polyamide (PA) and Submicron SAPO-34 zeolites filler was synthesized and evaluated for gas separation capabilities targeting CH_4, N_2, O_2 and CO_2. Mixed-matrix formulations represent a promising strategy to mitigate the permeability-selectivity compromise inherent in polymer membranes by integrating fillers. The properties of the filler are pivotal in dictating the performance of MMMs. MMMs were synthesized with varying weight percentages (0%, 5%, and 10%) of Submicron SAPO-34 zeolites filler incorporated into the semi-fluorinated PA matrix. The MMM incorporating 10 wt% Submicron SAPO-34 displayed CO_2 permeability and a selectivity of 44.20 for CO_2/CH_4 gas pairs, showcasing enhanced CO_2/CH_4 separation performance credited to the existence of Submicron fillers. SEM imaging confirmed the uniform combination of Submicron SAPO-34 filler into the polyamide matrix. This investigation presents a promising pathway for developing efficient and high-performance separation membranes.

Keywords: *Gas Permeability; Mixed-matrix Membranes; Poly(amide); SAPO-34*

Introduction

Membrane technology has developed as a proficient process for gas separation, due to the advantageous combination of cost-effectiveness, straightforward processing, and the innovative nature inherent in polymer materials (Usman, 2022). Particularly within the realm of gas separation, the operation of polymeric membranes for CO_2 separation has garnered significant attention due to its diverse potential applications, including carbon capture and natural gas refinement. Membranes are commonly categorized into groups based on their material composition: inorganic, polymeric and mixed organic-inorganic materials. Polymer membranes are favoured in manufacturing applications due to their low production prices, decent mechanical strength, flexibility, informal processing, and toughness related to inorganic membranes (Cardoso *et al*., 2023). However, they face limitations in gas separation performance, often characterized by the Robeson upper bound limit, which represents a trade-off between permeability and selectivity. Mixed matrix membranes (MMMs) offer a possible solution by incorporating high-execution zeolites, inorganic molecular sieves, into polymer matrices to enhance

separation performance (Cardoso *et al*., 2024a). MMMs combine the rewards of polymeric membranes with greater separation performances, surpassing the upper bound limits by Robeson. The addition of inorganic fillers to the matrix is anticipated to improve membrane belongings beyond those of consistent polymer membranes. The creation of MMMs often encounters challenges in weak filler-polymer matrix contact and poor filler distribution within the polymer matrix phase (Cardoso *et al*., 2024a). Polyamides (PAs) have been extensively studied as matrices for gas separation membranes due to their excellent chemical and thermal stability, as well as the selectivity of glassy polyimides, making them suitable for various gas separation processes, especially CO_2 separation. MMMs, which combine with polymer membranes and filler particles, exhibit an inclusive variety of gas separation application prospects. Crystalline zeolites (Hassan *et al*., 2023) inorganic structures possess of molecular dimensions formed by TO_4 (T = Si, Al, or P) with uniform-sized pores and are widely employed in adsorption and separation processes (Usman, 2022). SAPO-34 zeolite, CHA structure as a silicoaluminophosphate is shaped by the neutral $AlPO_4$ framework of Si atoms. The chemical composition of SAPO-34 is represented as $(SixAlyPz)O_2$, where x = 0.01–0.98, y = 0.01–0.60, z = 0.01–0.52, and x + z = y. SAPO-34's structure comprises eight-membered rings with a diameter of 9.4 Å (3.8 × 3.8), exhibiting unique shape selectivity, molecular sieving properties with a pore diameter of 0.38 nm, close to the kinetic diameter of CH_4, and a strong CO_2 adsorption capacity (Cardoso *et al*., 2024b). Its microporous nature, with a zeolitic pore volume of 0.310 $cm^3\ g^{-1}$ and pore sizes of 3.8 Å, makes it suitable for the adsorption of gas molecules (Carter *et al*., 2017). SAPO-34 possesses an approximate BET surface area of 600 $m^2\ g^{-1}$. The impact of adding SAPO-34 as a filler on the gas permeation properties of other polymers such as polyetherimide (Mirfendereski & Mazaheri, 2024), PEBAX, polyethersulfone, and polysulfone has been investigated (Ignatusha *et al*., 2024).

Cardoso *et al*. (2024a) investigated the combination of SAPO-34 with polyethersulfone (PES), observing significant enhancements in CH_4, CO_2 and H_2 permeabilities, albeit at the expense of decreased CO_2/CH_4 ideal selectivities. (Peydayesh *et al*., 2013; Alibak *et al*., 2022) developed SAPO-34/Matrimid 5218 MMMs, demonstrating notable improvements of 97% and 55% in permeability of CO_2 and selectivity of CO_2/CH_4, respectively, highlighting effective filler-polymer medium adhesion. (Carter *et al*., 2017) fabricated MMMs utilizing silica, SAPO-34, and ZIF-8, attributing pore size as the primary factor influencing gas permeability, with increased permeability observed. (Messaoud *et al*., 2015) reported a technique of dip-coating for SAPO-34/polyetherimide MMMs, attaining optimal molecular filtering routine with 5 wt% SAPO-34 MMMs, exhibiting high CO_2 permeability and selectivity. Zhao *et al*. (2014) discussed SAPO-34/Pebax1657 MMMs fabricated via solvent evaporation, wherein SAPO inclusion notably enhanced CO_2 permeability while maintaining constant selectivity. Santaniello

et al., (2020) described the incorporation of 200 nm SAPO-34 in a polyhexafluoropropylene PHFP matrix, resulting in MMMs with improved selectivity and permeability.

Despite extensive research on MMMs utilizing SAPO-34 for CO_2/CH_4 separation, there is limited investigation into incorporating particles into the semifluorinated aromatic polyamide (PA) matrix and the influence of SAPO-34 on the performance of membrane gas separation. This study goals to explore the effects of PA, SAPO-34 on final separation properties, specifically focusing on PA/SAPO-34 influences for CO_2/CH_4 parting. Characterization of MMMs with varying SAPO-34 loading ratios includes assessing structure, morphology, and gas permeation properties. Notably, membranes with a lesser Zeolite cargo ratio of 10.0 wt% exhibit significantly improved performance compared to pristine polymer membranes. Permeation tests (CO_2, CH_4, N_2 and O_2) are conducted on prepared MMMs, demonstrating the significant promotion of CO_2/CH_4 gas separation performance by incorporating SAPO-34 into PA. Furthermore, the study investigates the effects of SAPO-34 cargo on MMM construction and permeation belongings using Differential Scanning Calorimetric (DSC) techniques and scanning electron microscopy (SEM).

Experimental

Materials, Membrane Characterization and Gas Separation Measurements

SAPO-34 zeolite synthesis utilized phosphoric acid (H_3PO_4, 85 wt% aqueous solution, Merck), aluminum triisopropylate ($Al(i\text{-}C_3H_7O)_3$), tetra-ethyl ammonium hydroxide (TEAOH, Merck), and Ludox AS-40 colloidal silica sol (SiO_2, Aldrich). The synthesis of 2,6-bis[3'-trifluoromethyl-4'(4'' carboxyphenoxy)benzyl]pyridine (2) acid was earlier described (Bisoi *et al*., 2015). The m-phenyl diamine monomer was procured from SD Chemicals, India. The permeation of O_2, N_2, CO_2 and CH_4 gases was restrained over the polymer membranes utilizing an automated Diffusion Permeameter (DP-100-A) manufactured by Porous Materials, Inc., USA, at a temperature of 35°C and functional gas pressure of 3.5 bar.

Polymerization

Aromatic diamine, Triphenylamine (1), was reacted with a dicarboxylic acid monomer (2) in a 1:1 molar ratio with NMP as a solvent and triphenyl phosphite (TPP), $CaCl_2$, and pyridine, as illustrated in Scheme 1. The polymerization (PY PA) proceeded as follows: a mixture of the diamine, m-triphenylamine (0.686 g, 6.01 mmol) (1), and 2,6-bis[3'-trifluoromethyl-4'(4''-carboxyphenoxy)benzyl]pyridine (2) (0.494 g, 6.01 mmol), $CaCl_2$ (0.25 g), pyridine (1.2 mL), NMP (3 mL) and TPP (1.2 mL, 4.94 mmol), in a round-bottom flask and reflux condenser. The blend was intense at 110°C for 6 hours. Subsequently,

the mixture was transferred to methanol, resulting in the formation of a fibrous polymer. The fibrous polymer (PY-PA) was then dried in a vacuum (Bisoi *et al*., 2015).

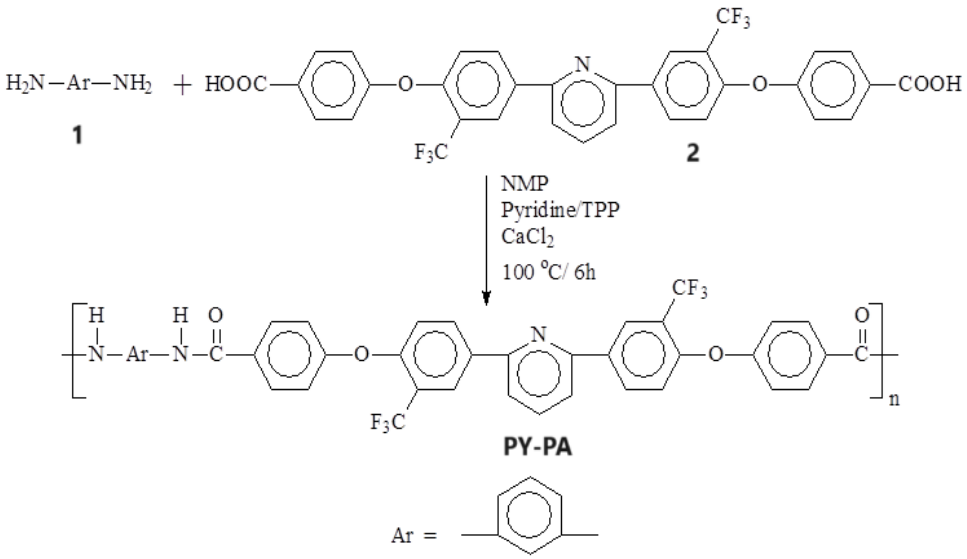

Scheme 1: Preparation of the poly(amide)s (PY PA) (Bisoi *et al*., 2015)

SAPO-34 zeolite synthesis

The hydrothermal technique was used for SAPO-34 zeolite synthesis. Initially, silica and tetraethylammonium hydroxide (TEAOH) were allowed to hydrolyze for 16 hours at room temperature. Subsequently, aluminum triisopropylate $Al(OiPr)_3$ was stimulated for 15 minutes in water, and phosphoric acid (H_3PO_4) was supplementary dropwise to form an alumina gel. The 1.0 Al_2O_3:1.0 P_2O_5:0.3 SiO_2:1.2 TEAOH:60 H_2O molar composition was used. A teflon-lined, stainless steel autoclave is used for crystal formation and growth. The product was recovered by centrifugation at 2700 rpm for 10 hours. The precipitate was dried (Messaoud *et al*., 2015).

Polymeric Membrane Preparation

Polymeric membranes were cast in clean glass Petri dishes at 80°C and 150°C in an oven 6 hours. Membranes were extracted from Petri dishes in hot water. Membranes were dried under vacuum at 160°C for 4 hours. The flexible membranes were obtained.

Physical properties are summarized in Table 1 for membranes. The fractional free volume (FFV) is calculated using the equation $FFV = (V-1.3V_w)/ V_w$, where V represents the specific volume ($V = 1/\rho$), density values (ρ). The Hyperchem computer program was used for van der Waals volume (V_w) calculation (Hypercube, 2019).

Preparation of SAPO-34 MMMs

For mixed matrix membranes (MMMs) preparation, PY-PA solution was dissolved in DMF of 0.6 g of polymer. Ultrasonication is used for the dispersion of SAPO-34 in DMF. A polymer solution was added to the SAPO-34 suspension and stirred overnight. Membranes were fabricated by casting the homogeneous polymer solution in DMF onto clean glass Petri dishes. And heating to 80°C to 150°C continued for 6 hours. This process yielded free-standing, stretchy membranes. To maintain consistency, the weight ratio of filler to total filler and polymer was kept constant for MMMs. MMMs were arranged with SAPO-34 loadings of 0%, 5%, and 10% by weight of the fillers. This approach ensured the systematic investigation of the belongings of varying SAPO-34 loading (Nawaz *et al*., 2024).

Results and Discussion

Polymer Synthesis and Their Properties

Polyamide was produced via the typical polycondensation-based phosphorylation with dicarboxylic acid (2) and diamine (1) (Scheme 1). Repeat unit structures of polymers confirmed NMR. The polymer repeat unit structures were consistent with ^{1}H-NMR spectra. The ^{1}H-NMR spectrum in pyridine-d_5 of PY-PA displayed a singlet above 11.39 ppm (amide proton). Physical properties were found to be consistent with the previously reported results (Bisoi *et al*., 2015).

***Table 1**: Physical properties of the polyamide*

Polymer	η_{inh} (dL g^{-1})[a]	Density (g cm^{-3})[b]	V_w (cm^3 mol^{-1})[c]	FFV
PY-PA	0.37	1.228	318.7	0.117

[a]η_{inh} = inherent viscosity at 30 °C. [b]Density measured at 30 °C. [c]V_w = Vander Waals volume, FFV = Fractional Free Volume (Bisoi et al., 2015).

Morphology: Synthesis of Nanoparticles of SAPO-34

Figure 1 illustrates the XRD spectra, showcasing the distinctive peaks of pure SAPO-34. High crystallinity specifies the synthesis of zeolite. Clearly visible in the picture are the cubic crystals of SAPO-34, aligning with previously reported findings (Wang *et al*., 2024). The sheet-like morphology in the SEM image depicted in Figure 2 confirms SAPO-34 crystals. Crystals exhibit an average length of 750 nm and a thickness of 75 nm. These observed particles display flat outer tops with a cubic morphology, distinguishing the crystals of SAPO 34. This observation aligns with the conclusions stated by Wang *et al*. (2024). Additionally, Messaoud *et al*. (2015) demonstrated the fabrication of both plate-like and cubic SAPO-34 morphologies. Initially, plate-like SAPO-34 is produced for use as seeds, followed by the formation of cubic SAPO-34.

doi: 10.31674/book.2024ecc.002

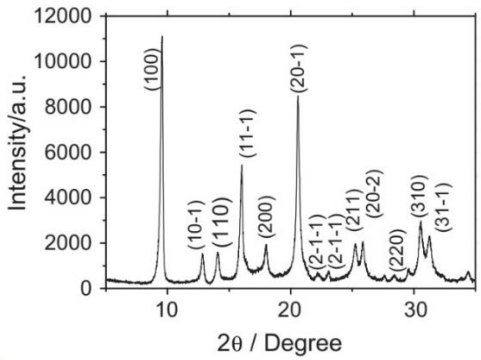

Figure 1: XRD patterns of SAPO-34 *(Messaoud et al., 2015)*

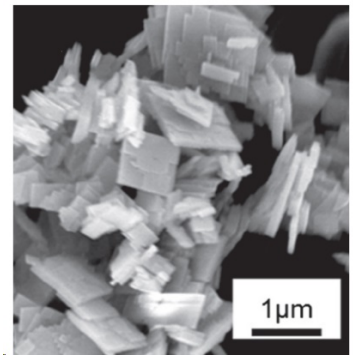

Figure 2: SEM images of SAPO-34 *(Messaoud et al., 2015)*

Processing of Mixed Matrix Membranes

Notably, the glass transition temperature (T_g) values ranged from 274 to 278ºC in DSC subversions (Figure 3), with no idea of crystallization temperatures. The T_g of pristine PY-PA was determined to be 274°C, consistent with previously reported findings. Disturbance in the stacking of polymer matrix is the reason for increased T_g values, which suggest the incorporation of SAPO-34 (Peydayesh *et al*., 2013).

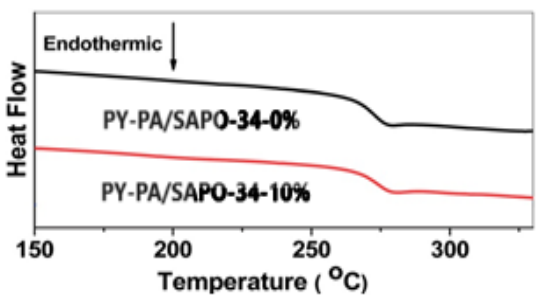

Figure 3: DSC curves of the MMMs *(Bisoi et al., 2015)*

The surfaces of the obtained MMMs are depicted in Figure 4. Both the PY-PA/SAPO-34-0% and PY-PA/SAPO-34-5% membranes exhibit no inadequacies and display similarity throughout the membrane. MMMs with distributed SAPO-34 crystals in the medium boost the performance of the membrane. However, the PY-PA/SAPO-34-10% membrane exhibited particle agglomeration. In Fig 4c, agglomeration ascends due to incompatibility between the SAPO-34 and matrix.

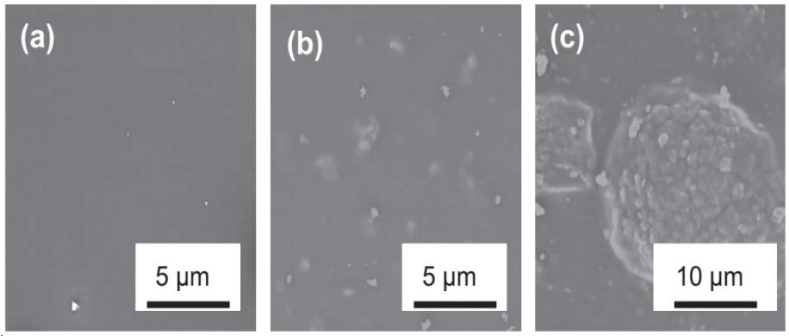

Figure 4: SEM images of PY-PA/SAPO-34 membranes with SAPO-34 loading of (a, b & c) 0 wt %, 5 wt % and 10 wt % (Usman, 2022)

Gas permeation

Effect of SAPO 34 on gas permeation properties

The gas permeation measurements of all MMMs were conducted at 3.5 bar and 293 K. The constant-volume method used for checking permeability of all the membranes of different gases (O_2, N_2, CO_2 and CH_4) in the MMMs is presented in Table 2. Gas permeability of the four different gases through these MMMs membranes follows the order of P (CO_2) > P (O_2) > P (N_2) > P (CH_4) (Bisoi *et al*., 2015). The solution-diffusion model used for transport mechanisms is broadly reported in the literature. Assimilation of SAPO-34 significantly enhances the permeability of the PA membrane, with an observed increase in gas permeabilities as the SAPO-34 concentration increases. This enhancement is attributed to SAPO-34's sieve effect on the gas molecule. The increased selectivity of CO_2/CH_4 with growing SAPO-34 loading (0 wt % to 10.0 wt %) is attributed to the decent dispersion of particles in MMMs. Mesopores in matrix pass gas molecules enhanced ideal CO_2/CH_4 selectivity.

***Table 2**: Gas permselectivities and permeability of the MMMs*

MMMs	P(CO_2)	P(O_2)	P(N_2)	P(CH_4)	α(CO_2/CH_4)	α(O_2/N_2)
PY-PA/SAPO-34-0%	65.0	12.2	1.59	1.54	36.50	7.86
PY-PA/SAPO-34-5%	78.0	13.9	1.77	1.65	37.30	7.79
PY-PA/SAPO-34-10%	80.0	14.1	1.91	2.33	44.20	9.13

P = gas permeability coefficient in barrer

Corelation of gas permeabilities of MMMs with membranes

The gas permselectivity, permeability and values of these MMMs (PY-PA/SAPO-34-0-10%) were related to the other polymers Matrimid, Extem, and Ultem (Bisoi *et al*., 2015). A thorough comparison of CO_2/CH_4 permselectivity vs. CO_2 gas permeability (Figure 5) and O_2/N_2 permselectivity vs. O_2 gas permeability (Figure 6) was conducted to obtain a better understanding through Robeson plots (Robeson, 2008). The data in Robson's line

touches indicate the separation capability of the membrane. In general, combination permeability and higher selectivity were observed for MMMs. The prepared membrane revealed better permeability than previously reported polymers. Here, the data's of MMMs in Robeson's upper bound was not surpassed, though the overall performance of the MMMs significantly improved. PY-PA/SAPO-34-10% displayed improved CO_2 gas permeability along with an enhancement in permselectivity compared to PAs. The optimal performance of MMMs was achieved with the highest SAPO-34 zeolite loading of 10wt%. These PAs demonstrated notable enhancements in gas-separation performance, as evidenced by their Robeson's trade-off points in the upper bound.

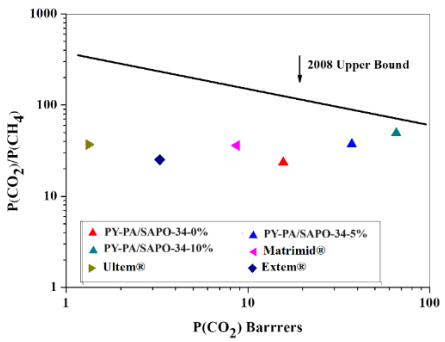

Figure 5: Robeson plot of CO_2/CH_4 selectivity vs. CO_2 permeability *(Bisoi et al., 2015)*

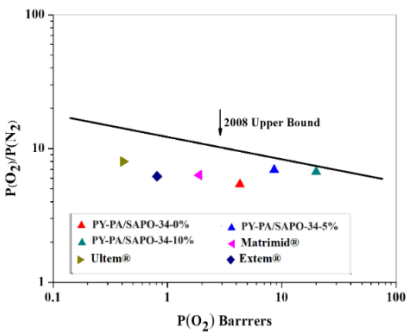

***Figure 6**: Robeson plot of O_2/N_2 selectivity vs. O_2 permeability* (Bisoi et al., 2015)

Conclusion

In summary, mixed-matrix membranes (MMMs) comprising semi-fluorinated polyamide (PY-PA) as the base polymer, along with incorporated SAPO-34, were prepared via a solvent-evaporation method. SAPO-34 filler materials were introduced to boost the proficiency of CO_2/CH_4 separation in the MMMs. SAPO-34 played a pivotal role in determining the performance of the MMMs. A fluorinated PA membrane containing a pyridine part in the polymer spine was hired to study its properties in combination with SAPO-34. Among the membranes tested, the one with 5 wt% SAPO-34 demonstrated a clear molecular sieving effect and exhibited the highest performance, with a permeability of CO_2 of 80 Barrer and a selectivity of CO_2/CH_4 of 44.2. The above findings suggest that PY-PA/SAPO-34 MMMs hold promise for gas separation applications. The preparation protocol employed for the MMMs occasioned in a uniform dispersal of SAPO 34 within the PY-PA. The experimental increase in permeability with growing SAPO-34 cargoes was attributed to the operational properties of SAPO-34, which exhibited excellent chemical compatibility with PY-PA. This innovative approach of incorporating SAPO-34 as filler materials into PY-PA-based MMMs presents a promising pathway for the enterprise of advanced membranes tailored for sustainable applications in gas transportation.

Acknowledgment

The authors acknowledge Narajole Raj College, India for providing them research facility to carry out this work. The authors also acknowledge the Material Science Centre, Indian Institute of Technology Kharagpur, India for providing the instrument facilities used in this work.

References

Alibak, A. H., Alizadeh, S. M., Davodi Monjezi, S., Alizadeh, A., Alobaid, F., & Aghel, B. (2022). Developing a Hybrid Neuro-Fuzzy Method to Predict Carbon Dioxide (CO_2) Permeability in Mixed Matrix Membranes Containing SAPO-34 Zeolite. In *Membranes*, *12*(11). https://doi.org/10.3390/membranes12111147

Bisoi, S., Bandyopadhyay, P., Bera, D., & Banerjee, S. (2015). Effect of bulky groups on gas transport properties of semifluorinated poly(ether amide)s containing pyridine moiety. *European Polymer Journal*, *66*, 419–428. https://doi.org/10.1016/j.eurpolymj.2015.03.008

Cardoso, J. S., Fonseca, J. P., Lin, Z., Brito, P., & Gando-Ferreira, L. M. (2024a). Optimization and performance studies of PES/SAPO-34 membranes for CO_2/N_2 gas separation. *Microporous and Mesoporous Materials*, *364*, 112845. https://doi.org/10.1016/j.micromeso.2023.112845

Cardoso, J. S., Lin, Z., Brito, P., & Gando-Ferreira, L. M. (2023). The Functionalization of PES/SAPO-34 Mixed Matrix Membrane with [emim][Tf2N] Ionic Liquid to Improve CO2/N2 Separation Properties. *Inorganics*, *11*(11), 447. https://doi.org/10.3390/inorganics11110447

Cardoso, J. S., Lin, Z., Brito, P., & Gando-Ferreira, L. M. (2024). Surface Functionalized SAPO-34 for Mixed Matrix Membranes in CO_2/CH_4 and CO_2/N_2 Separations. *Separation & Purification Reviews*, *53*(2), 180–193. https://doi.org/10.1080/15422119.2023.2204080

Carter, D., Tezel, F. H., Kruczek, B., & Kalipcilar, H. (2017). Investigation and comparison of mixed matrix membranes composed of polyimide matrimid with ZIF - 8, silicalite, and SAPO - 34. *J. Membr. Sci.*, *544*, 35–46.

Hassan, N. S., Jalil, A. A., Bahari, M. B., Khusnun, N. F., Aldeen, E. M. S., Mim, R. S., Firmansyah, M. L., Rajendran, S., Mukti, R. R., Andika, R., & Devianto, H. (2023). A comprehensive review on zeolite-based mixed matrix membranes for CO_2/CH_4 separation. *Chemosphere*, *314*, 137709. https://doi.org/10.1016/j.chemosphere.2022.137709

Hypercube, Inc. (25th December 2019). *HyperChem(TM) Professional 7.51* [Computer software]. Hypercube, Inc. https://lammpstube.com/2019/12/25/hyperchem/

Ignatusha, P., Lin, H., Kapuscinsky, N., Scoles, L., Ma, W., Patarachao, B., & Du, N. (2024). Membrane Separation Technology in Direct Air Capture. In *Membranes*, *14*(2). https://doi.org/10.3390/membranes14020030

Messaoud, S. B., Takagaki, A., Sugawara, T., Kikuchi, R., & Oyama, S. T. (2015). Mixed matrix membranes using SAPO-34/polyetherimide for carbon dioxide/methane separation. *Separation and Purification Technology*, *148*, 38-48. https://doi.org/10.1016/j.seppur.2015.04.017

Mirfendereski, S. M., & Mazaheri, T. (2024). Highly Permeable and Well-Oriented SAPO-34 Membranes for CO_2 Removal. *Chem & Bio Engineering*. https://doi.org/10.1021/cbe.3c00081

Nawaz, S., Sarfraz, M., Qaiser, A. A., Alomar, M., Gouadria, S., & BaQais, A. A. (2024). Quest for high performance carbon capture membranes: Fabrication of SAPO-34 and CNTs-doped

polyethersulfone-based mixed-matrix membranes. *Journal of Applied Polymer Science*, *141*(8), e54971. https://doi.org/10.1002/app.54971

Peydayesh, M., Asarehpour, S., Mohammadi, T., & Bakhtiari, O. (2013). Preparation and characterization of SAPO-34 – Matrimid® 5218 mixed matrix membranes for CO_2/CH_4 separation. *Chemical Engineering Research and Design*, *91*(7), 1335–1342. https://doi.org/10.1016/j.cherd.2013.01.022

Robeson, L. M. (2008). The upper bound revisited. *Journal of Membrane Science*, *320*(1–2), 390–400. http://dx.doi.org/10.1016/j.memsci.2008.04.030

Santaniello, A., Di Renzo, A., Di Maio, F., Belov, N. A., Yampolskii, Y. P., & Golemme, G. (2020). Competing non ideal behaviour of SAPO-34 and Poly(hexafluoropropylene) in mixed matrix membranes. *Microporous and Mesoporous Materials*, *303*, 110241. https://doi.org/10.1016/j.micromeso.2020.110241

Usman, M. (2022). Recent Progress of SAPO-34 Zeolite Membranes for CO_2 Separation: A Review. In *Membranes*, *12*(5), 507). https://doi.org/10.3390/membranes12050507

Wang, G., AlMasoud, N., Alomar, T. S., Azman, Y. N., Maireles-Torres, P., Chia, S., Juan, J. C., Ling, T. C., El-Bahy, Z. M., & Ng, E.-P. (2024). Direct evidence of time-dependent crystallization evolution of SAPO-34 and SAPO-20 zeolites directed by trimethylbenzylammonium hydroxide for microwave-assisted ethanolysis of furfuryl alcohol. *New Journal of Chemistry*, *48*(15), 6875–6885. https://doi.org/10.1039/D4NJ00875H

Zhao, D., Ren, J., Li, H., Hua, K., & Deng, M. (2014). Poly(amide-6-b-ethylene oxide)/SAPO-34 mixed matrix membrane for CO2 separation. *Journal of Energy Chemistry, 23*(2), 227–234. https://doi.org/10.1016/S2095-4956(14)60140-6

doi: 10.31674/book.2024ecc.003

A Brief Review on Recent Rh-Catalyzed C-H Bond Activation in Pyridines and Quinolines

Rupankar Paira

Department of Chemistry, Maharaja Manindra Chandra College, Kolkata, India

Corresponding Author's Email: rupankarpaira85@gmail.com

Abstract

In this short review article, attempts have been made to provide a concise pathway towards the recent advancements of organometallic chemistry, showcasing the broad spectrum of applications of Rh-catalysis in C-H bond activation and the transformative impact it has on society. By exploring these current developments of the last decade and the future opportunities of various sub-disciplines, it can certainly be hoped that the implementation of these works on other pyridine, oxazole, and aza-heterocycle derivatives will instigate further research and collaborative endeavors, fostering a deeper understanding of the limitless potential of rhodium chemistry. The continuous exploration and application of Rh-catalyzed C-H activation promise to revolutionize synthetic methodologies, driving innovation and progress across multiple scientific domains.

Keywords: *C-H activation; Pyridine; Quinolone; Rhodium-Catalysis*

Introduction

Chemistry, often regarded as the central science, has consistently played a crucial role in shaping humanity's understanding of the surrounding world. From decoding the intricate mechanistic paths of biological processes to engineering novel, newer materials with unparalleled functionalities, the applications of chemical science span a vast spectrum of fields, making it one of the most fundamental disciplines in scientific research and technological achievements (Blakemore *et al*., 2018). In this brief review article, the author will dive into some recent developments and some of the ground-breaking advancements in organometallic chemistry from various C-H activation protocols in pyridine and quinolone-based nitrogen heterocycles through Rh-catalysis (Lam, Wu & Yu, 2021). Through this endeavour, the diverse applications of rhodium catalysis and the potential opportunities they hold for the future. Heterocycles are fundamental components of numerous natural products, agrochemicals, and pharmaceuticals. Nitrogen-containing heterocycles, in particular, are especially significant as a rich source of therapeutic drugs in medicinal chemistry (Mohanty *et al*., 2024). The selection of aza-heterocycles primarily stems from their extensive use in various industries and academic fields (Campos *et al*., 2019). This is mainly because

such motifs exist in numerous fields, such as engendering new pharmaceuticals to fight diseases, designing eco-friendlier materials to minimize environmental impacts, or unveiling energy storage solutions for a sustainable future. The current review article also aims to showcase some of the remarkable advancements in organometallic chemistry, which range from inorganic and organic chemistry to physical and analytical chemistry. This article aims to highlight the key outcomes and breakthroughs from these areas, while also providing readers with a summarized overview of recent developments in the field and their potential implications. C–H bonds are more challenging to utilize than their pre-functionalized counterparts, they are not entirely inert. With the right catalyst, these bonds can be cleaved and used as latent substitutes for various functional groups (Zhang *et al*., 2024). It goes without saying that the future opportunities presented by the C-H activation processes in these compounds are truly exciting. As the understanding of these transition metal chemical pathways continues to evolve, it is fair to anticipate the emergence of newer materials with extraordinary properties along with the discovery of more potent catalysts for such chemical reactions. Additionally, the amalgamation of organometallic chemistry with other scientific streams, such as biological and material sciences, will likely promote unprecedented advancements in the fields of drug discovery, biotechnology, and nanotechnology.

Recent developments

I. Rhodium(I)-directed Aylation of Azines

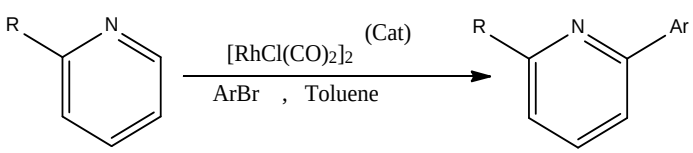

Scheme 1: Aylation of Azines *(Source: Berman et al., 2010)*

Direct arylation of the azines (scheme-1) can be accomplished with the employment of $[RhCl(CO)_2]_2$. The following diagram illustrates the mechanistic pathway of the arylation reaction between azine compounds and bromoarenes. Initially, a $[RhCl(CO)_2]_2$ molecule forms a bond with the 2-substitute pyridines and transforms into an N-heterocyclic carbene. After the reductive elimination of an HX molecule, A 2-substituted pyridinium Rh-complex is obtained (scheme-2), which readily proceeds along an oxidative addition pathway with the aryl bromide. The subsequent reductive elimination step produces a nitrogen-bound Rh-complex through an exchange with the pyridine starting material, resulting in the formation of the intended product (Berman, Bergman & Ellman, 2010).

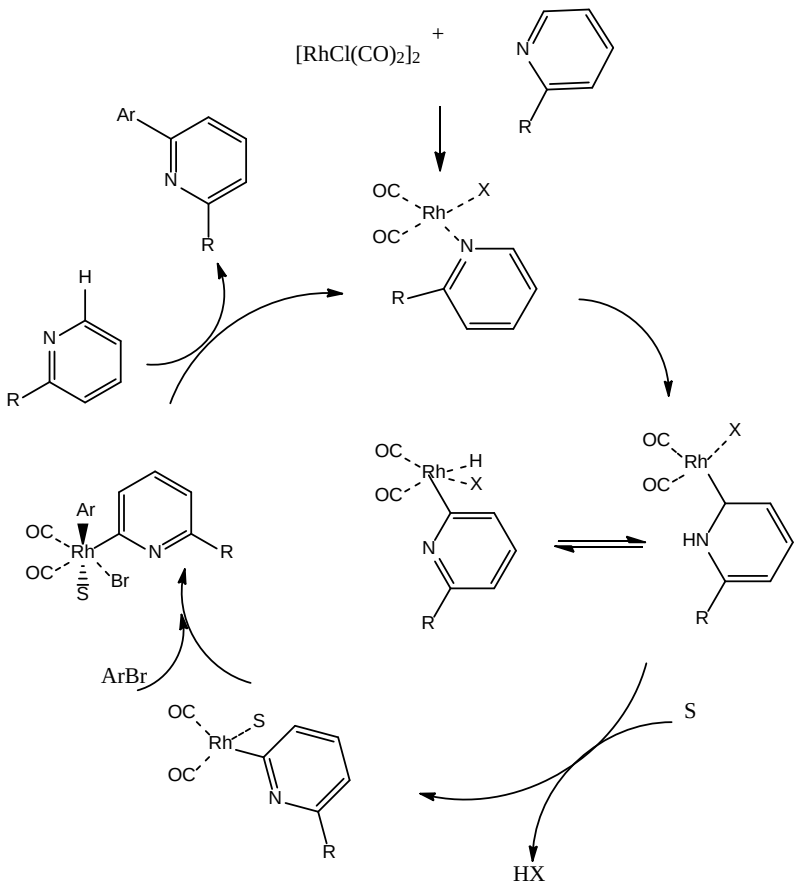

Scheme 2: Mechanism of arylation *(Source: Berman et al., 2010)*

Once this protocol is optimized, the authors invoke an electronically deficient catalyst $[RhCl(CO)_2]_2$ in the system, where the limiting reagent is aryl bromide. The authors extensively evaluated the scope of heterocycles and established that many ortho-, meta-, and para-substituted pyridines, as well as an array of heterocycles such as quinolines, effectively participate in this reaction under these sets of optimized reaction conditions. Several straight chain, R-branched, and also aliphatic group-substituted *β*-branched pyridines and quinolines in the C2 position are well tolerated, and all of them undergo efficient C-H activation (scheme-3).

However, in contrast, when the authors used a substrate in which the C2 site was vacant, the arylation reaction didn't proceed. The authors made these observations when they attempted to arylate a pyridine molecule.

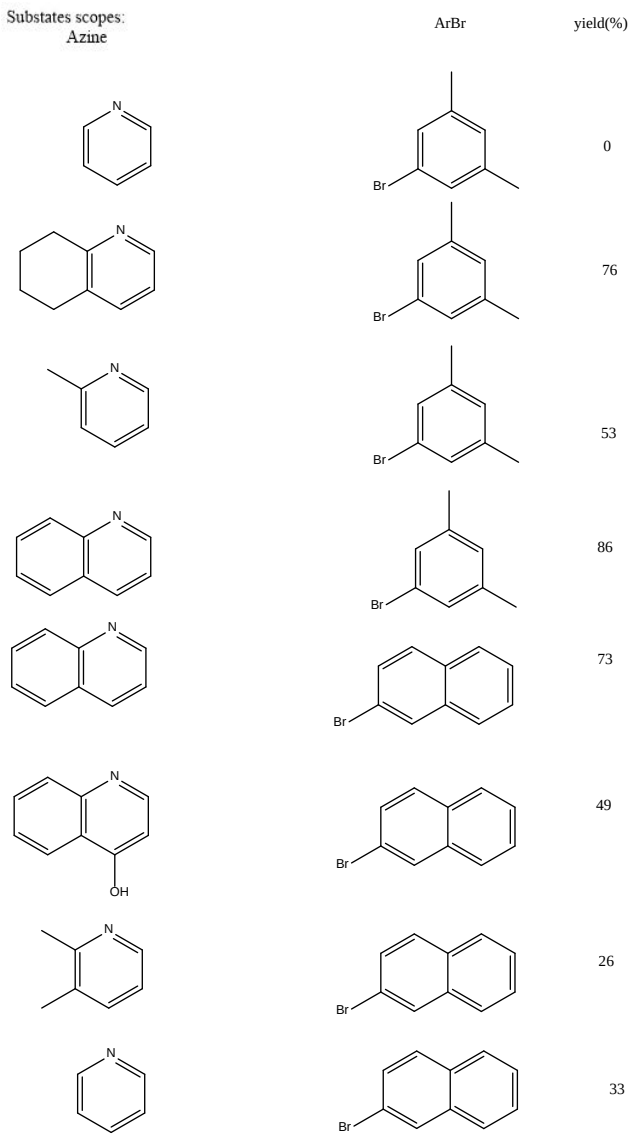

Scheme 3: Substrate Scope *(Source: Berman et al., 2010)*

II. Synthetic protocols of Quinoline systems through Rhodium (III)-promoted Oxidative Annulation reaction of Pyridines

Cupric acetate has been used as the oxidant in Rhodium-catalyzed concomitant C-H activation of pyridines (scheme-4) to create selective synthetic roads to quinolines through oxidative annulation of ortho/meta/para functionalized pyridine moieties and two alkyne counterparts. Nevertheless, the competitive coordination routes (scheme-5) of the pyridine nitrogen atom might block the C-H bond activation of pyridines, leading to a decrease in catalytic efficiency (Song, Gong & Li, 2011).

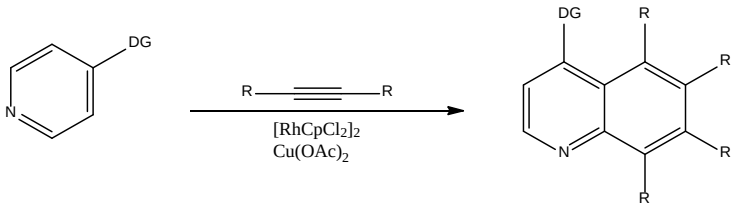

Scheme 4: Oxidative Annulation reaction of Pyridines *(Source: Song et al., 2011)*

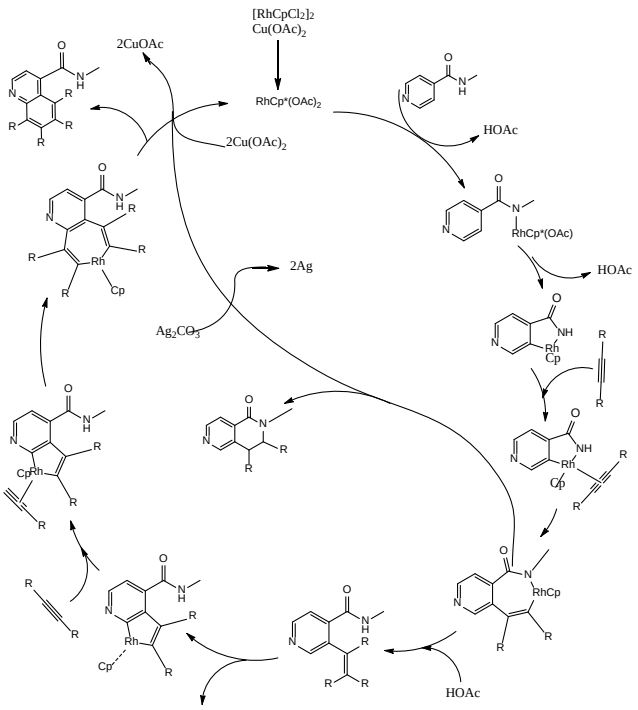

Scheme 5: Mechanism of the reaction *(Source: Song et al., 2011)*

Studies reveal that pyridines with an electronically deficient group (scheme-6) participate efficiently to produce the intended quinoline products in good yields. However, adding a methoxy moiety at the 3-position results in a significant reduction in catalytic efficiency. Moreover, a C2-substitution of the pyridines is very well tolerated. Scheme 6 demonstrates that activating a C3 C-H position typically takes place at a less crowded site. Further, the employment of quinoline-4-carboxamide under optimized conditions leads to an acridine with a good yield.

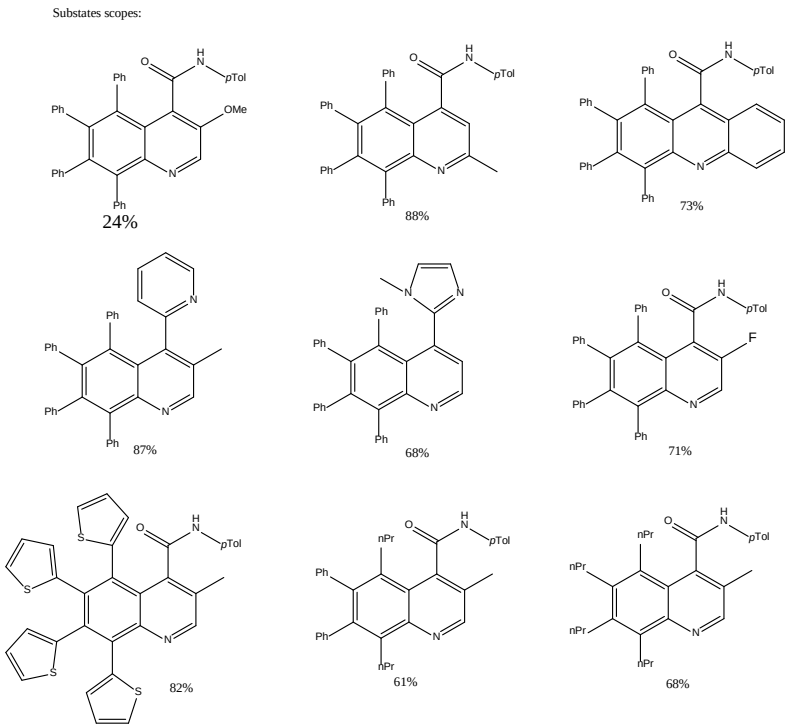

Scheme 6: Substrate Scope (Source: Song *et al.,* 2011)

III. Rhodium (III)-promoted Heteroarylation/Vinylation Protocol of Some Pyridine 1,6-Difluoroaryl Acrylamides

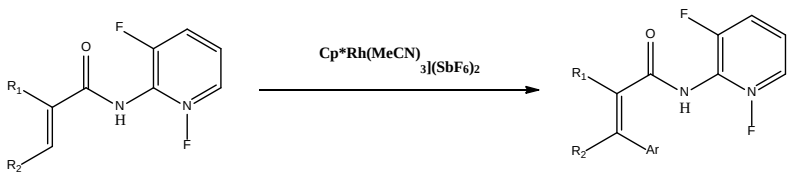

Scheme 7: Heteroarylation/Vinylation of Pyridine Acrylamides
(Source: Wang et al., 2021)

At the outset (scheme-7), the Rhodium catalyst gets attached with the amide, which gives rise to a five-membered rhodium-plugged cyclic species though a C−H activation reaction. The arylboronic acid pinacol esters then coordinate to the same Rhodium-centre, resulting in the emergence of the Rhodium species 4 (scheme-8). then, a C−C reductive elimination process yields the arylated product and an Iodo-Rhodium species, which can then undergo oxidation to yield Rhodium (III) through AgOPiv (Wang *et al*., 2021).

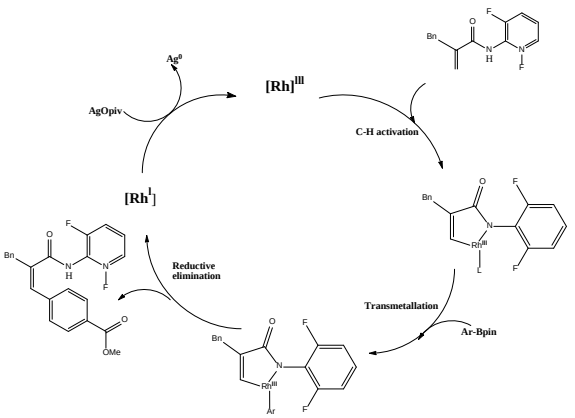

Scheme 8: Mechanism of the reaction *(Source: Wang et al., 2021)*

Generally, the present C−H bond functionalization strategy can be proved to be a nice fit for a vast array of the pinacol esters derived from aryl boronic acid. Also, it is generally applicable to electronically rich or deficient substrates, producing the desired structures with satisfactory yields. Moreover, the meta-substitution as well as the disubstitution with an electron-withdrawing arylboronate can give excellent yields. Additionally, a nice 82% yield could be achieved by employing 2-naphthyl boronates (scheme-9).

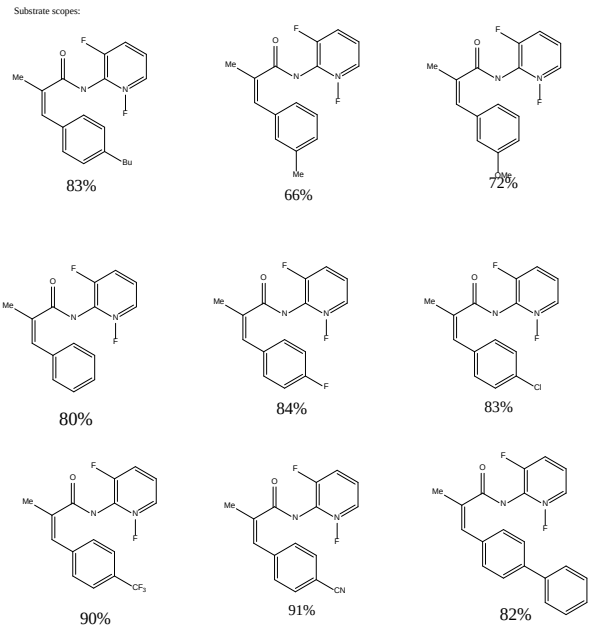

Scheme 9: Substrate Scope *(Source: Wang et al., 2021)*

Exploration of Chemical Complexity

IV. Rhodium-promoted straightforward C-H Addition reaction of 3,4-Dihydroquinazoline systems with Alkenes and its application in total synthesis of Vasicoline

During the intramolecular couplings of the unactivated alkenes (scheme-10), the 3,4-dihydroquinazolines can be produced, employing a Rh (I) catalyst (Wiedemann, Ellman, & Bergman, 2006).

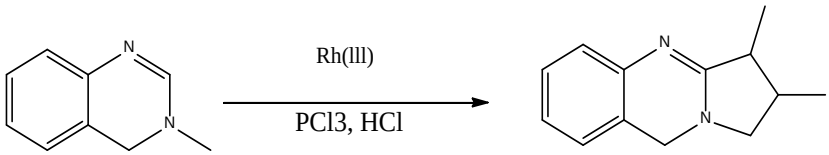

Scheme 10: C-H Addition reaction of 3,4-Dihydroquinazoline *(Source: Wiedemann et al., 2006)*

A wide application of this protocol on various motifs (scheme-11), including multisubstituted olefinic substrates, selectively afforded the tetracyclic product (cis-fusion), as desired by the authors. Through this technique, we can efficiently produce quinazoline natural products, which are mainly available from plant and microbial sources, for their antimalarial, antiinflamatory, and antitumor activities.

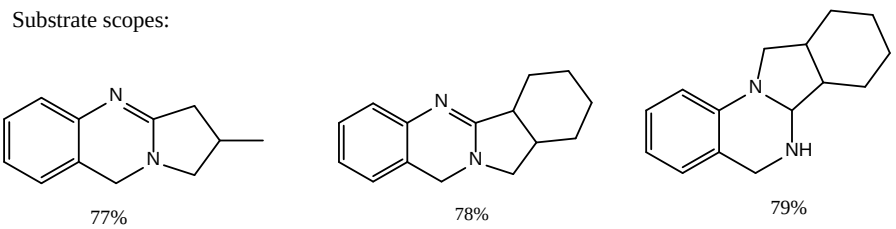

Scheme 11: Substrate Scope *(Source: Wiedemann et al., 2006)*

V. Cooperative sp^3/sp^2 C-H Activation protocol of 2-Ethylpyridines by using Copper and Rhodium towards Quinolizinium Salts

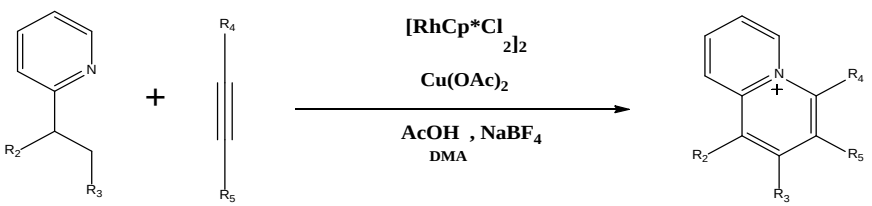

Scheme 12: C-H Activation of 2-Ethylpyridines *(Source: Luo et al., 2015)*

The cooperative sp^3/sp^2 C-H activation protocol (scheme-12) commenced with an initial dehydrogenation reaction of 2-ethylpyridine. The reaction is promoted through

cupric acetate to produce 2-vinylpyridine. After that, a coordination reaction takes place between the Rhodium center and the 2-vinylpyridine, which was formed in situ, followed by a cyclometalation reaction via the cleavage of the vinylic C−H linkage (scheme-13). This process led to a rhodium-implanted five-membered metalacycle and easily proceeds through an anion exchange reaction with the BF_4^-. Naturally, a cationic metalacycle species with the BF_4^- counteranion, formed in the system, which pushed the species to undergo a reductive elimination step to yield the intended final quinolizinium salt and a monocationic Rh-species. Further oxidation of Rh (I), by cupric acetate, regenerates the Rh (III) reactive catalytic species (Luo *et al*., 2015).

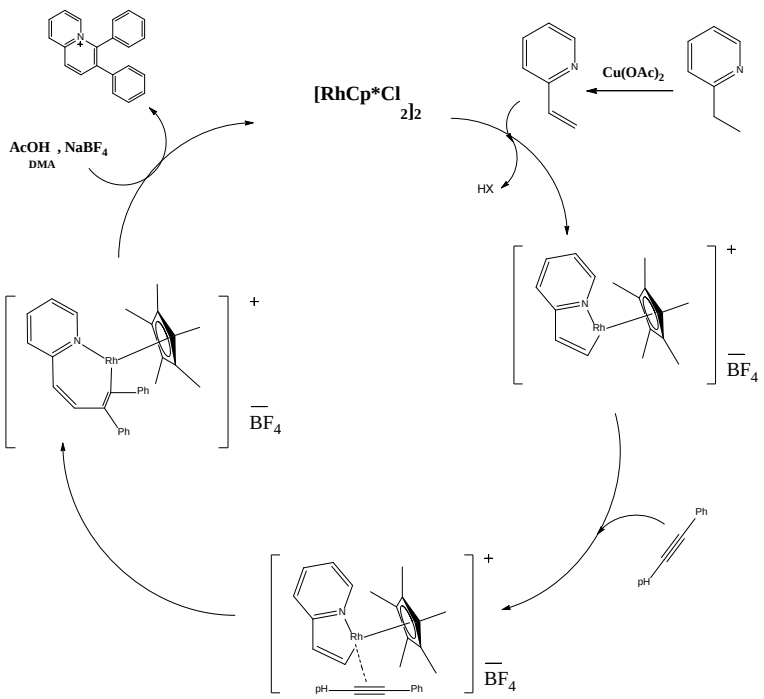

Scheme 13: Mechanism of the reaction *(Source: Luo et al., 2015)*

Further studies have shown that the electron-withdrawing groups have a high yield (scheme-14). Alkynes with different terminal moieties were also successfully invoked under this bimetal-mediated cooperative sp^3/sp^2 C-H activation protocol to form the intended quinolizinium salts with outstandingly high regioselectivity. But, terminal alkynes and dialkyl alkynes didn't yield the desired quinoliziniums.

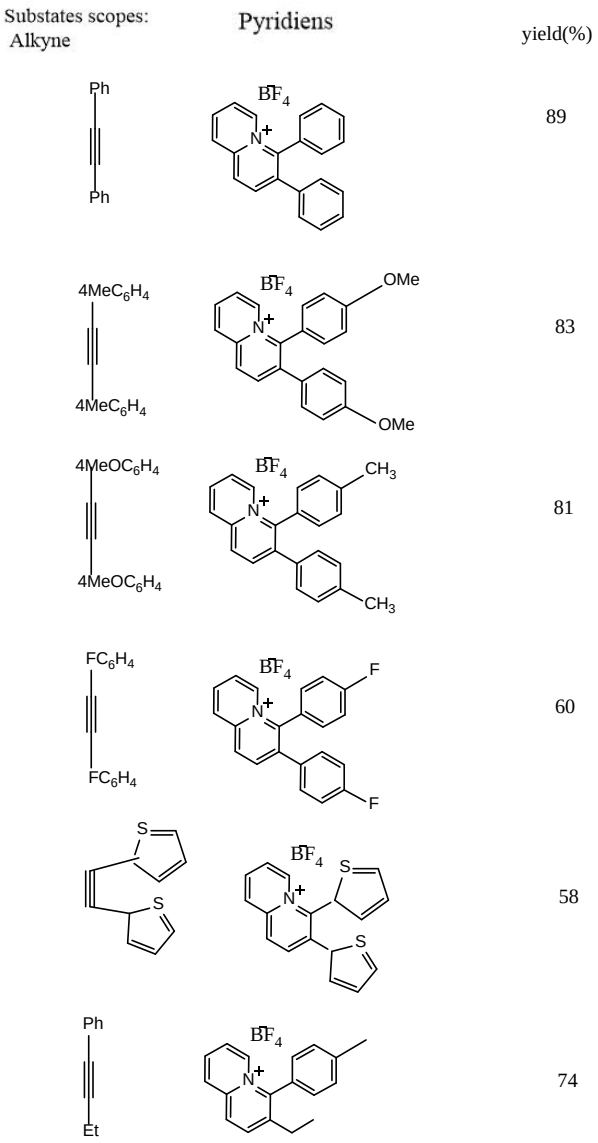

Scheme 14: Substrate Scope *(Source: Luo et al., 2015)*

VI. Synthetic route for the Functionalization of Pyridines through an Oxazoline-guided Regioselective C−H Amination Reaction

Differently functionalized pyridines can be obtained via an oxazoline-promoted regioselective C-H amination reaction (scheme-15). Interestingly, the presence of a C2-substituent is crucial for this transformation to be successful. Furthermore, it allows for extensive embellishment of the finished products. Note that, among these entities, 2-chloropyridines provide access to a wide range of building blocks, for example, a versatile azaquinazoline scaffold (Maiden *et al*., 2016).

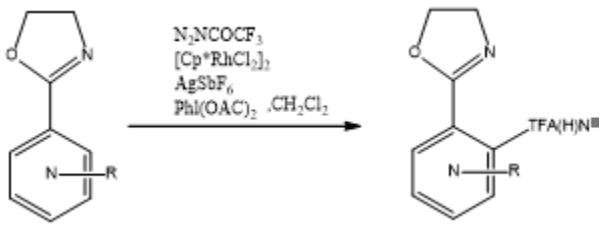

Scheme 15: Regioselective C−H Amination Reaction *(Source: Maiden et al., 2016)*

Both 2-halopyridine and 6-halopyridine participated (scheme-16) under the optimized conditions for smooth amidation to produce the aimed products with satisfactory yields. Also, a trifluoromethyl-substituted pyridine has excellent yield and selectivity.

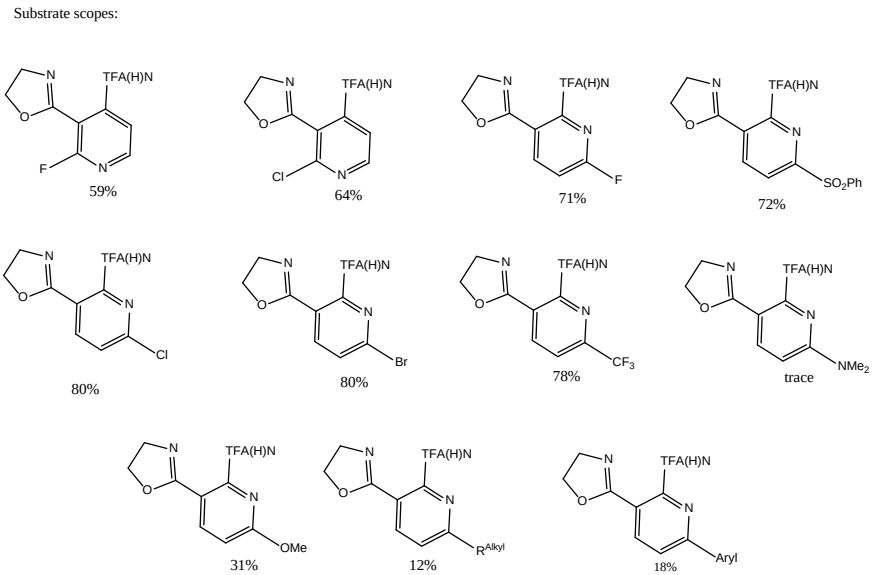

Scheme 16: Substrate Scope *(Source: Maiden et al., 2016)*

VII. Rhodium (III)-promoted Oxidative Annulation reaction of 7-Azaindoles with the Alkynes via two consecutive C−H Activation

This Rh (III)-catalyzed double C−H bond functionalization protocol (scheme-17) involves an ortho C−H activation step, which is guided by a nitrogen-based directing group. It is then followed by an ensuing roll-over reaction, which turns into another C−H bond functionalization step of the heterocyclic system. Note that, these 7-azaindole derivatives are generally very difficult to produce. But, under the present protocol, they can be achieved with excellent yields. The scope of the reaction is quite broad. Under the optimized protocol, the 7-azaindoles and also the internal alkynes successfully participated (Li *et al*., 2015).

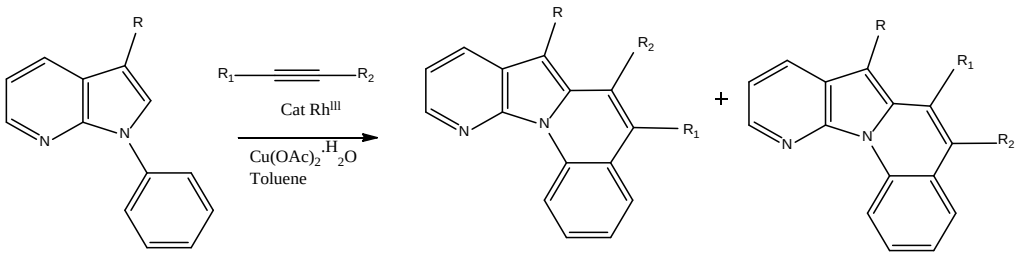

Scheme 17: Oxidative Annulation reaction of 7-Azaindoles *(Source: Li et al., 2015)*

The authors have employed both electron donating as well as electron retreating motifs at different sites (scheme-18) of the 7-azaindole species and engaged them under the standardized protocol to afford the desired products with great yields. As expected, an ortho-alkyl substitution on the benzene motif had obstructed the 2nd C-H activation process to produce the product with only 48% yield. Note that, the substrates, having a halogen motif on the pyridine ring were also proved fruitful under the optimized reaction protocol. Even, the alkyl substituted substrates reacted adequately in this coupling process, producing the products with good yields.

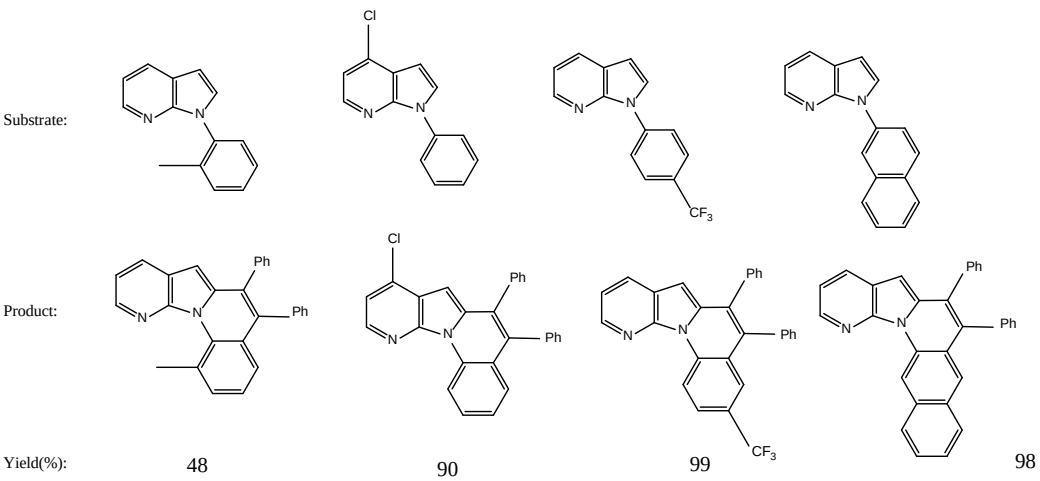

Scheme 18: Substrate Scope *(Source: Li et al., 2015)*

VIII. Rhodium (III)-promoted C-H Amidation Reaction on Indoles with Isocyanates

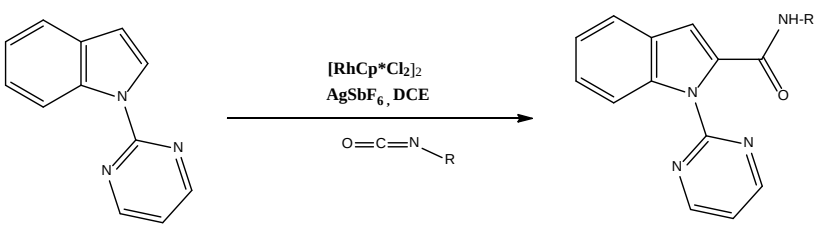

Scheme 19: C-H Amidation Reaction on Indoles *(Source: Jeong et al., 2015)*

When $[RhCp^*Cl_2]_2$ and $AgSbF_6$ react, a cationic Rh (III)-catalyst is formed, where the silver salt easily coupled with the pyrimidinyl nitrogen. Such catalysts can readily promote the C-H activation reversibly at the indole C2-site, thereby providing a rhodium-based metalacycle intermediate along with the release of a proton (H^+). The subsequent synchronization of the isocyanate then shaped an intermediate compound, which, on an additional drifting insertion into the Rhodium-Carbon bond, formed a complex that, upon accepting a proton, yielded the intended product (schemes-19 & 20) and also regenerated the active Rhodium (III) catalyst (Jeong *et al*., 2015).

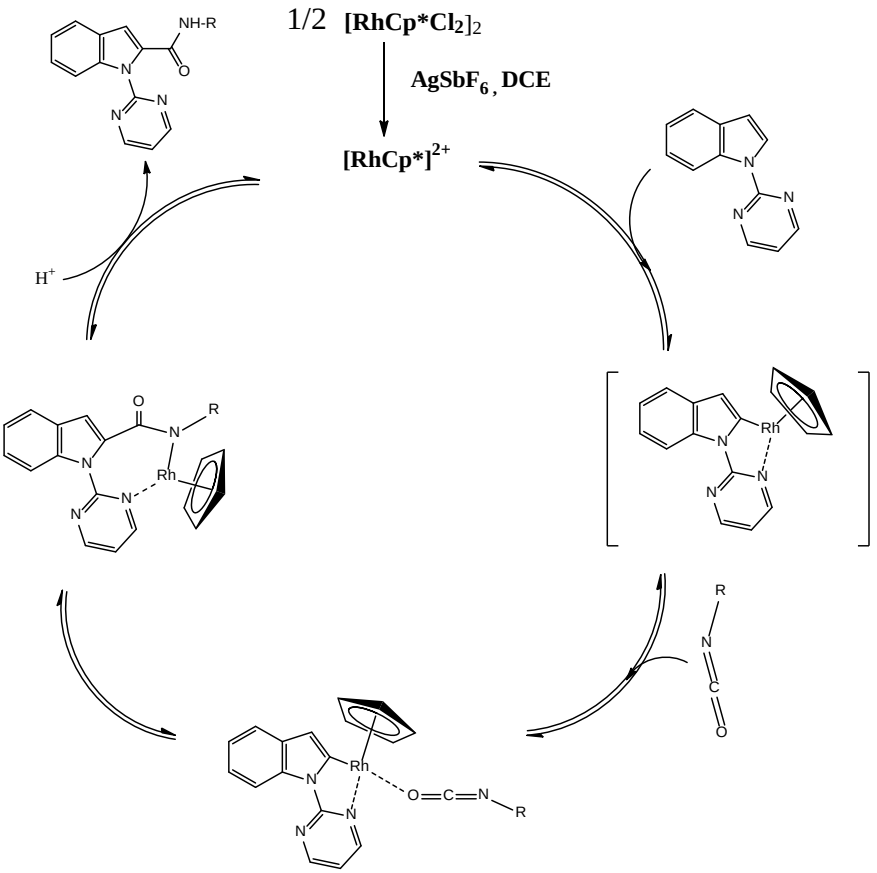

Scheme 20: Mechanism of the reaction *(Source: Jeong et al., 2015)*

The authors screened a variety of aryl isocyanates, both having electronically poor as well as electronically wealthy substituents (Me, Br, and CF_3) and they found that all were well endured under the given conditions and afforded the resultant products (scheme-21). But highly electronically scarce phenylsulfonyl isocynates tend to give low yields, possibly ascribed to the reversible nature of the amidation process.

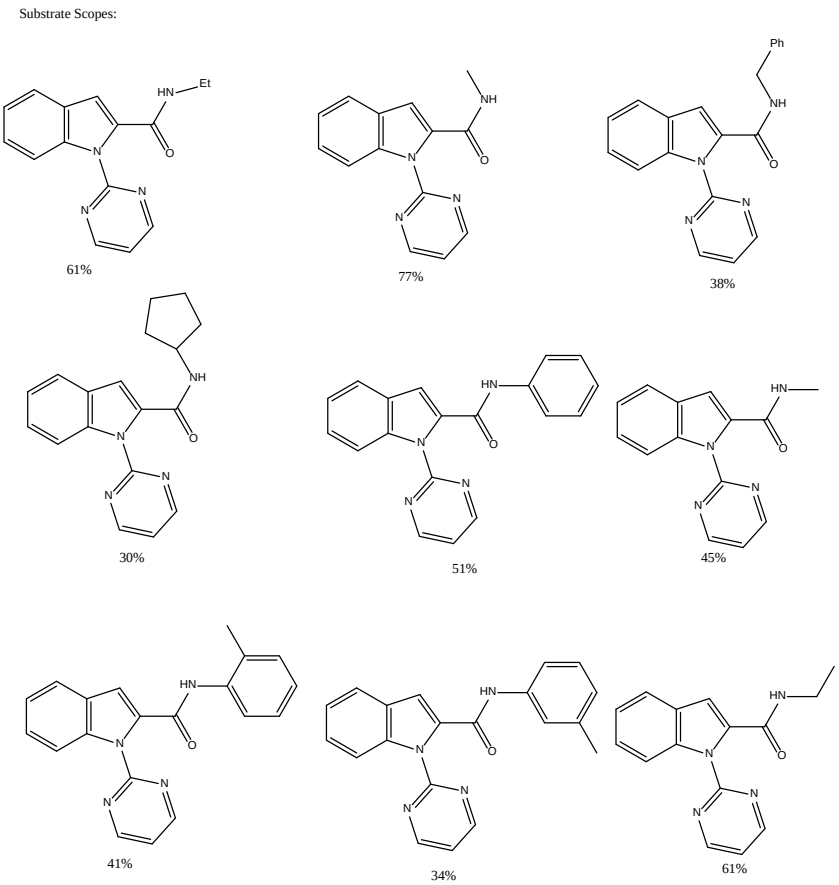

Scheme 21: Substrate Scope *(Source: Jeong et al., 2015)*

IX. Rhodium (III)-promoted C−H Activation reaction of Quinoline N-Oxides

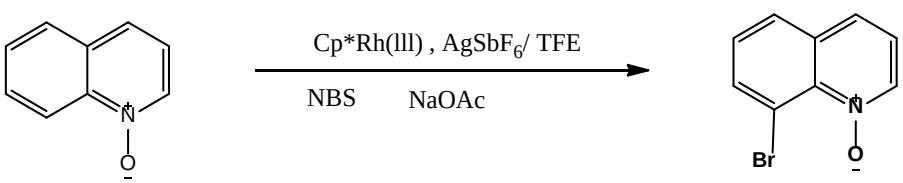

Scheme 22: C−H Activation of Quinoline N-Oxides *(Source: Dhiman et al., 2019)*

intermediate for such C8-functionalization (scheme-22) is a five-membered rhodacycle, formed in situ on reaction with the quinoline N-oxide. Dhiman *et al*. (2019) also used N-fluorobis-(phenylsulfonyl)-imide as the reagent for this C8-amidation technique of quinoline N-oxide unveiled by the authors. Both the bromination and amidation steps at the C8-site of the quinoline N-oxide systems were routed through this technique (scheme-23). This transformation has also been successfully

implemented, scaling up to a few-gram scale level. Such a scaled-up protocol also showed satisfactory functional group tolerance on a wide variety of substrates. A thorough mechanistic study revealed that the core intermediate for such C8-functionalization is a five-membered rhodacycle, formed in situ on reaction with the quinoline N-oxide. Dhiman *et al*. (2019) also used N-fluorobis-(phenylsulfonyl)-imide as the reagent for this C8-amidation technique of quinoline N-oxide.

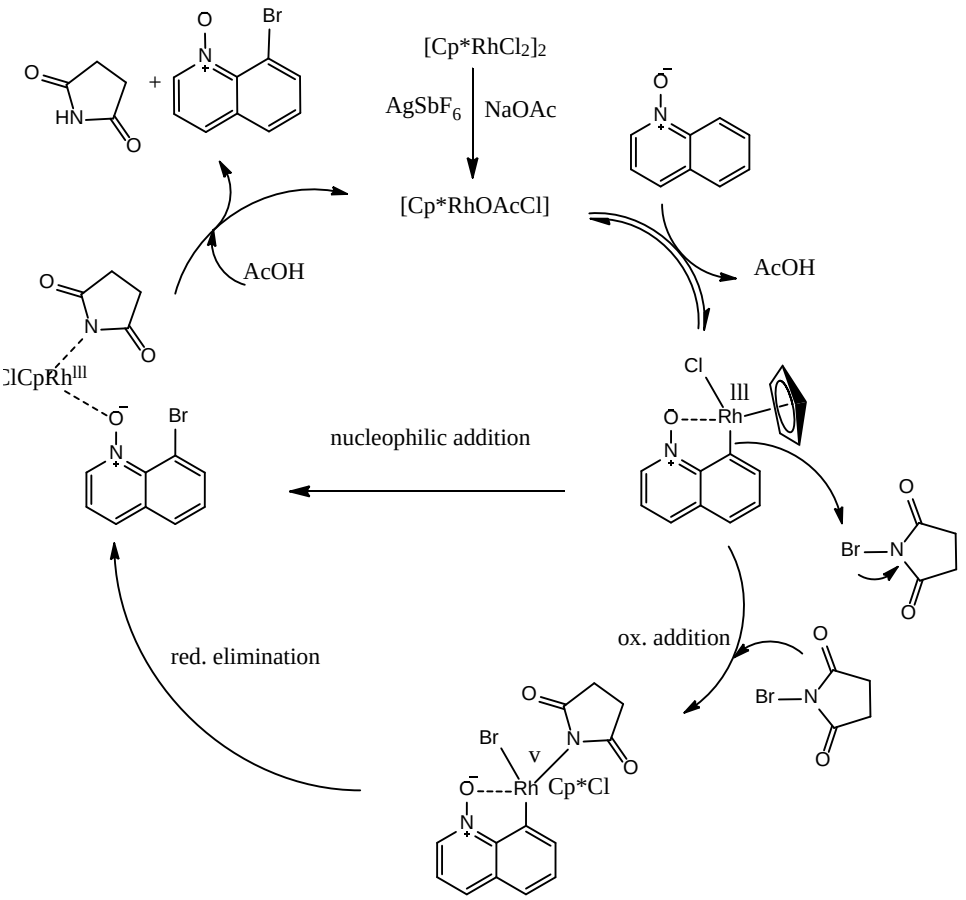

Scheme 23: Mechanism of the reaction *(Source: Dhiman et al., 2019)*

The authors screened various quinoline N-oxides to structure the substrate scope, and found that substituting OMe, iPr, t Bu, Br, Cl, and NH(Boc) at the C6 position of the system produced the intended product with moderate to high yields. Additionally, the authors observed a similar reactivity with 5-chloroquinoline N-oxide (scheme-24). However, when the substituent is situated at the C2-site, it was found that the yield is quite low, probably due to substantial steric hindrance at the site.

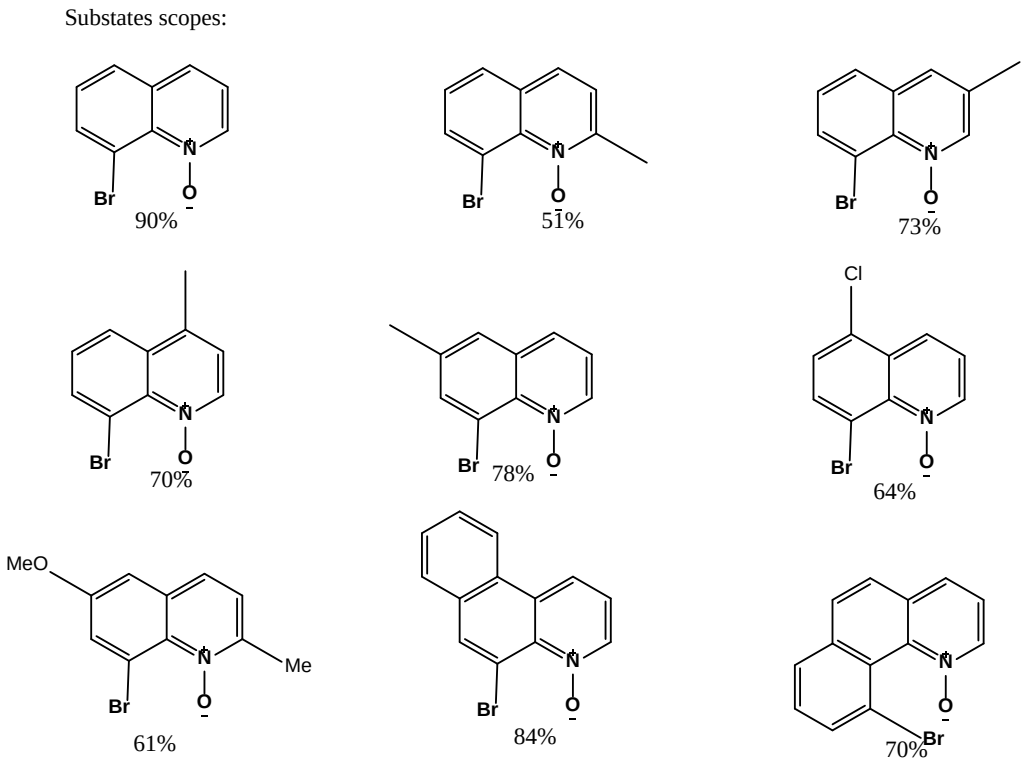

Scheme 24: Substrate Scope *(Source: Dhiman et al., 2019)*

X. Rhodium (I)-promoted Aryl C−H Carboxylation reaction of 2-Arylanilines with gaseous carbon dioxide

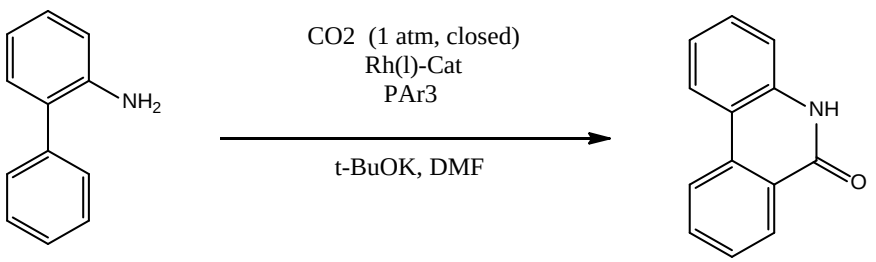

Scheme 25: Carboxylation reaction of 2-Arylanilines *(Source: Gao et al., 2019)*

This reaction (scheme-25) is an example of the oxidative addition process of an Iodo-rhodium species, which is reversible in nature. Subsequently, HX undergoes a clear reductive elimination. The process generates a rhodium-implanted metalacycle, subsequently undergoing a nucleophilic carboxylation step with carbon dioxide to form the rhodium carboxylate (scheme-26). The concluding lactamization reaction of rhodium carboxylate, promoted by potassium butoxide, eventually generated the product and reproduced the Rh (I) catalyst (Gao *et al*., 2019).

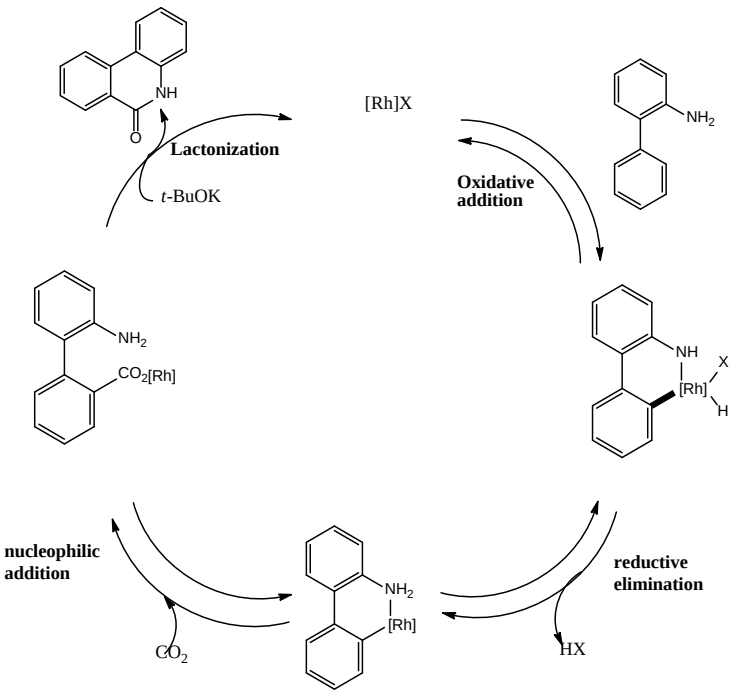

Scheme 26: Mechanism of the reaction *(Source: Gao et al., 2019)*

Substrate scopes:

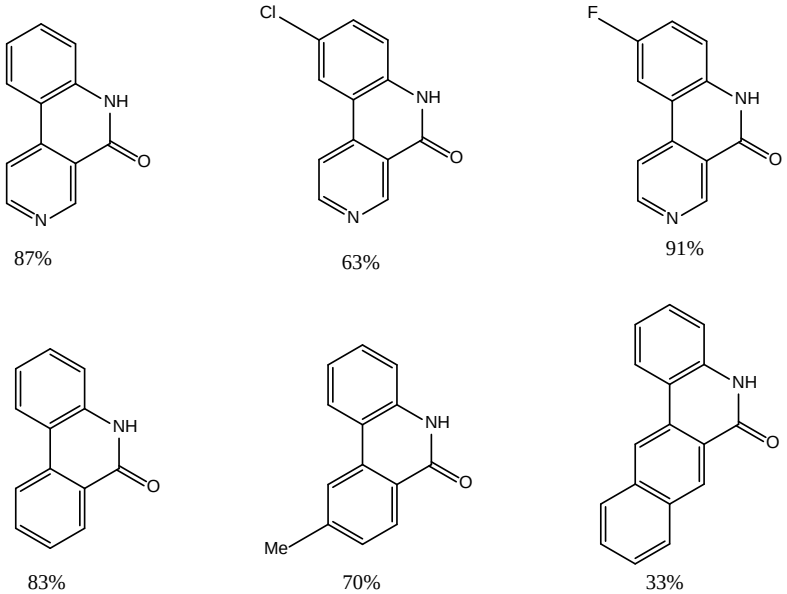

Scheme 27: Substrate Scope *(Source: Gao et al., 2019)*

Exploration of Chemical Complexity

In order to explore the substrate scope (scheme-27) with several electronically scarce as well as electronically rich substituents, the authors placed various substituents at the meta-position and para-position, and they were found to be fruitful under the optimized protocol. The yields of desired phenanthridinones are generally outstanding to excellent. Note that the electron-poor motifs like trifluoromethyl, amide, and cyanides were quite well tolerated with this reaction and smoothly led to a high-yielding synthetic protocol without the hydrolytic cleavage of these base-sensitive substituents.

Conclusion

This review article may be used as a window into the most recent developments in organometallic chemistry, highlighting the wide range of uses for Rh-catalysis in C-H bond activation procedures as well as the revolutionary effects it has had on society. One can definitely apply these works to other pyridine, oxazole, and aza-heterocycle derivatives to incite further research and collaborative endeavors, fostering a deeper understanding of the boundless potential of Rhodium chemistry. This can be achieved by exploring the current developments of the last ten years and the future opportunities of various sub-disciplines.

Acknowledgment

The author would like to thank the teacher in charge of Maharaja Manindra Chandra College, India for providing office space and internet facilities. The author also acknowledges the constant support extended by his colleagues in the Department of Chemistry at Maharaja Manindra Chandra College.

References

Berman, A. M., Bergman, R. G., & Ellman, J. A. (2010). Rh (I)-catalyzed direct arylation of azines. *The Journal of organic chemistry*, *75*(22), 7863-7868. https://doi.org/10.1021/jo101793r

Blakemore, D. C., Castro, L., Churcher, I., Rees, D. C., Thomas, A. W., Wilson, D. M., & Wood, A. (2018). Organic synthesis provides opportunities to transform drug discovery. *Nature chemistry*, *10*(4), 383-394. https://doi.org/10.1038/s41557-018-0021-z

Campos, K. R., Coleman, P. J., Alvarez, J. C., Dreher, S. D., Garbaccio, R. M., Terrett, N. K., ... & Parmee, E. R. (2019). The importance of synthetic chemistry in the pharmaceutical industry. *Science*, *363*(6424), eaat0805. https://doi.org/10.1126/science.aat0

Dhiman, A. K., Gupta, S. S., Sharma, R., Kumar, R., & Sharma, U. (2019). Rh (III)-catalyzed C (8)–H activation of quinoline N-Oxides: regioselective C–Br and C–N bond formation. *The Journal of Organic Chemistry*, *84*(20), 12871-12880. https://doi.org/10.1021/acs.joc.9b01538

Gao, Y., Cai, Z., Li, S., & Li, G. (2019). Rhodium (I)-catalyzed aryl C–H carboxylation of 2-arylanilines with CO2. *Organic letters*, *21*(10), 3663-3669. https://doi.org/10.1021/acs.orglett.9b01105

Jeong, T., Han, S., Mishra, N. K., Sharma, S., Lee, S. Y., Oh, J. S., ... & Kim, I. S. (2015). Rh (III)-Catalyzed C–H Amidation of Indoles with Isocyanates. *The Journal of Organic Chemistry*, *80*(14), 7243-7250. https://doi.org/10.1021/acs.joc.5b00763

Lam, N. Y., Wu, K., & Yu, J. Q. (2021). Advancing the logic of chemical synthesis: C− H activation as strategic and tactical disconnections for C− C bond construction. *Angewandte Chemie*, *133*(29), 15901-15924. https://doi.org/10.1002/ange.202011901

Li, S. S., Wang, C. Q., Lin, H., Zhang, X. M., & Dong, L. (2015). Rhodium (III)-catalyzed oxidative annulation of 7-azaindoles and alkynes via double C–H activation. *Organic letters*, *17*(12), 3018-3021. https://doi.org/10.1021/acs.orglett.5b01228

Luo, C. Z., Gandeepan, P., Wu, Y. C., Tsai, C. H., & Cheng, C. H. (2015). Cooperative C (sp3)–H and C (sp2)–H Activation of 2-Ethylpyridines by Copper and Rhodium: A Route toward Quinolizinium Salts. *ACS Catalysis*, *5*(8), 4837-4841. https://doi.org/10.1021/acscatal.5b01244

Maiden, T. M., Swanson, S., Procopiou, P. A., & Harrity, J. P. (2016). Synthesis of Functionalized Pyridines via a Regioselective Oxazoline Promoted C–H Amidation Reaction. *Organic letters*, *18*(14), 3434-3437. https://doi.org/10.1021/acs.orglett.6b01612

Mohanty, S. R., Prusty, N., Nanda, T., Mahulkar, P. S., & Ravikumar, P. C. (2024). Directing group-assisted selective C–H activation of six-membered N-heterocycles and benzo-fused N-heterocycles. *Organic Chemistry Frontiers*, *11*(2), 540-575. https://doi.org/10.1039/D3QO01396K

Song, G., Gong, X., & Li, X. (2011). Synthesis of quinolines via Rh (III)-catalyzed oxidative annulation of pyridines. *The Journal of Organic Chemistry*, *76*(18), 7583-7589. https://doi.org/10.1021/jo201266u

Wang, H. W., Qiao, Y. H., Wu, J. X., Wang, Q. P., Tian, M. X., Li, Y. F., ... & Lu, Y. (2021). RhIII-Catalyzed C–H (Het) arylation/Vinylation of N-2, 6-Difluoroaryl Acrylamides. *Organic Letters*, *23*(3), 656-662. https://doi.org/10.1021/acs.orglett.0c03688

Wiedemann, S. H., Ellman, J. A., & Bergman, R. G. (2006). Rhodium-Catalyzed Direct C− H Addition of 3, 4-Dihydroquinazolines to Alkenes and Their Use in the Total Synthesis of Vasicoline. *The Journal of Organic Chemistry*, *71*(5), 1969-1976. https://doi.org/10.1021/jo052345b

Zhang, Y., Zhang, J. J., Lou, L., Lin, R., Cramer, N., Wang, S. G., & Chen, Z. (2024). Recent advances in Rh (I)-catalyzed enantioselective C–H functionalization. *Chemical Society Reviews*. https://doi.org/10.1039/D3CS00762F

doi: 10.31674/book.2024ecc.004

Diversity of Zinc Oxide-Nanoconjugate: Photophysical and Photochemical Aspect

Piyali Mitra

Department of Chemistry (UG+PG), Trivenidevi Bhalotia College, Paschim Bardhaman, West Bengal, India

Corresponding Author's Email: mitra.piyali.2009@gmail.com

Abstract

Photophysical and photochemical studies of anticancer drug-functionalized nanoparticles are of enormous significance. Now adays, these nanoconjugates have greater application in the field of novel photo-based nanodevices for photocatalysis and drug delivery. Moreover, nanoconjugates are anticipated to be excellent revenue of assimilating attractive features of molecular as well as bulk regimes. Nanostructured materials produce the electronic excited states, or excitons, during light-matter interactions. It is interesting to be acquainted with diverse kinds of electrons. Furthermore, gaining knowledge about a diverse range of materials is energizing, as it allows us to understand the formation of electronically excited states and progress into femtosecond and nanosecond time domains. The mechanism of solar energy conversion, which is a solely photo-initiated process using ultrafast lasers, as well as finding out about new photonic and biphotonic applications, are also important areas of now days' research. Researchers use hundreds of light-absorbing molecules, known as chromophores, to harvest sunlight. Chromophores also play an important role in directing the excitation energy to nature's solar cells- proteins, which are called reaction centers.

Keywords: *Biophotonic; Excitons; Graphene; Photodynamic Therapy; Quantum Dots (Qds); Reactive Oxygen Species (ROS); Solar Energy; Ultrafast Spectroscopy*

Introduction

Metal oxide nanomaterials have received a lot of attention due to their current and potential commercial importance. ZnO, in particular, is an excellent candidate for applications in photocatalyst, photodetector, and biomedicine. To date, a number of strategies have been employed to improve the photocatalytic operation of ZnO, primarily to reduce the recombination of photogenerated electrons and holes. In general, ZnO nanoparticles have gotten a lot of attention because they are very sensitive to light, strong at high temperatures, cheap, safe, and compatible with living things. This makes them a good choice for studying photocatalytic action as well as their important roles in biology (Yuan, Hein & Misra, 2010). First, Yuan, Hein and Misra (2010) used ZnO QDs

(quantum dots) attached to biodegradable molecules, like chitosan, to deliver drugs specifically to tumors. Specifically, they encrusted ZnO QDs with folate-conjugated chitosan via electrostatic interaction. The conjugation serves the purpose of loading the ZnO QDs with doxorubicin (DOX), a widely used chemotherapy drug, to achieve a 75% efficiency in action. Furthermore, Liu *et al*. (2016) reported a pH-responsive drug delivery system based on ZnO NP loaded with the anticancer drug, DOX. Moreover, numerous literature reports have demonstrated the enhanced photocatalytic and antibacterial activity of noble metal/zinc oxide hybrid nanostructures, indicating their immense potential for use in water purification and various pathogenic applications (He *et al*., 2014; Hu *et al*., 2016; Kumar *et al*., 2014; Mao *et al.,* 2017). ZnO nanostructured substances don't dissolve well in physiological media, but they can dissolve as nontoxic ions in acidic media, like the late endosome and lysozome of tumor cells (Wang *et al*., 2014; Xiong, 2013; Cho *et al*., 2011), and they can also dissolve in basic media (Abdelmonem *et al*., 2015). Because of their excellent properties, ZnO NPs have become very important as multifunctional nanocarriers that make the release process easier (Zhou *et al*., 2006). Also, ZnO nanoparticles can effectively carry drugs in photodynamic therapies (PDT) by stopping a lot of drug buildup at the desired site (Zhang *et al.,* 2013).

It is made up of 9AA-HCl (9-aminoacridine hydrochloride hydrate), which is an organic molecule whose spectral properties are very sensitive to its surroundings. Moreover, 9AA-HCl exists in three different structures depending on the pH of the medium (Scheme 1) (Mitra *et al*., 2014). In addition, it acts as one of the important drugs for antibacterial, mutagenic, and antitumor effects (Zhu *et al*., 1994). One intriguing biological use of 9AA-HCl is as an intercalant agent, which means it can mix with DNA (Rehn and Pindur, 1996; Wynn *et al*., 2017; Graham *et al*., 2011; Ceron-Carrasco *et al*., 2017). Latterini and Tarpani (2011), apply the fluorescent drug for membrane imaging after doping with silica nanoparticles. Furthermore, conjugation with gold nanoparticles also enhances the antibacterial activity of 9AA-HCl (Mitra, Chakraborty & Basu, 2014). The literature also reports that the PP-ZnO nanohybrid demonstrates enhanced photodynamic action to inhibit E. coli growth (Sardar *et al*., 2015). During the interaction between PDT drugs and semiconductor nanoparticles, the development of reactive oxygen species (ROS) is the foremost factor. ROS oxidizes the organic compound; therefore, ROS generation may also influence the photocatalytic action of semiconductors (Zhou *et al*., 2011). The quick recombination of photogenerating electron-hole pairs, faster than surface redox reactions, reduces the quantum efficiency of photocatalysis of the semiconductor (Hoffmann *et al*., 1995). Therefore, Luo *et al*. (2012) conjugate the semiconductor nanoparticles with other molecules or materials to enhance charge separation and prevent the recombination of the respective electron and hole pairs.

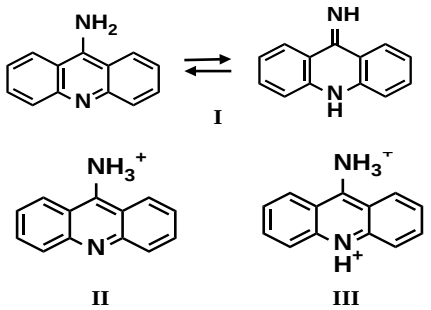

Scheme 1: The pH-responsive drug 9AA-HCl comes in various forms:(I) neutral; (II) protonated; (III) doubly protonated

Methodology and synthesis of ZnO nanoparticles

A transmission electron microscope (JEOL-TEM 2100 with an operating voltage of 200 kV) was used for the purpose of taking TEM images. To find out the crystal structures of the samples, an X-ray diffractometer with the model number Seifert 3000P and CuKa radiation (λ = 1.54178É) was used. The XPS data was obtained using Omicron nanotechnology. Zetasizer Nanosystem, Malvern Instruments Ltd., was used to calculate the DLS and zeta potential. A UV-vis spectrophotometer (SHIMADZU) was employed to measure the optical absorption spectra at room temperature. The fluoromax spectrophotometer of HORIBA JOBIN YVON was used to record the respective emission spectra (photoluminescence). Moreover, TCSPC, i.e., time-correlated single-photon counting measurement, was performed using picosecond NANO-LED. Using a previously reported method, ZnO NPs were synthesized (Barman *et al*., 2017).

Results and Discussion

Transmission electron microscope *i.e.,* TEM, Fourier transform infrared spectroscopy *i.e.,* FTIR and Raman spectroscopy are being used to establish the formation of nanoparticles as well as nano conjugation.

Zinc oxide nanoparticles

Figure 1A. depicts the TEM image with the particle size distribution, which depicts a monodispersed character with a particle size of ~6 ± 0.5 nm. Figure 1B. illustrates the XRD model for NPs. As expected, the XRD data shows that the nanoparticles are exactly the same as ZnO in its pure form, with a wurtzite nature configuration and a hexagonal crystal phase. Additionally, the XPS spectrum having two structural peaks implies ZnO of pure phase (at 1020.5 eV, it signifies $Zn2p_{3/2}$, and at 1043.9 eV, it signifies $Zn2p_{1/2}$). The UV-Vis spectrum shows evidence of pure ZnO NP, which corresponds to a band peak at 334 nm as depicted in Figure 1C. This UV data indicates that there is a restricted

size distribution of NP. Moreover, ZnO NP at 557 nm exhibits a strong yellow emission (Figure 1C), which is primarily caused by an oxygen vacancy defect in ZnO. Figure 1D. displays the TCSPC data for ZnO NP, which depicts defect emission with bi-exponential decay kinetics**.**

Furthermore, it is calculated from the obtained data that the lifetimes of the faster component are 7.69 ns (55%), and the slower component is 42.99 ns (45%), with an average lifetime of ~23.74 ns. While the emissions in the visible region are a tranquil topic of argument and quite a lot of explanations have been projected, the photoluminescence lifetime determines the concentration of defects. This type of emission occurs owing to the recombination of a trivial trapped electron in the midst of a profoundly trapped hole. In this current scenario, 43.0 ns, which signifies the longer lifetime component, happens owing to such recombination in the course of surface defects responsible for O^{2-}/O^{-}. The faster lifetime factor of ~7.7 ns originates from the band gap correlated with exciton recombination.

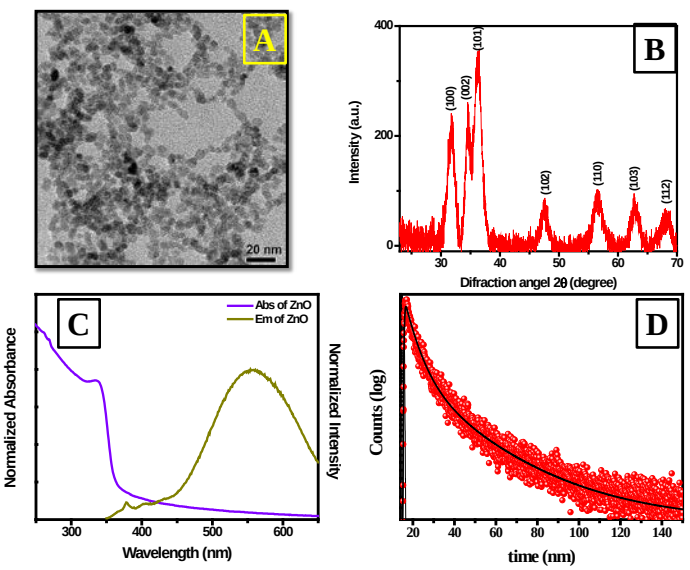

Figure 1: Zinc oxide nanoparticles (A) TEM image; (B) XRD pattern; (C) absorption and emission spectra; and (D) time-resolved decay curve *(Source: Baarman et al., 2017)*

Zinc oxide nanoconjugates

Small and consistently sized particles are of significant necessity to modulate physico-chemical properties, together with luminescence and drug-loading ability. The TEM image of nanohybrid is depicted in Figure 2. The consistencies of nearly spherical nanocrystals are confirmed.

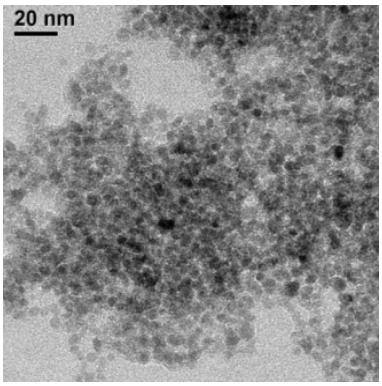

Figure 2 : ZnO-9AA-HCl nanoconjugate: Transmission electron micrograph.
(Source : Mitra et al., 2018)

Fourier transform infrared (FTIR) technique was used for studying the conjugation among the drug and the NP. The binding is a very essential factor for biological application. The FTIR spectra (Figure 3) having distinctive peak at 3337 $cm^{-1}$of drug molecule corresponds toward the amine group (-NH_2) stretching frequency (Mitra *et al*., 2014). However, subsequent to conjugation along with the NP, the stretching frequency which is responsible for of the -NH_2 moiety of the bare drug molecule is altered as well as broadened. The IR data signifies the fact that the covalent bonding is responsible for stretching frequency shifting. The covalent bond is formed between the -NH_2 (amine group) of the drug molecule and ZnO NP (Sardar *et al*., 2015). Moreover, owing to the conjugation, the surface hydroxyl groups of the ZnO (Liu *et al*., 2014, Tu *et al*., 2011) are affected (3370-3400 cm^{-1} and 1630-1635 cm^{-1}). This diminution in the intensity as well as shifting of the band position signifies the presence of hydrogen bonding interaction between nanoprticle and drug molecule (Das *et al*., 2017, Zhang *et al*. 2015).

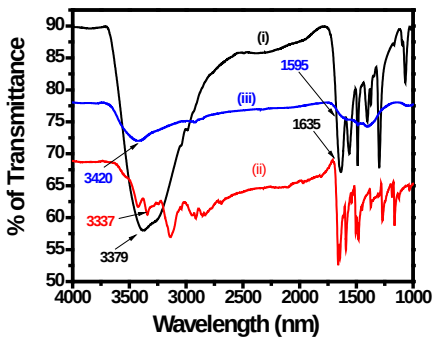

Figure 3: FTIR spectra of (i) NP, (ii) Drug molecule, and (iii) conjugate
(Source: Mitra et al., 2018)

The changes in the vibrational mode of ZnO NP after conjugation were investigated using a Raman spectroscopic study at room temperature. The results are illustrated in Figure 4. After excitation at 532 nm, due to high fluorescence, the Raman spectrum of 9AA-HCl does not illustrate any peak in the wave number range of 300–600 cm^{-1}. On the other hand, from the space group theory, it is well known that $A_1 + 2E_2 + E_1$ are the Raman active vibrational modes of the ZnO structure. It is evident from the figure that the Raman spectrum of ZnO NP exhibits four vibration peaks at 328 cm^{-1}, 378 cm^{-1}, 438 cm^{-1} and 577 cm^{-1}, which signifies the presence of a wurtzite structure (Zhang *et al*., 2003). The strong characteristic peak at 438 cm^{-1}can be consigned to the nonpolar optical phonon E_2 mode of ZnO NP at high frequency, which is associated with oxygen deficiency, whereas the peaks at 378 cm^{-1} and 577 cm^{-1} correspond to the polar transverse A_1 and longitudinal E_1 optical phonon modes, respectively. The peak at 332 cm^{-1} is attributed to the E_2^{high}-E_2^{low} mode. The most important thing is that the E_2 mode characteristic band, which is linked to flaws in ZnO NP, changes a lot after conjugation. This change implies that the passivation of the NPs surface states upon binding with the drug molecule. However, the presence of other characteristic bands indicates good wurtzite structure retention during interaction.

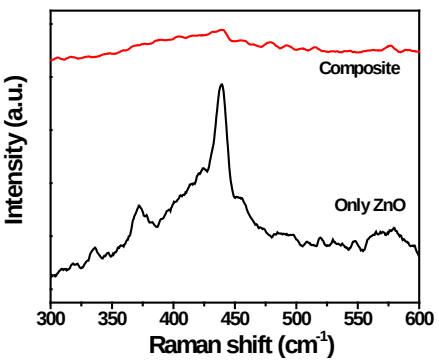

Figure 4: Raman spectra of ZnO NP (black) and conjugates (Red)
(Source: Mitra et al., 2018)

Steady state and Time resolved spectroscopic studies of ZnO-9AA-HCl system

Furthermore, visible spectroscopy helps characterize the nanoconjugate's creation. This therapeutic drug, having two pK_a values (-2.0 and 10.0), can exist in three different forms (Schuldiner *et al*., 1972). In concentrated strong acid (at pH < -2.0), the dominant form of the photodynamic drug is the doubly protonated form, while having -2.0 < pH < 10.0, the protonated form, *i.e.,* 9AAH+, exists. In pH > 10.0, the neutral form prevails through the deprotonation of the protonated form (II) and maintains equilibrium among its amino acids and iminotautomers (Murza *et al*., 2000). Figure 5 displays the UV-vis absorption spectra of only nanoparticles, drug molecules, and the conjugated form, ZnO-9AA-HCl.

At 345 nm, the ZnO NPs show evidence of a threshold band gap of 3.59 eV. However, the drug molecule has the highest absorbance at 400 nm. Note that the spectra of the nanoconjugate show no discernible peak of the drug molecule. The reason for this spectral nature is due to the extremely low concentration of 9AA-HCl and the significant scattering of the ZnO NPs. Moreover, the conjugate's UV-vis peak exhibits a slight shift towards the blue region, compared to the nanoparticle's 338 nm (3.67 eV). Therefore, it is reasonable to conclude that nanohybrids are formed more willingly than only physical absorption due to the interaction between the drug's NP and amine moiety.

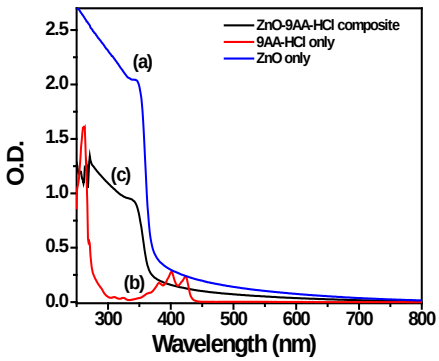

Figure 5: a) ZnO NP, b) 9AA-HCl, and c) ZnO-9AA-HCl; UV-Vis absorption spectra of only nanoparticles *(Source: Mitra et al., 2018)*

The Literature Survey revealed an excited state interaction between NP and carbon dot (Barman *et al*., 2017). Researchers using emission quenching and laser flash photolysis found that light can move electrons between NPs of different sizes and methyl viologen (Mitra *et al*., 2017). NPs, known for their oxygen vacancies, give rise to green emission in the visible region (Vietmeyer *et al*., 2007).

Figure 6(A) portrays suv-visible emission of NP, which is responsible for the surface states. The drug's presence tailors the surface of NPs, eliminating the possibility of energy transfer due to the lack of specific spectral overlap between NPs and drugs. Therefore, in the visible region, the emission quenching is exclusively due to photo-induced electron transfer.

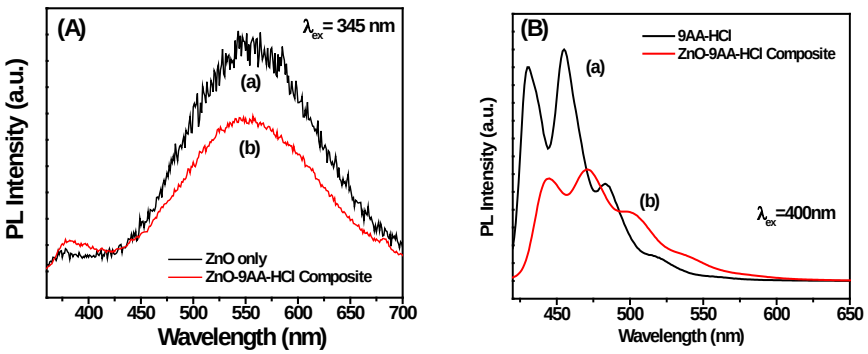

Figure 6: (A) PL spectra (a) NPs and (b) nanoconjugate; (B) PL spectra (a) NPs and (b) nanoconjugate *(Source : Mitra et al., 2018)*

Figure 6 (B) demonstrates the fact that the emission of drug molecules is quenched as well as blue-shifted due to their attachment to NP. Upon conjugation with ZnO NP, the drug molecule's PL spectrum nearly blends into its neutral form. This result indicates that the neutral form of the drug molecule prevails, which might be due to donating the H^+ to the ZnO NP (through hydrogen bonding) after binding with ZnO NP. These modes of binding are well corroborated with the results obtained from FTIR studies, as pointed out in the previous segment.

In order to confirm the occurrence of electron transfer interactions between NP and drug molecules, a time-resolved fluorescence spectroscopic study was performed. To conduct the experiment for the lifetime measurements, 9AA-HCl was excited at a wavelength of 371 nm, and the respective emission was monitored at 455 nm. Pant *et al*. (1986) previously reported the nearly equal lifetimes of the singly protonated and neutral forms. As a result, lifetime measurements are unlikely to identify the species that will prevail during the interaction. There is a single exponential decay in the drug molecule's fluorescence that lasts for 12.89 ns (Figure 7); however, there is a bi-exponential decay in the bioconjugate. The presence of a faster component (0.65 ns with a contribution of 78%) and a slower component (12.87 ns with a contribution of 22%) signify the curve's bi-exponential nature. The slower component, *i.e.,* 12.87 ns, is reliable with the excited-state lifetime of the drug molecule. However, the faster component may be due to the electron migration time from the drug molecule to the NP, as suggested by Kathiravan *et al*. (2009). In this way, the drug molecule adds a second pathway, specifically by connecting 9AA-HCl to ZnO NPs electronically. In addition, the decrease in average lifetime (from 12.89 ns to 3.34 ns) may be linked to the photoinduced electron transfer (PET) from the lowest unoccupied molecular orbital (LUMO) of the drug molecule to the conduction band of the semiconductor through a nonradiative pathway. The apparent non-radiative rate constant (k_{nr}) is determined by

comparing the lifetimes of 9AA-HCl in the absence (τ_0) and in the presence (τ) of ZnO NP, using the following equation:

$$k_{nr} = \frac{1}{<\tau>} - \frac{1}{<\tau_0>} \quad (1)$$

The rate of the electron transfer process from the excited state of the drug molecule to the conduction band of the ZnO NP is estimated to be 1.54×10^9 s^{-1} when considering only the faster component. The obtained k_{nr} value may indicate that the electron transfer process is an ultrafast phenomenon, and it is quite similar to the values reported in the literature (Kathiravan *et al*., 2009). So, having ZnO NPs around could help the PET between the excited state of 9AA-HCl and the semiconductor surface, which would make the photocatalytic and biological actions better.

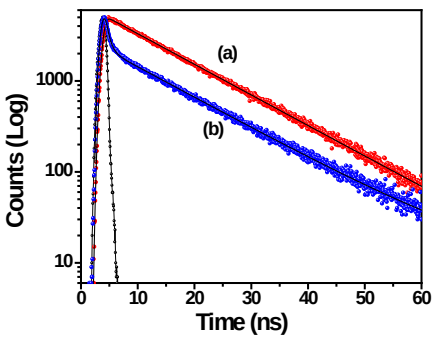

Figure 7: TCSPC curves of (a) the drug molecule and (b) the conjugates Ex-371 nm and Em-455 nm *(Source: Mitra et al., 2018)*

Table 1: *Time-resolved decay parameters of only the drug and the composite, measured at 455 nm under a 371 nm excitation wavelength*

System	τ_1 (ns) [b] (a_1)	τ_2 (ns) [b] (a_2)	τ_{avg} (ns) [b]
9AA-HCl	12.89 (100)	-	12.89
ZnO NP-9AA-HCl	12.87 (0.22)	0.65 (0.78)	3.34

Source: Mitra et al. (2018)

Several experiments have mimicked a natural light harvesting scheme using self-assembled molecules, specifically DNA-conjugated systems and supra-molecular organization of conjugated molecules (fluorophores, dendrimers, organogels, etc.). Adding a fluorophore to a confined matrix is another way to make a light-harvesting device. This gives the molecular arrangement more stability, functionality, and freedom from clumping together. However, the fabrication of light harvesting devices using both donor-acceptor-incorporated host materials encounters several limitations. Firstly, aggregation-based emission quenching may be possible inside the microchannel.

Secondly, it is sometimes necessary for both the donor and acceptor molecules to have similar molecular structures. To avoid such inconveniences, a distinct arrangement of donor-acceptor moieties can be plausible. For this purpose, dye-doped organic-polymer fluorescent nanoparticles may be appropriate as an acceptor system. Furthermore, in the search for a light-absorbing substance, it is currently well established that inorganic nanocrystals, or quantum dots (QDs), are extremely valuable for enhancing the light harvesting process due to their ability to absorb light over a broad spectral window. Particularly, the efficient absorption of visible light by variable-sized quantum dots with tunable band gap energies has established considerable concentration for resourceful solar light energy harvesting systems. To the best of our knowledge, we have not thoroughly studied the rotational relaxation of photoactive molecules inside the polymer nanoparticle, despite it being a suitable means of probing the microenvironment of these nanoparticles. A time-resolved anisotropy study is critical to understanding the source of the dye's rotational relaxation activities inside the polymer nanosphere. The encapsulation of the dye in polymer nanoparticles will constrain its rotational motion. Reorientation times, coupled to the wobbling motion and lateral diffusion of the dye in the nanoparticles, adequately explain the anisotropy decay of the dye molecule in the polymer nanoparticles.

Conclusion

Nowadays, the designing of artificial light harvesting systems using nanomaterials is a challenging task. A thorough understanding of photo physical properties and the carrier relaxation dynamics of photo excited nanocrystals (NCs) is of key importance for both basic research and technological applications. The photo physical properties of semiconductor NCs are considerably different from those of bulk materials as of quantum confinement effect and an enhanced surface-to-volume ratio. The meticulous understanding of the carrier relaxation dynamics is necessary for the reason that it dictates the general efficiency in diverse optoelectronics, photovoltaic, photo catalysis, light-harvesting as well as sensing applications.

Acknowledgement

The author expresses sincere thanks and deep respect to Prof. Amitava Patra. The author extends profound gratitude to Prof. Samita Basu, the research supervisor, for her unwavering cooperation. Special thanks are given to Prof. Nikhil Guchhait for his kind suggestions and discussions whenever needed. The author is deeply indebted to all his colleagues in the Chemistry Department at Triveni Devi Bhalotia College, India for their inspiration. This work would not have been possible without their constant encouragement and support.

References

Abdelmonem, A. M., Pelaz, B., Kantner, K., Bigall, N. C., Del Pino, P., & Parak, W. J. (2015). Charge and agglomeration dependent in vitro uptake and cytotoxicity of zinc oxide nanoparticles. *Journal of Inorganic Biochemistry*, *153*, 334-338. https://doi.org/10.1016/j.jinorgbio.2015.08.029

Barman, M. K., Mitra, P., Bera, R., Das, S., Pramanik, A., & Parta, A. (2017). An efficient charge separation and photocurrent generation in the carbon dot–zinc oxide nanoparticle composite. *Nanoscale*, *9*(20), 6791-6799. https://doi.org/10.1039/C7NR01663H

Cerón-Carrasco, J. P., Ruiz, J., Vicente, C., de Haro, C., Bautista, D., Zuniga, J., & Requena, A. (2017). DFT Simulation of structural and optical properties of 9-aminoacridine half-sandwich Ru (II), Rh (III), and Ir (III) antitumoral complexes and their interaction with DNA. *Journal of Chemical Theory and Computation*, *13*(8), 3898-3910. https://doi.org/10.1021/acs.jctc.7b00139

Cho, N. H., Cheong, T. C., Min, J. H., Wu, J. H., Lee, S. J., Kim, D., ... & Seong, S. Y. (2011). A multifunctional core–shell nanoparticle for dendritic cell-based cancer immunotherapy. *Nature nanotechnology*, *6*(10), 675-682. https://www.nature.com/articles/nnano.2011.149

Das, S., Pramanik, S., Chatterjee, S., Das, P. P., Devi, P. S., & Suresh Kumar, G. (2017). Selective binding of genomic Escherichia coli DNA with ZnO leads to white light emission: a new aspect of nano–bio interaction and interface. *ACS Applied Materials & Interfaces*, *9*(1), 644-657. https://doi.org/10.1021/acsami.6b11109

Graham, L. A., Wilson, G. M., West, T. K., Day, C. S., Kucera, G. L., & Bierbach, U. (2011). Unusual reactivity of a potent platinum–acridine hybrid antitumor agent. *ACS medicinal chemistry letters*, *2*(9), 687-691. https://doi.org/10.1021/ml200104h

He, W., Kim, H. K., Wamer, W. G., Melka, D., Callahan, J. H., & Yin, J. J. (2014). Photogenerated charge carriers and reactive oxygen species in ZnO/Au hybrid nanostructures with enhanced photocatalytic and antibacterial activity. *Journal of the American Chemical Society*, *136*(2), 750-757. https://doi.org/10.1021/ja410800y

Hoffmann, M. R., Martin, S. T., Choi, W., & Bahnemann, D. W. (1995). Environmental applications of semiconductor photocatalysis. *Chemical reviews*, *95*(1), 69-96. https://doi.org/10.1021/cr00033a004

Hu, J., Zhong, Z., Zhang, F., Xing, W., Jin, W., & Xu, N. (2016). High-efficiency, synergistic ZnO-coated SiC photocatalytic filter with antibacterial properties. *Industrial & Engineering Chemistry Research*, *55*(23), 6661-6670. https://doi.org/10.1021/acs.iecr.6b00988

Kathiravan, A., Kumar, P. S., Renganathan, R., & Anandan, S. (2009). Photoinduced electron transfer reactions between meso-tetrakis (4-sulfonatophenyl) porphyrin and colloidal metal-semiconductor nanoparticles. *Colloids and Surfaces A: Physicochemical and Engineering Aspects*, *333*(1-3), 175-181. https://doi.org/10.1016/j.colsurfa.2008.09.042

Kumar, R., Anandan, S., Hembram, K., & Narasinga Rao, T. (2014). Efficient ZnO-based visible-light-driven photocatalyst for antibacterial applications. *Acs applied materials & interfaces*, *6*(15), 13138-13148. https://doi.org/10.1021/am502915v

Latterini, L., & Tarpani, L. (2011). Hierarchical assembly of nanostructures to decouple fluorescence and photothermal effect. *The Journal of Physical Chemistry C*, *115*(43), 21098-21104. https://doi.org/10.1021/jp208124x

Liu, D., Lv, Y., Zhang, M., Liu, Y., Zhu, Y., Zong, R., & Zhu, Y. (2014). Defect-related photoluminescence and photocatalytic properties of porous ZnO nanosheets. *Journal of Materials Chemistry A*, *2*(37), 15377-15388. https://doi.org/10.1039/C4TA02678K

Liu, J., Ma, X., Jin, S., Xue, X., Zhang, C., Wei, T., ... & Liang, X. J. (2016). Zinc oxide nanoparticles as adjuvant to facilitate doxorubicin intracellular accumulation and visualize pH-responsive release for overcoming drug resistance. *Molecular pharmaceutics*, *13*(5), 1723-1730. https://doi.org/10.1021/acs.molpharmaceut.6b00311

Luo, Q. P., Yu, X. Y., Lei, B. X., Chen, H. Y., Kuang, D. B., & Su, C. Y. (2012). Reduced graphene oxide-hierarchical ZnO hollow sphere composites with enhanced photocurrent and photocatalytic activity. *The Journal of Physical Chemistry C*, *116*(14), 8111-8117. https://doi.org/10.1021/jp2113329

Mao, C., Xiang, Y., Liu, X., Cui, Z., Yang, X., Yeung, K. W. K., ... & Wu, S. (2017). Photo-inspired antibacterial activity and wound healing acceleration by hydrogel embedded with Ag/Ag@ AgCl/ZnO nanostructures. *ACS nano*, *11*(9), 9010-9021. https://doi.org/10.1021/acsnano.7b03513

Mitra, P., Dutta, D., Das, S., Basu, T., Pramanik, A., & Patra, A. (2018). Antibacterial and photocatalytic properties of ZnO–9-aminoacridine hydrochloride hydrate drug nanoconjugates. *ACS Omega*, *3*(7), 7962-7970. https://doi.org/10.1021/acsomega.8b00568

Mitra, P., Barman, M. K., Basu, S., Das, S., Pramanik, A., & Patra, A. (2017). Interfacial charge transfer between zinc oxide nanoparticles and methyl viologen: influence of size. *ChemistrySelect*, *2*(30), 9869-9877. https://doi.org/10.1002/slct.201701938

Mitra, P., Chakraborty, P. K., Saha, P., Ray, P., & Basu, S. (2014). Antibacterial efficacy of acridine derivatives conjugated with gold nanoparticles. *International journal of pharmaceutics*, *473*(1-2), 636-643. https://doi.org/10.1016/j.ijpharm.2014.07.051

Mitra, P., Chakraborty, B., & Basu, S. (2014). A spectroscopic investigation of the photophysical behaviour of 9-aminoacridine hydrochloride hydrate in presence of organic amines in homogeneous and heterogeneous media. *Journal of luminescence*, *149*, 221-230. https://doi.org/10.1016/j.jlumin.2014.01.034

Murza, A., Sánchez-Cortés, S., García-Ramos, J. V., Guisan, J. M., Alfonso, C., & Rivas, G. (2000). Interaction of the antitumor drug 9-aminoacridine with guanidinobenzoatase studied by spectroscopic methods: A possible tumor marker probe based on the fluorescence exciplex emission. *Biochemistry*, *39*(34), 10557-10565. https://doi.org/10.1021/bi000583p

Pant, D. D., Joshi, G. C., & Tripathi, H. B. (1986). Photophysics of 9-aminoacridinium hydrochloride. *Pramana*, *27*, 161-170. https://doi.org/10.1007/BF02846336

Rehn, C., & Pindur, U. (1996). Molecular Modeling von Interkalationskomplexen antitumoraktiver 9-Aminoacridine sowie eines [d, e]-anellierten Isochinolinderivates mit basengepaarten Desoxytetranukleotiden. *Monatshefte für Chemie/Chemical Monthly*, *127*, 645-658. https://doi.org/10.1007/BF0081725

Sardar, S., Chaudhuri, S., Kar, P., Sarkar, S., Lemmens, P., & Pal, S. K. (2015). Direct observation of key photoinduced dynamics in a potential nano-delivery vehicle of cancer drugs. *Physical Chemistry Chemical Physics*, *17*(1), 166-177. https://doi.org/10.1039/C4CP03749A

Schuldiner, S., Rottenberg, H., & Avron, M. (1972). Determination of ΔpH in chloroplasts: 2. Fluorescent amines as a probe for the determination of ΔpH in chloroplasts. *European Journal of Biochemistry*, *25*(1), 64-70. https://doi.org/10.1111/j.1432-1033.1972.tb01667.x

Tu, W., Lei, J., Wang, P., & Ju, H. (2011). Photoelectrochemistry of Free-Base-Porphyrin-Functionalized Zinc Oxide Nanoparticles and Their Applications in Biosensing. *Chemistry–A European Journal*, *17*(34), 9440-9447. https://doi.org/10.1002/chem.201100577

Vietmeyer, F., Seger, B., & Kamat, P. V. (2007). Anchoring ZnO particles on functionalized single wall carbon nanotubes. Excited state interactions and charge collection. *Advanced Materials*, *19*(19), 2935-2940. https://doi.org/10.1002/adma.200602773

Mitra, P., Barman, M. K., Basu, S., Das, S., Pramanik, A., & Patra, A. (2017). Interfacial charge transfer between zinc oxide nanoparticles and methyl viologen: influence of size. *ChemistrySelect*, *2*(30), 9869-9877. https://doi.org/10.1002/slct.201701938

Wynn, J. E., Zhang, W., Falkinham III, J. O., & Santos, W. L. (2017). Branched peptides: Acridine and boronic acid derivatives as antimicrobial agents. *ACS medicinal chemistry letters*, *8*(8), 820-823. https://doi.org/10.1021/acsmedchemlett.7b00119

Xiong, H. M. (2013). ZnO nanoparticles applied to bioimaging and drug delivery. *Advanced Materials*, *25*(37), 5329-5335. https://doi.org/10.1002/adma.201301732

Wang, Y. W., Cao, A., Jiang, Y., Zhang, X., Liu, J. H., Liu, Y., & Wang, H. (2014). Superior antibacterial activity of zinc oxide/graphene oxide composites originating from high zinc concentration localized around bacteria. *ACS applied materials & interfaces*, *6*(4), 2791-2798. https://doi.org/10.1021/am4053317

Yuan, Q., Hein, S., & Misra, R. D. K. (2010). New generation of chitosan-encapsulated ZnO quantum dots loaded with drug: synthesis, characterization and in vitro drug delivery response. *Acta biomaterialia*, *6*(7), 2732-2739. https://doi.org/10.1016/j.actbio.2010.01.025

Zhang, J., Zhao, B., Pan, Z., Gu, M., & Punnoose, A. (2015). Synthesis of ZnO nanoparticles with controlled shapes, sizes, aggregations, and surface complex compounds for tuning or switching the photoluminescence. *Crystal Growth & Design*, *15*(7), 3144-3149. https://doi.org/10.1021/cg5017017

Zhang, Y., Jia, H., Wang, R., Chen, C., Luo, X., Yu, D., & Lee, C. (2003). Low-temperature growth and Raman scattering study of vertically aligned ZnO nanowires on Si substrate. *Applied physics letters*, *83*(22), 4631-4633. https://doi.org/10.1063/1.1630849

Zhang, Z. Y., Xu, Y. D., Ma, Y. Y., Qiu, L. L., Wang, Y., Kong, J. L., & Xiong, H. M. (2013). Biodegradable ZnO@ polymer core–shell nanocarriers: pH-triggered release of doxorubicin in vitro. *Angewandte chemie*, *125*(15), 4221-4225. https://doi.org/10.1002/anie.201300431

Zhou, J., Xu, N. S., & Wang, Z. L. (2006). Dissolving behavior and stability of ZnO wires in biofluids: a study on biodegradability and biocompatibility of ZnO nanostructures. *Advanced Materials*, *18*(18), 2432-2435. https://doi.org/10.1002/adma.200600200

Zhou, K., Zhu, Y., Yang, X., Jiang, X., & Li, C. (2011). Preparation of graphene–TiO 2 composites with enhanced photocatalytic activity. *New Journal of Chemistry*, *35*(2), 353-359. https://doi.org/10.1039/C0NJ00623H

Zhu, H., Clark, S. M., Benson, S. C., Rye, H. S., Glazer, A. N., & Mathies, R. A. (1994). High-sensitivity capillary electrophoresis of double-stranded DNA fragments using monomeric and dimeric fluorescent intercalating dyes. *Analytical chemistry*, *66*(13), 1941-1948. https://doi.org/10.1021/ac00085a004

doi: 10.31674/book.2024ecc.005

Oxidation of Nitrite by an $\{Mn_4O_6\}^{4+}$ Core in Aqueous Media: Proton Coupled Electron Transfer

Suranjana Chatterjee

Department of Chemistry, Ananda Mohan College, Kolkata, West Bengal, India

Corresponding Author's Email: ranjanasur@yahoo.com

Abstract

Nitrous acid and its conjugate base nitrite are quantitatively oxidised to N(V) species in aqueous acidic (pH 2.0-6.0) media by a tetranuclear higher valent manganese complex $[Mn_4(\mu\text{-}O)_6(bipy)_6]^{4+}$(1, bipy = 2,2′-bipyridine), and its conjugate acid $[Mn_4(\mu\text{-}O)_5(\mu\text{-}OH)(bipy)_6]^{5+}$ ($1H^+$). As usual, protonated metal oxidant $1H^+$ reacts faster than 1, but an unusual observation of these reactions is the kinetic predominancy of HNO_2 over its conjugate base NO_2^-. Title complex 1 is stable in aqueous media over a long pH region and shows no ligand dissociative equilibria in the presence or absence of reducing agent. The reaction shows a remarkable kinetic isotope effect by increasing the reaction rate in D_2O media. A hydrogen atom transfer (HAT) mechanism (1e, $1H^+$; electroprotic) is appropriate to explain the isotope effect.

Keywords: *Isotope Effect; Kinetics; Manganese; Nitrite*

Introduction

Molecular dioxygen is generated in living systems by photosynthesis with the help of the oxygen evolving complex (OEC), which contains four manganese atoms at the reaction centre in close proximity to one another (Kirby *et al*., 1981; McEvoy & Brudvig, 2004; Yamaguchi *et al*., 2022; Burnap *et al*., 2022). The Mn aggregate is capable of cycling between five distinct oxidation levels, labeled as S_0 – S_4, as was demonstrated in the pioneering work of Kok, Forbush and McGloin (1970), which involves metal oxidation states II–IV (Dekker *et al*., 1984).

The site would contain two di-μ-oxo units linked by a μ-oxo-bis-μ-carboxylate bridge. The chosen oxidant $[Mn_4(\mu\text{-}O)_6(bipy)_6]^{4+}$ (**1**, Figure 1, bipy = 2,2′-bipyridine) of this study is topologically equivalent to Klein's proposal for OEC. Its one-electron reduced species, mixed-valent $Mn^{IV}_3Mn^{III}$ form, resembles the EPR spectroscopic model for the S_2 state (Philouze *et al*., 1994).

The N(III) atoms in the form of HNO_2 or NO_2^- have a varied redox role (Wilmarth *et al*., 1983; Rhodes, Barley & Meyer, 1991; Wu *et al*., 2020) in both oxidation and reduction purposes. The overall reactivity of N(III) in aqueous media not only results from NO_2^- and HNO_2, but also depends on the acidity of the aqueous solution and the total concentration of reagents used. NO^+ or even different redox species like NO, NO_2 and

N_2O_3 with notable acid-base features have a significant contribution to the reactivity. The study of aqueous N(III) chemistry thus remains a fertile endeavor. In view of the above discussion, it is believed that the redox reactivity of the title oxidant with N(III) will be informative in understanding the electron transfer mechanism in photosystem II.

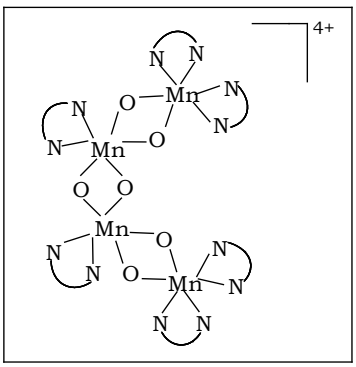

Figure 1: Schematic drawing of $[Mn_4(\mu\text{-}O)_6(bipy)_6]^{4+}$. $\overset{\frown}{N\quad N}$ is 2,2′-bipyridine
(Source: Das & Mukhopadhyay, 2007b)

Experimental

Materials

Pure crystals of title salt hydrate $[Mn_4(\mu\text{-}O)_6(bipy)_6](ClO_4)_4.2H_2O$ (**1**) were prepared according to the method described (Philouze *et al*., 1994). The tetrameric compound 1 used in all the experiments, thus seems to be almost pure monohydrated species. The solution of complex in water is stable in acidic environment up to pH 6.0. Sodium nitrite solution was prepared by dissolving recrystallised $NaNO_2$ in a hot ethanol-water mixture. The stock nitrite solution was standardised against $KMnO_4$. All used solutions were found to be unchanged for at least 24 hours at 10 °C and in a lower pH range up to pH 6.0.

$NaNO_3$ solution was standardised with a Dowex cation-exchange resin (in acid form), and the effluent acid was titrated with a standard base solution of NaOH with phenolphthalein indicator. 2,2′-bipyridine (G. R., E. Merck) solid was used as received without any further purification. D_2O (99.9 atom % D, Sigma) was used for the measurements of kinetic isotope effects. DNO_3 (99+ atom % D) was also from Sigma. Sulfanilic acid and a-naphthylamine were of E. Merck, G. R. grade. All other chemicals were of reagent grade. Throughout the experiments, doubly distilled deionized water was used to prepare all the solutions.

Equilibrium measurements

pH-metric titrations were performed to evaluate dissociation constants (K_a) of the acid HNO_2 in 95% D_2O media using a Metrohm 736-GP-Titrino autotitrator at I = 1.0 M ($NaNO_3$) at 25 °C. Similar methods were tried for the title complex over a long pH scale 2.0 – 8.0 to check oxo-bridge basicity.

Stoichiometric measurements

Overall stoichiometry of both reactions was determined in both kinetic ([reagent] >> [complex]) and non-kinetic conditions ([complex] > [reagent]). Unused amount of N(III) in the final solution state were colourimetrically determined, when 0.5 – 1.50 mM of 1 was allowed to react with 2.5 – 7.5 mM of reducing agent. After appropriate dilution, the remaining reaction mixtures were tested with sulfanilic acid and a-naphthylamine when a characteristic red dye was measured at 520 nm ($\varepsilon = 4.0 \times 10^4\ M^{-1}\ cm^{-1}$). The only reaction product, nitrate (NO_3^-) was detected by following the same procedure described above, but only Zn dust was added before the coupling reaction. Quantitative generation of NO_3^- was detected by the above method from the solutions having complex N(III) ratios between 1 : 2 to 1 : 4. The Mn complex, Mn^{II}, bipy and ClO_4^- did not interfere in this colorimetric study. Quantitative generation of bivalent manganese as the ultimate end product of the reduction could be estimated by complexometric method. In kinetic condition, an aliquot of the final product solutions was adjusted at pH 10 by ammonia-ammonium chloride buffer and estimated with standard EDTA using EBT indicator. At the end point, colour of the solution sharply changed from red to blue. It was also verified that other chemical species present in the product solution did not interfere in the complexometric titration. In non-kinetic situation, the tetrameric complex (0.10 – 0.50 mM) solution was allowed to react with the reagent concentration, which was less than the stoichiometric amount. After a definite interval of time, the absorbance of equilibrated solutions was measured at 420 nm ($\varepsilon = 7.5 \times 10^3\ M^{-1}\ cm^{-1}$) to evaluate the amount of Mn_4 complex left unreacted.

Physical measurements and kinetics

All physical parameters, like absorbances and spectra, of the described reaction were recorded with a Shimadzu (1601 PC) spectrophotometer using 1.00 cm quartz cells. The kinetics was monitored *in situ* with the instrument in “kinetic mode” at 420 nm in an electrically controlled thermostated 25.0(± 0.1) °C cell housing (CPS –240 A).

Except the Mn oxidant all other reaction partners are transparent at that (420 nm) wavelength. The ionic strength was normally maintained at 1.0 M with $NaNO_3$. Ligand bipyridine used in excess concentration (1 – 80 mM) over the complex, (C_{bipy} = [$(Hbipy)^+$] + [bipy]) acted as a good buffer. The pH value is increased by 0.4 units in D_2O media relative to the measured pH in water medium. In all the kinetic measurements, reducing agents were maintained in excess of the complex concentration.

Results and Discussion

Equilibrium measurements

The pK_a values of the title acid N(III) in 95% deuterated media and in aqueous media are found to be 3.80 ± 0.10 (Das & Mukhopadhyay, 2005) and 3.00, respectively. at 25.0

^{o}C and at I = 1.0 M ($NaNO_3$). Several attempts have been made to evaluate any ionisation constant for the oxidant in the working pH region (2.0–6.0) but have not resulted in any value.

Stoichiometric measurements

Stoichiometric determinations result in the average value $\triangle[Mn^{IV}_4]/\triangle[T_R]= 0.25 \pm 0.02$ where T_R = [N(III)] = [HNO_2] + [NO_3^-] i.e., analytical concentration of the reducing species. EDTA titration revealed that Mn^{II} is the final state of complex 1 in almost quantitative way. The ultimate reduced form of the tetravalent-tetramer is divalent manganese, which exists as a Mn^{II}- bipy complex at working condition. Existence of this complex is confirmed by the superposition of the optical spectra of ultimate product solutions and the mixture of manganese nitrate and 2,2'-bipyridine under the same conditions. Equation (1) is able to describe all the above findings.

$$[Mn_4O_6(bipy)_6]^{4+} + 4NO_2^- + 4H^+ \longrightarrow 4Mn^{2+} + 4NO_3^- + 6bipy + 2H_2O \quad (1)$$

Kinetics

The findings of decay in absorbance vs. time of the above kinetics are graphically posted and it is fitted finely in a standard first-order decay curve for at least four half-lives. The coloured oxidant is the only photoactive species in the working wavelength region (380 – 500 nm) where it absorbs sufficiently and the reaction rate constants do not vary with the wavelength. Each k_0 value measured is the average of at least three independent determinations where the coefficients of variation (CV) were within a maximum of 3%. The decay in absorbances at 420 nm is recorded, and $\log_{10}$(absorbance) *versus* time plots are excellent straight lines ($r \geq 0.98$) and slope of these lines directly produces k_0, the first order rate constants. Observed rate constants increase parallelly with the acidity of the reaction condition. The rate of the reactions remained unchanged when the amount of externally added bipy was varied in the range of 3–80 mM. Constancy in the k_0 values with the variation of bipy concentration ruled out the chance of any ligand releasing equilibrium in the parent complex solution. The rate of the reactions exhibits first-order dependencies on total reductant agent concentration over the working pH region and no T_R independent term is collected in the overall reaction. The observed rate constants were also found to be identical when complex concentrations were varied (0.05 – 0.2 mM) or in the presence or absence of ambient light in the reaction media. The reaction rate increases with decrease in ionic strength in the higher pH region and the reaction rates remain unaltered with the variation of ionic strength in the lower pH range. All these effects of ionic strength variation demonstrate the reaction between oppositely charged species and between charged and neutral species, respectively, at different pH regions.

Table 1: *Some representatives first-order rate constants*

pH	T_R, M	C_{bipy}, mM	$10^4 k_0$, s^{-1}
2.50	0.05	3.0	491 (500)
2.82	0.05	3.0	197 (202)
3.14	0.05	3.0	74.0 (76.6)
3.78	0.05	3.0	11.2 (10.4)
4.18	0.05	3.0	3.44 (3.34)
4.75	0.05	3.0	0.74 (0.78)
5.15	0.05	3.0	0.28 (0.30)
5.56	0.05	3.0	0.11 (0.11)
4.69	0.025	3.0	0.43 (0.45)
4.69	0.075	3.0	1.39 (1.35)
4.67	0.01	3.0	1.81 (1.89)
4.15	0.05	20	3.66 (3.62)
4.13	0.05	50	3.81 (3.82)
4.13	0.05	80	4.03 (3.82)
3.22	0.05	20	57.8 (59.6)
3.24	0.05	50	58.9 (56.0)
3.23	0.05	80	59.2 (57.8)
4.71	0.05	3.0	1.06[a]
4.70	0.05	3.0	1.39[b]
2.51	0.05	3.0	496[a]
2.53	0.05	3.0	499[b]

[a]I = 0.5 M ($NaNO_3$). [b]I = 0.1 M ($NaNO_3$)

Source: Das & Mukhopadhyay,2007b

The oxidation of nitrite by the title complex (0.10 mM) at T = 25.0 ^oC, I = 1.0 M ($NaNO_3$). Values within the parenthesis are calculated from equation (9) using the rate constants reported in Table 2.

The observed pH variation of the aforesaid redox can be explained and justified by the following reaction scheme, where simultaneously two protic equilibria equation (2) and equation (3) are considered. Here RH represents the protonated reductant, HNO_2 and R^- stands for the corresponding deprotonated species, i.e., NO_2^-.

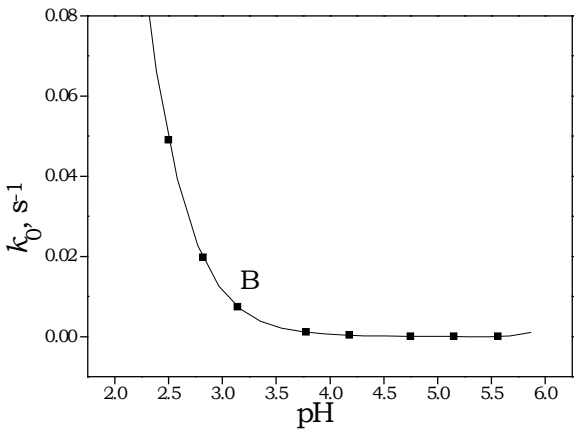

Figure 2: Plot of k_0 versus [H$^+$]. [complex]=0.10 mM, =25.0 °C, I=1.0 M ($NaNO_3$), C_{bipy}=3.0 *mM*
(Source: Das & Mukhopadhyay, 2007b)

$$RH \overset{K_a}{\rightleftharpoons} R^- + H^+ \quad (2)$$

$$\mathbf{1} + H^+ \overset{K_1}{\rightleftharpoons} \mathbf{1}H^+ \quad (3)$$

$$\mathbf{1}H^+ + RH \xrightarrow{k_1} \text{Products} \quad (4)$$

$$\mathbf{1}H^+ + R^- \xrightarrow{k_2} \text{Products} \quad (5)$$

$$\mathbf{1} + RH \xrightarrow{k_3} \text{Products} \quad (6)$$

$$\mathbf{1} + R^- \xrightarrow{k_4} \text{Products} \quad (7)$$

Scheme 1

The scheme 1 leads to the rate law equation (8).

$$k_0(1 + K_1[H^+])(K_a + [H^+])/T_R = k_1K_1[H^+]^2 + (k_2K_1K_a + k_3)[H^+] + k_4K_a \quad (8)$$

K_1 is the protonation constant of complex 1. The protonation occurs at the oxo-bridge of the oxidant. Several attempts have been made to evaluate the protonation constant of the title oxidant in the working pH range. Also, no pK_a value was obtained from the pH-meric titration of the complex soluton, indicating very weak basic nature of the oxo-bridges in water solution. Available literature reports on the study of numerous multicore higher-valent Mn complexes (Thorp *et al*., 1989) suggest the very weak basic nature of the oxo-bridges in an aqueous medium. Hence, from all the above information, it may be assumed that in this system, $K_1[H^+] << 1$. The maximum concentration of H$^+$ used is of the order of 10^{-2}. Therefore, $(K_1)_{max}10^{-2} << 1$, i.e., $(K_1)_{max} << 10^2$, so $(K_1)_{max} \leq 10$, i.e.,

the upper limit of K_1 is nearly at 10. Now, applying the assumption $K_1[H^+] << 1$, the equation (8) is simplified and takes the form described in equation (9).

$$k_0(K_a + [H^+])/T_R = k_1K_1[H^+]^2 + (k_2K_1K_a + k_3)[H^+] + k_4K_a \qquad (9)$$

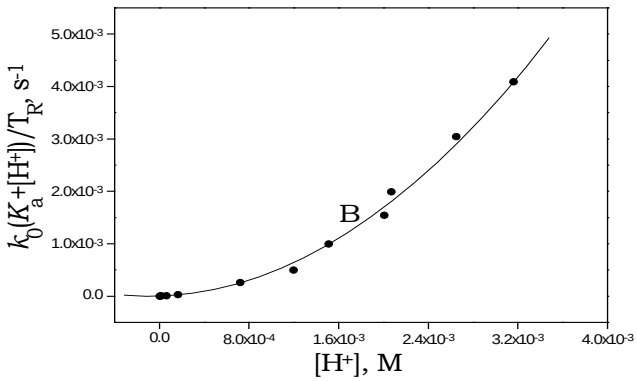

Figure 3: Plot of LHS of equation (9) versus $[H^+]$. [complex] = 0.10 mM, T = 25.0 °C, I = 1.0 M ($NaNO_3$), C_{bipy} = 3.0 mM *(Source: Das & Mukhopadhyay, 2007b)*

The left-hand side of equation (9) plotted against $[H^+]$, a well fitted polynomial curve obtain for the redox (Figure 3, $r > 0.98$), whence the rate parameters k_1K_1, ($k_2K_1K_a + k_3$) and k_4 (Table 2) were calculated. All these rate constants, if reused they reproduced experimentally observed k_0 values quite satisfactorily (within 7%). The k_0 values obtained from D_2O media also fit well with Scheme 1 and the rate parameters are determined in the same way, are listed in Table 2.

Table 2: *Rate constants for the reduction of 1 by nitrite at T = 25.0 °C, I = 1.0 M ($NaNO_3$)*

Reaction Path	k_1K_1 ($M^{-2}s^{-1}$)	($k_2K_1K_a + k_3$) ($M^{-1}s^{-1}$)	k_4 ($M^{-1}s^{-1}$)
H_2O medium	390 ± 20	$(8.2 \pm 0.5) \times 10^{-2}$	0
95% D_2O medium	760 ± 45	$(5.0 \pm 0.3) \times 10^{-2}$	0

(Source: Das & Mukhopadhyay, 2007b)

From Table 2, It can be noted that the value of k_4 path (**1**+R^- → Products) in both water and in D_2O media are statistically zero indicating non-existence of k_4 path. Eliminating k_4 term from equation (9), the polynomial changes to a simplified linear equation (10).

$$k_0(K_a + [H^+])/T_R = k_1K_1[H^+]^2 + (k_2K_1K_a + k_3)[H^+]$$

Dividing both side by $[H^+]$,

$$k_0(K_a + [H^+])/(T_R[H^+]) = k_1K_1[H^+] + (k_2K_1K_a + k_3) \qquad (10)$$

Thus, a plot of LHS of equation (10) *versus* $[H^+]$ (Figure 4) was found to be a straight line ($r > 0.98$) and slope $k_1K_1 = 384 \pm 15\ M^{-2}s^{-1}$ and intercept = $(8.0 \pm 0.3) \times 10^{-2}\ M^{-1}s^{-1}$.

The values of k_1K_1 and ($k_2K_1K_a + k_3$) obtained in the above-described manner are in close valuation (within 5%) with the reported values in Table 2, again confirming the absence of k_4 path in oxidation reaction.

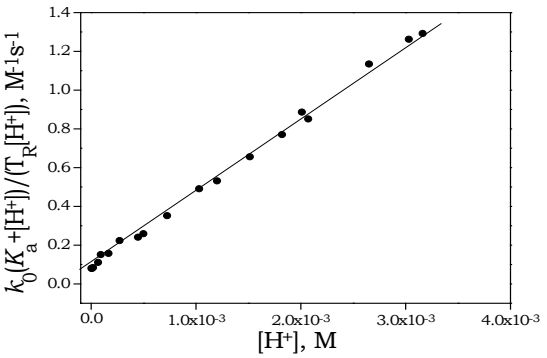

Figure 4: Plot of $k_0(K_a + [H^+])/(T_R[H^+])$ versus $[H^+]$. [Mn complex] = 0.10 mM, T = 25.0 °C, I = 1.0 M ($NaNO_3$) *(Source: Das & Mukhopadhyay, 2007b)*

An alternative to Scheme 1 that also explains the experimental findings is shown in Scheme 2 comprising only HNO_2 as reactive reductant.

$$\mathbf{1} + HNO_2 \xrightarrow{k'_2} \text{Products} \quad (11)$$

$$\mathbf{1}H^+ + HNO_2 \xrightarrow{k'_1} \text{Products} \quad (12)$$

Scheme 2

The calculated rate law for Scheme 2 is equation (13)

$$k_0/[HNO_2] = k'_1K_1[H^+] + k'_2 \quad (13)$$

Using the same procedure equation (13) is solved and obtain a good straight line with $k'_1K_1 = 390\ M^{-2}\ s^{-1}$ and $k'_2 = 0.082\ M^{-1}\ s^{-1}$. Value of the k'_1K_1 (reaction of $\mathbf{1}H^+$ with HNO_2) and k'_2 (reaction between **1** and HNO_2) path of Scheme 2 match well with the values reported for k_1K_1 and k_3 (taking k_2 path zero) in Scheme 1. Thus, this alternate scheme (Scheme 2) rules out any reactivity of nitrite anion with the tetrameric oxidant and with the protonated form of it. Therefore, the N(III) redox process is completely driven by the reactive protonated reductant HNO_2.

The alternative scheme (Scheme 2) of Scheme 1 for nitrite oxidation cannot confirm the non-reactivity of nitrite anion specially the non-existence of k_2 path i.e., the reaction between protonated metal oxidant ($\mathbf{1}H^+$) and the nitrite anion as the k_4 path which is the reaction between metal oxidant **1** and the NO_2^- is absent in scheme 1 also. Results of ionic strength variation at pH 4.7 (where $[NO_2^-] >> [HNO_2]$) indicated that reactions between oppositely charged ions as the first-order rate constants were decreased with

increasing ionic strength. Therefore, a significant role of the k_2 path may thus be expected when the k_4 path is totally absent in the kinetics. Protonated metal oxidants are kinetically superior to their deprotonated analogue, and hence **1**H^+ would oxidise NO_2^-. Kinetic differentiation of the k_2 and k_3 path is impossible due to proton-ambiguity of both the terms. It should be recalled that the k_1 path is effective towards the observed rate at pH $\leq$ 5.0. At lower pH, around pH 2.5 the kinetic superiority of acid form over its anionic conjugate form is reflected when media ionic strength is varied. The measured rate constants remain unaffected due to the change in ionic strength value of reactions indicating reaction between charged (**1** and **1**H^+) and neutral species (HNO_2).

From Table 2, It can be suggested that the maximum value of k_3 path (reaction between **1** and RH) would be 8.2×10^{-2} M^{-1} s^{-1} for N(III) oxidation.

Initially assumption was that $K_1[H^+]$ is much lower than **1**, and it draws an upper limit value for the K_1 of nearly 10. Taking the consideration that diffusion-controlled rate limit is 10^{11} M^{-1} s^{-1}, the assumed lower limit value of K_1 as found from the k_1K_1 value listed in Table 2 is around 10^{-9}.

Mechanism

The total eight electron transfers in this described redox are not in a single step but are the sum of several electronic transactions, but no immediate spectral changes were observed in working conditions. Moreover, in the working pH region, the linear dependence of k_0 on reagent concentration suggests a weak adduct formation, between the tetrameric Mn complex and the reducing agents. The electrochemistry of $[Mn_4(\mu\text{-}O)_6(bipy)_6]^{4+}$ has been extensively studied by Dunand-Sauthier *et al.* (1997, 1998, 1999). They prepared the title complex both electrochemically and chemically and also studied the electrochemical conversion of 1 into dinuclear ($[Mn^{III,IV}{}_2(\mu\text{-}O)_6(bipy)_4]^{3+}$) and mononuclear manganese ($[Mn^{II}(bipy)_3]^{2+}$) systems and *vice versa*. In nitric acid solution at pH = 2 the complex solution was decolourised upon application of 0.05 V *versus* SCE, indicates the final state is Mn^{II}. An overall eight electron reduction takes place. It is difficult to achieve the mono reduced form $[Mn^{IV}{}_3Mn^{III}(\mu\text{-}O)_6(bipy)_6]^{3+}$ by standard chemical reduction. The monoreduced form was generated by cryogenic radiolytic reduction of **1** (Blondin *et al.,* 1997) the very high reactivity of these monoreduced form was documented. This monoreduced one is not at all stable, even at low temperature (190 K). From the above discussion, it can be concluded that the tetrameric complex is not a powerful oxidant. The overall process of reducing the tetramer Mn^{IV} to Mn^{II} is a smooth transition, but initially, monoelectronic transfer to generate the mixed valent tetramer is energetically unfavourable process. In the overall reaction (equations 9 – 12), it is assumed initial mono electronic transfer is the rate limiting step, that produces the reactive intermediate $[Mn^{IV}{}_3Mn^{III}(m\text{-}O)_6(bipy)_6]^{3+}$, which is quickly reduced to final product form in the presence of excess reducing material or the produced radicals at the

rds. No polymerisation was observed when the reactions were carried out in a 6% v/v acrylonitrile solution, but this cannot prove the chance of the formation of radical as the radicals may react very fast with the mono-reduced Mn tetramer to initiate polymerisation. Basic nature of oxo-bridges of **1** or **1**H^+ tetramer highly increases due to one-electron reduction, which causes immediate grabbing of a proton from the reaction medium, which removes thermodynamic or kinetic barriers of reduction to the next level. The mono reduced form would have much more basic oxo-bridges, which could remove thermodynamic or kinetic barriers and facilitate further reduction (Baldwin & Pecoraro, 1996; Vrettos, Limburg & Brudvig, 2001) and it is one of the key points in the redox process of the Kok cycle in PS II (Renger, 2004).

In general, weak acids in H_2O become much weaker in D_2O, (Wiberg, 1955; Ghosh *et al*., 2002) and it was observed that pK_a's are considerably increased in D_2O for several reducing acids. Glyoxylic (Das, Bhattacharyya & Mukhopadhyay, 2006), pyruvic (Das, Bhattacharyya & Mukhopadhyay, 2006), nitrous (Das & Mukhopadhyay, 2007a) and hydroxylammonioum cations Therefore, for the tetrameric complex, the protonation constant (K_1) should increase in D_2O i.e., higher concentration of **1**H^+ is expected to be available in D_2O media compared to that in aqueous media. A structured network of hydrogen bonding in OEC is revealed during the molecular mechanics computation of the structure of the OEC cluster (Jeans *et al*., 2002; Russell & Vinyard, 2024; Matta, 2021), thereby providing an insight into the movement of proton and water in the site.

Conclusion

The reflection of the increase in K_1 value in D_2O media shows in the increment in k_1K_1 value, which effectively ruled over the decreased value of k_1 value (electroprotic mechanism). The reaction may be attributed to a secondary isotope effect where, during the substitution of isotopic (H *versus* D) no oxygen bonds to H/D are made or broken during the rate-limiting step and indicates that the isotopic atom is bonded more strongly through the H-bond in the transition state. This experimental fact again supports the existence of a postulated hydrogen-bonding network in the OEC. K_a value in D_2O media decreases compared to that in H_2O, which causes the lowering of the composite ($k_2K_1K_a$ + k_3) value in deuterated media. The contribution of the reaction path of NO_2^- with **1** in Scheme 1 towards the overall rate is found to be very small. Even, $(k_2K_1)_{max}$ value is found to be much lower than k_1K_1, therefore is expected a major contribution of k_3 path to evaluated composite term. Thus, in the described reduction process of tetramer (for both **1** and **1**H^+) the acidic format HNO_2 is more reactive than the conjugated basic form NO_2^-. The mechanistic pathways revealed the initial electron transaction by producing the nitrite radical ($NO_2^{\cdot}$) along with the protonated oxo-bridge in the mixed-valent tetramer in conjugation with a Hydrogen atom transfer (HAT) in the reducing agent. This mechanistic approach justifies the kinetic superiority of HNO_2 over its anion. In the protonated form of the tetramer **1**H+, a relatively stronger hydrogen bonding framework

forms between oxo-bridges and oxygens and hydrogens of the reducing species, which helps in the propagation of hydrogen or hydrogen ion and eventually this makes the species **1**H^+ kinetically superior.

Acknowledgment

The author thanks the higher authorities of Ananda Mohan College, Kolkata, India, for their continuous support.

References

Baldwin, M. J., & Pecoraro, V. L. (1996). Energetics of proton-coupled electron transfer in high-valent $Mn_2(\mu\text{-}O)_2$ systems: models for water oxidation by the oxygen-evolving complex of Photosystem II. *Journal of the American Chemical Society*, *118*(45), 11325-11326. https://doi.org/10.1021/ja9626906

Blondin, G., Davydov, R., Philouze, C., Charlot, M. F., Åkermark, B., Girerd, J. J., & Boussac, A. (1997). Electron paramagnetic resonance study of the S= ½ ground state of a radiolysis-generated manganese (III)–trimanganese (IV) form of $[Mn^{IV}_4 O_6 (bipy)_6]^{4+}$(bipy= 2, 2′-bipyridine). Comparison with the photosynthetic Oxygen Evolving Complex. *Journal of the Chemical Society, Dalton Transactions*, (21), 4069-4074. https://doi.org/10.1039/A703381H

Das, A., & Mukhopadhyay, S. (2005). Kinetic and Mechanistic Studies on the Oxidation of Nitrogen (III)(HNO_2/NO_2^-) by the Tris (biguanide) manganese (IV) Ion in Aqueous Acidic Media. *Helvetica Chimica Acta*, *88*(9), 2561-2572. https://doi.org/10.1002/hlca.200590195

Das, S., & Mukhopadhyay, S. (2007a). Mechanistic studies on oxidation of nitrite by a $\{Mn_3O_4\}^{4+}$ core in aqueous acidic media. *Dalton Transactions*, (22), 2321-2327. https://doi.org/10.1039/B702740K

Das, S., & Mukhopadhyay, S. (2007b). Oxidation of N^{III} and N^{-I} by an $\{Mn_4O_6\}^{4+}$ Core in Aqueous Media: Proton-Coupled Electron Transfer. https://doi.org/10.1002/ejic.200700363

Das, S., Bhattacharyya, J., & Mukhopadhyay, S. (2006). Mechanistic Studies on the Oxidation of Glyoxylic and Pyruvic Acid by a $[Mn_4O_6]^{4+}$ Core in Aqueous Media: Kinetics of Oxo-Bridge Protonation. *Helvetica Chimica Acta*, *89*(9), 1947-1958. https://doi.org/10.1002/hlca.200690186

Dekker, J. P., Van Gorkom, H. J., Wensink, J., & Ouwehand, L. (1984). Absorbance difference spectra of the successive redox states of the oxygen-evolving apparatus of photosynthesis. *Biochimica et Biophysica Acta (BBA)-Bioenergetics*, *767*(1), 1-9. https://doi.org/10.1016/0005-2728(84)90073-2

Dunand-Sauthier, M. N. C., Deronzier, A., & Piron, A. (1999). Electrochemical behaviour of $[Mn_2^{III,IV}O_2 (phen)_4]^{3+}$ complex in aqueous phen+ phenH+ buffer; phen= 1, 10-phenanthroline. *Journal of Electroanalytical Chemistry*, *463*(1), 119-122. https://doi.org/10.1016/S0022-0728(98)00429-X

Dunand-Sauthier, M. N. C., Deronzier, A., Piron, A., Pradon, X., & Ménage, S. (1998). New chemical and electrochemical synthesis of the $[Mn_4^{IV}O_6(bpy)_6]^{4+}$ Cluster. Electrochemical interconversion with corresponding Bi-and mononuclear complexes. *Journal of the American Chemical Society*, *120*(22), 5373-5380. https://doi.org/10.1021/ja974246o

Dunand-Sauthier, M. N. C., Deronzier, A., Pradon, X., Ménage, S., & Philouze, C. (1997). Electrochemical interconversion of mono-, bi-, and tetranuclear (bipyridyl) manganese

complexes in buffered aqueous solution. *Journal of the American Chemical Society*, *119*(13), 3173-3174. https://doi.org/10.1021/ja964102u

Ghosh, D., Shukla, A. D., Banerjee, R., & Das, A. (2002). Kinetics of oxidation of ascorbic acid and 1, 4-dihydroxybenzene by semiquinone radical bound to ruthenium (ii). *Journal of the Chemical Society, Dalton Transactions*, (6), 1220-1225. https://doi.org/10.1039/B104585G

Jeans, C., Schilstra, M. J., Ray, N., Husain, S., Minagawa, J., Nugent, J. H. A., & Klug, D. R. (2002). Replacement of tyrosine D with phenylalanine affects the normal proton transfer pathways for the reduction of $P680^+$ in oxygen-evolving photosystem II particles from Chlamydomonas. *Biochemistry*, *41*(52), 15754-15761. https://doi.org/10.1021/bi020558e

Kirby, J. A., Robertson, A. S., Smith, J. P., Thompson, A. C., Cooper, S. R., & Klein, M. P. (1981). State of manganese in the photosynthetic apparatus. 1. Extended x-ray absorption fine structure studies on chloroplasts and di-. mu.-oxo-bridged dimanganese model compounds. *Journal of the American Chemical Society*, *103*(18), 5529-5537. https://doi.org/10.1021/ja00408a042

Kok, B., Forbush, B., & McGloin, M. (1970). Cooperation of charges in photosynthetic O_2 evolution–I. A linear four step mechanism. *Photochemistry and Photobiology*, *11*(6), 457-475. https://doi.org/10.1111/j.1751-1097.1970.tb06017.x

Matta, D. K. (2021). *Role of Protonation State Changes and Hydrogen Bonding Around the Oxygen Evolving Complex of Photosystem II* (Doctoral dissertation, City University of New York).

McEvoy, J. P., & Brudvig, G. W. (2004). Structure-based mechanism of photosynthetic water oxidation. *Physical Chemistry Chemical Physics*, *6*(20), 4754-4763. https://doi.org/10.1039/B407500E

Oliver, N., Avramov, A. P., Nürnberg, D. J., Dau, H., & Burnap, R. L. (2022). From manganese oxidation to water oxidation: assembly and evolution of the water-splitting complex in photosystem II. *Photosynthesis Research*, *152*(2), 107-133. https://doi.org/10.1007/s11120-022-00912-z

Philouze, C., Blondin, G., Girerd, J. J., Guilhem, J., Pascard, C., & Lexa, D. (1994). Aqueous chemistry of high-valent manganese. Structure, magnetic, and redox properties of a new type of Mn-Oxo cluster,$[Mn_4^{IV}O4\ (bpy)_6]^{4+}$: relevance to the oxygen evolving center in plants. *Journal of the American Chemical Society*, *116*(19), 8557-8565. https://doi.org/10.1021/ja00098a016

Renger, G. (2004). Coupling of electron and proton transfer in oxidative water cleavage in photosynthesis. *Biochimica et Biophysica Acta (BBA)-Bioenergetics*, *1655*, 195-204. https://doi.org/10.1016/j.bbabio.2003.07.007

Rhodes, M. R., Barley, M. H., & Meyer, T. J. (1991). Electrocatalytic reduction of nitrite ion by edta complexes of iron (II) and ruthenium (II). *Inorganic Chemistry*, *30*(4), 629-635. https://doi.org/10.1021/ic00004a008

Russell, B. P., & Vinyard, D. J. (2024). Conformational changes in a Photosystem II hydrogen bond network stabilize the oxygen-evolving complex. *Biochimica et Biophysica Acta (BBA)-Bioenergetics*, *1865*(1), 149020. https://doi.org/10.1016/j.bbabio.2023.149020

Thorp, H. H., Sarneski, J. E., Brudvig, G. W., & Crabtree, R. H. (1989). Proton-coupled electron transfer in manganese complex $[(bpy)_2Mn(O)_2Mn(bpy)_2]^{3+}$. *Journal of the American Chemical Society*, *111*(26), 9249-9250. https://doi.org/10.1021/ja00208a029

Vrettos, J. S., Limburg, J., & Brudvig, G. W. (2001). Mechanism of photosynthetic water oxidation: combining biophysical studies of photosystem II with inorganic model chemistry. *Biochimica et*

Biophysica Acta (BBA)-Bioenergetics, *1503*(1-2), 229-245. https://doi.org/10.1016/S0005-2728(00)00214-0

Wiberg, K. B. (1955). The deuterium isotope effect. *Chemical Reviews*, *55*(4), 713-743. https://doi.org/10.1021/cr50004a004

Wilmarth, W. K., Stanbury, D. M., Byrd, J. E., Po, H. N., & Chua, C. P. (1983). Electron-transfer reactions involving simple free radicals. *Coordination Chemistry Reviews*, *51*(2), 155-179. https://doi.org/10.1016/0010-8545(83)85010-3

Wu, Y., Bu, L., Duan, X., Zhu, S., Kong, M., Zhu, N., & Zhou, S. (2020). Mini review on the roles of nitrate/nitrite in advanced oxidation processes: Radicals transformation and products formation. *Journal of Cleaner Production*, *273*, 123065. https://doi.org/10.1016/j.jclepro.2020.123065

Yamaguchi, K., Shoji, M., Isobe, H., Kawakami, T., Miyagawa, K., Suga, M., ... & Shen, J. R. (2022). Geometric, electronic and spin structures of the $CaMn_4O_5$ catalyst for water oxidation in oxygen-evolving photosystem II. Interplay between experiments and theoretical computations. *Coordination Chemistry Reviews*, *471*, 214742. https://doi.org/10.1016/j.ccr.2022.214742

doi: 10.31674/book.2024ecc.006

Anticancer Activities of 1,3-Diaryltriazene Based Compounds: An Overview

Chhandasi Guha Roy Sarkar

Department of Chemistry, Hooghly Mohsin College, Chinsurah, Hooghly, West Bengal, India

Corresponding Author's Email: chhandasi22@gmail.com

Abstract

The present article discusses the anticancer and antitumor properties of aliphatic and aromatic triazene compounds and their derivatives. The triazene molecule is an essential tool in organic synthesis, acting as the starting material or the reactive intermediate in various organic transformations. In addition, it possesses interesting biological properties. The most explored biological application of the triazene moiety is its cytotoxic effect. The present review highlights the antineoplastic activities of the triazene molecule *in vitro* and *in vivo,* as well as its different derivatives and complexes.

Keywords: *Anticancer Properties;1,3-Diaryltriazene; Metal Complexes*

Introduction

The 1,3-diaryltriazene ligands are azo compounds characterized by a diazoamino group (N=N–NH) consisting of three consecutive nitrogen centers (Kölmel, Jung & Braese, 2013). The synthesis of the first triazene ligand can be traced back to 1859, when the ligand 1,3-bisphenyltriazene was described in connection with diazonium salt preparation (Griess, 1859). The ligands are isoelectronic with amidinates, although the central nitrogen imparts greater acidity to the N-H protons in triazenes. Triazenes and its derivatives consist of a versatile and diverse group of compounds and have received considerable attention in the research arena due to its varied coordination modes (Garzon *et al*., 2015). The ligand usually functions as a bidentate, monoanionic N, N-chelating ligand through dissociation of the acidic N–H proton. It coordinates with the metal center, forming a four-membered chelate ring (Guha Roy*,* Butcher *&* Bhattacharya, 2008). The 1,3-diaryltriazenide anion is a 'short-bite' ligand, having the capacity to act as a bidentate chelating ligand, as stated earlier, along with being a monodentate and a bridging ligand (Nimitsiriwat *et al*., 2007). The ligands are important in natural product preparations, combinatorial chemistry, and biological applications (Canakci *et al*., 2019). The biomedical applications include antibacterial (Abd Halim *et al*., 2023; Cappoen *et al*., 2014) and antifungal properties (Ombaka*,* Muguna *&* Gichumbi, 2012), efficient carbonic anhydrase inhibition (Işık *et al*., 2020; Supuran, 2017), and prolific use in the evolution of numerous anticancer compounds.

The discovery of the antitumor properties of cisplatin heralded a new era of synthetic chemistry in the field of metal-dependent anticancer drugs (Rosenberg, Van Camp & Krigas, 1965). However, cis-platin and other platinum-based drugs possess a lot of undesired effects *viz*., high toxicity and the development of strong resistance to drugs (Heffeter *et al*., 2008). As a result, there is a need to explore newer chemotherapeutic agents. Keeping this in mind, 1,3-diaryltriazenes were selected as the preferred ligand to complex with suitable metals because of its demonstrated ability as antitumor agents. The present review consists of a brief discussion of the anticancer properties of free 1,3-diaryltriazenes and its derivatives, along with some of its complexes.

Discussion

Triazenes as Alkylating agents

Dacarbazine 5-(3,3-dimethyl-1-triazenyl)-imidazole-4-carboxamide (DTIC) (2) is a triazene that is used in the treatment of cancer (Meer *et al*., 1986). It has been sanctioned by the Food and Drug Administration (FDA) for medical use. The synthesis of dacarbazine is presented in Figure 1.

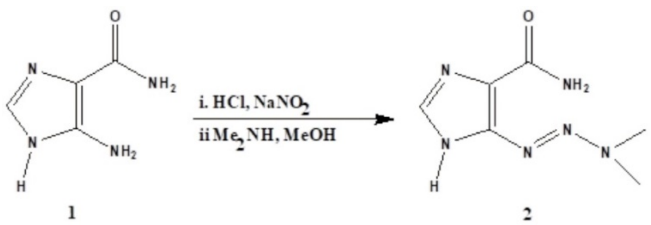

Figure 1: Synthesis of Dacarbazine

On being activated by the hemeprotein enzyme *viz.*, cytochrome P450, dacarbazine undergoes proteolytic decomposition under *in vivo* conditions. This decomposition results in the formation of methyldiazonium ion, which is extremely reactive and effective in the alkylation of DNA (Meer *et al*., 1986). The N^7 position of the guanine base serves as the most common site of DNA alkylation. However, methylguanine adducts formed at the DNA O^6 position are mainly responsible for cytotoxicity and genetic mutation because they can disturb the base pairing, generating an incorrect base pair and causing cell death. Dacarbazine has been one of the most long-established drugs used to treat Hodgkin disease and melanoma (Ogura *et al*., 2010). However, it causes severe side effects in the form of skin toxicity, bone marrow suppression, cardiac and hepatic toxicity, and nausea.

It is worthwhile to note at this point that numerous reports were published prior to the synthesis of dacarbazine, putting forward evidence of the strong antineoplastic activity of 1-phenyl-3,3-dimethyltriazene (3, Figure 2). This resulted in the use of aryl groups

other than those obtained from aniline to produce dimethylaryl triazenes for anticancer study, eventually culminating in the synthesis and use of dacarbazine (Kimball & Haley, 2002).

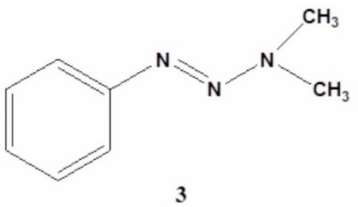

Figure 2: Structure of 1-phenyl-3,3-dimethyltriazene (*Kimball & Haley, 2002*)

Another triazene based antineoplastic compound is diminazene aceturate (Berenil) (4, Figure 3). It forms facile complexes by binding smoothly into the minor groove of AT-rich domains of DNA. Berenil indicates a weak anticancer property against L1210 leukaemia cells (Cimbora-Zovko *et al*., 2011).

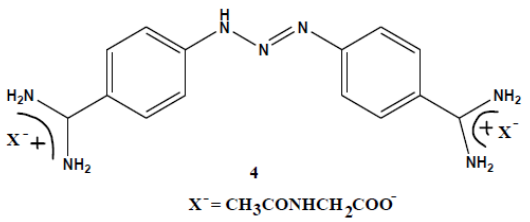

Figure 3: Structure of Berenil

A list of the most prominent molecules exhibiting antineoplastic effects among those discussed in this article is presented in Table 1. The table expresses the cell lines against which the molecules display anticancer activity along with their efficiency in terms of IC_{50} or GI_{50} values. It reveals that the 1,3-diaryltriazene molecules manifest antineoplastic characteristics against a variety of cell lines with satisfactory efficiency.

Table 1: *A List of the Most Prominent Molecules Exhibiting Antineoplastic Effects*

Name of the molecules	Working cell lines	Efficiency
3-acetyl-1,3-bis(2-chloro-4-nitrophenyl)-1-triazene	HeLa	IC_{50} :0.63±0.05 μM
1-(4-nitrophenyl)-3-(3-hydroxyphenyl) triazene	HT29, PC3, HepG2 HL60, HeLa, MCF7, Jurkat, K562	IC_{50} :1.51-8.87 μM
1-(4-nitrophenyl)-3-(2-hydroxyphenyl) triazene	HT29, PC3, HepG2 HL60, HeLa, MCF7, Jurkat, K562	IC_{50} :1.13-4.20 μM
1, 3-bis (2-cyanophenyl) triazene	HT29, PC3, HepG2 HL60, HeLa, MCF7, Jurkat, K562	IC_{50} :1.04-2.39 μM

1,3-bis(2-ethoxyphenyl) triazene	HT29, PC3, HepG2 HL60, HeLa, MCF7, Jurkat, K562	IC_{50} :0.67-3.33 μM
Ethyl 2-(3,3-dibuthyl-1-triazenyl)-1H-pyrido[2,3-c] pyrrolo-3-carboxylate	Jurkat, K562	GI_{50} :2.2-5.5 μM
Ethyl 2-(3,3-dibenzyl1-triazenyl)-1H-pyrido[2,3-c] pyrrolo-3-carboxylate	Jurkat, K562	GI_{50} :2.5-8.2 μM
1-(4-(3-(benzo[d]thiazol-2-yl) triaz-2-en-1-yl)phenyl)ethan-1-one	MCF7, HCT116	IC_{50} :10-50 μM
1-(2-chloroethyl)-3-methyl-3-carbethoxytriazene	H125, U251, MCF7, OVCAR4, MALME-3M, LOX	IC_{50} :2.5-25 μM
1-(2-chloroethyl)-3-methy-3-(methylcarbamoyl)triazene	H125, U251, MCF7, OVCAR4, MALME-3M, LOX	IC_{50} :10-30 μM
4-(3-(4-chlorophenyl) triaz-1-en-1-yl)-(pyrimidin-2-yl) benzenesulfonamide	BHK21	IC_{50} :0.03 μg/mL
Ag(I) and Cu(II) complexes of 1,3-diaryltriazene-substituted sulfonamide	MDA-MB231, DLD1, ECC1, HeLa, PC3, HT29, DU145	IC_{50} :2.1-28.2 μM
1,3-diaryltriazenido(*p*-cymene) ruthenium(II) complexes	HeLa	IC_{50} :0.103 ± 0.006 μM

Acyl substitution in Triazenes

Diminazene aceturate, or Berenil, has two amidinium functionalities that are strong electron-withdrawing groups. Taking this fact into account, Cimbora-Zovko *et al.* (2011) studied a series of triazene compounds having electron withdrawing groups in both the benzene rings of 1,3-diphenyltriazene. Various triazene derivatives bearing fluoro, trifluoromethyl, chloro, bromo and nitro substitutions were synthesized. Cimbora-Zovko *et al.* (2011) reported the compounds to be active against HeLa cells. They further stated that the presence of an acetyl group, resulted in increased cytotoxicity. This was probably since acytylated triazenes can selectively transfer an acetyl group to various amino moieties in different solutions *viz*., aqueous, and alcoholic solutions. The compounds that demonstrated substantial antitumor activities against HeLa cells are represented in Figure 4.

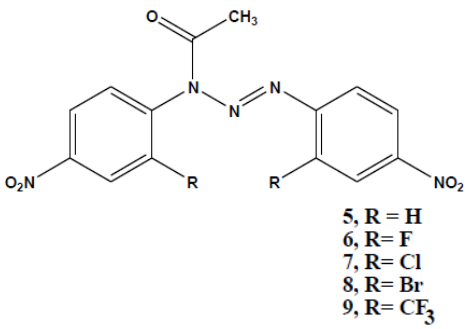

5, R = H
6, R= F
7, R= Cl
8, R= Br
9, R= CF_3

Figure 4: Acetyl substituted 1,3-diaryltriazenes

Farina *et al.* (1982) discussed the cytotoxic property of 1-(4-acetylphenyl)-3.3-dimethyltriazene (10) against isolated mouse hepatocytes *in vitro* and mouse TLXS lymphoma *in vivo*. They put forward the mechanism that the dimethyltriazenes undergo oxidative N-demethylation, forming monomethyltriazenes, which is the active cytotoxic moiety (Figure 5). It is intriguing to note that Farina *et al.* (1982) demonstrated *in vivo* anticancer activity of acetyl substituted triazenes. In addition, since the mechanism and the active species have been clearly understood, it can be stated that acyl substitution in triazenes has adequate potential as antineoplastic agents.

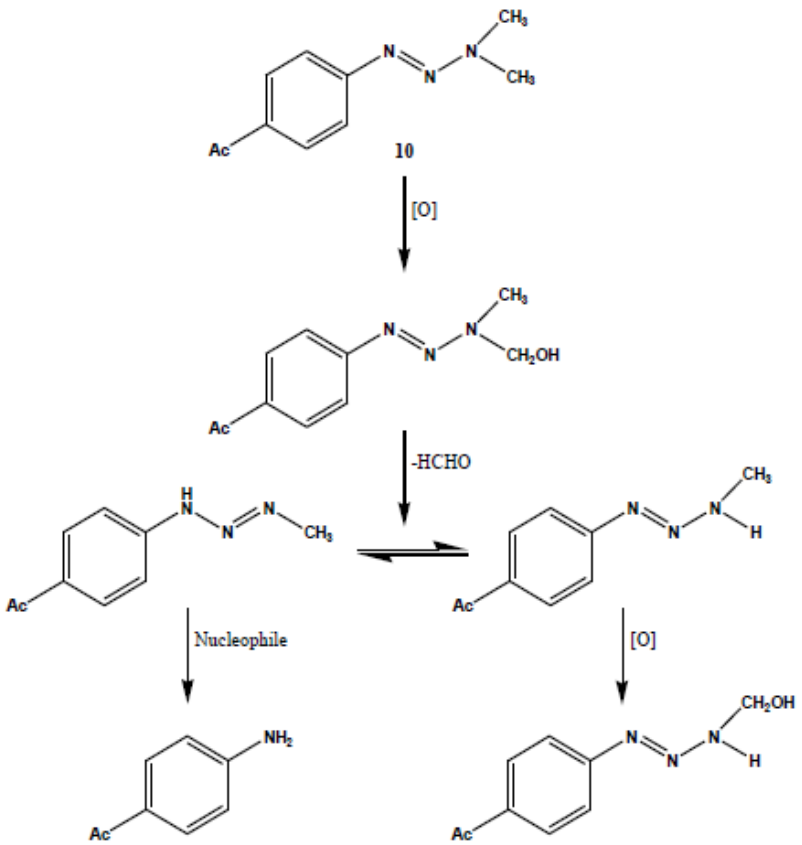

Figure 5 : Oxidative N-demethylation of dimethyltriazene (*Farina et al., 1982*)

Hydroxy substitution in Triazenes

Adibi *et al.* (2013) reported that the hydroxy substituted 1,3-diaryltriazenes (Figure 6) displayed cytotoxic activity against cancer cell lines *viz*., HT29, PC3, HepG2 HL60, HeLa, MCF7,

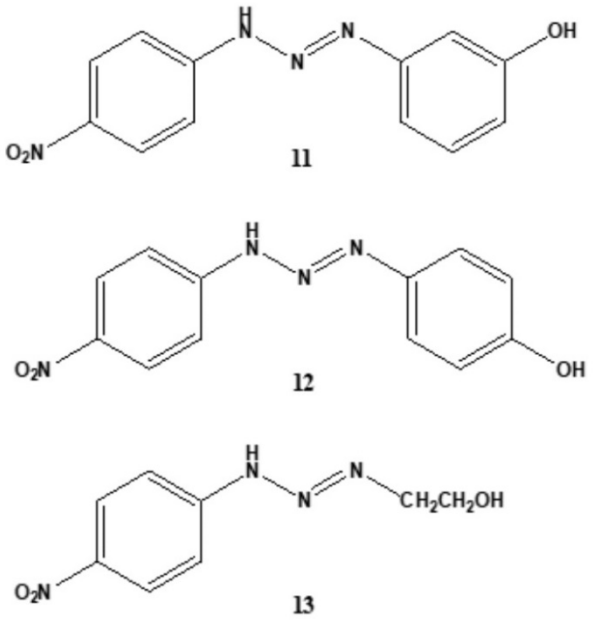

Figure 6: Hydroxy substituted 1,3-diaryltriazenes

Jurkat and K562 and a normal cell line *viz*., HUVEC (Adibi *et al*., 2013). In addition, they also prepared compounds 14,15,16 (Figure 7). 1,3-bis(2-ethoxyphenyl) triazene had IC_{50} value in the range of 0.56-3.33 μM on cancer cell lines and 12.61 μM on non-cancerous cell line. The vast difference between toxic dosage on cancer and normal cell line is a notable factor as this may cause less toxic chemotherapeutic side effects under physiological conditions. However, 1-(4-nitrophenyl)-3-(2-hydroxyethyl) triazene demonstrated weaker impact on cancer cell lines than the other compounds having IC_{50} value in the range 3-15 μM. Adibi *et al.* (2013) concluded that the absence of aromatic ring reduced the selectivity and effectiveness of the triazenes.

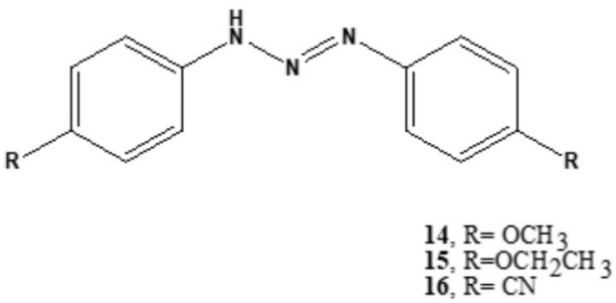

Figure 7: Methoxy, Ethoxy and Cyano substituted 1,3-diaryltriazenes

Heteroaryl Triazeno derivatives

The anticancer activity displayed by dacarbazine led to the development of several heteroaryl triazeno derivatives (El-Moghazy Aly *et al*., 2007). Among the various substituted triazenes synthesized, the azole derivatives were of utmost significance. Triazenotriazoles, pyrazoles, and imidazoles indicated antitumor activities against several types of tumors. The heterocyclic moiety probably controlled the antineoplastic activity such that the efficiency increased with the increase in nucleophilic characteristic of the heterocyclic ring (Diana *et al*., 2011). Based on this idea, Diana *et al.* (2011) discussed the antineoplastic activity of some pyrrole and indole substituted triazenes (Figure 8).

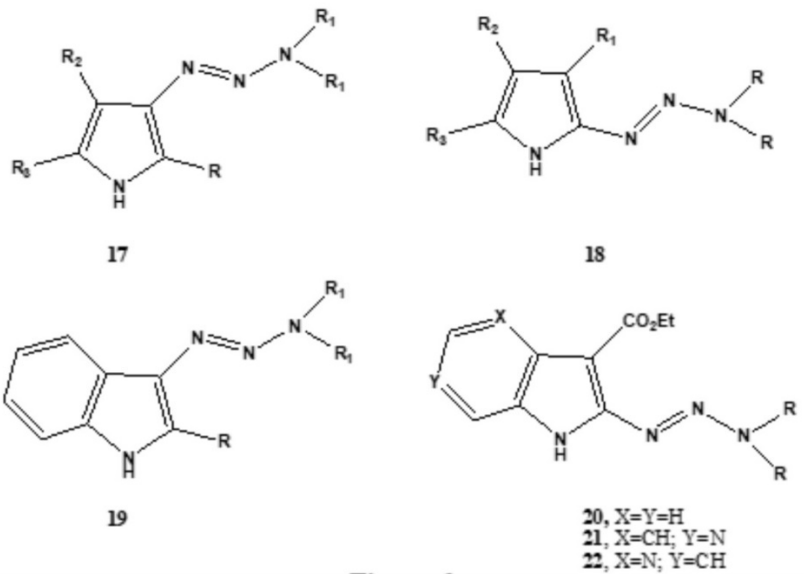

Figure 8: Pyrrole and indole substituted triazenes *(Diana et al., 2011)*

The first heterocyclic triazene synthesized (17) displayed antitumor property against Friend erythroleukemia cells (FLC) with IC_{50} value between 1.1- 3.1 μM. The indole derivative (19) proved to be 20-40 times more active than the triazenopyrrole compounds against multidrug-resistant cells and erythroleukemia with IC_{50} values between 0.10-0.14 μM and 0.053-0.080 μM, respectively. Another pyrrole derivative (18) showed cytotoxicity against leukaemia and lymphoma with an IC_{50} value of 3.9-21 μM. The last compound synthesized was a group of benzofused triazene (20, 21, 22) which expressed antineoplastic activity against Jurkat and K562 cell lines with GI_{50} values between 2.2-12.6 μM.

Alamri *et al*. (2021) worked with three benzothiazole based triazene molecules and found them to be cytotoxic against MCF7 and HCT116 cell lines with IC_{50} values around

40-47 μM and 10-20 μM for MCF7 and HCT116 cell lines respectively. A representative structure is given as Figure 9 (23).

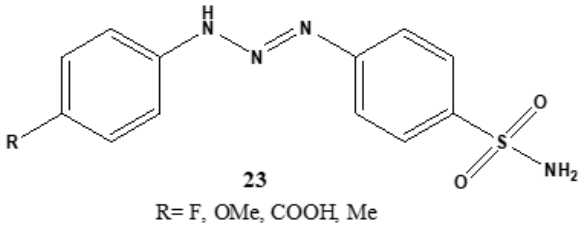

23

R= F, OMe, COOH, Me

Figure 9: Benzothiazole based triazene *(Alamri et al., 2021)*

Aliphatic Triazenes

Much less is known about the anti-tumor properties of aliphatic triazenes. Smith, Scudiero and Michejda (1990) probed into the antitumor properties of aliphatic triazenes, as these molecules could form alkyldiazonium ions without enzymatic activation (Smith, Scudiero and Michejda, 1990). In this backdrop, they explored the antineoplastic activities of many aliphatic triazenes. They reported that 1,3-diethyltriazene was a potent carcinogen in rats. They synthesized 1,3-dialkyl-3-acyltriazenes and 1-(2-chloroethyl)-3-methyl-3-acyltriazenes which proved to be cytotoxic against several human cancer cell lines *in vitro*. Another compound *viz.*, 1-(2-chloroethyl)-3-methyl-3-carbethoxytriazene (CMC), was most active against leukaemia cells while 1-(2-chloroethyl)-3-methy-3-(methylcarbamoyl)triazene (CMM) was primarily cytotoxic against leukaemia, melanoma, and mammary carcinoma. Rouzer *et al.* (1996) also worked with CMM along with 1-(2-chloroethyl)-3- benzyl-3-(methylcarbamoyl)triazene (CBzM). Both compounds possessed antineoplastic activity *in vivo*, against specific tumor xenografts embedded in nude mice.

Complexes of 1,3-diayltriazenes

A series of silver (I) and copper (II) complexes of 1,3-diaryltriazene-substituted sulfonamide (24, Figure 10) derivatives were investigated by Canakci *et al.* (2019).

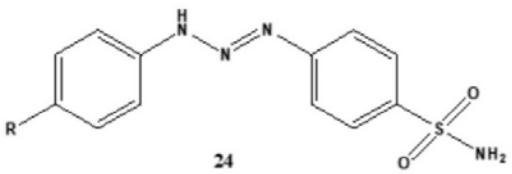

24

R= F, OMe, COOH, Me

Figure 10: 1,3-diaryltriazene-substituted sulfonamide *(Canakci et al., 2019)*

The anticancer activity of the free ligands and their Ag (I) and Cu (II) complexes was explored against the reported cancer cell lines *viz*., MDA-MB231, DLD1, ECC1, HeLa, PC3, HT29 and DU145 and non-cancerous cell lines *viz*., PNT1A, HEK293 and ARPE19. A vast majority of the complexes exhibited enhanced antitumor activity compared to their corresponding free ligands. The potency of some of the metal complexes was comparable to that of 5-Fluorouracil (5-FU), which is a widely used drug with IC_{50} value of 19.15 μM. The -COOH substituted triazene complexes presented cytotoxic activity much greater than the other complexes. This is probably due to the electron withdrawing (-I and -R) effects of the carboxylic acid group. In this context, it is relevant to mention that Aydin *et al*. (2023) synthesized a series of sulfadiazine derivatives of 1,3-diaryltriazine compounds that manifested *in vitro* antineoplastic activity against BHK21 cell line, exhibiting IC_{50} values between 0.03-0.18 μg/mL (25, Figure 11).

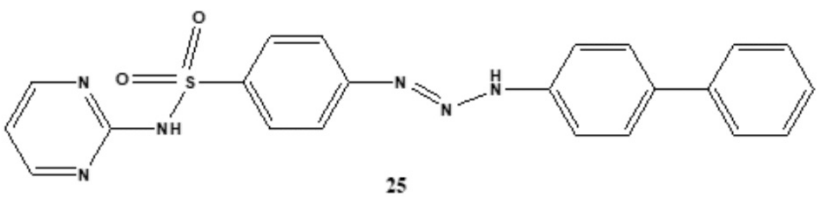

25

Figure 11: Sulfadiazine derivative of triazine

Another metal that has been receiving constant attention among researchers because of its antitumor properties is ruthenium. This is mainly because the ruthenium complexes are less toxic and can mimic iron under certain physiological conditions (Vajs *et al*., 2015). The rapidly dividing cancer cells have significant affinity for iron. Thus, ruthenium, which belongs to the same group as iron in the periodic table, accumulates more in tumor cells than in normal cells. Till date, two ruthenium complexes *viz*., KP1019 {(IndH)[*trans*-$RuCl_4(Ind)_2$], Ind = indazole} and NAMI-A {(ImH)[*trans*-$RuCl_4$(dmso-S)(Im)], Im = imidazole} have reached human clinical trials (Alessio & Messori, 2019). This prompted the researchers to synthesize ruthenium complexes of 1,3-diaryltriazenes as it has been a well-established concept that a synergistic effect can occur from the unification of two pharmacophores into one compound. Vajs *et al*. (2015) synthesized ruthenium complexes of a series of substituted 1,3-diaryltriazenes using $[RuCl_2(\eta^6$-p-cymene$)]_2$ as the starting material. They introduced electron withdrawing groups *viz*., -F, -Cl, -Br, -CN and $-CF_3$ in the 1,3-diphenyltriazene backbone. The cytotoxic property of the complexes was probed using human cervical carcinoma HeLa cells. All the complexes revealed prominent antitumor property with IC_{50} below 6 μM. The ruthenium complex having chloro and trifluromethyl disubstituted triazene ligand was found to show highest cytotoxicity with IC_{50} of 0.103 ± 0.006 μM at the end of 72 h incubation period.

Overall, the anticancer property of the complexes was found to be much enhanced than that of the corresponding free ligands confirming the phenomenon of synergistic effect.

Conclusion

The overview traces the journey of 1,3-diaryltriazene as a potential antineoplastic agent. It is interesting to note that many of the triazene based molecules have shown considerable promise as anticancer agents *in vivo*. It is also worthwhile to mention that the triazene molecules with electron withdrawing groups displayed a greater cytotoxic effect. Despite its importance, few researches have been found in the literature on the antitumor property of these molecules. Consequently, there is much scope for the expansion of research focused on the cytotoxic properties of molecules with the triazene scaffold.

Acknowledgement

The author would like to express gratitude to the Department of Chemistry at Hooghly Mohsin College in Chinsurah, Hooghly, West Bengal, India.

References

Abd Halim, A. N., Hussin, A. S. M., Ngaini, Z., Zamakshshari, N. H., & Haron, I. Z. (2023). Synthesis, antibacterial potential and in silico molecular docking analysis of triazene compounds via diazo coupling reactions of an amine. *Tetrahedron Letters*, *132*, 154803. https://doi.org/10.1016/j.tetlet.2023

Adibi, H., Majnooni, M. B., Mostafaie, A., Mansouri, K., & Mohammadi, M. (2013). Synthesis, and in-vitro cytotoxicity studies of a series of triazene derivatives on human cancer cell lines. *Iranian Journal of Pharmaceutical Research: IJPR*, *12*(4), 695–703.

Alamri, M. A., Al-Jahdali, M., Al-Radadi, N. S., & Hussien, M. A. (2021). Biological activity evaluation and computational study of novel triazene derivatives containing benzothiazole rings. *Journal of Molecular Structure*, *1227*, 129507. https://doi.org/10.1016/j.molstruc.2020.129507

Alessio, E., & Messori, L. (2019). NAMI-A and KP1019/1339, two iconic ruthenium anticancer drug candidates face-to-face: A case story in medicinal inorganic chemistry. *Molecules*, *24*(10), 1995. https://doi: 10.3390/molecules24101995

Aydin, H., Akocak, S., Lolak, N., Uslu, U., Sait, A., Korkmaz, S., ... & Aksakal, A. (2023). In vitro multitarget activity of sulfadiazine substituted triazenes as antimicrobial, cytotoxic, and larvicidal agents. *Journal of Biochemical and Molecular Toxicology*, *37*(10), e23467. https://doi.org/10.1002/jbt.23467

Canakci, D., Koyuncu, I., Lolak, N., Durgun, M., Akocak, S., & Supuran, C. T. (2019). Synthesis and cytotoxic activities of novel copper and silver complexes of 1,3-diaryltriazene-substituted sulfonamides. *Journal of Enzyme Inhibition and Medicina Chemistry*, *34*(1), 110-116. https://doi.org/10.1080/14756366.2018.1530994

Cappoen, D., Vajs, J., Uythethofken, C., Virag, A., Mathys, V., Kočevar, M., ... & Košmrlj, J. (2014). Anti-mycobacterial activity of 1, 3-diaryltriazenes. *European Journal of Medicinal Chemistry*, *77*, 193-203. https://doi.org/10.1016/j.ejmech.2014.02.065

Čimbora-Zovko, T., Brozovic, A., Piantanida, I., Fritz, G., Virag, A., Alič, B., ... & Osmak, M. (2011). Synthesis and biological evaluation of 4-nitro-substituted 1, 3-diaryltriazenes as a novel class of potent antitumor agents. *European Journal of Medicinal Chemistry*, *46*(7), 2971-2983. https://doi.org/10.1016/j.ejmech.2011.04.024

Diana, P., Stagno, A., Barraja, P., Carbone, A., Parrino, B., Dall'Acqua, F., ... & Cirrincione, G. (2011). Synthesis of triazenoazaindoles: A new class of triazenes with antitumor activity. *ChemMedChem*, *6*(7), 1291-1299. https://doi.org/10.1002/cmdc.201100027

El-Moghazy Aly, S. M., Georgey, H. H., Mohammed, M. A., Abdel Gawad, N. M., & Amin, N. H. (2007). Synthesis and antineoplastic activity of certain triazene and triazeno-acridine combilexin derivatives. *Bulletin of Pharmaceutical Sciences. Assiut*, *30*(2), 89-110. https://doi.org/10.21608/bfsa.2007.64146

Farina, P., Gescher, A., Hickman, J. A., Horton, J. K., D'Incalci, M., Ross, D., ... & Torti, L. (1982). Studies of the mode of action of antitumour triazenes and triazines—IV. The metabolism of 1-(4-acetylphenyl)-3, 3-dimethyltriazene. *Biochemical Pharmacology*, *31*(10), 1887-1892. https://doi:10.1016/0006-2952(82)90492-0

Garzon, L. R., Nunes, M. S., Martini, R., Rampelotto, R. F., Hörner, R., Locatelli, A., & Hörner, M. (2015). Complexos triazenidos de platina (II): Avaliação in vitro da atividade antibacteriana e citotóxica frente a bactérias e células de medula óssea de pacientes leucêmicos de um hospital escola. *Revista de Ciências Farmacêuticas Básica e Aplicada*, *36*(2).

Griess, J. P. (1859). V. On new nitrogenous derivatives of the phenyl-and benzoyl-series. *Proceedings of the Royal Society of London*, (9), 594-597. https://doi.org/10.1098/rspl.1857.0113

GuhaRoy, C., Butcher, R. J., & Bhattacharya, S. (2008). Rhodium complexes of 1,3-diaryltriazenes: Usual coordination, N–H bond activation and, N–N and C–N bond cleavage. *Journal of Organometallic Chemistry,* *693*(26), 3923-3931. https://doi.org/10.1016/j.jorganchem.2008.10.006

Heffeter, P., Jungwirth, U., Jakupec, M., Hartinger, C., Galanski, M. S., Elbling, L., ... & Berger, W. (2008). Resistance against novel anticancer metal compounds: differences and similarities. *Drug Resistance Updates*, *11*(1-2), 1-16. https://doi.org/10.1016/j.drup.2008.02.002

Işık, M., Akocak, S., Lolak, N., Taslimi, P., Türkeş, C., Gülçin, İ., ... & Beydemir, Ş. (2020). Synthesis, characterization, biological evaluation, and in silico studies of novel 1, 3-diaryltriazene-substituted sulfathiazole derivatives. *Archiv Der Pharmazie*, *353*(9), 2000102. https://doi.org/10.1002/ardp.202000102

Kimball, D. B., & Haley, M. M. (2002). Triazenes: a versatile tool in organic synthesis. *Angewandte Chemie International Edition*, *41*(18), 3338-3351. https://doi.org/10.1002/1521-3773(20020916)41:18<3338::AID-ANIE3338>3.0.CO;2-7

Koelmel, D. K., Jung, N., & Braese, S. (2013). Azides–diazonium ions–triazenes: Versatile nitrogen-rich functional groups. *Australian Journal of Chemistry*, *67*(3), 328-336. https://doi.org/10.1071/CH13533

Meer, L., Janzer, R. C., Kleihues, P., & Kolar, G. F. (1986). In vivo metabolism and reaction with DNA of the cytostatic agent, 5-(3, 3-dimethyl-1-triazeno) imidazole-4-carboxamide (DTIC). *Biochemical Pharmacology*, *35*(19), 3243-3247. https://doi.org/10.1016/0006-2952(86)90419-3

Nimitsiriwat, N., Gibson, V. C., Marshall, E. L., Takolpuckdee, P., Tomov, A. K., White, A. J. P., Williams, D. J., Elsegood, M. R. J., & Dale, S. H. (2007). Mono- versus bis-chelate formation in triazenide and amidinate complexes of magnesium and zinc. *Inorganic Chemistry*, *46*(23), 9988-9997. https://doi.org/10.1021/ic701061q

Ogura, M., Itoh, K., Kinoshita, T., Fukuda, H., Takenaka, T., Ohtsu, T., ... & Shimoyama, M. (2010). Phase II study of ABVd therapy for newly diagnosed clinical stage II–IV Hodgkin lymphoma: Japan Clinical Oncology Group study (JCOG 9305). *International Journal of Hematology*, *92*, 713-724. https://doi.org/10.1007/s12185-010-0712-8

Ombaka, A. O., Muguna, A. T., & Gichumbi, J. M. (2012). Antibacterial and antifungal activities of novel hydroxytriazenes. *J Environ Chem Ecotoxicol*, *4*(7), 133-136. https://doi.org/10.5897/JECE12.006

Rosenberg, B., Van Camp, L., & Krigas, T. (1965). Inhibition of cell division in Escherichia coli by electrolysis products from a platinum electrode. *Nature*, *205*(4972), 698-699. https://doi.org/10.1038/205698a0

Rouzer, C. A., Sabourin, M., Skinner, T. L., Thompson, E. J., Wood, T. O., Chmurny, G. N., ... & Michejda, C. J. (1996). Oxidative metabolism of 1-(2-chloroethyl)-3-alkyl-3-(methylcarbamoyl) triazenes: Formation of chloroacetaldehyde and relevance to biological activity. *Chemical Research in Toxicology*, *9*(1), 172-178. https://doi.org/10.1021/tx9500639

Smith, Jr., R. H., Scudiero, D. A., & Michejda, C. J. (1990). 1,3-Dialkyl-3-acyltriazenes, a novel class of antineoplastic alkylating agents. *Journal of Medicinal Chemistry*, *33*(9), 2579-2583. https://doi.org/10.1021/jm00171a036

Supuran, C. T. (2017). Advances in structure-based drug discovery of carbonic anhydrase inhibitors. *Expert Opinion on Drug Discovery*, *12*(1), 61-88. https://doi.org/10.1080/17460441.2017.1253677

Vajs, J., Steiner, I., Brozovic, A., Pevec, A., Ambriović-Ristov, A., Matković, M., ... & Košmrlj, J. (2015). The 1, 3-diaryltriazenido (p-cymene) ruthenium (II) complexes with a high in vitro anticancer activity. *Journal of Inorganic Biochemistry*, *153*, 42-48. https://doi:10.1016/j.jinorgbio.2015.09.005

doi: 10.31674/book.2024ecc.007

Redefining Chemical Practices for a Low-Carbon Future through Sustainability with Eco-Chemistry

Amit Kumar Kundu[1*], Aniruddha Mondal[2], Prasenjit Mandal[3]

[1]Department of Chemistry, Sripat Singh College, Murshidabad, West Bengal, India
[2]Department of Chemistry, Harindanga High School, Harindanga, West Bengal, India
[3]Department of Chemistry, Santipur College, Nadia, West Bengal, India

**Corresponding Author's Email: amitnml@gmail.com*

Abstract

The urgency to combat climate change and mitigate carbon emissions has spurred a growing fascination with low-carbon technologies spanning multiple sectors. In the field of chemistry, the emergence of Eco-Chem - a discipline centered on leveraging low-carbon chemistry principles - stands out as a beacon of hope for realizing sustainability objectives. Eco-Chem embodies a holistic approach that integrates sustainable practices into every facet of chemical processes, aiming to minimize environmental impact while maximizing efficiency. At its essence, this paradigm shift entails reimagining chemical synthesis, production, and consumption through a lens of environmental stewardship and resource conservation. The review elucidates key strategies inherent to Eco-Chem, emphasizing the importance of green solvents, renewable feedstocks, and energy-efficient processes. By prioritizing these elements, Eco-Chem endeavours to reduce carbon footprints, minimize waste generation, and foster closed-loop systems that promote circularity and sustainability. Furthermore, the paper explores cutting-edge technologies underpinning the Eco-Chem framework, ranging from catalysis and biotechnology to materials science and process engineering. These innovative solutions showcase the versatility and adaptability of Eco-Chem principles across diverse industries, offering scalable and economically viable alternatives to traditional chemical practices. Importantly, the review underscores the transformative potential of Eco-Chem in shaping a cleaner future. By embracing this paradigm, industries can mitigate greenhouse gas emissions, enhance resource efficiency, and drive the transition toward a low-carbon economy. Moreover, the adoption of Eco-Chem principles fosters collaboration, innovation, and knowledge-sharing, propelling us closer to achieving global sustainability goals. The review paper serves as a roadmap for navigating the evolving landscape of Eco-Chem, highlighting its role as a catalyst for positive change in the realm of chemistry and beyond. By embracing Eco-Chem principles and leveraging innovative technologies, it can forge a path toward a more sustainable and resilient future for generations to come.

Keywords: *Clean Chemistry; Cutting-edge Technologies; Eco-Chemistry; Low-Carbon; Sustainability*

Introduction

Climate change stands as one of the most pressing challenges of our time, demanding urgent and concerted action from every corner of society (Aarya, 2024). With rising global temperatures, extreme weather events, and escalating environmental degradation, the need for sustainable solutions has never been more critical (Khayyam & Tariq, 2022; Nguyen *et al*., 2023). In this context, the role of chemistry emerges as both pivotal and transformative. Through the lens of Eco-Chemistry, a burgeoning discipline at the intersection of chemistry and sustainability, innovative pathways toward a low-carbon economy and a more resilient future for the planet can be explored (Matlin *et al*., 2023). Chemistry, often dubbed the central science, underpins much of modern civilization, powering industries, shaping technologies and driving innovation. Yet, traditional chemical processes have also been a significant contributor to environmental degradation, from greenhouse gas emissions to pollution of air, water, and soil (Yoro & Daramola, 2020). As the impacts of climate change escalate, there is a growing imperative to harness the power of chemistry for positive change - to transition from a linear, resource-intensive economy to one that is regenerative, circular, and low in carbon emissions (Kandpal *et al*., 2024). Enter Eco-Chemistry - a paradigm shift that seeks to align chemical principles with environmental stewardship and sustainability goals. At its core, Eco-Chemistry embodies the principles of green chemistry, advocating for the design of products and processes that minimize environmental impact, conserve resources, and prioritize human health and safety (Chawla *et al*., 2022). However, Eco-Chemistry extends beyond the confines of green chemistry by integrating broader ecological perspectives, systems thinking, and interdisciplinary collaboration.

The significance of Eco-Chemistry becomes apparent when viewed through the lens of climate change mitigation and adaptation. As human civilization confronts the realities of a warming planet and escalating carbon emissions, there is a growing recognition that technological innovation alone will not suffice. Systemic change - an overhaul of industrial systems, energy infrastructure, and consumption patterns - is needed to achieve meaningful progress towards a sustainable future (Scoones *et al*., 2020). Here, Eco-Chemistry emerges as a powerful catalyst for transformation, offering a framework to reimagine chemical processes, materials, and products in alignment with environmental sustainability goals. Central to the ethos of Eco-Chemistry is the concept of carbon neutrality - the idea that chemical processes should strive to minimize or offset carbon emissions throughout their lifecycle. This entails a holistic assessment of carbon footprints, from raw material extraction and production to transportation, use, and end-of-life disposal. By optimizing process efficiencies, utilizing renewable resources, and

adopting carbon capture and utilization technologies, Eco-Chemistry aims to decouple chemical production from fossil fuel dependency, paving the way for a low-carbon economy. Moreover, Eco-Chemistry emphasizes the importance of circularity - the idea that waste should be minimized, and resources should be reused, recycled, or repurposed whenever possible. This involves redesigning chemical processes and materials to minimize waste generation, enhance recyclability, and promote closed-loop systems (Roy Chowdhury *et al*., 2023; de la Guardia & Garrigues, 2012). By closing the loop on resource flows, Eco-Chemistry not only reduces environmental pollution but also conserves finite resources and fosters economic resilience in the face of resource scarcity.

Beyond technical innovations, Eco-Chemistry also encompasses broader socio-economic dimensions, recognizing the interconnectedness of environmental sustainability, social equity, and economic prosperity (Ivanov, 2022). As the transition towards a low-carbon economy occurs, it is essential to ensure that the benefits of sustainability are equitably distributed and that vulnerable communities are not left behind (Siciliano *et al*., 2021). This requires inclusive decision-making processes, capacity-building initiatives, and policies that prioritize environmental justice and equitable access to green technologies and opportunities. The urgency of addressing climate change demands bold and transformative action across all sectors of society, with chemistry playing a central role in driving sustainable solutions. Through the lens of Eco-Chemistry, there is an opportunity to harness the power of chemistry for positive environmental and social impact, paving the way towards a low-carbon economy and a more resilient future for generations to come.

Definition and scope of Eco-Chem

Eco-Chem, or Ecological Chemistry, represents a multifaceted approach to chemical production that places paramount importance on environmental sustainability, human health, and economic viability (Mohan & Katakojwala, 2021). At its core, Eco-Chem seeks to revolutionize traditional chemical processes by integrating principles from various disciplines such as green chemistry, circular economy, and sustainable manufacturing (Hessel *et al*., 2021). By doing so, it aims to mitigate the detrimental environmental impacts associated with conventional chemical production methods. Central to the philosophy of Eco-Chem is the recognition that chemical processes, while essential for various industrial applications, often come at a significant cost to the environment. Traditional methods of chemical production typically involve the consumption of large quantities of natural resources, the generation of hazardous waste, and the emission of pollutants into the air, water, and soil. These practices not only contribute to environmental degradation but also pose serious risks to human health and well-being (Barinova, Gaeva & Krasnov, 2020). In contrast, Eco-Chem advocates for a

paradigm shift towards more sustainable and environmentally friendly practices. This entails designing and implementing chemical processes that minimize resource consumption, waste generation, and adverse environmental effects throughout the entire product life cycle - from raw material extraction to final disposal or recycling (Mondal, Acharjee & Saha, 2022). By adopting a holistic approach, Eco-Chem aims to achieve the triple bottom line of environmental, social, and economic benefits.

One of the key principles underlying Eco-Chem is green chemistry, which focuses on the development of chemical products and processes that are inherently benign to the environment (Zehra *et al*., 2020). This includes the use of renewable feedstocks, elimination or reduction of hazardous substances, and optimization of reaction conditions to maximize efficiency and minimize waste. By adhering to the principles of green chemistry, Eco-Chem endeavors to create a more sustainable chemical industry that is less reliant on fossil fuels and more in tune with the natural world (Sigsgaard, 2021). Furthermore, Eco-Chem embraces the concept of a circular economy, which seeks to minimize waste and maximize resource efficiency by closing the loop on material flows (Lim *et al*., 2022). This involves designing products for durability, reparability, and recyclability, as well as implementing strategies for recovering and reusing valuable materials from waste streams. By transitioning towards a circular economy model, Eco-Chem aims to reduce the environmental burden associated with chemical production and promote a more regenerative approach to resource management. In addition to green chemistry and circular economy principles, Eco-Chem also encompasses the principles of sustainable manufacturing, which emphasize the importance of energy efficiency, pollution prevention, and social responsibility in industrial processes (Panchal, Singh & Diwan; 2021; Sheldon, 2018). By integrating these principles into chemical production practices, Eco-Chem seeks to foster innovation, promote collaboration, and drive continuous improvement toward a more sustainable future. By embracing principles from green chemistry, circular economy, and sustainable manufacturing, Eco-Chem aims to revolutionize traditional chemical processes and pave the way towards a more sustainable and resilient chemical industry. Through collaborative efforts and innovation, Eco-Chem holds the promise of creating a brighter and more sustainable future for generations to come.

Crore principle of eco-chemistry

The core principles of Eco-Chem revolve around the integration of green chemistry, circular economy, and sustainable manufacturing practices to foster environmentally responsible and economically viable chemical production processes. Each of these principles plays a pivotal role in ensuring that chemical manufacturing is conducted in a manner that minimizes its environmental footprint while maximizing resource efficiency and social responsibility (Chen *et al*., 2020). Green chemistry serves as the foundation

of Eco-Chem, emphasizing the design of chemical products and processes that prioritize environmental sustainability. This involves the reduction or elimination of hazardous substances, the minimization of waste generation, and the conservation of energy and resources. By adhering to principles such as the use of renewable feedstocks, solvent selection, energy efficiency, and the design of safer chemicals, green chemistry promotes the development of chemical products and processes that are not only environmentally benign but also economically viable in the long term. Complementing green chemistry, the principles of the circular economy advocate for the efficient use and reuse of materials throughout their lifecycle. In the context of Eco-Chem, circular economy principles are applied to chemical production to minimize waste generation, maximize resource efficiency, and promote the reuse and recycling of materials (Ncube *et al*., 2023). This involves designing products and processes with end-of-life considerations in mind and implementing closed-loop systems for resource recovery. By closing material loops and enabling reuse, recycling, and resource recovery, circular economy approaches contribute to the overall sustainability of chemical manufacturing.

Sustainable manufacturing serves as the overarching framework that integrates green chemistry and circular economy principles into the design and operation of chemical production facilities (Cagno *et al*., 2023). Sustainable manufacturing strategies and practices optimize resource utilization, minimize environmental impact, and enhance social responsibility throughout the manufacturing process. In Eco-Chem, sustainable manufacturing principles guide decision-making regarding energy consumption, emissions reduction, and waste management, ensuring that chemical production aligns with long-term sustainability goals (Figure 1).

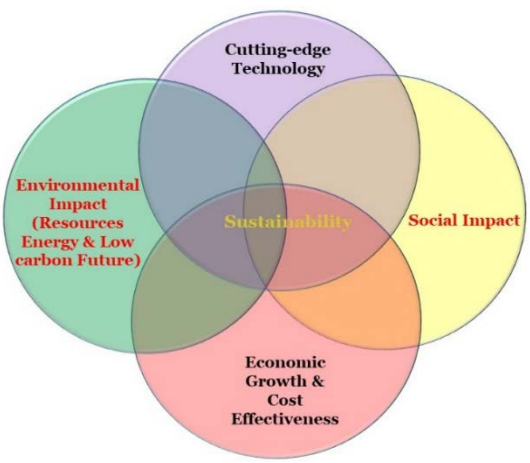

Figure 1: Core Principle of Eco-Chemistry

By integrating environmental, economic, and social considerations, sustainable manufacturing enables chemical producers to achieve holistic sustainability and

contribute positively to the transition towards a more sustainable future. By incorporating these principles into their operations, chemical manufacturers can mitigate environmental impact, conserve resources, and foster social responsibility, ultimately contributing to a more sustainable and resilient chemical industry.

Importance of minimizing carbon footprint and reducing reliance on fossil fuels

The importance of minimizing carbon footprint and reducing reliance on fossil fuels cannot be overstated in the context of environmental sustainability and combating climate change (Usman & Radulescu, 2022). Fossil fuel-based chemical production processes, in particular, have significant environmental impacts that underscore the urgent need for a transition to renewable feedstocks and energy sources. Fossil fuel-based chemical production is a major contributor to greenhouse gas emissions, air and water pollution, and depletion of natural resources. These processes involve the extraction, processing, and combustion of fossil fuels, resulting in the release of carbon dioxide (CO_2), methane (CH_4), and other greenhouse gases into the atmosphere. These emissions exacerbate climate change and contribute to environmental degradation, including air pollution, acid rain, and water contamination. Moreover, the reliance on finite resources such as crude oil and natural gas for chemical production poses additional challenges. These resources are subject to price volatility and geopolitical tensions, making the supply chain vulnerable to disruptions and economic instability (Blondeel *et al*., 2021). As these resources become increasingly scarce, the environmental and economic costs of their extraction and utilization escalate.

To address these challenges, there is a pressing need to transition to renewable feedstocks and energy sources in chemical production. This transition is essential for minimizing the carbon footprint of chemical manufacturing and promoting environmental sustainability. Renewable feedstocks, including biomass, CO_2, and other sustainable sources, offer a promising alternative to traditional fossil fuel-based feedstocks (Hasan *et al*., 2021). Biomass, derived from organic materials such as plants and agricultural residues, can be converted into bio-based chemicals through processes such as fermentation and thermochemical conversion. Unlike fossil fuels, biomass is renewable and carbon-neutral, as it absorbs CO_2 during growth, offsetting emissions from its combustion. Similarly, CO_2 can be utilized as a feedstock for chemical production through processes such as carbon capture and utilization (CCU) (Desport & Selosse, 2022). By capturing CO_2 emissions from industrial sources and converting them into value-added products, such as chemicals and fuels, CCU technologies can help reduce greenhouse gas emissions and mitigate climate change (Alok *et al*., 2022).

In addition to transitioning to renewable feedstocks, integrating renewable energy sources into chemical manufacturing is crucial for reducing reliance on fossil fuels and lowering emissions. Renewable energy sources, including solar, wind, and hydroelectric

power, offer clean and sustainable alternatives to fossil fuels for powering industrial processes. Solar energy, harvested through photovoltaic panels or concentrated solar power systems, can provide reliable and cost-effective electricity for chemical production facilities (Shahabuddin *et al*., 2021). Wind energy, generated by wind turbines, can supplement or replace fossil fuel-based electricity generation, reducing emissions and environmental impact (Wolniak & Skotnicka-Zasadzień, 2023) Likewise, hydroelectric power, generated by harnessing the energy of flowing water, can provide a renewable source of electricity for industrial applications (Yadav, Kumar & Jaiswal, 2023). Overall, the transition to renewable feedstocks and energy sources is imperative for minimizing the environmental impacts of fossil fuel-based chemical production. By reducing greenhouse gas emissions, air and water pollution, and reliance on finite resources, this transition can promote environmental sustainability, mitigate climate change, and support a more resilient and sustainable economy.

Key strategies and technologies in eco-chem

In the pursuit of a sustainable future, the field of eco-chemistry emerges as a beacon of hope, offering innovative solutions to address the environmental challenges associated with traditional chemical practices. By integrating key strategies and cutting-edge technologies, eco-chemistry seeks to minimize the carbon footprint of chemical production while maximizing resource efficiency. In this paradigm shift towards sustainability, several critical areas of focus have emerged, each playing a pivotal role in reshaping the landscape of chemical manufacturing. At the heart of eco-chemistry lies the utilization of renewable feedstocks, such as biomass, CO_2, and other sustainable sources, for chemical production. Through advancements in bio-based materials and processes, including bio-refineries, fermentation, and enzymatic catalysis, the industry is poised to transition away from fossil fuels towards greener alternatives. By harnessing the power of nature's building blocks, eco-chemistry enables the production of chemicals in a manner that is both economically viable and environmentally friendly. Another cornerstone of eco-chemistry is the pursuit of energy efficiency throughout the chemical manufacturing process. By implementing innovative technologies such as process optimization, heat integration, and cogeneration, companies can minimize energy consumption and reduce their reliance on non-renewable resources (Bagherian & Mehranzamir, 2020). Furthermore, the integration of renewable energy sources such as solar panels, wind turbines, and biomass boilers further enhances the sustainability of chemical production, mitigating greenhouse gas emissions and contributing to a cleaner, greener future.

Advancements in catalysis and reaction engineering play a pivotal role in driving the transition towards eco-friendly chemical practices. Through the development of catalytic processes, including heterogeneous catalysis, enzymatic catalysis, and photocatalysis,

researchers are able to achieve selective and efficient chemical transformations with minimal environmental impact. Moreover, innovations in reaction engineering, such as process intensification and continuous flow systems, optimize yield, selectivity, and energy efficiency, further enhancing the sustainability of chemical manufacturing processes. The integration of unit operations and the application of process intensification techniques are key strategies in streamlining chemical processes and minimizing resource consumption. By integrating unit operations, companies can reduce energy and resource consumption while simultaneously minimizing waste generation. Additionally, the adoption of process intensification techniques such as micro-reactors, membrane separation, and reactive distillation enables compact and efficient production of chemicals, further contributing to a low-carbon future (Burek *et al*., 2022).

Waste minimization and Valorization

Waste minimization and valorization strategies are essential for closing the loop on chemical production and maximizing resource efficiency (Mostaghimi & Behnamian, 2023). By implementing recycling, reuse, and recovery initiatives, companies can reduce waste generation and maximize the valorization of by-products. Moreover, recycling and upcycling approaches such as chemical recycling, bioremediation, and resource recovery create value from waste streams, further enhancing the sustainability of chemical manufacturing processes (Kumar *et al*., 2023). The eco-chemistry offers a promising pathway toward a low-carbon future by redefining traditional chemical practices through sustainability. By embracing renewable feedstocks, enhancing energy efficiency, advancing catalysis and reaction engineering, optimizing processes through intensification and integration, and prioritizing waste minimization and valorization, the industry can achieve significant reductions in its environmental footprint while simultaneously driving economic growth and innovation. Through collaborative efforts and continued investment in research and development, eco-chemistry has the potential to revolutionize the way chemicals are produced, paving the way for a more sustainable and prosperous future for generations to come.

Conclusion

Eco-Chem represents a transformative paradigm in chemical production, encapsulating a multifaceted approach that harmonizes the principles of green chemistry, circular economy, and sustainable manufacturing. This integrated framework lays the groundwork for a more resilient and environmentally responsible chemical industry. At its core, Eco-Chem emphasizes the imperative of minimizing environmental impact while maximizing resource efficiency throughout the entire chemical production lifecycle. Central to Eco-Chem are a series of strategic initiatives and technological advancements aimed at driving sustainable practices. These encompass a spectrum of methodologies, including leveraging renewable feedstocks, enhancing energy

efficiency, optimizing catalysis and reaction engineering, implementing process intensification and integration, and prioritizing waste minimization and valorization. By embracing these strategies, Eco-Chem endeavors to not only mitigate the ecological footprint of chemical processes but also foster economic viability and societal well-being. Looking ahead, the future trajectory of Eco-Chem hinges on sustained efforts to propel innovation and address evolving challenges. Research and development endeavors must prioritize the refinement and proliferation of sustainable technologies, with a keen emphasis on optimizing resource utilization and tackling emergent environmental and social concerns. However, this journey is not without obstacles. Technological barriers, economic constraints, and the need for supportive policy frameworks present formidable challenges that must be navigated to realize the full potential of Eco-Chem. Nevertheless, the implications of embracing Eco-Chem principles are profound and far-reaching. By aligning chemical practices with sustainability imperatives, Eco-Chem holds the promise of advancing global efforts towards achieving sustainable development goals, combatting climate change, and safeguarding environmental integrity for future generations. Realizing this vision necessitates concerted collaboration among diverse stakeholders, including industry leaders, academic institutions, governmental bodies, and civil society organizations. Through collective action and knowledge sharing, these stakeholders can catalyze the transition towards a low-carbon future founded on the principles of sustainability and Eco-Chemistry.

Acknowledgement

The authors would like to thank the principal, Dr. Kamal Krishna Sarkar, Sripat Singh College, Jiaganj; Dr. Sagar Simlandy, IQAC Coordinator, Sripat Singh College, Jiaganj and all the staff of the Department of Chemistry, Sripat Singh College, Jiaganj, India for their valuable suggestions and help.

References

Aarya, A. K. (2024). Global Eco-Politics: Media Discourse and Conflicting Climate Change Frameworks. In *Eco-Politics and Global Climate Change* (pp. 189-214). Cham: Springer Nature Switzerland.

Alok, A., Shrestha, R., Ban, S., Devkota, S., Uprety, B., & Joshi, R. (2022). Technological advances in the transformative utilization of CO_2 to value-added products. *Journal of Environmental Chemical Engineering*, *10*(1), 106922. https://doi.org/10.1016/j.jece.2021.106922

Bagherian, M. A., & Mehranzamir, K. (2020). A comprehensive review on renewable energy integration for combined heat and power production. *Energy Conversion and Management*, *224*, 113454. https://doi.org/10.1016/j.enconman.2020.113454

Barinova, G.M., Gaeva, D.V., Krasnov, E.V. (2020). Hazardous Chemicals and Air, Water, and Soil Pollution and Contamination. In: Leal Filho, W., Wall, T., Azul, A.M., Brandli, L., Özuyar, P.G. (eds) Good Health and Well-Being. Encyclopedia of the UN Sustainable Development Goals. *Springer, Cham*. https://doi.org/10.1007/978-3-319-95681-7_48

Blondeel, M., Bradshaw, M. J., Bridge, G., & Kuzemko, C. (2021). The geopolitics of energy system transformation: A review. *Geography Compass*, *15*(7), e12580. https://doi.org/10.1111/gec3.12580

Burek, B. O., Dawood, A. W., Hollmann, F., Liese, A., & Holtmann, D. (2022). Process intensification as game changer in enzyme catalysis. *Frontiers in Catalysis*, *2*, 858706. https://doi.org/10.3389/fctls.2022.858706

Cagno, E., Negri, M., Neri, A., & Giambone, M. (2023). One framework to rule them all: an integrated, multi-level and scalable performance measurement framework of sustainability, circular economy and industrial symbiosis. *Sustainable Production and Consumption*, *35*, 55-71. https://doi.org/10.1016/j.spc.2022.10.016

Chawla, S., Rai, P., Garain, T., Uday, S., & Hussain, C. M. (2022). Green carbon materials for the analysis of environmental pollutants. *Trends in Environmental Analytical Chemistry*, *33*, e00156. https://doi.org/10.1016/j.teac.2022.e00156

Chen, T. L., Kim, H., Pan, S. Y., Tseng, P. C., Lin, Y. P., & Chiang, P. C. (2020). Implementation of green chemistry principles in circular economy system towards sustainable development goals: Challenges and perspectives. *Science of the Total Environment*, *716*, 136998. https://doi.org/10.1016/j.scitotenv.2020.136998

de la Guardia, M., & Garrigues, S. (Eds.). (2012). *Handbook of Green Analytical Chemistry* (Vol. 794). Chichester: John Wiley & Sons. https://doi.org/10.1002/9781119940722

Desport, L., & Selosse, S. (2022). An overview of CO_2 capture and utilization in energy models. *Resources, Conservation and Recycling*, *180*, 106150. https://doi.org/10.1016/j.resconrec.2021.106150

Hasan, M. F., Rossi, L. M., Debecker, D. P., Leonard, K. C., Li, Z., Makhubela, B. C., ... & Kleij, A. (2021). Can CO_2 and renewable carbon be primary resources for sustainable fuels and chemicals?. *ACS Sustainable Chemistry & Engineering*, *9*(37), 12427-12430. https://doi.org/10.1021/acssuschemeng.1c06008

Hessel, V., Escriba-Gelonch, M., Bricout, J., Tran, N. N., Anastasopoulou, A., Ferlin, F., ... & Vaccaro, L. (2021). Quantitative sustainability assessment of flow chemistry–from simple metrics to holistic assessment. *ACS Sustainable Chemistry & Engineering*, *9*(29), 9508-9540. https://doi.org/10.1021/acssuschemeng.1c02501

Ivanov, T. (2022). Higher Education for Interdisciplinary Education in Sustainable Development. *UNSS yearbook*, *1*(1), 173-212.

Kandpal, V., Jaswal, A., Santibanez Gonzalez, E.D.R., & Agarwal, N. (2024). Circular Economy Principles: Shifting Towards Sustainable Prosperity. In: Sustainable Energy Transition. Circular Economy and Sustainability. *Springer, Cham*. https://doi.org/10.1007/978-3-031-52943-6_4

Khayyam, U., & Tariq, I. (2022). Environmental Degradation and Global Warming. In: Baikady, R., Sajid, S., Przeperski, J., Nadesan, V., Rezaul, I., Gao, J. (eds) The Palgrave Handbook of Global Social Problems. *Palgrave Macmillan, Cham*. https://doi.org/10.1007/978-3-030-68127-2_80-1

Kumar, M., Bolan, S., Padhye, L. P., Konarova, M., Foong, S. Y., Lam, S. S., ... & Bolan, N. (2023). Retrieving back plastic wastes for conversion to value added petrochemicals: opportunities, challenges and outlooks. *Applied Energy*, *345*, 121307. https://doi.org/10.1016/j.apenergy.2023.121307

Lim, M. K., Lai, M., Wang, C., & Lee, Y. (2022). Circular economy to ensure production operational sustainability: A green-lean approach. *Sustainable Production and Consumption*, *30*, 130-144. https://doi.org/10.1016/j.spc.2021.12.001

Matlin, S. A., Mehta, G., Cornell, S. E., Krief, A., & Hopf, H. (2023). Chemistry and pathways to net zero for sustainability. *RSC Sustainability*, *1*(7), 1704-1721. https://doi.org/10.1039/D3SU00125C

Mohan, S. V., & Katakojwala, R. (2021). The circular chemistry conceptual framework: A way forward to sustainability in industry 4.0. *Current Opinion in Green and Sustainable Chemistry*, *28*, 100434. https://doi.org/10.1016/j.cogsc.2020.100434

Mondal, S., Acharjee, A., & Saha, B. (2022). Utilization of natural surfactants: an approach towards sustainable universe. *Vietnam Journal of Chemistry*, *60*(1), 1-14. https://doi.org/10.1002/vjch.202100137

Mostaghimi, K., & Behnamian, J. Waste minimization towards waste management and cleaner production strategies: a literature review. *Environ Dev Sustain 25*, 12119–12166 (2023). https://doi.org/10.1007/s10668-022-02599-7

Ncube, A., Mtetwa, S., Bukhari, M., Fiorentino, G., & Passaro, R. (2023). Circular economy and green chemistry: the need for radical innovative approaches in the design for new products. *Energies*, *16*(4), 1752. https://doi.org/10.3390/en16041752

Nguyen, T. T., Grote, U., Neubacher, F., Do, M. H., & Paudel, G. P. (2023). Security risks from climate change and environmental degradation: implications for sustainable land use transformation in the Global South. *Current Opinion in Environmental Sustainability*, *63*, 101322. https://doi.org/10.1016/j.cosust.2023.101322

Panchal, R., Singh, A., & Diwan, H. (2021). Does circular economy performance lead to sustainable development? - A systematic literature review. *Journal of Environmental Management*, *293*, 112811. https://doi.org/10.1016/j.jenvman.2021.112811

Roy Chowdhury, P., Medhi, H., Bhattacharyya, K. G., & Hussain, C. M. (2023). Future of Carbon Materials in Environmental Analysis. In *Green Carbon Materials for Environmental Analysis: Emerging Research and Future Opportunities* (pp. 195-231). American Chemical Society. https://doi.org/10.1021/bk-2023-1441.ch009

Scoones, I., Stirling, A., Abrol, D., Atela, J., Charli-Joseph, L., Eakin, H., ... & Yang, L. (2020). Transformations to sustainability: combining structural, systemic and enabling approaches. *Current Opinion in Environmental Sustainability*, *42*, 65-75. https://doi.org/10.1016/j.cosust.2019.12.004

Shahabuddin, M., Alim, M. A., Alam, T., Mofijur, M., Ahmed, S. F., & Perkins, G. (2021). A critical review on the development and challenges of concentrated solar power technologies. *Sustainable Energy Technologies and Assessments*, *47*, 101434. https://doi.org/10.1016/j.seta.2021.101434

Sheldon, R. A. (2018). Metrics of green chemistry and sustainability: past, present, and future. *ACS Sustainable Chemistry & Engineering*, *6*(1), 32-48. https://doi.org/10.1021/acssuschemeng.7b03505

Siciliano, G., Wallbott, L., Urban, F., Dang, A. N., & Lederer, M. (2021). Low-carbon energy, sustainable development, and justice: Towards a just energy transition for the society and the environment. *Sustainable Development*, *29*(6), 1049-1061. https://doi.org/10.1002/sd.2193

Sigsgaard, T. (2021). Implementation of green chemistry: real-world case studies. *Green Chem. Beginners*, *205*.

Usman, M., & Radulescu, M. (2022). Examining the role of nuclear and renewable energy in reducing carbon footprint: does the role of technological innovation really create some difference?. *Science of The Total Environment*, *841*, 156662. https://doi.org/10.1016/j.scitotenv.2022.156662

Wolniak, R., & Skotnicka-Zasadzień, B. (2023). Development of Wind Energy in EU Countries as an Alternative Resource to Fossil Fuels in the Years 2016–2022. *Resources*, *12*(8), 96. https://doi.org/10.3390/resources12080096

Yadav, P. K., Kumar, A., & Jaiswal, S. (2023). A critical review of technologies for harnessing the power from flowing water using a hydrokinetic turbine to fulfill the energy need. *Energy Reports*, *9*, 2102-2117. https://doi.org/10.1016/j.egyr. 2023.01.033

Yoro, K. O., & Daramola, M. O. (2020). CO2 emission sources, greenhouse gases, and the global warming effect. In *Advances in Carbon Capture* (pp. 3-28). Woodhead Publishing. https://doi.org/10.1016/B978-0-12-819657-1.00001-3

Zehra, A., Meena, M., Swapnil, P., Raytekar, N.A., & Upadhyay, R.S. (2020). Sustainable Approaches to Remove Heavy Metals from Water. In: Singh, J., Vyas, A., Wang, S., Prasad, R. (eds) Microbial Biotechnology: Basic Research and Applications. *Environmental and Microbial Biotechnology*. Springer, Singapore. https://doi.org/10.1007/978-981-15-2817-0_6

doi: 10.31674/book.2024ecc.008

Applications of Green Solvents for the Development of Sustainable Chemical Process

Aniruddha Mondal[1*], Amit Kumar Kundu[2], Prasenjit Mandal[3]

[1]Department of Chemistry, Harindanga High School, Harindanga, West Bengal, India
[2]Department of Chemistry, Sripat Singh College, Jiaganj, Murshidabad, West Bengal, India
[3]Department of Chemistry, Santipur College, Nadia, West Bengal, India

**Corresponding Author's Email: aniruddha.chem007@gmail.com*

Abstract

The pursuit of sustainable chemical processes has prompted a substantial emphasis on the advancement and utilization of green solvents and reaction media. Conventional solvents and reaction conditions frequently present environmental and health risks, underscoring the necessity for alternative, environmentally friendly solutions. Green solvents, distinguished by their low toxicity, renewable origins, and minimal environmental footprint, present promising avenues to tackle these issues. This paper offers a comprehensive overview of green solvents, encompassing their classification, properties, and applications across various chemical processes. Additionally, the significance of designing sustainable reaction media and their role in augmenting the efficiency and environmental sustainability of chemical reactions are deliberated upon. By embracing green solvents and reaction media, the chemical industry can transition towards more sustainable practices, thereby contributing to the realization of a greener future. This review highlights the critical importance of transitioning towards sustainable chemical practices by leveraging green solvents and reaction media, emphasizing their potential to mitigate environmental and health hazards associated with conventional approaches. Through comprehensive coverage of their classification, properties, and applications, the abstract underscores the multifaceted benefits of adopting green solvents and the pivotal role they play in advancing sustainability within the chemical industry.

Keywords: *Environmental Impact; Green Chemistry; Green Solvents; Reaction Media; Renewable Resources; Sustainable Chemistry*

Introduction:

In modern chemistry, the choice of solvents and reaction media plays a crucial role not only in the efficiency of chemical processes but also in their environmental impact. Traditional solvents, while effective in facilitating reactions and dissolving compounds, often pose significant challenges due to their toxicity, volatility, and adverse effects on human health and the environment (Joshi & Adhikari, 2019; Jv, 2001; Hansen & Wilbur,

1994). However, with the growing recognition of the importance of sustainable development, the principles of green chemistry (Erythropel *et al*., 2018; Anastas & Warner, 2000) have emerged as a guiding framework for designing chemical processes that minimize environmental impact while maximizing efficiency and safety. This article provides an overview of the environmental challenges associated with traditional solvents and reaction media, discusses the principles of green chemistry (Erythropel *et al*., 2018; Anastas & Warner, 2000) and their significance in sustainable development, and introduces green solvents as alternatives to conventional counterparts. Additionally, it explores the classification, properties, and examples of commonly used green solvents, highlighting their role in promoting environmentally friendly practices in the field of chemistry. Traditional solvents, such as chlorinated hydrocarbons, aromatic hydrocarbons, and volatile organic compounds (VOCs), have long been utilized in various chemical processes due to their solvating power and versatility. However, these solvents pose significant environmental and health risks. VOCs, for instance, contribute to air pollution and can have detrimental effects on human health, including respiratory problems and neurological disorders. Moreover, many traditional solvents are non-renewable, derived from fossil fuels, and contribute to carbon emissions and the depletion of natural resources.

In response to the environmental challenges posed by traditional solvents, the principles of green chemistry have gained prominence in recent years. Green chemistry emphasizes the design of chemical products and processes that reduce or eliminate the use and generation of hazardous substances, thus minimizing environmental impact and promoting sustainability. Green solvents (Capello, Fischer & Hungerbühler, 2007; Clarke *et al*., 2018) represent a fundamental aspect of green chemistry, offering sustainable alternatives to conventional solvents. These solvents are characterized by their low toxicity, minimal environmental impact, and renewable or biodegradable nature (Winterton, 2021; Byrne *et al*., 2016). By replacing traditional solvents with green alternatives, chemists can significantly reduce the environmental footprint of chemical processes while maintaining high levels of efficiency and performance (Devi *et al*., 2020; Welton, 2015).

Classification and properties of green solvents

Green solvents can be classified based on various criteria, including their origin, toxicity, and environmental impact.

Table 1: *Different type of Green Solvents*

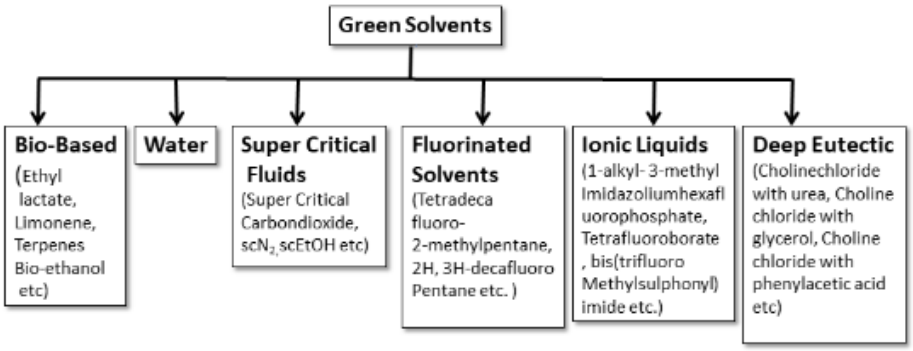

Common classifications include renewable solvents derived from biomass, bio-based solvents (Vovers, Smith & Stevens, 2017) synthesized from renewable feedstocks, and natural solvents extracted from plants or minerals. Additionally, green solvents are characterized by properties such as low volatility, biodegradability, and non-toxicity, which contribute to their environmental benefits. Water is perhaps the most abundant and environmentally friendly solvent available (Zhou, Hearne & Li, 2019). It is non-toxic, readily available, and can dissolve a wide range of organic and inorganic compounds. Supercritical carbon dioxide (CO_2) is gaining prominence as a green solvent due to its low toxicity, non-flammability, and minimal environmental impact (Madan, 2018). Under supercritical conditions, CO_2 exhibits both gas-like and liquid-like properties, making it an efficient solvent for extraction, purification, and reaction processes (Budisa & Schulze-Makuch, 2014). Most fluorinated solvents have high thermostability, chemostability, and low toxicity (Gladysz & Emnet, 2004; Nakamura *et al*., 2003). They neither mix with common organic solvents nor with water at room temperature, thus forming biphasic systems, and they dissolve fluorine-rich compounds well. Ionic liquids (Lei *et al*., 2017; Welton, 2018) are salts that exist in a liquid state at relatively low temperatures, often below 100°C. They are characterized by their low volatility (Earle *et al*., 2006), wide liquid range, and tunable properties, making them versatile solvents for various chemical reactions, including catalysis and separation processes (Shah, An & Muhammad, 2020). Deep eutectic solvents (DES) are a class of solvents formed by mixing two or more solid or liquid components to create an eutectic mixture with a lower melting point than each individual component (Smith, Abbott & Ryder, 2014). DES exhibits properties similar to traditional organic solvents but with lower toxicity and environmental impact, making them suitable for a wide range of applications, including biomass processing and organic synthesis (Zhang *et al*., 2012; Hansen *et al*., 2020).

Applications of green solvents in chemical processes

In recent years, there has been a growing emphasis on sustainability and environmental responsibility in the chemical industry. One area where significant progress has been made is in the development and application of green solvents and reaction media (Hessel *et al*., 2022; Sheldon, 2005). These environmentally friendly alternatives offer numerous benefits across various chemical processes, from solvent extraction and organic synthesis to polymerization and cleaning processes. In this article, we'll explore the applications of green solvents in chemical processes, with a focus on solvent extraction and separation techniques, organic synthesis and catalysis, polymerization and material synthesis, cleaning and degreasing processes and their importance as sustainable reaction media. Solvent extraction and separation techniques play a crucial role in various industries, including pharmaceuticals, mining and waste treatment (Brahmachari, 2015; Chaudhuri, Ghosh & Chattopadhyay, 2021). Traditional organic solvents used in these processes, such as chlorinated hydrocarbons and aromatic compounds, often pose significant environmental and health risks. Green solvents offer a safer and more sustainable alternative by reducing toxicity and environmental impact. For example, supercritical carbon dioxide (CO_2) has been widely used for extraction processes due to its low toxicity, non-flammability, and recyclability (Zorić *et al*., 2022; Gulzar *et al*., 2020).

In organic synthesis and catalysis, the choice of solvent can profoundly influence reaction outcomes in terms of yield, selectivity, and reaction rate. Green solvents, such as water, ionic liquids, and fluorinated solvents, have emerged as viable alternatives to conventional organic solvents. Water, in particular, is abundant, cheap, and environmentally benign, making it an attractive solvent for a wide range of chemical processes, including hydrothermal reactions and aqueous-phase catalysis (Simon & Li, 2012; Lajoie, Fabiano-Tixier & Chemat, 2022; Castro-Puyana, Marina, & Plaza, 2017). Ionic liquids, on the other hand, offer unique properties such as low volatility, high thermal stability, and tunable solvation properties, making them versatile reaction media for various catalytic processes (Tang *et al*., 2012; Greer, Jacquemin & Hardacre, 2020). Different fluorinated solvents are used for cell culture (Kasuya *et al*., 2011) and batteries (Narayan & Dominko, 2022; Besenhard *et al*., 1999).

Polymerization and material synthesis represent another area where green solvents play a significant role in reducing environmental impacts. Conventional polymerization processes often rely on volatile organic solvents, which can contribute to air pollution and pose health risks to workers. Green solvents, such as bio-based solvents derived from renewable resources, offer a more sustainable alternative for polymerization processes. For example, bio-based solvents like ethanol and glycerol have been successfully used in the synthesis of biodegradable polymers and composites (Gu & Jérôme, 2013). Cleaning and degreasing processes in industries such as automotive,

aerospace and electronics manufacturing typically involve the use of hazardous solvents like chlorinated hydrocarbons and petroleum-based solvents. These solvents not only pose risks to human health and the environment but also contribute to air and water pollution. Green solvents, such as terpenes, d-limonene, and soy-based solvents, offer effective alternatives for cleaning and degreasing applications. These solvents are derived from renewable resources, are biodegradable and have low toxicity, making them environmentally friendly choices for industrial cleaning processes. In the pharmaceutical and agrochemical industries, the development of green solvents and reaction media is of paramount importance due to the stringent regulations and growing consumer demand for sustainable products. Green solvents offer several advantages in pharmaceutical and agrochemical synthesis, including improved reaction selectivity, reduced waste generation, and lower environmental impact. For example, the use of ionic liquids as reaction media has enabled the synthesis of pharmaceutical intermediates with higher purity and yield compared to conventional solvents (Petkovic *et al*., 2011). Deep Eutectic solvents are used for protein extraction (Bowen *et al*., 2022), in drug discovery (Oyoun *et al*., 2023) and cellulose dissolution (Chen *et al*., 2019). DES is the solvent for 21stcentury (Paiva *et al*., 2014).

In addition to specific applications, the importance of green reaction media lies in their role as sustainable alternatives that contribute to the overall reduction of environmental impact in chemical processes. Design considerations for green reaction media include solvent-free systems, aqueous solutions, ionic liquids, and other environmentally benign solvents. By optimizing reaction conditions and choosing appropriate green solvents, chemists can achieve enhanced reaction rates, selectivity, and yield while minimizing waste generation and energy consumption. Several case studies demonstrate the successful implementation of green reaction media in various chemical transformations. For instance, the use of water as a solvent for metal-catalyzed reactions has led to significant advancements in cross-coupling reactions, hydrogenation, and C-H activation (Cortes-Clerget *et al*., 2021). Similarly, ionic liquids have been employed as reaction media for biomass conversion, olefin metathesis, and organocatalytic reactions, showcasing their versatility and efficacy in sustainable synthesis. By choosing environmentally friendly alternatives and optimizing reaction conditions, chemists can achieve more sustainable and environmentally responsible chemical transformations. Through continued research and innovation, the widespread adoption of green solvents is poised to play a crucial role in shaping the future of the chemical industry in a more sustainable and environmentally friendly direction.

Challenges and future perspectives

The adoption of green solvents and reaction media represents a significant step towards enhancing the sustainability of chemical processes. However, several challenges (Castiello *et al*., 2023) remain in achieving widespread adoption and maximizing their

potential impact on environmental and human health. One of the primary challenges lies in the limited availability of green solvents that can effectively replace conventional, often hazardous, solvents across a wide range of chemical reactions. While significant progress has been made in identifying and developing alternative solvents, there are still many reactions for which suitable green alternatives have not been found. Additionally, the scalability and cost-effectiveness of these green solvents remain important considerations, especially for industrial applications. Further research is essential to address these challenges and advance the development of novel green solvents and reaction systems. This research should focus on designing solvents with tailored properties to meet the specific requirements of different reactions, as well as improving their synthesis processes to enhance efficiency and reduce costs. Additionally, exploring innovative approaches such as solvent-free and aqueous-based reactions can expand the repertoire of green reaction media available to chemists.

Integration of green solvent principles into chemical education and industrial practices is another critical aspect that requires attention. Educating future generations of chemists about the importance of sustainability and providing training on green chemistry principles will foster a culture of responsible chemical design and synthesis. Similarly, incorporating green solvent metrics and guidelines into industrial practices can help industries make informed decisions to minimize their environmental footprint and comply with regulatory requirements. Looking toward the future, the widespread adoption of green solvents and reaction media holds immense promise for advancing sustainability in the chemical industry. By reducing reliance on hazardous and non-renewable resources, these greener alternatives can significantly decrease the environmental impact of chemical processes, mitigating pollution and conserving natural resources. Moreover, the adoption of green chemistry principles can drive innovation and lead to the development of cleaner, more efficient technologies, ultimately benefiting both the industry and society as a whole.

Conclusion

Green solvents and reaction media play a pivotal role in advancing sustainable chemical processes, heralding a transformative shift towards environmentally conscious practices within the chemical industry. Their significance lies in their ability to mitigate the environmental impact traditionally associated with chemical synthesis while enhancing efficiency and safety. By substituting hazardous solvents with eco-friendly alternatives derived from renewable resources or possessing minimal toxicity, green chemistry principles are upheld, fostering a more harmonious relationship between chemical production and the ecosystem. The adoption of green solvents and reaction media is imperative in addressing pressing environmental challenges such as pollution, resource depletion, and climate change. These alternatives minimize the generation of harmful by-products, reduce energy consumption, and offer safer working conditions for

personnel, thereby aligning chemical processes with sustainability goals. Moreover, their implementation promotes circular economy principles by facilitating the recycling and reuse of resources, contributing to the conservation of natural resources and reducing waste. To further propel the integration of green solvents and reaction media into mainstream chemical practices, continued research and innovation are paramount. Collaborative efforts among academia, industry, and government entities should be intensified to develop novel green solvents, optimize existing processes, and enhance their scalability and cost-effectiveness. Additionally, educational initiatives should be bolstered to raise awareness among stakeholders about the benefits of green chemistry and foster a culture of sustainability within the chemical community. Looking ahead, envisioning a greener and more sustainable future in the chemical industry necessitates a steadfast commitment to green chemistry principles and the widespread adoption of environmentally benign practices. By embracing innovation, collaboration, and responsible stewardship, the industry can transition towards a circular economy model characterized by resource efficiency, waste reduction, and ecological integrity. Through concerted action and collective determination, we can pave the way for a thriving chemical sector that not only meets the demands of the present but also safeguards the well-being of future generations and the planet. Let us seize this opportunity to catalyze positive change and forge a path towards a truly sustainable future.

Acknowledgment

The authors would like to thank Dr. Indranil Kar, Principal, Surendranath College, Mr. Arpan Kantal and Mr. Nabendu Mandal, Assistant Teacher of Harindanga High School, India for their constant support and encouragement.

References

Anastas, P. T., & Warner, J. C. (2000). *Green Chemistry: Theory and Practice*. Oxford university press. https://doi.org/10.1093/oso/9780198506980.001.0001

Besenhard, J., Möller, K. C., Winter, M., Wrodnigg, G., & Hodal, T. (1999). Fluorinated organic solvents in electrolytes for lithium ion cells. *ITE Battery Letters*, *1*, 105-105.

Bowen, H., Durrani, R., Delavault, A., Durand, E., Chenyu, J., Yiyang, L., ... & Fei, G. (2022). Application of deep eutectic solvents in protein extraction and purification. *Frontiers in Chemistry*, *10*, 912411. https://doi.org/10.3389/fchem.2022.912411

Brahmachari, G. (2015). Green synthetic approaches for biologically relevant 2-amino-4H-pyrans and 2-amino-4H-pyran-annulated heterocycles in aqueous media. In *Green Synthetic Approaches for Biologically Relevant Heterocycles* (pp. 185-208). Elsevier. https://doi.org/10.1016/B978-0-12-820792-5.00016-0

Budisa, N., & Schulze-Makuch, D. (2014). Supercritical carbon dioxide and its potential as a life-sustaining solvent in a planetary environment. *Life*, *4*(3), 331-340. https://doi.org/10.3390/life4030331

Byrne, F. P., Jin, S., Paggiola, G., Petchey, T. H., Clark, J. H., Farmer, T. J., ... & Sherwood, J. (2016). Tools and techniques for solvent selection: green solvent selection guides. *Sustainable Chemical Processes*, *4*, 1-24. https://doi.org/10.1186/s40508-016-0051-z

Capello, C., Fischer, U., & Hungerbühler, K. (2007). What is a green solvent? A comprehensive framework for the environmental assessment of solvents. *Green Chemistry*, *9*(9), 927-934. https://doi.org/10.1039/B617536H

Castiello, C., Junghanns, P., Mergel, A., Jacob, C., Ducho, C., Valente, S., & Mai, A. (2023). GreenMedChem: the challenge in the next decade toward eco-friendly compounds and processes in drug design. *Green Chemistry*, *25*(6), 2109-2169. https://doi.org/10.1039/D2GC03772F

Castro-Puyana, M., Marina, M. L., & Plaza, M. (2017). Water as green extraction solvent: Principles and reasons for its use. *Current Opinion in Green and Sustainable Chemistry*, *5*, 31-36. https://doi.org/10.1016/j.cogsc.2017.03.009

Chaudhuri, S., Ghosh, A., & Chattopadhyay, S. K. (2021). Green synthetic approaches for medium ring–sized heterocycles of biological and pharmaceutical interest. In *Green Synthetic Approaches for Biologically Relevant Heterocycles* (pp. 617-653). Elsevier. https://doi.org/10.1016/B978-0-12-820792-5.00004-4

Chen, Y. L., Zhang, X., You, T. T., & Xu, F. (2019). Deep eutectic solvents (DESs) for cellulose dissolution: a mini-review. *Cellulose*, *26*, 205-213. https://doi.org/10.1007/s10570-018-2130-7

Clarke, C. J., Tu, W. C., Levers, O., Brohl, A., & Hallett, J. P. (2018). Green and sustainable solvents in chemical processes. *Chemical Reviews*, *118*(2), 747-800. https://doi.org/10.1021/acs.chemrev.7b00571

Cortes-Clerget, M., Yu, J., Kincaid, J. R., Walde, P., Gallou, F., & Lipshutz, B. H. (2021). Water as the reaction medium in organic chemistry: from our worst enemy to our best friend. *Chemical science*, *12*(12), 4237-4266. https://doi.org/10.1039/D0SC06000C

Devi, B. K., Naraparaju, S., Soujanya, C., & Gupta, S. D. (2020). Green chemistry and green solvents: an overview. *Current Green Chemistry*, *7*(3), 314-325. https://doi.org/10.2174/2213346107999200709132815

Earle, M. J., Esperança, J. M., Gilea, M. A., Canongia Lopes, J. N., Rebelo, L. P., Magee, J. W., ... & Widegren, J. A. (2006). The distillation and volatility of ionic liquids. *Nature*, *439*(7078), 831-834. https://doi.org/10.1038/nature04451

Erythropel, H. C., Zimmerman, J. B., de Winter, T. M., Petitjean, L., Melnikov, F., Lam, C. H., ... & Anastas, P. T. (2018). The Green ChemisTREE: 20 years after taking root with the 12 principles. *Green Chemistry*, *20*(9), 1929-1961. https://doi.org/10.1039/C8GC00482J

Gladysz, J. A., & Emnet, C. (2004). Fluorous solvents and related media. *Handbook of Fluorous Chemistry*, 11-23. https://doi.org/10.1002/3527603905.ch3

Greer, A. J., Jacquemin, J., & Hardacre, C. (2020). Industrial applications of ionic liquids. *Molecules*, *25*(21), 5207. https://doi.org/10.3390/molecules25215207

Gu, Y., & Jérôme, F. (2013). Bio-based solvents: an emerging generation of fluids for the design of eco-efficient processes in catalysis and organic chemistry. *Chemical Society Reviews*, *42*(24), 9550-9570. https://doi.org/10.1039/C3CS6024

Gulzar, A., Gulzar, A., Ansari, M. B., He, F., Gai, S., & Yang, P. (2020). Carbon dioxide utilization: A paradigm shift with CO_2 economy. *Chemical Engineering Journal Advances*, *3*, 100013. https://doi.org/10.1016/j.ceja.2020.100013

Hansen, B. B., Spittle, S., Chen, B., Poe, D., Zhang, Y., Klein, J. M., & Sangoro, J. R. (2020). Deep eutectic solvents: A review of fundamentals and applications. *Chemical Reviews*, *121*(3), 1232-1285. https://doi.org/10.1021/acs.chemrev.0c00385

Hansen, H., & Wilbur, S. B. (1994). *Toxicological profile for acetone*. U.S. Department of Health and Human Services Public Health Service

Agency for Toxic Substances and Disease Registry, Atlanta, Georgia

Hessel, V., Tran, N. N., Asrami, M. R., Tran, Q. D., Long, N. V. D., Escribà-Gelonch, M., ... & Sundmacher, K. (2022). Sustainability of green solvents–review and perspective. *Green Chemistry*, *24*(2), 410-437.

Joshi, D. R., & Adhikari, N. (2019). An overview on common organic solvents and their toxicity. *Journal of Pharmaceutical Research International*, *28*(3), 1-18. https://doi.org/10.9734/jpri/2019/v28i330203

Jv, B. (2001). Toxic effect of solvents and vapors. *Casarett & Doull's Toxicology. The Basic Science of Poisons*.

Kasuya, M. C. Z., Wen, X., Hatanaka, K., & Akashi, K. (2011). Fluorous solvent for cell culture. *Journal of Fluorine Chemistry*, *132*(11), 978-981. https://doi.org/10.1016/j.jfluchem.2011.06.028

Lajoie, L., Fabiano-Tixier, A. S., & Chemat, F. (2022). Water as green solvent: methods of solubilisation and extraction of natural products—past, present and future solutions. *Pharmaceuticals*, *15*(12), 1507. https://doi.org/10.3390/ph15121507

Lei, Z., Chen, B., Koo, Y. M., & MacFarlane, D. R. (2017). Introduction: ionic liquids. *Chemical Reviews*, *117*(10), 6633-6635. https://doi.org/10.1021/acs.chemrev.7b00246

Madan, V. K. (2018). Supercritical Carbon Dioxide as Greener Solvent of 21 st Century. *Asian Journal of Chemistry*, *30*(4). https://doi.org/10.14233/ajchem.2018.21150A

Nakamura, H., Usui, T., Kuroda, H., Ryu, I., Matsubara, H., Yasuda, S., & Curran, D. P. (2003). Fluorous solvent as a new phase-screen medium between reagents and reactants in the bromination and chlorination of alcohols. *Organic Letters*, *5*(8), 1167-1169. https://doi.org/10.1021/ol034060w

Narayan, R., & Dominko, R. (2022). Fluorinated solvents for better batteries. *Nature Reviews Chemistry*, *6*(7), 449-450. https://doi.org/10.1038/s41570-022-00387-5

Oyoun, F., Toncheva, A., Henríquez, L. C., Grougnet, R., Laoutid, F., Mignet, N., ... & Corvis, Y. (2023). Deep Eutectic Solvents: An Eco-friendly Design for Drug Engineering. *ChemSusChem*, *16*(20), e202300669. https://doi.org/10.1002/cssc.202300669

Paiva, A., Craveiro, R., Aroso, I., Martins, M., Reis, R. L., & Duarte, A. R. C. (2014). Natural deep eutectic solvents–solvents for the 21st century. *ACS Sustainable Chemistry & Engineering*, *2*(5), 1063-1071. https://doi.org/10.1021/sc500096j

Petkovic, M., Seddon, K. R., Rebelo, L. P. N., & Pereira, C. S. (2011). Ionic liquids: a pathway to environmental acceptability. *Chemical Society Reviews*, *40*(3), 1383-1403. https://doi.org/10.1039/C004968A

Shah, F. U., An, R., & Muhammad, N. (2020). Properties and applications of ionic liquids in energy and environmental science. *Frontiers in Chemistry*, *8*, 627213. https://doi.org/10.3389/fchem.2020.627213

Sheldon, R. A. (2005). Green solvents for sustainable organic synthesis: state of the art. *Green Chemistry*, *7*(5), 267-278. https://doi.org/10.1039/B418069K

Simon, M. O., & Li, C. J. (2012). Green chemistry oriented organic synthesis in water. *Chemical Society Reviews*, *41*(4), 1415-1427. https://doi.org/10.1039/C1CS15222J

Smith, E. L., Abbott, A. P., & Ryder, K. S. (2014). Deep eutectic solvents (DESs) and their applications. *Chemical Reviews*, *114*(21), 11060-11082. https://doi.org/10.1021/cr300162p

Tang, B., Bi, W., Tian, M., & Row, K. H. (2012). Application of ionic liquid for extraction and separation of bioactive compounds from plants. *Journal of Chromatography B*, *904*, 1-21. https://doi.org/10.1016/j.jchromb.2012.07.020

Vovers, J., Smith, K. H., & Stevens, G. W. (2017). Bio-based molecular solvents. In *The Application of Green Solvents in Separation Processes* (pp. 91-110). Elsevier. https://doi.org/10.1016/B978-0-12-805297-6.00004-8

Welton, T. (2015). Solvents and sustainable chemistry. *Proceedings of the Royal Society A: Mathematical, Physical and Engineering Sciences*, *471*(2183), 20150502. https://doi.org/10.1098/rspa.2015.0502

Welton, T. (2018). Ionic liquids: a brief history. *Biophysical Reviews*, *10*(3), 691-706. https://doi.org/10.1007/s12551-018-0419-2

Winterton, N. (2021). The green solvent: A critical perspective. *Clean Technologies and Environmental Policy*, *23*(9), 2499-2522. https://doi.org/10.1007/s10098-021-02188-8

Zhang, Q., Vigier, K. D. O., Royer, S., & Jérôme, F. (2012). Deep eutectic solvents: syntheses, properties and applications. *Chemical Society Reviews*, *41*(21), 7108-7146. https://doi.org/10.1039/C2CS35178A

Zhou, F., Hearne, Z., & Li, C. J. (2019). Water—the greenest solvent overall. *Current Opinion in Green and Sustainable Chemistry*, *18*, 118-123. https://doi.org/10.1016/j.cogsc.2019.05.004

Zorić, M., Banožić, M., Aladić, K., Vladimir-Knežević, S., & Jokić, S. (2022). Supercritical CO2 extracts in cosmetic industry: Current status and future perspectives. *Sustainable Chemistry and Pharmacy*, *27*, 100688. https://doi.org/10.1016/j.scp.2022.100688

.

doi: 10.31674/book.2024ecc.009

Recent Developments in the Biological Activities of 2-Pyrazoline Derivatives

Attreyee Mukherjee

Department of Chemistry, Ananda Mohan College, Kolkata, West Bengal, India

Corresponding Author's Email: attreyee.m@gmail.com

Abstract

Pyrazolines, a significant class of heterocyclic compounds, have gathered attention in medicinal chemistry for their diverse biological activities. In recent years, scientists have explored structural modifications, leading to pharmacologically active derivatives incorporated into therapeutic agents. 2-pyrazoline scaffold is found to be present in various important drug molecules e.g antipyrine, phenylbutazone, oxyphenbutazone, ibipinabant, ramiphenazone etc. 2- Pyrazoline derivatives have been reported to possess broad-spectrum biological activities such as antimalarial, antidepressant, antiinflammatory, antitumor, antibacterial, anticancer and also MAO (monoamine oxidase), acetylcholine esterase (AChE), cannabinoid (CB_1) etc. inhibitory activities. Pyrazoline based drugs are also used to treat neurodegenerative diseases such as Alzheimer's disease, Perkinson's disease, psychiatric disorders etc. The variation of substituents in the pyrazoline scaffold has had a tremendous impact on biological activity. It has been shown from different research studies that the electronegativity and steric factor of the substituents present in N-1, C-3 and C-5 positions have a great influence on the biological properties of the compounds. This article will cover numerous biological significances of 2-pyrazoline based compounds in medicinal chemistry and SAR (structure-activity relationship) for the improvement of therapeutic implications.

Keywords: *Biological Activity; Pharmacologically Active; 2-Pyrazoline; Structure-Activity Relationship*

Introduction

Pyrazolines, five-membered heterocycles with two adjacent nitrogens, have emerged with huge attention from organic and medicinal chemists due to their potent biological activities and the numerous possibilities for structural diversification. Among three isomers of pyrazolines, 2-pyrazoline is most common in the literature and it has huge applications in the field of medicine. 2-pyrazoline scaffold is present in a number of drug molecules, such as antipyrine, ibipinabant, ramiphenazone, oxyphenbutazone, phenylbutazone etc. A wide spectrum of biological activities has been found in the pyrazoline based heterocyclic compounds (Nehra *et al.*, 2020). Pyrazoline derivatives are reported to possess biological activities such as anti-inflammatory (Mantzanidou, Pontiki & Hadjipavlou-Litina, 2021), antimalarial (Ravindar *et al.,* 2023), anticancer

(Haider *et al.,* 2022), antitubercular (Joshi *et al.,* 2016), antifungal (Elewa *et al*., 2020), antidepressant (Kaplancıklı *et al.,* 2010), antitumor (Matiadis & Sagnou, 2020) and cholinesterase (Mishra & Sasmal, 2013), EGFR tyrosine kinase (Sahoo *et al.,* 2010), cannabinoid CB1 (Lange *et al.,* 2010) inhibitory activities. Modern research on pyrazoline scaffold reveals that the biological property of this heterocycle is largely influenced by the substituents present N1, C3, C5 position. This review covers the various biological activities of pyrazoline derivatives.

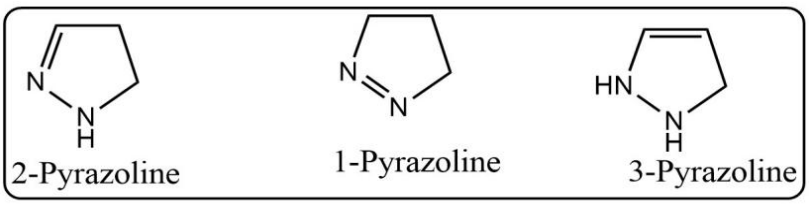

Scheme 1

Biological Activities of 2-Pyrazoline Derivatives

Antiinflammatory activity

Eid and George (2018) synthesised new pyrazoline derivatives attached to the furan and thiophene ring at C-3 and acetyl and amide group at N1and examined *in vivo* anti-inflammatory activity. The compounds are reported to exhibit potent anti-inflammatory activity. It was also shown by the researcher that furan appended N-acetyl pyrazolines possess better activity than the thiophene pyrazoline derivatives.

New phenyl-pyrazoline-coumarin hybrids were synthesised by Chen *et al.* (2017) and the results of *in vivo* anti-inflammatory activity showed significant inhibition in edema.

Abdel-Sayed *et al.* (2016) synthesised 1,3,5-trisubstituted pyrazoline derivatives and evaluated for *in vivo* anti-inflammatory activity. Some of the compounds showed no inhibition of COX-1 up to 100 μM, but 3-phenyl 5-(4-nitrophenyl)N-acetylphenylpyrazoline and 3-(4-fluorophenyl) 5-(4-nitrophenyl)N-acetylphenylpyrazoline exhibited *in vitro* COX-2 inhibitory activity with IC_{50} values of 10 and 12.1, respectively. Barsoum, Hosni and Girgis (2006) synthesized novel bis(1-acyl-2-pyrazolines) derivatives and reported remarkable anti-inflammatory properties with a lower ulcerogenic liability than standard drug used. The synthesis and *in vivo* screening of a new series of fluoro substituted pyrazoline derivatives were reported by Jadhav *et al.* (2013) and the results showed that the compounds exhibited antiinflammatory and analgesic activity.

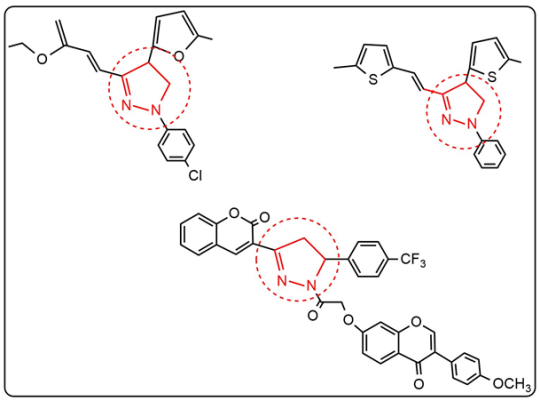

Figure 1: Pyrazoline as anti-inflammatory agents

Antimalarial activity

A series of novel pyrazolepyrazoline derivatives bearing benzenesulfonamide were synthesized (Kumar *et al.*, 2018) and evaluated for *in vitro*, and *in vivo* antimalarial activity. The test results revealed that some of the compounds exhibited significant activity against CQS and CQR strains of *P. falciparum*. It was observed by the researchers that the substituents on the pyrazole and pyrazoline rings control the activity. R_1= -Me, -OMe enhances the activity, while monohalo and dihalo substitutions lower the activity.

The antimalarial activity of a series of newly synthesised oxazoline pyrazoline derivatives was evaluated (Pandey *et al.*, 2016); among them, compounds with 4-methoxyphenyl substitution showed significant potential against *P. falciparum.* Both *in vivo* and *in vitro* studies against *P. falciparum* and *P. berghei* showed satisfactory result with 79.33% and 63.89% suppression of parasitemia at a dose of 50 mg/kg and 25 mg/kg, respectively, on day 4.

Marella *et al.* (2015) synthesised and examined new pyrimidine cubbed nitrile-pyrazoline hybrid derivatives for *in vitro* gametocytocidal activity, and the results indicated that most of the compounds exhibited promising antimalarial activity against the chloroquine-sensitive (CQS, 3D7) strain of *P. falciparum.* SAR studies showed that (a) -OMe substitution in ring A enhances the potency; (b) dimethoxy and trimethoxy substitution in ring C was reported to be most effective.

Akhter *et al.* (2015) reported a series of coumarin based pyrazoline derivatives and examined antimalarial and antimicrobial activity. The compound with 3,4,5-trimethoxybenzene showed the highest inhibitory activities against CQs strain of *P. falciparum* with IC_{50} 11.63 µg/mL. The activity was enhanced by (a) the number of methoxy group present in the phenyl group. (b) Bulky group substituted N1and acyl, phenyl substituted N1. Some synthesized derivatives were also evaluated for antimicrobial activity against *E. coli* and *S. aureus* and fungal strains *R. oryza* and

P.citrum with MIC values 10, 12.5 and 12.5 µg/mL against *S.aureus, E.coli* and *R.oryza* respectively.

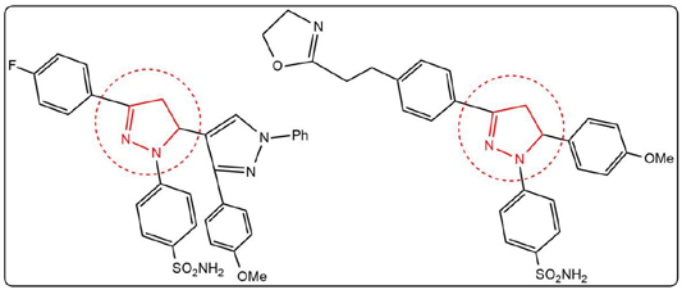

Figure 2: Pyrazoline as anti-malarial agents

Anticancer activity

In recent years, a number of chemotherapeutic drugs have been used that contain nitrogen heterocycles and pyrazoline moiety, such as axitinib (Wu, Nielsen & Clausen, 2015) (renal cell carcinoma treatment) and ibrutinib (Byrd *et al.*, 2013) (chronic lymphocytic leukemia treatment).

Some of the compounds were reported as therapeutic agents to treat drug-resistant breast cancer. The compounds were synthesised and evaluated by Luan *et al.* (2017) and it has been shown that these have high sensitivity against MCF-7/Adr cell lines.

The coumarin based pyrazolines showed antiproliferative activity and some of the compounds were also treated as cytotoxic agents.

Wu and coworkers (2014) showed inhibitory activity against tolemerase with IC_{50} 0.92 µM, supposed to cause the inhibition of cancer cells growth. Wei and coworkers (2018) synthesised pyrazolines and examined for anticancer activity and concluded that this compound exhibited inhibitiry activity with IC_{50} 4.7 for A549 lung cancer cell.

Mehmood *et al.* (2022) synthesised a series of 1,3,5-triaryl 2-pyrazoline and examined for anticancer activity. The compound showed inhibitory activities against urease and some of the synthesised compounds were found to inhibit strongly against α-glucosidase. SAR studies revealed that size and ewg and edg group affected the activity. The compounds were also found to have cytotoxic activity against MCF-7 and HeLa cell lines.

The author synthesised series of pyrazoloyl pyrazoline and one of the compounds (5-ethoxy pyrazoline derivative) coupled with doxorubicine (PYZ-DOX) was applied for bioimaging in the living HepG2 cells (Rana, Dhar & Bhattacharya, 2014; Mukherjee & Mahalanabis, 2009). The Compound showed fluorescent blue image while incubated to living HepG2 cells but when coupled with DOX, it showed strong fluorescent red image.

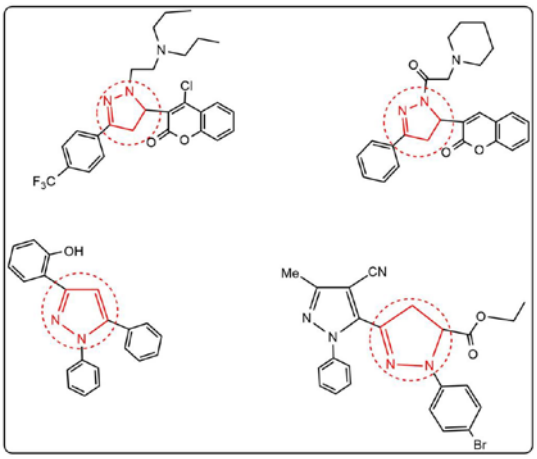

Figure 3: Pyrazoline as anticancer agents

Antibacterial and antifungal activity

The design and synthesis of a series of new 1,3,5-trisubstitutedpyrazolines were reported by Mishra *et al*. (2017) and compounds with fluoro/chlorophenyl substitution at 3-position of pyrazoline derivatives showed strong antibacterial activity against bacterial strains *S. aureus* and *B. subtilis* (gram positive) and *E. coli* (gram negative) having MIC values3.25-25µg/Ml. *In vitro* antifungal study of one of the pyrazoline derivative in the series showed very satisfactory result.

The new series of thiophene based pyrazolines was reported by Edrees *et al.* (2018) and their antifungal evaluation showed potent activity against the fungal strains *A. fumigatus* and *C. albicans*.

Montoya *et al.* (2016) synthesised novel substituted 2-pyrazoline derivatives containing 7-chloro 4-aminoquinoline moiety and evaluation of antifungal test showed satisfactory results. The strong antofungal effects were shown against *C. albicans and C. neoformans* compared to the drug Amphotericin B.

Some pyrazoline derivatives with a sulfonamide moiety (Sadashiva *et al.,* 2017) found to exhibit antituberculosis activities with MIC values 0.8 to 100 µg/mL compared to pyrazinamide (3.125µg/mL). All the compounds were reported to possess antibacterial and antifungal activity against *S. aureus* and *B. subtilis* (gram positive) and *E. coli*, *P. aeruginosa* (gram negative) bacteria and *A. niger, C. albicans, A. fumigatus* and *A. flavus* fungal strains. In vitro antimicrobial studies showed that most of the compounds in this series exhibited strong antibacterial and antifungal activities.

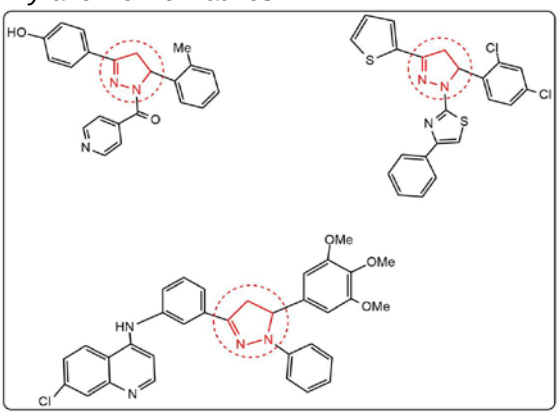

Figure 4: Pyrazoline as antibacterial and antifungal agents

MAO inhibitory activities

Salgin-Goksen *et al*. (2021) synthesised new 2-pyrazoline and acetohydrazide derivatives and tested for MAO inhibitory activity. The results showed the selective MAO-A inhibitor activity. The in vitro studies of hydrazone derivatives revealed the compounds exhibit strong inhibition toward hMAO-A.

All of the compounds exhibited antidepressant activity (Salgin-Goksen *et al*., 2021). It has been reported by Nair *et al.* (2021) that the halogenated phenyl ring at the 5-position of the pyrazoline ring increases the potency against MAO-B and the activity increases in the order F>Cl>Br> I. Tripathi and his coworkers (2016) designed some novel 3,5-disubstituted 2-pyrazoline derivatives and the *in vivo* antidepressant study showed a good to moderate response.

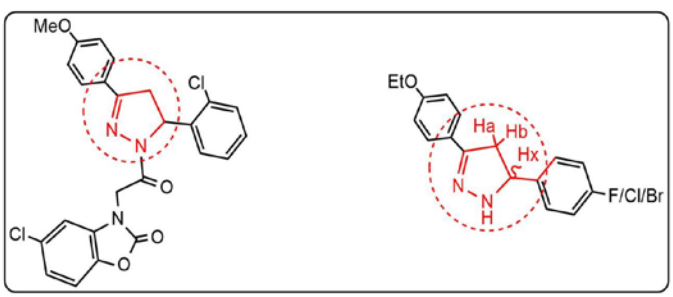

Figure 5: Pyrazoline having MAO Inhibitory Activities

Carbonic anhydrase inhibitory activities

Carbonic anhydrase is an enzyme that helps in the interconversion of CO_2 and H_2O and dissociates ions of carbonic acid. Several diseases epilepsy, glaucoma, obesity, cancer, tumor cell growth are associated with CA. CA inhibition controls these diseases. Alaa and co-workers (2019) reported the synthesis of some novel 1,3,5-trisubstituted 2-pyrazoline derivatives with benzene sulfonamide fragments, and in vitro assay results

revealed the inhibitory effect against hCA1. Moi *et al*. (2019) synthesised and evaluated pyrazoline based aromatic sulfamate derivatives and in vitro studies of most of the compounds showed strong inhibition against hCAII.

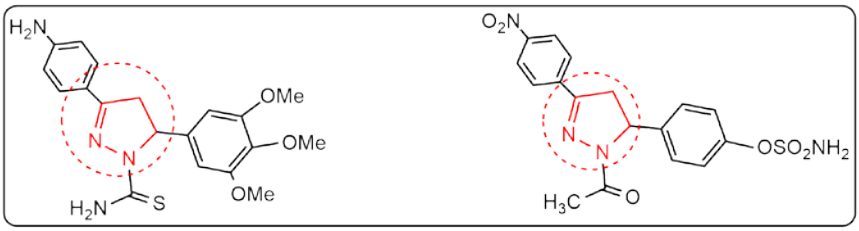

Figure 6: Pyrazoline having Carbonic anhydrase Inhibitory Activities

Table 1: *Clinically used Drugs containing pyrazoline ring*

Sl. no.	**Name of the drug**	**Structure of the compound**	**Clinical Use**
1.	Phenylbutazone	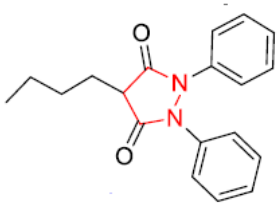	Anti-inflammatory drug (NSID), analgesic, antipyretic.
2.	Antipyrine	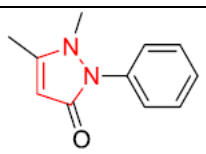	Anti-inflammatory drug (NSID), analgesic, antipyretic
3.	Metamizole	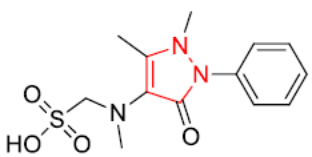	analgesic, antipyretic
4.	Enficoxib (E-6087)	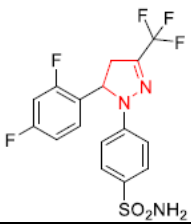	NSID for treatment of osteoarthritis pain, inhibits selectively the enzyme COX-2.

5.	(SLV-330)	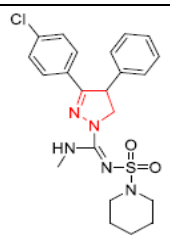	CB_1 receptor antagonist for the treatment of CNS disorder
6.	GDC-0941	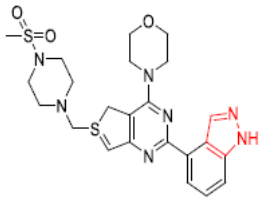	Anticancer agent, P13 kinase inhibitor
7.	YC-1	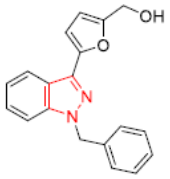	Anticancer agent, inhibits abnormal cell growth
8.	Axinib	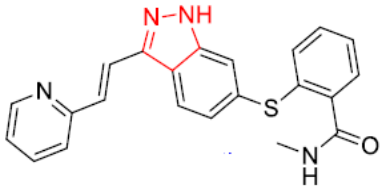	Anticancer drug for the treatment of metastatic renal cell carcinoma.

Conclusion

In this review, the biological activities such as anti-inflammatory, antimalarial, anticancer, antibacterial, MAO inhibitory activities, and CA inhibitory activities of various pyrazoline derivatives have been discussed. The SAR study reveals that the activity of pyrazoline derivatives depends on the substituents present in pyrazoline. The biological activities are evaluated by in vitro and in vivo studies of the compounds discussed in this literature. In conclusion, pyrazoline is now an important pharmacophore for new drug design.

Acknowledgement

The author is thankful to the Department of Chemistry, Ananda Mohan College, Kolkata. The author is grateful to Prof. K. K. Mahalanabis, Department of Chemistry, Jadavpur University, for his constant support.

References

Abdel-Sayed, M. A., Bayomi, S. M., El-Sherbeny, M. A., Abdel-Aziz, N. I., ElTahir, K. E. H., Shehatou, G. S., & Alaa, A. M. (2016). Synthesis, anti-inflammatory, analgesic, COX-1/2 inhibition activities and molecular docking study of pyrazoline derivatives. *Bioorganic & Medicinal Chemistry*, *24*(9), 2032-2042. https://doi.org/10.1016/j.bmc.2016.03.032

Akhter, W., Marella, A., Shaquiquzzaman, M., Akhter, M., & Alam, M. M. (2015). Microwave assissted synthesis of pyrazoline-coumarin hybrids and their in-vitro antimalarial evaluation. *Journal of Pharmacy Research*, *9*(5), 318-322.

Alaa, A. M., El-Azab, A. S., Bua, S., Nocentini, A., El-Enin, M. A. A., Alanazi, M. M., ... & Supuran, C. T. (2019). Design, synthesis, and carbonic anhydrase inhibition activity of benzenesulfonamide-linked novel pyrazoline derivatives. *Bioorganic Chemistry*, *87*, 425-431. https://doi.org/10.1016/j.bioorg.2019.03.052

Barsoum, F. F., Hosni, H. M., & Girgis, A. S. (2006). Novel bis (1-acyl-2-pyrazolines) of potential anti-inflammatory and molluscicidal properties. *Bioorganic & Medicinal Chemistry*, *14*(11), 3929-3937. https://doi.org/10.1016/j.bmc.2006.01.042

Byrd, J. C., Furman, R. R., Coutre, S. E., Flinn, I. W., Burger, J. A., Blum, K. A., ... & O'Brien, S. (2013). Targeting BTK with ibrutinib in relapsed chronic lymphocytic leukemia. *New England Journal of Medicine*, *369*(1), 32-42. https://doi.org/10.1056/NEJMoa1215637

Chen, L. Z., Sun, W. W., Bo, L., Wang, J. Q., Xiu, C., Tang, W. J., ... & Liu, X. H. (2017). New arylpyrazoline-coumarins: Synthesis and anti-inflammatory activity. *European Journal of Medicinal Chemistry*, *138*, 170-181. https://doi.org/10.1016/j.ejmech.2017.06.044

Edrees, M. M., Melha, S. A., Saad, A. M., Kheder, N. A., Gomha, S. M., & Muhammad, Z. A. (2018). Eco-friendly synthesis, characterization and biological evaluation of some novel pyrazolines containing thiazole moiety as potential anticancer and antimicrobial agents. *Molecules*, *23*(11), 2970. https://doi.org/10.3390/molecules23112970

Eid, N. M., & George, R. F. (2018). Facile synthesis of some pyrazoline-based compounds with promising anti-inflammatory activity. *Future Medicinal Chemistry*, *10*(02), 183-199. https://doi.org/10.4155/fmc-2017-0144

Elewa, S. I., Mansour, E., Nassar, I. F., & Mekawey, A. A. (2020). Synthesis of some new pyrazoline-based thiazole derivatives and evaluation of their antimicrobial, antifungal, and anticancer activities. *Russian Journal of Bioorganic Chemistry*, *46*, 382-392.

Haider, K., Shafeeque, M., Yahya, S., & Yar, M. S. (2022). A comprehensive review on pyrazoline based heterocyclic hybrids as potent anticancer agents. *European Journal of Medicinal Chemistry Reports*, *5*, 100042. https://doi.org/10.1016/j.ejmcr.2022.100042

Jadhav, S. Y., Shirame, S. P., Kulkarni, S. D., Patil, S. B., Pasale, S. K., & Bhosale, R. B. (2013). PEG mediated synthesis and pharmacological evaluation of some fluoro substituted pyrazoline derivatives as antiinflammatory and analgesic agents. *Bioorganic & Medicinal Chemistry Letters*, *23*(9), 2575-2578. https://doi.org/10.1016/j.bmcl.2013.02.105

Joshi, S. D., Dixit, S. R., Kirankumar, M. N., Aminabhavi, T. M., Raju, K. V. S. N., Narayan, R., ... & Yang, K. S. (2016). Synthesis, antimycobacterial screening and ligand-based molecular docking studies on novel pyrrole derivatives bearing pyrazoline, isoxazole and phenyl thiourea moieties. *European Journal of Medicinal Chemistry*, *107*, 133-152. https://doi.org/10.1016/j.ejmech.2015.10.047

Kaplancıklı, Z. A., Özdemir, A., Turan-Zitouni, G., Altıntop, M. D., & Can, Ö. D. (2010). New pyrazoline derivatives and their antidepressant activity. *European Journal of Medicinal Chemistry*, *45*(9), 4383-4387. https://doi.org/10.1016/j.ejmech.2010.06.011

Kumar, G., Tanwar, O., Kumar, J., Akhter, M., Sharma, S., Pillai, C. R., ... & Zama, M. S. (2018). Pyrazole-pyrazoline as promising novel antimalarial agents: A mechanistic study. *European Journal of Medicinal Chemistry*, *149*, 139-147. https://doi.org/10.1016/j.ejmech.2018.01.082

Lange, J. H., Attali, A., van der Neut, M. A., Wals, H. C., Mulder, A., Zilaout, H., ... & van Vliet, B. J. (2010). Two distinct classes of novel pyrazolinecarboxamides as potent cannabinoid CB1 receptor agonists. *Bioorganic & Medicinal Chemistry Letters*, *20*(17), 4992-4998. https://doi.org/10.1016/j.bmcl.2010.07.056

Luan, S., Zhong, H., Zhao, X., Yang, J., Jing, Y., Liu, D., & Zhao, L. (2017). Synthesis, anticancer evaluation and pharmacokinetic study of novel 10-O-phenyl ethers of dihydroartemisinin. *European Journal of Medicinal Chemistry*, *141*, 584-595. https://doi.org/10.1016/j.ejmech.2017.10.023

Mantzanidou, M., Pontiki, E., & Hadjipavlou-Litina, D. (2021). Pyrazoles and pyrazolines as anti-inflammatory agents. *Molecules*, *26*(11), 3439. https://doi.org/10.3390/molecules26113439

Akhter, W., Marella, A., Shaquiquzzaman, M., Akhter, M., & Alam, M. M. (2015). Microwave assissted synthesis of pyrazoline-coumarin hybrids and their *in-vitro* antimalarial evaluation. *Journal of Pharmacy Research, 9*(5), 318-322.

Matiadis, D., & Sagnou, M. (2020). Pyrazoline hybrids as promising anticancer agents: An up-to-date overview. *International Journal of Molecular Sciences*, *21*(15), 5507. https://doi.org/10.3390/ijms21155507

Mehmood, R., Sadiq, A., Alsantali, R. I., Mughal, E. U., Alsharif, M. A., Naeem, N., ... & Ahmed, S. A. (2022). Synthesis and evaluation of 1, 3, 5-triaryl-2-pyrazoline derivatives as potent dual inhibitors of urease and α-glucosidase together with their cytotoxic, molecular modeling and drug-likeness studies. *ACS omega*, *7*(4), 3775-3795. https://doi.org/10.1021/acsomega.1c06694

Mishra, N., & Sasmal, D. (2013). Additional acetyl cholinesterase inhibitory property of diaryl pyrazoline derivatives. *Bioorganic & Medicinal Chemistry Letters*, *23*(3), 702-705. https://doi.org/10.1016/j.bmcl.2012.11.100

Mishra, V. K., Mishra, M., Kashaw, V., & Kashaw, S. K. (2017). Synthesis of 1, 3, 5-trisubstituted pyrazolines as potential antimalarial and antimicrobial agents. *Bioorganic & Medicinal Chemistry*, *25*(6), 1949-1962. https://doi.org/10.1016/j.bmc.2017.02.025

Moi, D., Nocentini, A., Deplano, A., Balboni, G., Supuran, C. T., & Onnis, V. (2019). Structure-activity relationship with pyrazoline-based aromatic sulfamates as carbonic anhydrase isoforms I, II, IX and XII inhibitors: Synthesis and biological evaluation. *European Journal of Medicinal Chemistry*, *182*, 111638. https://doi.org/10.1016/j.ejmech.2019.111638

Montoya, A., Quiroga, J., Abonia, R., Derita, M., Sortino, M., Ornelas, A., ... & Insuasty, B. (2016). Hybrid molecules containing a 7-chloro-4-aminoquinoline nucleus and a substituted 2-pyrazoline with antiproliferative and antifungal activity. *Molecules*, *21*(8), 969. https://doi.org/10.3390/molecules21080969

Mukherjee, A., & Mahalanabis, K. K. (2009). Preparation of 4-Cyano-3-methyl-1-phenyl-1H-pyrazole-5-(4-bromophenyl) nitrile Imine: Regio-and Stereoselective Synthesis of a New Class of Substituted 3-Pyrazolines and Pyrazoles. *Heterocycles*, *78*(4), 911. https://doi.org/10.3987/COM-08-11531

Nair, A. S., Oh, J. M., Koyiparambath, V. P., Kumar, S., Sudevan, S. T., Soremekun, O., ... & Kim, H. (2021). Development of halogenated pyrazolines as selective monoamine oxidase-B Inhibitors: Deciphering via molecular dynamics approach. *Molecules*, *26*(11), 3264. https://doi.org/10.3390/molecules26113264

Nehra, B., Rulhania, S., Jaswal, S., Kumar, B., Singh, G., & Monga, V. (2020). Recent advancements in the development of bioactive pyrazoline derivatives. *European Journal of Medicinal Chemistry*, *205*, 112666. https://doi.org/10.1016/j.ejmech.2020.112666

Pandey, A. K., Sharma, S., Pandey, M., Alam, M. M., Shaquiquzzaman, M., & Akhter, M. (2016). 4, 5-Dihydrooxazole-pyrazoline hybrids: Synthesis and their evaluation as potential antimalarial agents. *European Journal of Medicinal Chemistry*, *123*, 476-486. https://doi.org/10.1016/j.ejmech.2016.07.055

Rana, D. K., Dhar, S., & Bhattacharya, S. C. (2014). An intriguing pH-triggered FRET-based biosensor emission of a pyrazoline–doxorubicin couple and its application in living cells. *Physical Chemistry Chemical Physics*, *16*(13), 5933-5936. https://doi.org/10.1039/C3CP54527J

Ravindar, L., Hasbullah, S. A., Rakesh, K. P., & Hassan, N. I. (2023). Pyrazole and pyrazoline derivatives as antimalarial agents: A key review. *European Journal of Pharmaceutical Sciences*, *183*, 106365. https://doi.org/10.1016/j.ejps.2022.106365

Sadashiva, R., Naral, D., Kudva, J., Shivalingegowda, N., Lokanath, N. K., & Pampa, K. J. (2017). Synthesis, spectral, biological activity, and crystal structure evaluation of novel pyrazoline derivatives having sulfonamide moiety. *Medicinal Chemistry Research*, *26*, 1213-1227. https://doi.org/10.1007/s00044-017-1838-5

Sahoo, A., Yabanoglu, S., Sinha, B. N., Ucar, G., Basu, A., & Jayaprakash, V. (2010). Towards development of selective and reversible pyrazoline based MAO-inhibitors: Synthesis, biological evaluation and docking studies. *Bioorganic & Medicinal Chemistry Letters*, *20*(1), 132-136. https://doi.org/10.1016/j.bmcl.2009.11.015

Salgin-Goksen, U., Telli, G., Erikci, A., Dedecengiz, E., Tel, B. C., Kaynak, F. B., ... & Gokhan-Kelekci, N. (2021). New 2-pyrazoline and hydrazone derivatives as potent and selective monoamine oxidase A inhibitors. *Journal of Medicinal Chemistry*, *64*(4), 1989-2009. https://doi.org/10.1021/acs.jmedchem.0c01504

Tripathi, A. C., Upadhyay, S., Paliwal, S., & Saraf, S. K. (2016). An expeditious one-pot microwave facilitated versus conventional syntheses: in vivo biological screening and molecular docking studies of some 3, 5-disubstituted-4, 5-dihydro-(1 H)-pyrazole derivatives. *Medicinal Chemistry Research*, *25*, 390-406. https://doi.org/10.1007/s00044-015-1489-3

Wei, Q., Ning, J. Y., Dai, X., Gao, Y. D., Su, L., Zhao, B. X., & Miao, J. Y. (2018). Discovery of novel HSP90 inhibitors that induced apoptosis and impaired autophagic flux in A549 lung cancer cells. *European Journal of Medicinal Chemistry*, *145*, 551-558. https://doi.org/10.1016/j.ejmech.2018.01.024

Wu, P., Nielsen, T. E., & Clausen, M. H. (2015). FDA-approved small-molecule kinase inhibitors. *Trends in Pharmacological Sciences*, *36*(7), 422-439. https://doi.org/10.1016/j.tips.2015.04.005

Wu, X. Q., Huang, C., Jia, Y. M., Song, B. A., Li, J., & Liu, X. H. (2014). Novel coumarin-dihydropyrazole thio-ethanone derivatives: Design, synthesis and anticancer activity. *European Journal of Medicinal Chemistry*, *74*, 717-725. https://doi.org/10.1016/j.ejmech.2013.06.014

doi: 10.31674/book.2024ecc.010

An Attempt to Understand the Food in Packages: Food Additive Chemicals

Subhrajit Banerjee

Department of Physiology, Surendranath College, University of Calcutta, Kolkata, West Bengal, India

Corresponding Author's Email: subhrajitphysiology@gmail.com

Abstract

The presence of food additive chemicals in packaged foods has become a significant concern for consumers and researchers alike. This chapter aims to explore the various aspects of food additives, including their types, uses, and potential impacts on human health. Food additives are substances added to processed and packaged foods to enhance shelf life, texture, flavour, and appearance. While some additives are derived from natural sources, others are synthesized chemically. This chapter delves into the different categories, purposes, and specific chemical natures of food additives, such as preservatives, flavour enhancers, emulsifiers, and stabilizers, among others. Additionally, the regulations and safety measures surrounding the use of food additives, as well as exploring the role of governmental agencies and international organizations in establishing guidelines and tolerable limits, are envisaged.

Keywords: *Chemicals; Food Additives; Health; Preservatives; Toxic Effects*

Introduction

In an era of packed and packaged ready-to-eat fast foods and processed and semi-processed food, it's always a good idea to read food labels carefully and to choose products that are made by reputable brands and manufacturers. To foster a better understanding of the topic, the study highlights the necessity of accurate labelling and transparency in the food industry. The importance of informed consumer choices is to encourage individuals to be aware of the additives present in packaged foods we consume. Alternative and traditional strategies that can be employed to reduce reliance on synthetic additives and promote healthier and more sustainable food products are explored. Detailed analysis and referral of norms with regard to food categories and levels of use are required nowadays. Packaged products are approved by regulatory authorities. In India, local products like bread and different munching and snacking items of local bakery products like biscuits, chips, and other fried ready-to-eat items like *Chanachur* are devoid of any labelling in packaging. This chapter aims to introduce the readers to the various groups of food additives and their categorization according to safety norms issued by regulatory agencies like the FDA and other international bodies,

as well as national bodies like FSSAI in India. Food adulteration refers to the addition of harmful or inferior-quality substances to food products in order to increase their quantity or enhance their appearance, which is not dealt with here and is not to be confused with food additives.

An Introduction to Different Classes of Food Additives

Food additives are substances that are numerous and fall into different classes. The most important to start with are preservatives, which are chemicals that increase shelf life; similarly, taste enhancers increase tastes like sweet, sour, salty, and umami. Examples include monosodium glutamate (MSG) and yeast extracts. Sweeteners can be either natural (e.g., sucrose, honey) or artificial (e.g., aspartame, saccharin). Additives that enhance or intensify the aroma of food products are called flavour enhancers and are discussed in detail in this chapter. Colorants are additives that provide or enhance the colour of food products. They can be natural (e.g., beet juice, turmeric) or artificial (e.g., FD&C dyes). Emulsifiers, stabilizers, and thickeners are added to food products to improve their texture and appearance. Acidity regulators help control and adjust the acidity or pH levels of food products, enhancing flavour and improving preservation. Antioxidants inhibit or delay the oxidation process in food, preventing rancidity and extending shelf life. Examples include ascorbic acid (vitamin C) and tocopherols (vitamin E). Bulking agents add bulk or volume to food products without significantly contributing to their caloric content. Examples include cellulose and maltodextrin. Humectants retain moisture in food products, preventing drying out or staleness. Examples include maltitol, glycerol and propylene glycol. Leavening agents help dough or batter rise by releasing gases. Examples include baking powder, yeast, and ammonium bicarbonate. Firming agents help maintain or enhance the texture and firmness of fruits and vegetables during processing. Examples include calcium citrate, calcium chloride and calcium lactate. Enzymes are proteins that catalyse specific biochemical reactions in food products, aiding in processes like fermentation, tenderization, and flavour development. Stabilizers and Thickeners enhance the texture, consistency, and stability of food products. Examples include agar, carrageenan, and xanthan gum. Anticaking agents prevent the formation of lumps or clumps in powdered food products, improving flowability. Examples include silicon dioxide and calcium silicate. Foaming agents can reduce the surface tension of water to form foam. Examples include quillaia extract and Polysorbate (20, 40 and 60). Bulking agents increase the bulk of a food without affecting its nutritional value. Examples include starch and potassium tartrates. Glazing agents provide a shiny appearance and give foods a foods a protective coating. Examples include Beeswax, carrageenan, carnauba wax, and shellac. Sequestrants enhance the quality and stability of foods. Examples include Calcium disodium and ethylene diamine tetraacetate (Inetianbor, Yakubu & Ezeonu, 2015; O’Brien-Nabors, 2012)

Here in this text, a detailed listing of emulsifiers, flavouring agents, and preservatives is done and readers are directed to further refer sites for further analysis of the other heads from referred sites, take careful note of food labels, store packets for further reading and also refer to Table 1. The deleterious effects of food chemicals or additives can vary depending on several factors, such as the type of additive, dosage, individual sensitivity, and overall dietary intake. While many food chemicals have been deemed safe for consumption by regulatory bodies such as the FDA and FSSAI when used within approved limits, excessive or inappropriate use of additives can potentially have negative health implications. It's important to note that the majority of these additives are considered safe for consumption when used in appropriate amounts as determined by regulatory authorities (FDA, n.d.; Zhou *et al*., 2023).

Emulsifiers

In the United States, emulsifiers are generally identified on food labels by their common names or by their International Numbering System (INS) codes. The INS is a system developed by the United Nations Food and Agriculture Organization (FAO) and the World Health Organization (WHO) to provide a global standard for food additives, including emulsifiers. The INS code consists of a three-digit number, where the first digit indicates the functional category of the additive (such as emulsifiers), and the second and third digits indicate the specific additive within that category. For example, the INS code for lecithin, a common emulsifier derived from soybeans, is E322. The use of emulsifiers in food products in India is regulated by the Food Safety and Standards Authority of India (FSSAI), the regulatory authority responsible for regulating food additives, and only those emulsifiers that are approved by the FSSAI can be used in food products. Food manufacturers in India are required to list all food additives, including emulsifiers, on product labels, along with their common names, chemical names, or ISI codes. Emulsifiers used in India may be identified on food labels using their common names, chemical names, or Indian Standards Institution (ISI) codes. FSSAI has established a list of approved food additives, which includes emulsifiers and has assigned codes to these additives. Emulsifiers are food additives that help to stabilize and homogenize mixtures of water and oil. The additives are coded "Food Additive Numbers" or FANS. The FANs for emulsifiers are listed under the functional class "Emulsifying, Gelling, Stabilizing, and Thickening Agents. Emulsifiers used in India are Lecithin: FAN - 322, Mono- and diglycerides of fatty acids: FAN - 471, Polysorbate 80: FAN - 433, Sodium stearoyl lactylate: FAN - 481, Similar ISI codes for Lecithin are: IS: 400, Mono- and diglycerides of fatty acids: ISI code - IS: 322, Polysorbate 80: ISI code - IS: 1430, Sodium stearoyl lactylate: ISI code - IS: 11193. An exhaustive list of Food Additive Numbers (FANs) approved for use in India is present on the official website of the Food Safety and Standards Authority of India (FSSAI) (https://www.fssai.gov.in/).

Exploration of Chemical Complexity

Some FDA-approved common emulsifiers are Lecithin, Mono- and Diglycerides, Polysorbates, Carrageenan, and Sodium Stearoyl Lactylate. It is important to note that (while these emulsifiers are FDA-approved) some studies have suggested that they may have negative health effects if consumed in large quantities. The use of non-FDA-approved emulsifiers in food products is illegal in the United States. However, some manufacturers may use these additives in their products without proper labelling or regulatory oversight. Consuming food products that contain non-FDA-approved emulsifiers can pose health risks, including allergic reactions, digestive problems, and chronic diseases. It's important to note that some of these emulsifiers may be considered safe by regulatory agencies in other countries, or may be used in small amounts that are considered safe for consumption.

Food additives that are classified as emulsifiers or stabilizers in the European Union's numbering system for food additives fall within the range of E400 to E499 (Food-Info.net, 2021). The website lists the emulsifiers and stabilizers within this range, along with their chemical names, functions, and examples of foods in which they are commonly used. Regulations and classifications of food additives can vary between different countries and regions, so it's always a beneficial idea to refer to the specific regulations and labelling requirements in your own country or region. Here are some websites that provide information on food additives and their regulations in India: Food Safety and Standards Authority of India (FSSAI) The website is https://www.fssai.gov.in/

Indian Standards Institution (ISI) - The ISI is a national standards body in India that develops standards for various products, including food additives. Their website provides information on Indian standards for food additives, including emulsifiers, along with their codes and specifications. The website is https://www.bis.gov.in/index.php/en/.

Central Food Technological Research Institute (CFTRI) (2024)- The CFTRI is a research institution in India that conducts research on various aspects of food science and technology. Their website provides information on food additives, including emulsifiers, along with their functions and applications in food products. The website is http://www.cftri.com.

Surveys conducted by the Food Safety and Standards Authority of India (FSSAI)(2024) include the National Milk Quality Survey, the National Food Safety and Quality Survey, and the National Survey on Milk Adulteration (https://www.fssai.gov.in/cms/national-surveys.php).

Natural Emulsifier

Lecithin is derived from soybeans, eggs, or sunflower seeds. It is commonly used in food products such as chocolate, baked goods, and margarine. Carrageenan, derived from seaweed, is commonly used in dairy products such as ice cream, chocolate milk, and

yogurt, almond milk. Xanthan gum is derived from bacteria used in salad dressings, sauces, and other food products. Though natural, some studies revealed digestive problems and other health issues (Blekas, 2016).

Synthetic Emulsifier

These additives as emulsifiers have not been evaluated (or not adequately evaluated) for safety or because they have been found to be unsafe. Examples and uses of emulsifiers are as follows. Mono- and diglycerides are commonly used in baked goods, ice cream, and peanut butter. Health effects include weight gain. Polysorbates are commonly used in ice cream, salad dressings, baked goods, and mayonnaise It has been linked to inflammation, gut dysbiosis (Food and Agriculture Organization of the United Nations, 2023). Sodium stearoyl lactylate is used in bread, pastries, and other baked goods. DATEM is a synthetic emulsifier that is commonly used in baked goods and other food products. It has been banned in some countries due to safety concerns (Bakerpedia, 2024a).

PVA is a synthetic emulsifier that is commonly used in instant noodles and other food products. It has been found to be unsafe for consumption and has been banned in some countries (Saxena, 2004). Azodicarbonamide (ADA) is a synthetic emulsifier that is commonly used in bread and other baked goods. It has been banned in some countries due to safety concerns (Bakerpedia, 2024b). SLS is a synthetic emulsifier that is commonly used in personal care products such as toothpaste and shampoo. It has been found to be unsafe for consumption and is not approved for use in food products (Chemical Safety Facts, 2022). Propylene glycol is used in baked goods, frosting, and other food products. Health effects include allergic reactions and skin irritation. Ethoxylated mono- and diglycerides are used in baked goods and other food products. Health effects include allergic reactions. Sodium carboxymethylcellulose used in processed foods and ice cream causes gut irritation and inflammation (Partridge *et al*., 2019). Glycerol ester of wood rosin (GEWR) is used in citrus-flavoured drinks and other beverages. Health effects include allergic reactions and skin irritation. PGEs are used in baked goods and confectionery. Health effects include allergic reactions and digestive problems. Calcium stearoyl lactylate (CSL) used in baked goods, margarine allergic reactions, skin irritation Butylated hydroxyanisole (BHA) used in snack foods, baked goods, and cereal. Health effects include cancer. Butylated hydroxytoluene (BHT) is used in food products such as potato chips, cereal, and baked goods. Health effects include cancer and liver damage. Titanium dioxide is used as a whitening agent in food products such as candy, gum, and frosting. Health effects are inflammation and DNA damage (denotes FDA non-approved).

Food Preservative

Salt has been used as a natural preservative for centuries. It can be used to preserve vegetables, meats, and fish by drawing out moisture and inhibiting the growth of bacteria. There are several healthy preservatives that can be used at home without causing harm, like vinegar, honey, alcohol, and citric acid. Sugar is a natural preservative that can be used to preserve fruits, jams, and jellies. Citric acid is used to preserve canned fruits and vegetables, and as a flavour enhancer. Sorbic acid is used to preserve cheese, wine, and baked goods. Tocopherols, natural forms of vitamin E, used to preserve oils, dressings, and baked goods. Carrageenan, a natural preservative used in dairy products, salad dressings, and other foods. Some examples of organic preservatives include rosemary extract, clove oil, and grapefruit seed extract. Rosemary is a natural antioxidant that can be used to preserve meats and other food products. It can also be used to prevent the oxidation of oils and fats. Ginger has antibacterial properties and can be used to preserve food. It's particularly effective in preserving pickles and other fermented foods. Tea tree oil has antibacterial and antifungal properties and can be used to preserve food. It's particularly effective in preserving fruits and vegetables. Oregano oil has antibacterial and antifungal properties and can be used to preserve food. It's particularly effective in preserving meats and other animal products. Cloves have antibacterial properties and can be used to preserve food. They're particularly effective at preserving fruits and vegetables. These ingredients have been used for centuries to preserve food, and are generally considered safe when used in appropriate amounts. Several spices have natural antimicrobial properties that can act as preservatives in food. Some of these spices are cinnamon, cloves, oregano, thyme, rosemary, sage, ginger, mustard, black pepper, and turmeric. Some other natural preservatives are nisin- a natural preservative used in cheese and other dairy products and natamycin- a natural preservative used in cheese and other dairy products.

There are several preservatives approved for use in food in India, each with its own chemical code. The preservatives listed are identified by their respective international numbering system, which is widely used across the globe, including India. The Indian food regulatory body (FSSAI), recognizes and approves the use of these preservatives based on their respective international codes. FSSAI has set maximum limits for certain preservatives in different food categories to ensure that the levels of these substances in the final product do not exceed the safe limits. Therefore, food manufacturers in India are required to comply with the FSSAI regulations related to the use of preservatives in food products, in addition to following the international codes for preservatives.:

Table 1: *Chemical synthetic preservatives used in food that are approved in India are mentioned below*

Sodium Benzoate (E211)	This preservative is commonly used in acidic foods, such as pickles, chutneys, and sauces, to prevent spoilage. and is a commonly used preservative in Indian street food. Some studies suggest that high levels of sodium benzoate in the diet may increase the risk of hyperactivity and behavioural problems in children. In addition, when combined with ascorbic acid (vitamin C), sodium benzoate may form benzene, a carcinogenic substance.
Potassium Sorbate (E202)	Some studies have linked potassium sorbate to skin irritation, allergic reactions, and digestive issues.
Calcium Propionate (E282)	High levels of calcium propionate may cause skin irritation, digestive issues, and headaches. In addition, some studies suggest that calcium propionate may have a negative impact on gut health.
Ascorbic Acid (Vitamin C) (E300)	Used as an antioxidant and preservative in a wide range of foods, including fruit juices, canned fruits and vegetables, and processed meats. A synthetic Vitamin C, it is also commonly used in jams, and other products to prevent oxidation and spoilage. While ascorbic acid is generally considered safe, high levels of vitamin C may cause digestive issues, such as diarrhoea and nausea.
Butylated Hydroxy anisole (BHA) (E320) and Butylated Hydroxytoluene (BHT) (E321)	Used as an antioxidant in many processed foods, including cereals, snack foods, and baked goods, to prevent the oxidation of fats and oils and extend the shelf life of the product. Some studies have linked BHA/BHT to cancer in animals. However, the evidence is not yet conclusive in humans. BHA/BHT is also used in cosmetics, pharmaceuticals, and rubber products to prevent oxidation.
Propyl Gallate (E310)	Some studies suggest that high levels of propyl gallate may be carcinogenic in animals. In addition to its use as a preservative in food products, propyl gallate is also used in cosmetics, pharmaceuticals, and toiletries as an antioxidant.
Ethylenediaminetetraacetic Acid (EDTA) (E385) -While EDTA	Generally considered safe, some studies have suggested that high levels of EDTA may have negative impacts on kidney function in some individuals. Used as a chelating agent to bind metal ions, such as calcium and iron, in canned and bottled foods to prevent spoilage and maintain the quality of the product.
Sodium Metabisulphite (E223)	This preservative is commonly used in dried fruits, such as raisins and apricots, to prevent spoilage and to maintain their colour and flavour. Used in juices and other beverages to prevent spoilage and to maintain their colour and flavour. Sulphites (sulphur dioxide, sodium sulphite, sodium bisulphite) – are often used to preserve wine and beer.
Sodium Nitrite/ Nitrate (E250/E251)	A fertilizer and a component in gunpowder; used in cured meats, such as bacon, ham, and sausages, to prevent the growth of bacteria, preserve color and flavour, and prevent spoilage. High levels of sodium nitrite may increase the risk of cancer, particularly colon cancer. Sodium nitrate is not tasteless. In fact, it has a slightly salty and bitter taste, and carcinogenic compounds called nitrosamines are formed in the body from nitrite.
Ethylenediaminetetraacetic Acid (EDTA) (E385)	In addition to its use as a preservative in canned and bottled foods, EDTA is also used in the cosmetics industry as a chelating agent and in the medical field as a treatment for heavy metal poisoning.
Methylcellulose	Synthetic preservative used to preserve processed meats and cheese.

Potential health risks associated with preservatives are often related to high levels of exposure over long periods of time, which is why regulatory bodies have set maximum

limits for the use of these substances in food products. Additionally, individual sensitivity to preservatives may vary, and some individuals may experience adverse effects at lower levels of exposure. Therefore, it's always a good idea to consume processed foods in moderation and read labels carefully. It's important to note that all food additives, including preservatives, have been thoroughly tested and approved for use by regulatory bodies such as the US Food and Drug Administration (FDA) and the European Food Safety Authority (EFSA). Studies have suggested that long-term exposure to high levels of certain preservatives may pose health risks to individuals (Mirza, Asema & Kasim, 2017).

The most common easily available preservatives in India that are used in roadside stalls and street food hawkers include sodium nitrate, sodium benzoate, sodium meta bi-sulphite, sodium citrate, EDTA (chelating agents are used to remove metal ions from food, which can cause spoilage and degradation), sodium lignosulphonate, citric acid, propionic acid, polyethylene glycol, 1,4 butane diols. Potassium sorbate, citric acid, calcium propionate are commonly used in carbonated drinks, fruit juices, and candies to add tartness and prevent spoilage. Calcium propionate - is commonly used in bread and baked goods and also in dairy products, and processed meats.

Examples of some other synthetic preservatives are sodium propionate - commonly used in bread and baked goods to prevent mould growth, butyrate - used in meat products to prevent the growth of bacteria and fungi, sodium erythorbate - used in meat products to help preserve the colour and prevent the growth of bacteria, potassium bromates - used in flour and baked goods to improve dough strength and shelf life. TBHQ (tertiary butylhydroquinone) – is used in oils, fats, and fried foods to prevent oxidation and extend shelf life. Antioxidants are a type of preservative that prevents food from becoming rancid or spoiled due to exposure to oxygen. Some common antioxidants used in food include ascorbic acid (vitamin C) and alpha-tocopherol (vitamin E).

Flavouring Chemicals

Flavouring chemicals can be found in various food products and beverages. A brief explanation of the flavours associated with some of the chemicals is provided here. It's worth noting that these flavours can be highly subjective and can vary depending on the concentration and context in which they are used. Additionally, some of these chemicals can have negative effects on health at high levels, so they are typically used in small amounts and regulated by food safety agencies. Flavouring chemicals are often used to create a more consistent and cost-effective flavour profile.

Vanillin is a sweet, creamy, and vanilla-like flavour commonly found in vanilla extract, baked goods, and desserts. Ethyl vanillin is a more intense and stronger version of vanillin, often used in imitation vanilla flavouring. Acetaldehyde is a fruity and slightly sweet flavour commonly found in ripe fruits and alcoholic beverages. Maltol is a caramel-

like flavour often used in baked goods and caramel-flavoured products. 2-acetyl pyrazine is a nutty and roasted flavour commonly found in coffee, chocolate, and other roasted or toasted foods. Cinnamaldehyde is a spicy and warm flavour commonly found in spicy foods. Limonene is a citrusy and fruity flavour commonly found in citrus fruit juices such as lemons and oranges. Eugenol - spicy and warm flavour commonly found in (clove-like) spicy foods. Menthol is a cool and refreshing flavour commonly found in mint and other mint-flavoured products. Linalool - floral and slightly spicy flavour. Isoamyl acetate- fruity and banana-like flavour. Ethyl acetate fruity - sweet flavour commonly found in fruit juices and drinks such as apples, pears, and grapes. Butyric acid is a cheesy and rancid flavour commonly found in aged cheese and other fermented foods. Propionic acid - slightly sour and tangy flavour commonly found in cheese and other fermented foods. 4-hydroxy-2,5-dimethyl-3(2H)-furanone (HDMF) is a sweet and caramel-like flavour commonly found in strawberries. Citral- citrusy and lemon-like flavour commonly found in lemongrass. Geraniol- rose flavour, Furfural- nutty and slightly burnt flavour commonly found in baked goods and roasted coffee. 2-methylbutyric acid - cheesy and rancid flavour commonly found in cheese and other fermented foods. 2,3-pentanedione - buttery and creamy flavour commonly found in butter and other dairy products (Branen *et al*., 2001).

Table 2: *Different types of food additives with their effect on human health*

Food Additive Types	Compounds	Deleterious Effect	Reference
Preservatives	Sorbic acid	Interactions with human serum albumins causing cytotoxicity, complication in immune balance, suppress immune function, hampering male reproductive system, gastric irritation, nausea, diarrhea, allergic reactions, asthma, skin rashes, dermatitis and allergies in the urticaria	Ambarwati, 2012; Herrero *et al*., 2013; Anand & Sati, 2013; Silva & Lidon, 2016
	Benzoic acid		
	Propionic acid		
	Methyl-, ethyl- , butyl- and propyl-esters of p-hydroxybenzoic acid (PHB, parabens)		
	Sodium acetate		
	Sodium benzoate		
	Potassium sorbate		
Antimicrobials	Nitrates	Methemoglobinemia, allergies, palpitations, headaches, risk of tumorigenesis, and even carcinogenesis	Nair & Elmore, 2003; Xie *et al*., 2011; Crowe, Elliott & Green, 2019
	Nitrites		
	Sulfites		
Antioxidants	Butylated hydroxyanisole (BHA)	Carcinogenic effect on liver and stomach tissues, immunotoxic effects like hypersensitivity, chronic inflammation, high toxicity and mutagenicity	Dolatabadi & Kashanian, 2010; Eskandani, Hamishehkar & Dolatabadi, 2014; Naidenko *et al*., 2021
	Butylated hydroxytoluene (BHT)		
	Tertiary butyl hydroquinone (TBHQ)		
	NDGA (Nor dihydroguaiaretic acid)		
	DG (dodecyl gallate)		
	PG (propyl gallate),		
	OG (octyl gallate)		

Colorants	Tartrazine	Hyperactivity in children, allergies, cancer	Abiega-Franyutti & Freyre-Fonseca, 2021; Dey & Nagababu, 2022; Sultana *et al*., 2023
	Titanium dioxide		
	Sunset Yellow FCF		
	Ponceau 4R		
	Allura Red AC		
	Quinoline yellow		
	Carmoisine		
	Greenplum Amaranth		
	Black PN		
	Cake Red 2G		
	Erythrosine		
	Green S		
	Brilliant Blue		
	Indigo carmine		
Flavour or Taste Enhancer	Monosodium glutamate (MSG)	Cytotoxic and genotoxic effects, potential DNA damage	Zanfirescu *et al*., 2019; Xu *et al*., 2022
	Monopotassium glutamate		
	Calcium Glutamate		
	Magnesium di-glutamate		
	Protein hydrolysate		
	Umami peptides		
	Dimethylpolysiloxane		
	Sodium Guanylate		
	Guanylic acid		
	Sodium Inosinate		
	Ethyl Maltol		
	Maltol Sodium5-Ribonucleotide		
Acidity Regulator	Sodium lactate	Stinging, swelling, shortness of breath, a big weight gain, allergic reaction, skin burn, liver damage, hyperkalemia and NH_3 toxicity	Cao *et al*., 2020
	Citric acid		
Anticaking Agents	Calcium phosphate	nausea/vomiting, bone/muscle pain, headache, oxidative stress, respiratory distress, allergic reactions	Athinarayanan *et al*., 2014
	Magnesium silicate		
	Sodium aluminosilicate		
	Sodium ferrocyanide		
	Potassium ferrocyanide		
Emulsifyers	Carboxymethylcellulose	Dysbiosis with overgrowth of mucus-degrading bacteria, deficiency in interleukin-10 or toll-like receptor 5, intestinal (small bowel) inflammation, food allergies, and risk of certain types of cancer, metabolic syndrome	Laudisi *et al*., 2019b; Naimi *et al.*, 2021; De Siena *et al*., 2022
	Lecithins		
	Mono- and diglycerides		
	Polysorbates		
	Carrageenans		
	Guar gums		
	Maltodextrin		
	Sodium stearoyl lactylate		
	Resistant starch		
	Sorbitans		
Stabilizer	Xanthan gum	Altered gut bacteria, irritating the intestinal lining	EFSA Panel on Food Additives and
	Carageenan		

	Gum arabic Magnesium stearate		Nutrient Sources added to Food *et al*., 2017
Sweeteners	Acesulfame-K	Neurological damage, risk factor for cardiovascular disease prevention, gut dysbiosis, impaired glucose metabolism, glucose tolerance and support weight gain by negatively affecting microbiota	Cao *et al*., 2020; Mahalak *et al*., 2019; Debras *et al*., 2022; Li *et al*., 2022
	Aspartame		
	Saccharin		
	Sucralose		
	Cyclamate		
	Neotame		
	Sorbitol		
	Erythritol		
Thickeners	Dextrin	Altered mucus barrier, increased intestinal inflammation	Laudisi *et al*., 2019a

Conclusion

The FDA follows a rigorous pre-market approval process for food additives, including food thickeners. Manufacturers must submit detailed safety data and evidence of the additive's safety and intended use before it can be approved for use. The FDA evaluates the safety of the additive and sets specific usage levels and conditions of use. Once approved, the FDA assigns a "Generally Recognized as Safe" (GRAS) status or issues a food additive regulation for the substance.

Food regulations as laid by authorities are binding across packaged foods from reputed industrial food manufacturers, while street foods and eateries all over India are flaunting these regulations and are mostly ignored by jurisdiction, surveillance, and regulatory authorities. Some commonly used preservatives (that are relatively inexpensive) and used in roadside stalls for storing curry, juices, and high-calorie products are sodium benzoate, potassium sorbate, nitrates (in curries), sodium metabisulfite for dried fruits, and ascorbic acid in fruit juice stalls. Some potential deleterious effects associated with food chemicals include allergic reactions in susceptible individuals and sensitivities or intolerances to specific food additives, resulting in digestive issues, headaches, or other adverse reactions. Individuals with specific health conditions, such as asthma, have sulfite sensitivity. Again, high doses or prolonged exposure due to overconsumption of packed meals and packaged foods with certain food additives may be consumed at higher than desirable levels, which will have toxic effects on the body. Additionally, different additives in combination with food can have complex effects that are not fully understood.

A balanced and varied diet that includes whole, minimally processed foods is generally recommended to minimize reliance on processed foods containing high levels of additives. Again, it's important to note that excessive or prolonged exposure to these substances may pose health risks, particularly for sensitive individuals. Readers are further advised to understand the health implications and current updated information like manufacturing practices, purity, and levels of use of these additives in different

categories of food and become aware as consumers. Therefore, it's always a beneficial idea to consume processed foods in moderation and be aware of the ingredients and additives.

Acknowledgement

The author acknowledges the untiring efforts of scientists and food regulatory bodies for their work to make food safe.

Reference

Abiega-Franyutti, P., & Freyre-Fonseca, V. (2021). Chronic consumption of food-additives lead to changes via microbiota gut-brain axis. *Toxicology*, *464*, 153001. https://doi.org/10.1016/j.tox.2021.153001

Ambarwati, R. (2012). Effect of sodium nitrite (NaNO2) to erithrocyte and hemoglobin profile in white rat (rattus norvegicus). *Folia Medica Indonesiana*, *48*(1), 1-5.

Anand, S. P., & Sati, N. (2013). Artificial preservatives and their harmful effects: looking toward nature for safer alternatives. *Int. J. Pharm. Sci. Res*, *4*(7), 2496-2501.

Athinarayanan, J., Periasamy, V. S., Alsaif, M. A., Al-Warthan, A. A., & Alshatwi, A. A. (2014). Presence of nanosilica (E551) in commercial food products: TNF-mediated oxidative stress and altered cell cycle progression in human lung fibroblast cells. *Cell Biology and Toxicology*, *30*, 89-100. https://doi.org/10.1007/s10565-014-9271-8

Bakerpedia. (2024a). Diacetyl Tartaric Acid Ester of Mono- and Diglycerides (DATEM). https://bakerpedia.com/ingredients/datem/. Accessed on 10th June 2024.

Bakerpedia. (2024b). Azodicarbonamide (ADA). https://bakerpedia.com/ingredients/azodicarbonamide-ada/. Accessed on 15th June 2024.

Blekas, G. (2016). *Food additives: classification, uses and regulation* (No. IKEEBOOKCH-2022-027, pp. 731-736). Academic Press; Elsevier. https://doi.org/10.1016/B978-0-12-384947-2.00304-4

Branen, A. L, Davidson, P. M., Salminen, S. & Thorngate III, J. H. (eds.) (2001). *Food Additives*, (2nd ed.). New York: Marcel Dekker, Inc.

Cao, Y., Liu, H., Qin, N., Ren, X., Zhu, B., & Xia, X. (2020). Impact of food additives on the composition and function of gut microbiota: A review. *Trends in Food Science & Technology*, *99*, 295-310. https://doi.org/10.1016/j.tifs.2020.03.006

Chemical Safety Facts. (October 14, 2022). Sodium lauryl sulfate (SLS). https://www.chemicalsafetyfacts.org/chemicals/sodium-lauryl-sulfate-sls/. Accessed on 15th June 2024.

Crowe, W., Elliott, C. T., & Green, B. D. (2019). A review of the in vivo evidence investigating the role of nitrite exposure from processed meat consumption in the development of colorectal cancer. *Nutrients*, *11*(11), 2673. https://doi.org/10.3390/nu11112673

De Siena, M., Raoul, P., Costantini, L., Scarpellini, E., Cintoni, M., Gasbarrini, A., ... & Mele, M. C. (2022). Food emulsifiers and metabolic syndrome: the role of the gut microbiota. *Foods*, *11*(15), 2205. https://doi.org/10.3390/foods11152205

Debras, C., Chazelas, E., Sellem, L., Porcher, R., Druesne-Pecollo, N., Esseddik, Y., ... & Touvier, M. (2022). Artificial sweeteners and risk of cardiovascular diseases: results from the prospective NutriNet-Santé cohort. *Bmj*, *378*. https://doi.org/10.1136/bmj-2022-071204

Dey, S., & Nagababu, B. H. (2022). Applications of food color and bio-preservatives in the food and its effect on the human health. *Food Chemistry Advances*, *1*, 100019. https://doi.org/10.1016/j.focha.2022.100019

Dolatabadi, J. E. N., & Kashanian, S. (2010). A review on DNA interaction with synthetic phenolic food additives. *Food Research International*, *43*(5), 1223-1230. https://doi.org/10.1016/j.foodres.2010.03.026

EFSA Panel on Food Additives and Nutrient Sources added to Food (ANS), Mortensen, A., Aguilar, F., Crebelli, R., Di Domenico, A., Frutos, M. J., ... & Dusemund, B. (2017). Re-evaluation of guar gum (E 412) as a food additive. *EFSA Journal*, *15*(2), e04669. https://doi.org/10.2903/j.efsa.2017.4669

Eskandani, M., Hamishehkar, H., & Dolatabadi, J. E. N. (2014). Cytotoxicity and DNA damage properties of tert-butylhydroquinone (TBHQ) food additive. *Food Chemistry*, *153*, 315-320. https://doi.org/10.1016/j.foodchem.2013.12.087

FDA. (n.d.). *Food Additive Status List*. U.S. Food & Drug Administration. https://www.fda.gov/food/food-additives-petitions/food-additive-status-list. Accessed on 8th June 2024.

Food and Agriculture Organization of the United Nations. (2003). Food additives. https://www.fao.org/3/y0474s/y0474s5a.htm

Food-Info.net. (5th September 2021). *E400- E500 Emulsifiers and thickening agents.* http://www.food-info.net/uk/e/e400-500.htm. Accessed on 10th June 2024.

Herrero, M., Castro-Puyana, M., Ibáñez, E., & Cifuentes, A. (2013). Compositional Analysis of Foods. In *Liquid Chromatography* (295–317). https://doi.org/10.1016/B978-0-12-415806-1.00011-5

Inetianbor, J. E., Yakubu, J. M., & Ezeonu, S. C. (2015). Effects of food additives and preservatives on man-a review. *Asian Journal of Science and Technology*, *6*(2), 1118-1135.

Laudisi, F., Di Fusco, D., Dinallo, V., Stolfi, C., Di Grazia, A., Marafini, I., ... & Monteleone, G. (2019a). The food additive maltodextrin promotes endoplasmic reticulum stress–driven mucus depletion and exacerbates intestinal inflammation. *Cellular and molecular gastroenterology and hepatology*, *7*(2), 457-473. https://doi.org/10.1016/j.jcmgh.2018.09.002

Laudisi, F., Stolfi, C., & Monteleone, G. (2019b). Impact of food additives on gut homeostasis. *Nutrients*, *11*(10), 2334.

Li, C. H., Wang, C. T., Lin, Y. J., Kuo, H. Y., Wu, J. S., Hong, T. C., ... & Wu, H. T. (2022). Long-term consumption of the sugar substitute sorbitol alters gut microbiome and induces glucose intolerance in mice. *Life Sciences*, *305*, 120770. https://doi.org/10.1016/j.lfs.2022.120770

Mahalak, K. K., Firrman, J., Tomasula, P. M., Nunez, A., Lee, J. J., Bittinger, K., ... & Liu, L. S. (2019). Impact of steviol glycosides and erythritol on the human and Cebus apella gut microbiome. *Journal of Agricultural and Food Chemistry*, *68*(46), 13093-13101. https://doi.org/10.1021/acs.jafc.9b06181

Mirza, S. K., Asema, U. K., & Kasim, S. S. (2017). To study the harmful effects of food preservatives on human health. *J. Med. Chem. Drug Discovery*, *2*, 610-616.

Naidenko, O. V., Andrews, D. Q., Temkin, A. M., Stoiber, T., Uche, U. I., Evans, S., & Perrone-Gray, S. (2021). Investigating molecular mechanisms of immunotoxicity and the utility of ToxCast for immunotoxicity screening of chemicals added to food. *International Journal of Environmental Research and Public Health*, *18*(7), 3332. https://doi.org/10.3390/ijerph18073332

Naimi, S., Viennois, E., Gewirtz, A. T., & Chassaing, B. (2021). Direct impact of commonly used dietary emulsifiers on human gut microbiota. *Microbiome*, *9*, 1-19. https://doi.org/10.1186/s40168-020-00996-6

Nair, B., & Elmore, A. R. (2003). Final report on the safety assessment of sodium sulfite, potassium sulfite, ammonium sulfite, sodium bisulfite, ammonium bisulfite, sodium metabisulfite and potassium metabisulfite. *International Journal of Toxicology*, *22*, 63-88. https://doi.org/10.1080/10915810305077x

O'Brien-Nabors, L. (ed.). (2012). *Alternative sweeteners*, 4th ed. Boca Raton: CRC Press. https://doi.org/10.1201/b11242

Partridge, D., Lloyd, K. A., Rhodes, J. M., Walker, A. W., Johnstone, A. M., & Campbell, B. J. (2019). Food additives: Assessing the impact of exposure to permitted emulsifiers on bowel and metabolic health–introducing the FADiets study. *Nutrition Bulletin*, *44*(4), 329-349. https://doi.org/10.1111/nbu.12408

Saxena, S. K. (2004). Chemical and Technical Assessment. *Polyvinyl Alcohol, 61st JECFA: FAO*. https://www.fao.org/fileadmin/templates/agns/pdf/jecfa/cta/61/PVA.pdf

Silva, M. M., & Lidon, F. C. (2016). Food preservatives-An overview on applications and side effects. *Emirates Journal of Food and Agriculture*, *28*(6), 366.

Sultana, S., Rahman, M. M., Aovi, F. I., Jahan, F. I., Hossain, M. S., Brishti, S. A., ... & Sharma, R. (2023). Food color additives in hazardous consequences of human health: An overview. *Current Topics in Medicinal Chemistry*, *23*(14), 1380-1393. https://doi.org/10.2174/1568026623666230117122433

Xie, T. P., Zhao, Y. F., Chen, L. Q., Zhu, Z. J., Hu, Y., & Yuan, Y. (2011). Long-term exposure to sodium nitrite and risk of esophageal carcinoma: a cohort study for 30 years. *Diseases of the Esophagus*, *24*(1), 30-32. https://doi.org/10.1111/j.1442-2050.2010.01080.x

Xu, J., Tang, M., Liu, Y., Xu, J., & Xu, X. (2022). Safety assessment of monosodium glutamate based on intestinal function and flora in mice. *Food Science and Human Wellness*, *11*(1), 155-164. https://doi.org/10.1016/j.fshw.2021.07.016

Zanfirescu, A., Ungurianu, A., Tsatsakis, A. M., Nițulescu, G. M., Kouretas, D., Veskoukis, A., ... & Margină, D. (2019). A review of the alleged health hazards of monosodium glutamate. *Comprehensive Reviews in Food Science and Food Safety*, *18*(4), 1111-1134. https://doi.org/10.1111/1541-4337.12448

Zhou, X., Qiao, K., Wu, H., & Zhang, Y. (2023). The impact of food additives on the abundance and composition of gut microbiota. *Molecules*, *28*(2), 631. https://doi.org/10.3390/molecules28020631

doi: 10.31674/book.2024ecc.011

Synthesis and Magnetic Properties of Polynuclear Complexes of 1st Transition Metals: A Mini Review

Apurba Biswas

Department of Chemistry, Surendranath College, Kolkata, India

Corresponding Author's Email Address: apurbacu@yahoo.co.in

Abstract

The design and synthesis of multinuclear complexes has attracted considerable interest for their utility in small memory devices and quantum phenomena. The studies of magnetic studies of those complexes are very important to know their behavior in presence of magnetic fields. Now a days, ongoing interest is to synthesis single molecule-based magnets (SMMs) that can be derived from transition metals with different ligands. Majority of the metals that are used for the synthesis of such single-molecule magnets are Co(II/III), Mn(II/III), Cu(II) and Ni(II). Different synthetic routes and ligands have been used to get multinuclear 1st transition metal complexes, especially bridging ligands such as azide, thiocyanate, cyanate, hydroxyl, carboxylates etc. along with phenol-based Schiff base ligands are widely used. The exchange coupling between the unpaired electrons of two metal centers connected through bridging ligands depends on several factors, such as metal metal distance, bridging angles, geometry, etc.

Keywords: *3d Metal Complex; High Nuclearity; Polynuclear; Single Molecule Magnet (SMM)*

Introduction

The polyuclear transition metal complexes are of ongoing interest for their relevance to biological systems (Messerschmidt *et al.,* 2001) due to their utility for designing active sites of metalloproteins, in molecular magnetism, especially for the single molecular magnets (SMM) (Miyasaka *et al.*, 2004; Sahu *et al.,* 2023; Dey *et al.,* 2023), and for devising nano-materials (Weiss, 2010) for their potential use in nanoscience and technology. Most importantly, the magnetic properties of the multinuclear complexes containing paramagnetic centers have taken great attention for their wide range of technological applications. The literature survey reveals that the coupling constant (*J*) depends on the M-A-M (M = metal, A = bridging atom) angle and M-A bond lengths (Nanda *et al*., 1994). The coupling between the metal centers can be modulated by changing the geometry of the complex around the metal center or by changing the bonding parameters that are associated with the interaction of the metal centers along with the bridging ligands. Therefore, appropriate metal ions as well as bridging ligands are vital for the formation of desired multinuclear complexes (Mukherjee *et al.,* 2009). Various synthetic methods have been developed for obtaining multinuclear transition

metal complexes. The synthetic strategies sometimes make it difficult to get predicted structure, but the targeted complexes that behave as single-molecule magnets (SMM's) are always a subject of extensive investigation. The large spin ground state and a significant negative (easy-axis) magneto anisotropy make the system an intrinsic bistability with very slow thermal relaxation of the magnetization at very low temperatures in the molecular magnets (Das *et al.,* 2011) that are widely used for their possible applications in small memory devices as well as in quantum computing (Thomas *et al.,* 1996).

Review of Literature

Polynuclear metal clusters with high nuclearity by using a variety of poly-pyridine and poly-ß-diketonate ligands and 3d metals V to Cu have gained attention for single-molecule magnets (SMMs). Many of these, specially $[Mn_{12}O_{12}(O_2CR)_{16}(H_2O)_4]$ and $[Mn_4O_3Cl_4(O_2CEt)_3(py)_3]_2$ compounds, can be given as examples of nanoscale magnets (Sessoli *et al.,*1993; Sieber *et al.,* 2005). Various polynuclear clusters form nanoscopic architectures with interesting magnetic properties (Gole, Mondal & Mukherjee, 2014). Mukherjee *et al.* (2003) also designed polynuclear complexes with bridging carboxylate groups and studied their magnetic properties. The magnetic nature of 1st transition metal complexes is shown in Table 1.

Table 1: *Some selective 1st transition metal complexes with their magnetic nature*

Compound	Magnetic Nature	*J* (cm^{-1})	Ref.
$[Cu(L)(\mu_{1,1}–N_3)(ClO_4)]_2$	Antiferromagnetic	–7.2	Nandy *et al.,* 2015
$[Cu(L)(\mu_{1,1}–NCO)(ClO_4)]_2$	Ferromagnetic	+0.41	Nandy *et al.,* 2015
$[\{Cu(L)(CF_3COO)\}_2]_n$	Antiferromagnetic	−0.47±0.01	Shit *et al.,* 2016
$[(maleate)_2Ni_3(bpe)_4(H_2O)_4](NO_3)_2.H_2O$	Ferromagnetic	+1.74	Mukherjee *et al.* 2003
[(adipate)Mn(bpe)]	Antiferromagnetic	−1.84 (0.015)	Mukherjee *et al.,* 2003
$[Mn_2O_2(O_2CCH_3)(bpea)_2](ClO_4)_3$	Antiferromagnetic	−124	Pal, Chan & Armstrong, 1992
$[Mn_3O_4(OH)(bpea)_3](ClO_4)_3$	Antiferromagnetic	−76	Pal, Chan & Armstrong, 1992
$[Cu_2L_2(N_3)]_2$	Antiferromagnetic	−8.5	Koner *et al.,* 2004
$[Cu(L^1)(N_3)]_n(ClO_4)_n$	Ferromagnetic	+2.15	Mukherjee *et al.,* 2002
$[Cu(L^2)(N_3)]_n(ClO_4)_n$	Ferromagnetic	+3.61	Mukherjee *et al.,* 2002
$[Ni_2L_2(N_3)_2(H_2O)_2]$	Ferromagnetic	+23.5	Mukherjee *et al.,* 2009
$[Ni_2L_2(NO_3)_2]$	Antiferromagnetic	−24.27	Mukherjee *et al.,* 2009
$[(CuL^1)_2Mn(o\text{-}(NO_2)C_6H_4CO_2)_2]$	Antiferromagnetic	–7.027(2)	Ganguly *et al.,* 2023

$[(NiL)_2Mn(NCS)_2(CH_3OH)_2]\cdot CH_3OH$	Antiferromagnetic	-4.84	Maity *et al.,* 2021
$[(NiL)_2Mn(N(CN)_2)_2(CH_3OH)_2]\cdot CH_3OH$	Antiferromagnetic	−5.23	Maity *et al.,* 2021
$[Mn_4L_2(\mu_3\text{-}Cl)_2Cl_2]$	Antiferromagnetic	−0.19(J_1), −6.87(J_2), −0.70(J_3)	Das *et al.,* 2019
$[Mn_4L_2(\mu_{1,1,1}\text{-}N_3)_2(N_3)_2]$	Antiferromagnetic	+0.11(J_1), −0.64(J_2), +0.11(J_3)	Das *et al.,* 2019
$[Ni_4(L^2)_2(\mu_3\text{-}OCH_3)_2(NO_3)](NO_3)\cdot CH_3OH$	Ferromagnetic	+0.64(J_1), +8.41 (J_2)	Ghosh *et al.,* 2019
$[Ni_6(L^2)_2(o\text{-}van)_2(\mu_3\text{-}OH)_4](NO_3)_2\cdot H_2O$	Antiferromagnetic	−5.60(J_1), −9.39 (J_2), −5.18(J_3), +3.72(J_4)	Ghosh *et al.,* 2019
$[Cu^{II}_2(L^7)_2\text{-}(\mu\text{-}Cl)_2][ClO_4]_2$	Ferromagnetic	+6.0(1)	Singh, Lloret & Mukherjee, 2014
$[Cu^{II}(L^6)(\mu\text{-}Cl)][ClO_4]\cdot CH_3CN$	Antiferromagnetic	–0.20(1)	Singh, Lloret & Mukherjee, 2014
$[(\mu_{1,3}\text{-}N_3)\{Co^{II}(L^1)(\mu\text{-}O_2CC_6H_4NO_2)Co^{III}(N_3)\}_2]PF_6$	Antiferromagnetic	−13.07	Banerjee *et al.,* 2019
$[Mn_2L_2(ClO_4)_2]$	Ferromagnetic	+1.95(2)	Seth, Giri & Ghosh, 2015
$[Mn_2L_2(NCS)_2]$	Ferromagnetic	+0.44(1)	Seth, Giri & Ghosh, 2015
$[Ni_2L_2(NO_2)_2]$	Antiferromagnetic	−39	Biswas *et al.,* 2017
$[Ni_3L_3(OH)(NO_2)]\cdot ClO_4$	Ferromagnetic	+18.2	Biswas *et al.,* 2017
$\{[(NiL)_2Co(NCNCN)_2]\cdot CH_3CN\}_\infty$	Ferromagnetic	+4.1	Ghosh *et al.,* 2013
$[(CuL^2)_2Co\{dca\}_2]\cdot H_2O$	Antiferromagnetic	−18.6	Biswas *et al.,* 2014

Multinuclear complexes with Schiff bases and coligands have shown interesting magnetic properties. The combined effect of phenoxide and carboxylate on magnetic properties of bridged complexes has also been studied (Nanda *et al.,* 1994). Salen type Schiff base ligands form Co(II/III) mixed valence complexes in *cis* and *trans* form by varying the solvent. Moreover, by changing the anionic coligands e.g. perchlorate, thiocyanate, dicyanamide etc., various phenoxido bridged Mn(III) complexes have been synthesized (Biswas *et al.,* 2011). The magnetic coupling between the metal centers was ferromagnetic in some of these complexes and antiferromagnetic in the others, which have been rationalized by DFT calculations and/or considering the structural parameters (Seth, Giri & Ghosh, 2015). The tridentate N_2O-donor Schiff base/reduced Schiff base ligands were utilized for the syntheses of complexes of Ni(II) and Cu(II) having various nuclearities. The magnetic measurements showed that the coupling between the metal centers can be ferro- or antiferromagnetic depending upon the bridging angles and bond distances (Biswas *et al.,* 2017). The supramolecular robustness of $\{[ML]_2M'\}$ type building blocks derived from N_2O_2 ligands has also been explored. Firstly, the linear-bent flexibility of the basic trinuclear structural unit $\{[NiL]_2M\}$

was evaluated with dicyanamide by varying M = Ni, Zn and Cd (Das, Gómez-García & Ghosh, 2015). Secondly, the use of flexible trinuclear metallatecton {$(CuL)_2Co$} as a building block to construct coordination complexes with ortho-, meta-, and para-benzenedicarboxylates for evaluating positional isomeric effects of the ligand. Both the results showed that the trinuclear units could conveniently be used as nodes for the synthesis of polynuclear complexes (Biswas *et al.,* 2014). Trinuclear heterometallic Cu^{II}–Mn^{II}, Cu^{II}–Co^{II} complexes have been prepared by N,O donor ligands with o-nitro benzoate anion (Ganguly *et al.,* 2023). The anionic coligands cyano, oximato, azido, dicyanomido, and thiocyanato are excellent for the formation of bridged one-dimentional, two-dimentional or three-dimentional dinuclear, trinuclear or tetranuclear complexes and these complexes play important role in understanding molecular magnetism. Among these pseudohalide anions, azide is the excellent for superexchange pathway between the paramagnetic centers of 3d transition metal ions (Adhikary & Koner, 2010). Azide containing μ-1,1 (end-on, EO) and μ-1,3 (end-to-end, EE) bridging Ni(II) and Mn(II) complexes have shown excellent magneto-structural correlations. Unprecedented end-on double azido bridged low Cu−N(azide)−Cu angles copper(II) complex have been reported with their magnetic properties (Koner *et al.,* 2004). Mukherjee *et al.* (2002) reported magnetic properties of three novel end-to-end single azido-bridged ferromagnetic copper(II) chains. Magneto-structural studies have been performed for the chlorido bridged coordination polymers (Singh, Lloret & Mukherjee, 2014). A rare defective dicubane tetranuclear μ_3-chlorido and a $\mu_{1,1,1}$-azido bridged Mn(II) complex have been reported and coupling constant values of the complex are rationalized by DFT calculations (Das *et al.,* 2019). Mixed bridged azido/cyanato copper(II) complexes have been studied with their magnetic studies (Nandy *et al.,* 2015).

Discussion

Different polynuclear 3d transition metal complexes have been prepared by using different types of ligands, most of them are Schiff bases derived from salicylaldehyde derivatives and diamines, phenoxido-bridged Cu(II) complexes are most frequent ones. The magnetic properties of the Cu_2O_2 core of these phenoxido-bridged complexes depend on several factors, such as coordination geometry of the metal centers, Cu–O bond lengths, Cu–O–Cu bond angles, Addition parameters, Cu···Cu distances, which are the parameters that have been shown to influence coupling constants (*J*) values (Biswas *et al.,* 2011). Thompson *et al.* (1996) observed that the *J* values strongly vary for μ-hydroxido, μ-alkoxido and μ-phenoxido bridged Cu(II) complexes. In general, larger the Cu–O–Cu angle favours large antiferromagnetic coupling between two paramagnetic centers. Simultaneously, Ni−O−Ni angles larger than 98° favour antiferromagnetic interactions for double alkoxido or hydroxido bridges Ni(II) complexes but the antiferromagnetic coupling becomes more strong for phenoxido bridged Ni(II) complexes whereas ferromagnetic coupling appears for angles close to 90°. The

presence of an additional *syn-syn* carboxylato bridge contributes weak or moderate antiferromagnetic coupling (Mukherjee *et al,* 2009). The magnetic coupling of heterometallic phenoxido-bridged Ni(II)–Mn(II) complexes is linearly dependent on the bridging angles. Antiferromagnetic exchange interaction increases with increasing Ni–O–Mn angles and the cross over angle is about ~98° for ferro- to antiferromagnetic exchange couplings (Maity *et al.,* 2021). The exchange coupling interaction of thiocyanato-bridged Ni(II) complexes depends on various factors such as bridging bond distances, bond angles and Ni–N–S–Ni torsion angle. The Ni–S–C and Ni–N–C angles which are close to 100° and greater than 160° respectively, are usually weak ferromagnetically coupled (Escuer *et al.,* 1996) and the antiferromagnetic coupling decreases with greater bridging bond distances. The bridging mode azide coligand influences the structure of the transition metal complexes and in general, end-on and end-to end coordination modes of azide ligand favour ferromagnetic and antiferromagnetic coupling between the paramagnetic metal centers, respectively (Adhikary & Koner, 2010). Most of the reported $\mu_{1,3}$-azido bridged Co(II) complexes are antiferromagnetic (Banerjee *et al.,* 2019).

Conclusion

This review shows the utility of different ligands for the assembly of multiple metal centers (whether homometallic or heterometallic) in a predetermined fashion. The factors that are responsible for determining the nuclearity and shape of the resultant clusters have been identified and monitored to get the desired products. The resultant polynuclear homometallic or heterometallic complexes were also utilized as a structural building block for the synthesis of coordination polymers. With the judicious variation of the ligands and metal ions, different research groups were able to synthesize complexes having wide variation of phenoxido bridging angles, which helped to draw magneto-structural correlations in different coordination complexes of 1st transition metals.

Acknowledgement

The author expresses his sincere thanks to Department of Biotechnology, Government of India, for the funding from DBT-STAR College grant, under which this review project was conducted. They are also grateful to the Principal and the DBT-STAR Coordinator, Surendranath College, for their support.

References

Adhikary, C., & Koner, S. (2010). Structural and magnetic studies on copper (II) azido complexes. *Coordination Chemistry Reviews*, *254*(23-24), 2933-2958. https://doi.org/10.1016/j.ccr.2010.06.001

Banerjee, A., Banerjee, S., Gómez García, C. J., Benmansour, S., & Chattopadhyay, S. (2019). Magnetic Properties of End-to-End Azide-Bridged Tetranuclear Mixed-Valence Cobalt (III)/Cobalt

(II) Complexes with Reduced Schiff Base Blocking Ligands and DFT Study. *ACS omega*, *4*(24), 20634-20643. https://doi.org/10.1021/acsomega.9b02764

Biswas, A., Drew, M. G., Gomez-Garcia, C. J., & Ghosh, A. (2017). Formation of a dinuclear and a trinuclear Ni (II) complex on slight variation of experimental conditions: Structural analysis and magnetic properties. *Polyhedron*, *121*, 80-87. https://doi.org/10.1016/j.poly.2016.09.050

Biswas, A., Drew, M. G., Ribas, J., Diaz, C., & Ghosh, A. (2011). Synthesis, Crystal Structures and Magnetic Properties of a Phenoxo-Bridged Dinuclear CuII Complex and a Dicyanamide Bridged Novel Molecular Rectangle Based on It. *European Journal of Inorganic Chemistry, 15*, 2405–2412. https://doi.org/10.1002/ejic.201100067

Biswas, S., Gomez-Garcia, C. J., Clemente-Juan, J. M., Benmansour, S., & Ghosh, A. (2014). Supramolecular 2D/3D isomerism in a compound containing heterometallic $Cu^{II}_2Co^{II}$ nodes and dicyanamide bridges. *Inorganic Chemistry*, *53*(5), 2441-2449. https://doi.org/10.1021/ic4023536

Das, A., Chakraborty, M., Maity, S., & Ghosh, A. (2019). The catalytic activities and magnetic behaviours of rare μ 3-chlorido and μ 1, 1, 1-azido bridged defective dicubane tetranuclear Mn (ii) complexes. *Dalton Transactions*, *48*(25), 9342-9356. https://doi.org/10.1039/C9DT01567A

Das, A., Gieb, K., Krupskaya, Y., Demeshko, S., Dechert, S., Klingeler, R., ... & Meyer, F. (2011). A new family of 1D exchange biased heterometal single-molecule magnets: observation of pronounced quantum tunneling steps in the hysteresis loops of quasi-linear $\{Mn_2Ni_3\}$ clusters. *Journal of the American Chemical Society*, *133*(10), 3433-3443. https://doi.org/10.1021/ja108740c

Das, L. K., Gómez-García, C. J., & Ghosh, A. (2015). Influence of the central metal ion in controlling the self-assembly and magnetic properties of 2D coordination polymers derived from $[(NiL)_2M]^{2+}$ nodes (M= Ni, Zn and Cd)(H_2 L= salen-type di-Schiff base) and dicyanamide spacers. *Dalton Transactions*, *44*(3), 1292-1302. https://doi.org/10.1039/C4DT02823F

Dey, A., Ali, J., Moorthy, S., Gonzalez, J. F., Pointillart, F., Singh, S. K., & Chandrasekhar, V. (2023). Field induced single ion magnet behavior in Co^{II} complexes in a distorted square pyramidal geometry. *Dalton Transactions*, *52*(41), 14807-14821. https://doi.org/10.1039/D3DT01769A

Escuer, A., Vicente, R., El Fallah, M. S., Solans, X., & Font-Bardía, M. (1996). Structure and magnetic behaviour of the first singly bridged nickel cyanate chain and a new dinuclear complex: an approximation to the superexchange mechanism for the nickel pseudohalide system. *Journal of the Chemical Society, Dalton Transactions*, (6), 1013-1019. https://doi.org/10.1039/DT9960001013

Ganguly, S., Bhunia, P., Mayans, J., & Ghosh, A. (2023). Trinuclear heterometallic CuII–MII (M= Mn and Co) complexes of N, O donor ligands with o-nitro benzoate anion: Structures, magnetic properties and catalytic oxidase activities. *Inorganica Chimica Acta*, *549*, 121404. https://doi.org/10.1016/j.ica.2023.121404

Ghosh, S., Mukherjee, S., Seth, P., Mukherjee, P. S., & Ghosh, A. (2013). Solvent-templated supramolecular isomerism in 2D coordination polymer constructed by Ni^{II}_2 Co II nodes and dicyanamido spacers: drastic change in magnetic behaviours. *Dalton Transactions*, *42*(37), 13554-13564. https://doi.org/10.1039/C3DT51326B

Ghosh, T. K., Mahapatra, P., Jana, S., & Ghosh, A. (2019). Variation of nuclearity in Ni^{II} complexes of a Schiff base ligand: crystal structures and magnetic studies. *CrystEngComm*, *21*(31), 4620-4631. https://doi.org/10.1039/C9CE00574A

Gole, B., Mondal, K. C., & Mukherjee, P. S. (2014). Tuning nuclearity of clusters by positional change of functional group: Synthesis of polynuclear clusters, crystal structures and magnetic properties. *Inorganica Chimica Acta*, *415*, 151-164. https://doi.org/10.1016/j.ica.2014.02.017

Koner, S., Saha, S., Mallah, T., & Okamoto, K. I. (2004). Unprecedented low Cu− N (azide)− Cu angles in end-on double azido bridged copper (II) complex. *Inorganic Chemistry*, *43*(3), 840-842. https://doi.org/10.1021/ic034347p

Maity, S., Mahapatra, P., Ghosh, T. K., Gomila, R. M., Frontera, A., & Ghosh, A. (2021). Synthesis of Ni (ii)–Mn (ii) complexes using a new mononuclear Ni (ii) complex of an unsymmetrical N_2O_3 donor ligand: Structures, magnetic properties and catalytic oxidase activity. *Dalton Transactions*, *50*(13), 4686-4699. https://doi.org/10.1039/D0DT04337K

Messerschmidt, A., Huber, R., Poulos, T., & Wieghardt, K. (2001). *Handbook of Metalloproteins* (Vol. 2). Chichester: John Wiley & Sons. http://dx.doi.org/10.1002/0470028637

Miyasaka, H., Clérac, R., Wernsdorfer, W., Lecren, L., Bonhomme, C., Sugiura, K. I., & Yamashita, M. (2004). A Dimeric Manganese (iii) Tetradentate Schiff Base Complex as a Single-Molecule Magnet. *Angewandte Chemie International Edition*, *43*(21), 2801-2805. https://doi.org/10.1002/anie.200353563

Mukherjee, P. S., Konar, S., Zangrando, E., Mallah, T., Ribas, J., & Chaudhuri, N. R. (2003). Structural analyses and magnetic properties of 3D coordination polymeric networks of nickel (II) maleate and manganese (II) adipate with the flexible 1, 2-bis (4-pyridyl) ethane ligand. *Inorganic Chemistry*, *42*(8), 2695-2703. https://doi.org/10.1021/ic026150n

Mukherjee, P. S., Maji, T. K., Escuer, A., Vicente, R., Ribas, J., Rosair, G., ... & Chaudhuri, N. R. (2002). Three Novel End-to-End Single Azido-Bridged Ferromagnetic Copper (II) Chains: Synthesis, Crystal Structure, and Magnetic Behavior. *European Journal of Inorganic Chemistry*, *2002*(4), 943-949. https://doi.org/10.1002/1099-0682(200203)2002:4%3C943::AID-EJIC943%3E3.0.CO;2-M

Mukherjee, P., Drew, M. G., Gomez-Garcia, C. J., & Ghosh, A. (2009). The crucial role of polyatomic anions in molecular architecture: structural and magnetic versatility of five nickel (II) complexes derived from AN, N, O-donor schiff base ligand. *Inorganic Chemistry*, *48*(13), 5848-5860. https://doi.org/10.1021/ic9001863

Nanda, K. K., Thompson, L. K., Bridson, J. N., & Nag, K. (1994). Linear dependence of spin exchange coupling constant on bridge angle in phenoxy-bridged dinickel (II) complexes. *Journal of the Chemical Society, Chemical Communications*, (11), 1337-1338. https://doi.org/10.1039/C39940001337

Nandy, M., Shit, S., Garribba, E., Gomez-Garcia, C. J., & Mitra, S. (2015). Double azido/cyanato bridged copper (II) dimers incorporating tridentate nitrogen donors Schiff base: Structure, EPR and magnetic studies. *Polyhedron*, *102*, 137-146. https://doi.org/10.1016/j.poly.2015.07.034

Pal, S., Chan, M. K., & Armstrong, W. H. (1992). Ground spin state variability in manganese oxo aggregates. Demonstration of an S= 3/2 ground state for $[Mn_3O_4(OH)(bpea)_3](ClO_4)$ 3. *Journal of the American Chemical Society*, *114*(16), 6398-6406. https://doi.org/10.1021/ja00042a016

Sahu, P. K., Kharel, R., Shome, S., Goswami, S., & Konar, S. (2023). Understanding the unceasing evolution of Co (II) based single-ion magnets. *Coordination Chemistry Reviews*, *475*, 214871. https://doi.org/10.1016/j.ccr.2022.214871

Sessoli, R., Tsai, H. L., Schake, A. R., Wang, S., Vincent, J. B., Folting, K., ... & Hendrickson, D. N. (1993). High-spin molecules:[$Mn_{12}O_{12}$ (O_2CR) $_{16}$ (H_2O) $_4$]. *Journal of the American Chemical Society*, *115*(5), 1804-1816. https://doi.org/10.1021/ja00058a027

Seth, P., Giri, S., & Ghosh, A. (2015). Tuning of exchange coupling by the Mn–O distance and phenoxido bridging angle: an experimental and theoretical study of the family of Mn (III) dimers with salen type ligands. *Dalton Transactions*, *44*(28), 12863-12870. https://doi.org/10.1039/C5DT01224D

Shit, S., Nandy, M., Rizzoli, C., Desplanches, C., & Mitra, S. (2016). Crystal structure, characterization and magnetic properties of a 1D copper (II) polymer incorporating a Schiff base with carboxylate side arm. *Journal of Chemical Sciences*, *128*, 913-920. https://doi.org/10.1007/s12039-016-1082-4

Sieber, A., Foguet-Albiol, D., Waldmann, O., Ochsenbein, S. T., Bircher, R., Christou, G., ... & Güdel, H. U. (2005). Direct Determination of the Anisotropy and Exchange Splittings in the Dimeric Single-Molecule Magnet [$Mn_4O_3Cl_4$ (O_2CEt) $_3$ (py) $_3$] $_2$⊙ 8MeCN by Inelastic Neutron Scattering. *Inorganic Chemistry*, *44*(19), 6771-6776. https://doi.org/10.1021/ic050764l

Singh, R., Lloret, F., & Mukherjee, R. (2014). Mono-and Di-chloro-bridged Discrete Dimers and Trimers and Mono-Chloro-Bridged 1D-Coordination Polymer of Copper (II). Magneto-structural Studies. *Zeitschrift Für Anorganische Und Allgemeine Chemie*, *640*(6), 1086-1094. https://doi.org/10.1002/zaac.201400005

Thomas, L., Lionti, F. L., Ballou, R., Gatteschi, D., Sessoli, R., & Barbara, B. (1996). Macroscopic quantum tunnelling of magnetization in a single crystal of nanomagnets. *Nature*, *383*(6596), 145-147. https://doi.org/10.1038/383145a0

Thompson, L. K., Mandal, S. K., Tandon, S. S., Bridson, J. N., & Park, M. K. (1996). Magnetostructural correlations in bis (μ2-phenoxide)-bridged macrocyclic dinuclear copper (II) complexes. Influence of electron-withdrawing substituents on exchange coupling. *Inorganic Chemistry*, *35*(11), 3117-3125. https://doi.org/10.1021/ic9514197

Weiss, J. (2010). Supramolecular approaches to nano and molecular electronics. *Coordination Chemistry Reviews*, *19*(254), 2247-2248. http://dx.doi.org/10.1016%2Fj.ccr.2010.06.002

doi: 10.31674/book.2024ecc.12

Green Hydrogen, an Alternative Renewable Energy Source: Based on Solar-Energy-Driven Water-Splitting Technology

Amit Kumar Dutta

Department of Chemistry, Bangabasi Morning College, Kolkata, West Bengal, India

Corresponding Author's Email: amitkumardutta@bangabasimorning.edu.in

Abstract:

The need for zero-emission, eco-friendly hydrogen fuel has increased enormously over the years due to adverse impacts on the environment caused by conventional fuels such as natural gas, coal, oil, fossil fuels, bio-mass etc. This chapter reports the safest and most efficient route for hydrogen-fuel production based on solar-energy-driven water-splitting technology over a heterogeneous photo-catalyst. Several challenges have been made for the extension of photo-catalyst, based on nano-sized semiconducting materials such as binary and ternary metal chalcogenides nano-materials, CuS, CdS, Fe_3O_4, $CuInO_2$, $CuInS_2$, $CuGaS_2$ and their composites with hetero-nanostructure. When the nano-structures have the ability to absorb solar-light-energy (having a narrow band gap energy < 3.6 eV), i.e., to utilise the most of the solar-spectrum, the photo-catalytic performances have increased much more. The catalytic performances of the semiconductors have also been improved for enhanced hydrogen production using nano-engineering technology, i.e., different modifications to the nano-catalyst surface and electronic energy structure, so that they can act as an efficient photo-catalyst for solar-energy driven water electrolysis to produce enhanced large-scale hydrogen-fuel. The possible mechanism of the photo-chemical processes has also been explored through the formation of free electron-hole pair (e^-/h^+) on suitable heterogeneous catalyst's surface and controlling the kinetics of hydrogen evolution reaction and oxygen evolution reaction. How the proposed nano-catalyst materials have been designed to optimize solar-to-hydrogen conversion efficiency, improve the rate of hydrogen production and commercialized for the sake of society has been deliberated.

Keywords: *Electro-Catalytic Activity; Photo-Catalysis; Semiconducting Nano-Materials; Solar-Energy-Driven Chemical Reactions; Water-Splitting; Zero Emission Hydrogen*

Introduction:

Natural fuel supplies are gradually running out, which is why there is a growing need for alternate, renewable, and non-fossil energy sources. Again Recently, much attention has been paid to 'hydrogen-fuel', as a next-generation energy carrier. Hydrogen is commonly known as 'Zero emission fuel (ZEF)' (Nnabuife *et al*., 2023) (Figure 1)

because when hydrogen entries into vehicles that run on hydrogen fuel, it produces only water vapour and generates almost no harmful air pollution, unlike conventional fuels such as natural gas, coal, oil, fossil fuel, bio-mass etc. which emit equally large amount (830 million tons) of carbon dioxide annually into the atmosphere (Höök & Tang, 2013). Due to presence of simplest chemical structure, where only two hydrogen atoms are stuck together by electrostatic force of attraction, hydrogen-fuel is non-toxic, odorless, and tasteless, unlike conventional fuels such as natural gas, coal, oil, fossil fuel, bio-mass etc. that contain toxic substances. With tremendous development of science and technology, Japan first achieved full-scale use of hydrogen-fuel as renewable energy source, like solar and wind-energy. In 2015, world's first publicly available Hydrogen Vehicle, commonly known as fuel cell electric vehicle, was launched in Japan, where energy is generated by converting chemical energy of hydrogen to mechanical energy in a fuel cell to rotate electric motor (Turoń, 2020). In this case, when hydrogen entries into fuel-cell device of a Hydrogen Car or Bus, it has been used as fuel and combines with oxygen from the air, creates electricity and water vapour through an electrochemical process. In this way, hydrogen and fuel cells can play an important role in the country-wide energy strategy, with the potential for use in a broad range of applications across all sectors—transportation, commercial, industrial, residential, etc.

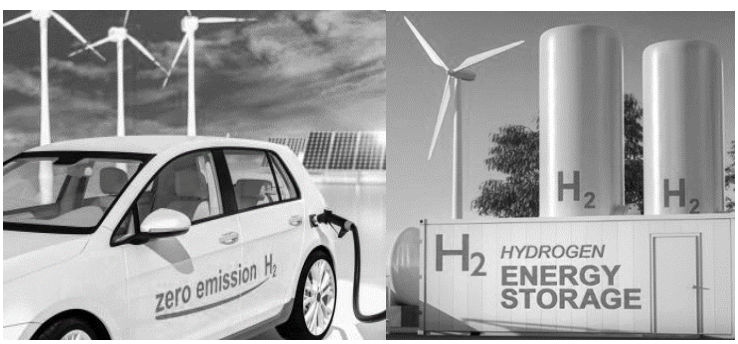

Figure 1: Zero emission future (Net Zero*) (Source: Nnabuife et al., 2023)*

Hydrogen is the simplest and most abundant chemical element in the universe. It was discovered in the Sun, Stars and the gas planets, but on earth, hydrogen doesn't exist in free form and is generally found in compounds with other elements such as carbon and oxygen, it exists mainly as methane (CH_4) and water (H_2O), respectively. To obtain pure hydrogen for industrial applications, it must be separated from the compounds to which it is bound. Since the beginning of the 19th century, hydrogen-fuel has been so chosen to be used to fuel cars, airships, spaceships etc. and most of the cases of hydrogen (in environment sense Grey Hydrogen) have been extracted commercially from fossil-fuels such as natural gas, coal, oil, bio-mass etc. that emit equally large amount of carbon dioxide into the atmosphere. So, focus needs to be put on replacing

that grey hydrogen with one that can reduce global warming, decrease fossil-fuel dependency through improving technologies for fully utilizing unlimited water resources. Since then, water-splitting or water-electrolysis process has become much desired, where pure green hydrogen can be produced by separating hydrogen from the oxygen in water. In 2022, Govt. of India established the national Green Hydrogen Mission and India's first 99.99% pure green-hydrogen-pilot-plant was commissioned by OIL (Oil India limited) where pure hydrogen has been generated by the electrolysis of water or water-splitting (Harichandan, Kar & Rai, 2023; Vardhan *et al*., 2022).

Now-a-days, solar-energy-driven water-splitting, over a nano-sized photo-catalyst material, is the most acceptable method for enhanced large-scale hydrogen production (Kim *et al*., 2019; Maji *et al*., 2012). Light is an outstanding source of energy and has been used as driving force to conduct chemical-pathways. When solar-energy is used in a photo-chemical reaction, it will be the most beneficial alternate sustainable-energy source as the abundance is virtually unlimited and free, making the hydrogen production process more cost-effective for the sake of society (Dutta *et al*., 2012). In the year 1967, Prof. Fujishima and Honda (1972) of Tokyo University of Science, Japan, first discovered the Photo-catalytic hydrogen production technology, which is basically analogous to the natural photo-synthesis technique in plant-leaves and similar types of photo-chemical reactions have been carried out under light irradiations (Figure 2). In their research works, it has been observed that, in a photo-electrochemical set up with Titanium dioxide (TiO_2) nano-material based working electrode and a Platinum cathode, when light falls on the TiO_2 surface, gas bubbles consisting of hydrogen have evolved from the surface of the TiO_2 anode while simultaneously oxygen gas has been generated at the Pt counter electrode from water splitting.

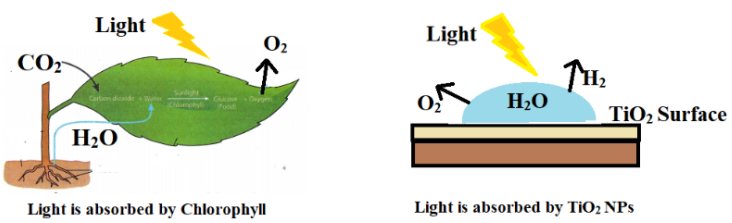

Figure 2: Photo-catalysis technology on TiO_2 surface, basically analogous to the photo-synthesis technique in plant *(Source: Fujishima & Honda, 1972)*

The possibility of hydrogen production from water opens the door for the development of hydrogen production technology by employing different nano-materials with very interesting physico-chemical features. As a catalyst material, nano-sized inorganic materials show remarkable efficiency in the field of photo-catalysis technology (Hoffmann *et al*., 1995). As the dimension of the nano-scaled materials is so small, new interesting properties have been generated, such as interesting chemical and physical

properties, large specific surface area, large specific surface-to-volume ratio, greater surface tension, greater surface activity, high catalyst-loading capacity and better light absorption capacity. Again, the nano-dimension having large surface-to-volume ratio can enormously increase the number of active sites at the nano-catalyst's surface, their interaction with different target-molecules/moieties and hence catalytic performances. Now-a-days, using nano-engineering technology, the nano-structure can be manipulated during nano-materials synthesis with specific control over size (quantum confinement), shape, morphology and hence the catalytic performances towards hydrogen production can be optimized.

When the nano-structures are semiconducting in nature, they possess suitable band-gap energies and flat band-potential levels that can easily absorb UV, visible, even solar-light-energy and accelerate the photo-chemical reaction rate (Nakata & Fujishima, 2012). Most of the metal chalcogenides nano-particles such as metal oxides, metal sulfides TiO_2, ZnO, CuO, FeS, ZnS NPs etc. are semiconducting in nature and have proper redox potentials, excellent electron transfer ability and outstanding stability in air and solutions (Sun *et al*., 2008).

Keeping in mind low-cost and large-scale hydrogen production for the sake of society, this chapter comprehensively summarizes how pure green hydrogen production technology has been developed in such a way that low-cost, large-scale commercially hydrogen has been obtained from unlimited and free water resources using unlimited and free solar-energy. It has also been discussed in detail about the fundamental principle of water-splitting technologies based on simplest photo-catalytic water-electrolysis. The possible mechanism of the photo-chemical processes has also been explored through the creation of free electron-hole pair (e^-/h^+) on suitable heterogeneous catalyst's surface and controlling the kinetics of hydrogen evolution reaction (HER) and oxygen evolution reaction (OER). A brief overview of recent trends in solar-energy-driven hydrogen-fuel production has been deliberated.

Fundamental principle of water-splitting technologies

Water is the most copious resource for hydrogen-production. Water-splitting technology breaks the water molecule into hydrogen and oxygen when suitable amount of energy is provided according to thermodynamic equation 1 and 2.

$$H_2(g) + \frac{1}{2}O_2(g) \rightarrow H_2O(l) + 237.2\,\text{kJ mol}^{-1} \quad (1)$$

$$\boldsymbol{H_2O \longrightarrow H_2 + \frac{1}{2}O_2 \quad (\Delta G = 237\ kJ/mol)} \quad (2)$$

As equation 1 involves thermodynamically uphill transformation, which is associated with positive 237.2 kJ/mol Gibbs free energy (Li & Li, 2017), in water-splitting reverse reaction

(equation 2), a certain amount of energy equivalent to Gibb's free energy (~237 kJ/mol) has to be supplied to the system comprising water, leading to the conversion (thermodynamically) into hydrogen and oxygen. Generally, in simplest way, electrical energy has been used to split water, which is commonly known as water-electrolysis. In this case, an electrical current has been passed through two electrodes (anode and cathode) of an electrochemical set-up containing water molecules to conduct two half-cell reactions, oxidation and reduction, leading to the formation of hydrogen and oxygen, respectively (Holladay *et al*., 2009). From the redox point of view, the reduction reaction by electrons to form H_2 (at the cathode) and oxidation reaction to form O_2 (at the anode) are commonly known as hydrogen evolution reaction (HER) and oxygen evolution reaction (OER), respectively (Li, Wang & Wang, 2021).

anode

$$H_2O \rightarrow 1/2O_2 + 2H^+ + 2e^- \quad (E^0 = 1.23 \text{ V vs. RHE})$$

cathode

$$2H^+ + 2e^- \rightarrow H_2 \qquad (E^0 = 0 \text{ V vs. RHE})$$

overall process

$$H_2O \rightarrow H_2 + 1/2O_2$$

The kinetics of HER requires redox potential of H^+/H_2 i.e., 0 V vs. NHE and standard reduction potential of 1.23 V vs. NHE (E^0 of O_2/H_2O) requires for evolution of oxygen. The total Gibb's free energy (237.2 KJ/mol) corresponds to 1.23 eV per electron have to be supplied to overcome the overall thermodynamic barricade of the water-splitting reaction is 1.23 V.

Photo–catalytic mechanism on water-splitting

When a heterogeneous semiconductor photo-catalyst has been employed in the above water-splitting chemical pathway, enhanced large-scale hydrogen-production has been obtained. Under light illumination. In a photo-chemical set up, suitable catalyst material plays important role in quickening the kinetics of both the OER and HER.

Numerous attempts have been covered to develop photo-catalyst materials in such a way that they can function under visible, even solar-light irradiation to efficiently utilize solar-energy. In photo-catalysis process, metal chalcogenide-based nanomaterials are chosen as heterogeneous photo-catalyst because they are semiconducting in nature and possess suitable band gap and flat band potential levels with filled valance band (VB) and vacant conduction band (CB) (Figure 3). Titanium dioxide (TiO_2) nano-material has been selected as the model material for basic investigation and to demonstrate

general surface photo-catalytic reactions of semiconductors. It is generally accepted that the main reaction responsible for photo-catalysis is the interfacial redox reaction of carriers generated when a certain amount of energy is absorbed by the semiconductor catalyst. If the band gap energy of the catalyst is equivalent to or less than the energy of incident light energy, the electrons (e^-) residing in VB will absorb the photon and be promoted to the CB, thus leaving behind a hole (h^+) in VB of the semiconducting nanomaterials (Figure 3).

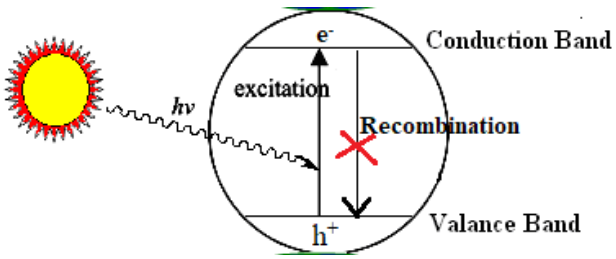

Figure 3: Illustration of photo-catalytic mechanism *(Source: Dutta, Maji & Adhikary, 2014)*

The photo-chemical reactions basically start with the free electron-hole pair (e^-/h^+) formation (Dutta, Maji & Adhikary, 2014). That 'e⁻' s and 'h⁺' s pass to the active sites of the surface of semiconductor photo-catalyst, acting as reducing or oxidizing agents to drive reduction/oxidation reaction on that surface. In water-splitting process, water molecules are reduced by the photo-induced electrons to form H_2 and similarly, water molecules are oxidized by the photo-induced holes to O_2 (Almomani, Shawaqfah & Alkasrawi, 2022) (Figure 4) according to equation:

$$2\,H_2O + 4\,h^+ \rightarrow 4\,H^+ + O_2\ (E^0 = 1.23\ \text{V vs. RHE})$$

$$2\,H^+ + 2\,e^- \rightarrow H_2\ (E^0 = 0\ \text{V vs. RHE})$$

The hydrogen gas that produced was collected using gas-tight syringe and analysed by gas chromatography.

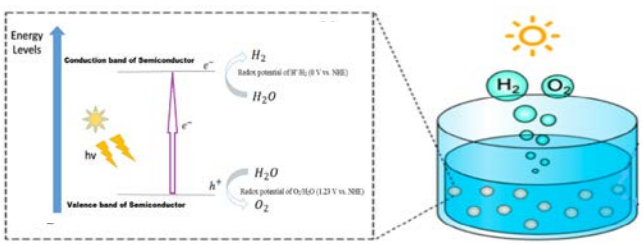

Figure 4: General illustration for photocatalysis-based water splitting on TiO_2 nano-materials *(Source: Almomani, Shawaqfah & Alkasrawi, 2022)*

Recent trends of Photo–catalytic (PC)-based hydrogen-fuel production

Inspiring from the first research work of Fujishima and Honda in 1972, so many researchers have paid considerable attention to increasing hydrogen production efficiency in a large-scale way using efficient catalyst materials such as metal oxides, metal sulphides, carbon-nitrides, polymers, hetero-nanostructures, even under natural solar-light illumination (Teixeira *et al*., 2018). In these cases, the catalyst materials can act as catalytically active sites to facilitate the corresponding HER, lowering the kinetics overpotentials of water-splitting.

From the above thermodynamic restrictions, a semiconductor photo-catalyst that has the ability to split water to produce hydrogen must have flat band-positions in such a way that the bottom level of the conduction band (CB) position should be more negative than the redox potential of H^+/H_2 (0 V vs. NHE) for evolution of hydrogen and the top level of the valence band (VB) needs to be more positive than the standard reduction potential of O_2/H_2O (1.23 V vs. NHE) for evolution of oxygen (Jafari *et al*., 2016). So, the minimum band-gap energy of a semiconductor photo-catalyst necessary for driving water-splitting process is 1.23 eV. To efficiently use solar-energy, the band-gap energy (E_g) should be in the range of 3.0 eV > E_g > 1.23 eV (Qiao *et al*., 2018). Figure 5 represents the band potential positions of several metal chalcogenide semiconductors relative to the water redox potential levels, which can efficiently split water to produce hydrogen.

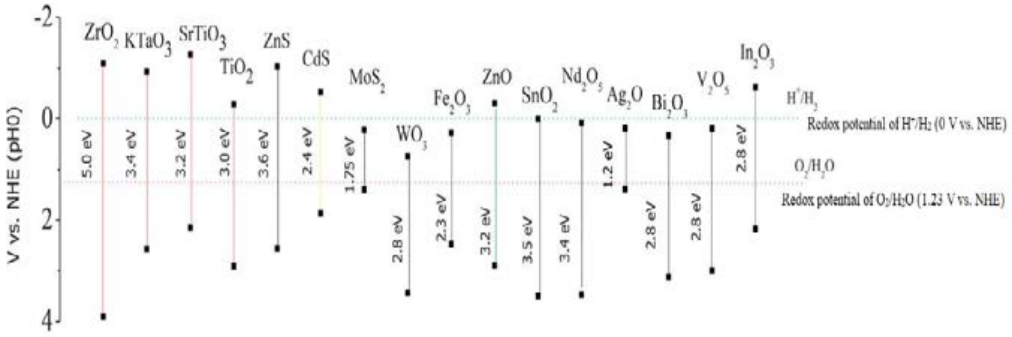

Figure 5: Band potential position of several metal chalcogenide semiconductors against normal hydrogen electrode (NHE) as a reference *(Source: Jafari et al., 2016)*

Though fulfilling thermodynamic potential level condition, some nano-materials cannot efficiently produce hydrogen, exhibit inacceptable photo-catalytic capability much below the expected level, due to their partial light utilization, inactive surface redox processes. Again, most of the photo-generated electrons and holes can re-combine (considerable electron–hole pair re-combination) on the photo-catalyst's surface in a very short-time.

Again, after formation of hydrogen, the back-ward reaction of H_2 and O_2 to H_2O occurs immediately.

Under these circumstances, in the recent trend, numerous effective strategies have been explored to increase light absorption, photo-generated charge separation and lower kinetic overpotentials of hydrogen evolution using different efficient nano-semiconductors, such as metal oxides, carbon-nitrides, polymers, and hetero-structures (Teixeira *et al*., 2018). In addition, different modifications on nano-catalyst surface, such as amalgamation of semiconductors with other components by ion-doping, hetero-structure fabrication, noble-metal loading, morphology or size modulation, defect engineering, tuning of active crystal facets etc. have also been adopted for enhancing the photo-catalytic capability. Using defect engineering, vacancy defects in semiconductors can enhance catalytic efficiency and improve photocatalytic water-splitting. Actually, vacancy defects can change the electronic structure of semiconductors and generate defective energy levels near the conduction-band (CB) or near the valence-band (VB) in case of n-type or p-type semiconductors, respectively. The newly formed energy level (Fermi level) in semiconductors can effectively prohibit electron–hole pair recombination, can effectively promote light absorption or improve visible light harvesting, promote charge carrier separation (photo-induced carrier separation) and photo-electron transfer, which really extend the carrier life-time, increase conductivity, and reduce the energy barriers for water-splitting. Again, in the cobalt sulphide/nickel sulphide hetero-structure, hybridization between two or more transition metal-based materials can synergistically enhance their catalytic performance and facilitate charge-transport ability, which provides a synergistic effect (Figure 6) toward HER and OER (Shit *et al*., 2018).

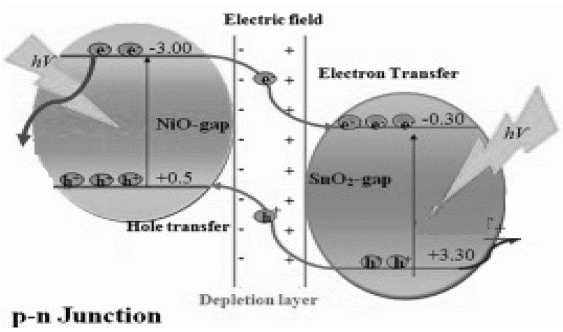

Figure 6: Illustration of synergistic effect on charge transport towards photo-catalytic reaction *(Source: Shit et al., 2018)*

Similarly, when some semiconductors (TiO_2) coupled with highly conductive supports such as metallic Silver, Gold, Pd, Pt or bimetallic PdPt NPs, they can strongly prevent the re-combination of photo-generated electrons in the semiconductor, enhance the

electron-transport behaviour and improve their photo-electrocatalysis performances towards water-splitting (da Silva *et al*., 2020). Also, active co-catalyst loading (say Ni_3N) onto semiconductor g-C_3N_4 support, can produce hydrogen under visible-light illumination with hydrogen evolution rate of ~305.4/mol/h/g, which is about three times higher than that of pristine g-C_3N_4 (Ge *et al*, 2019). ZnS nano-structure has excellent potential in solar-energy-driven hydrogen formation because of its ability to quickly generate photo-induced carriers. Again, zinc vacancies can modulate the electronic energy-level of ZnS and affect the CB and VB positions in such a way that it can decrease the oxidation capacity of the holes, protecting the Zn-deficient ZnS from photo-corrosion, leading to long-term photo-catalytic stability and exhibiting an outstanding light-energy-driven hydrogen productivity of ~338 μmol/h/g. Besides, Bi-based photo-catalysts, Bi_2WO_6 nano-bipyramids with "Bi–O" vacancy and $BiVO_4$ with enriched oxygen vacancies have been used for enhanced solar-energy-driven photocatalytic hydrogen production and show much stronger photo-sensitivity and photo-induced carrier separation ability owing to the formation of the intermediate defect energy-level in its band-gap (Kim *et al*., 2015).

Photo-electrocatalysis (PEC) technology on water-splitting

Photo-electrocatalysis technology (PEC) is gaining considerable interest for commercial green-hydrogen production owing to presence of lower system complexity, lower operation potential and higher hydrogen production efficiency. If in the above photo-chemical mechanism, an externally applied electrical bias (Figure 7) has been used in an electro-chemical setup having a photo-electrode (photo-anode) coating with a similar type of semiconducting nano-material and normal platinum counter electrode, photo-electrocatalysis i.e. 'electrochemically assisted photo-catalysis' technology, has been developed. Here, the photo-catalysis technology has been combined with electro-catalysis to make dual-functional catalysis work for green-hydrogen production (Chatterjee *et al*., 2022).

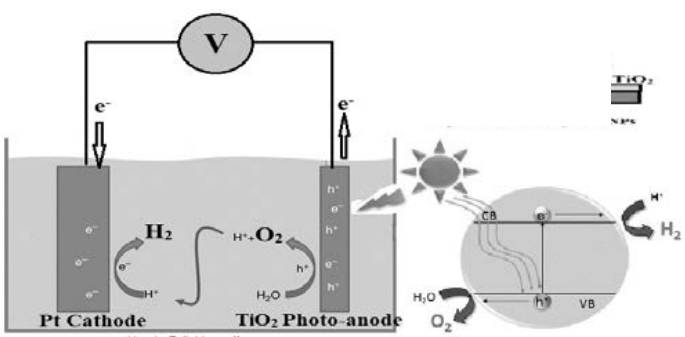

Figure 7: Schematic diagram of PEC water-splitting based on n-type photo-anode
(Source: Chatterjee et al., 2022)

In PEC water-splitting technology, the first electron-hole pair (e^-/h^+) is generated on the surface of a photo-electrode (generally photo-anode) upon light irradiation, followed by immediate transfer of those electrons to counter electrode through external circuit in the presence of external bias which promotes the HER redox reactions for hydrogen production (Figure 7). Here, the externally applied electrical bias plays an important role in preventing electron-hole pair (e^-/h^+) re-combination through the migration of electrons to counter electrode and thereby increasing the life-time of the generated electron–hole pairs, which can improve the hydrogen production reaction-rates. The photo-anode, where electrons are the majority carriers, is generally fabricated by immobilising a n-type semiconducting nano-material onto an electrically conducting supporting substrate such as metals, carbonous materials or conductive films such as indium-doped tin oxide (ITO) or fluorine-doped tin oxide (FTO). Owing to large number of electrons that migrate to counter electrode upon light irradiation, which is commonly known as photo-induced carrier transport properties, an anodic photo-current response has been generated and can be measured experimentally through linear sweep voltammetry in comparison to current in dark (Figure 8a). Similarly, cathodic photocurrents have been observed from photo-cathodes coated with p-type materials, where holes are the majority carriers (Figure 8b) (Sato,1998).

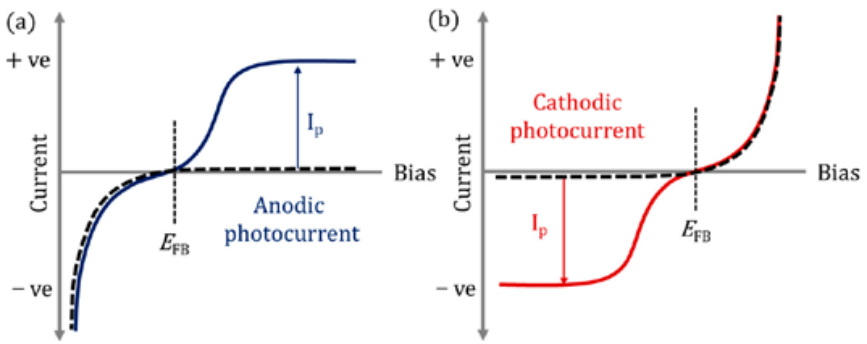

Figure 8: (a) Anodic photocurrent (Ip) response, (b) cathodic photocurrent (Ip) response; solid lines under irradiation; dashed lines in dark; EFB flat band potential (Sato,1998)

Various solar-energy-driven hydrogen production technologies have been greatly developed based on photo-electrochemical (PEC) water splitting with a high solar-to-hydrogen (STH) conversion efficiency. Different semiconductor electro-catalyst have been designed to optimize STH efficiency and improve rate of hydrogen production. Till now, $BiVO_4$ has been established to be the best metal oxide electro-catalyst material and has been used as photoanode, which exhibits a photocurrent density of ~4.5 mA cm−2 at 1.23 V under simulated sunlight irradiation, corresponding to high STH efficiency of 8.1% (Pihosh *et al*., 2015). According to R. Banerjee and his co-workers (2021), the rate of H_2 production from water over a heterogeneous photo-catalyst, CdS-

carbon nano-composite (40 MC/CdS of Figure 9), has been found to be much higher i.e., 37,641 μmol/g/h due to the presence of a suitable flat band potential and photo-generated charge separation ability of catalyst.

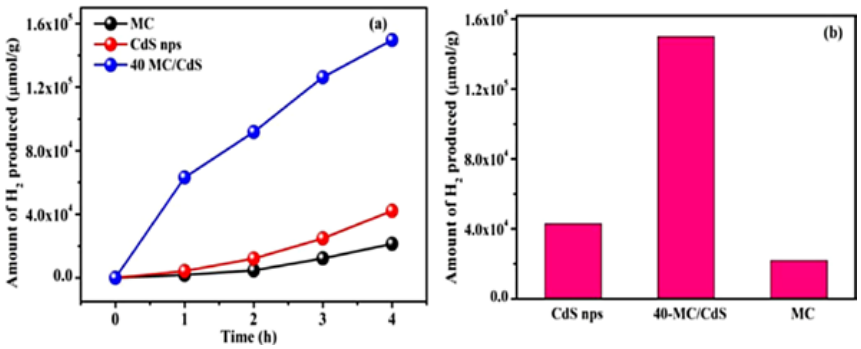

Figure 9: (a) Photo-catalytic hydrogen-fuel production (μmol/g/h) in presence of different CdS NPs (b) comparative study of H_2 production obtained after 4 h of light irradiation *(Source: Banerjee et al., 2021)*

In recent years, there has been considerable attention to use hetero-structured semiconductor nano-composites in water-splitting technology to improve catalytic performances for enhanced hydrogen production and catalyst stability. Owing to presence of effective exciton-plasmon coupling (Figure 10) at hetero-junction, some semiconductors coupled with highly conductive supports such as metallic Silver, Gold, Pd or Pt can strongly prevent the re-combination of photo-generated electrons of the semiconductor, enhance the electron transport behaviour and hence improve their photo-electrocatalysis performances. The Au–$CuGaS_2$ and Au–$CuInS_2$ twin-structures similarly exhibit plasmon enhanced superior charge-transport ability, generate abruptly high photocurrent-density and have been used as potential candidates for photo-electrochemical water-splitting (Ghosh *et al*., 2018).

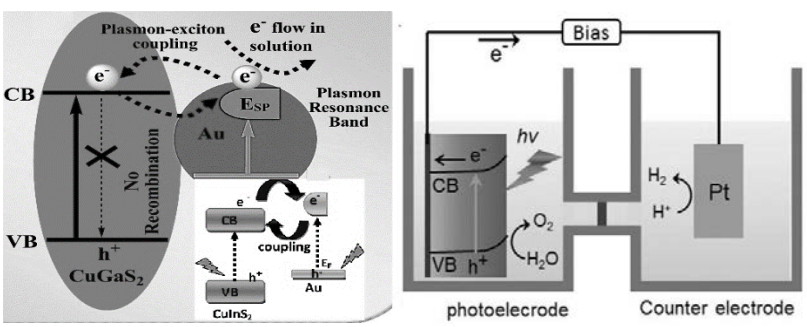

Figure 10: Basic mechanism of plasmon–exciton coupling in the Au–$CuGaS_2$ hetero-structure *(Ghosh et al., 2018)*

Again, water-splitting concerning OER and HER also depends upon overpotentials (η) and those overpotentials have been enormously minimized with the help of efficient and bi-functional electro-catalysts, silver permanganate ($AgMnO_4$ AMO)/Pd nano-composite (Mondal *et al*., 2021). The catalytic performances of simple $AgMnO_4$ (AMO) nano-materials had been improved for enhanced hydrogen production using nano-engineering technology through loading with highly conductive Pd over AMO and further modifying with PdOx (x = 1, 1.5, 2), having different oxidation states of $Pd^{\delta+}$ species produced at the AMO−Pd interface. It has been reported that the robust synergistic effect among AMO, Pd^{3+} and PdOx strongly contributes to remarkable OER/HER performances and AMO/PdOx/Pd-260 NComp (NComp-3) exhibits extremely low overpotentials (η10) (160 mV for OER, 58 mV for HER at 10 mA cm^{-2}), highest Turnover Frequency (TOF) (3.7×10^{-1} s^{-1}) and highest specific activity at η of 200 mV.

Conclusion

This chapter aims to give an overview of different low-cost, large-scale pure green-hydrogen production technologies in such a way that commercially hydrogen has been obtained from unlimited, free water resources using unlimited and free solar-energy. Heterogeneous photo-catalyst materials have been successfully developed based on nano-sized semiconducting materials such as binary and ternary metal chalcogenides nano-materials, CuS, CdS, Fe_3O_4, $CuInO_2$, $CuInS_2$, $CuGaS_2$ and their composites. The catalytic performances of the semiconductors have been successfully improved for enhanced hydrogen production using nano-engineering technology i.e., different modifications to the nano-catalyst surface and electronic energy structure, which can act as an efficient photo-catalyst for solar-energy driven water-electrolysis to produce large-scale hydrogen-fuel. The possible photo-catalytic mechanism has also been discussed through the detection of free electron-hole pairs (e^-/h^+) on a suitable catalyst's surface, which will act as reducing or oxidizing agents to drive reduction/oxidation reaction i.e., the hydrogen evolution reaction (HER) to form H_2 and oxygen evolution reaction (OER), respectively. The catalytic performances have also been improved by tuning shape, size, morphology and band-gap energy during synthesis process. A brief overview of recent trends in solar-energy driven hydrogen-fuel production has been deliberated and successfully commercialized for the sake of society so that most of the solar-spectrum and light energies can be utilized for large-scale applications.

Acknowledgement

The author is grateful to Prof. Bibhutosh Adhikary, Department of Chemistry, Indian Institute of Engineering Science and Technology (IIEST), Shibpur, for helpful discussions. He is indebted to UGC, India, for financial support through the MRP [PSW–066/15–16 (ERO)]. The author also acknowledges the MHRD (India) for providing instrumental facilities to the Department of Chemistry, IIEST Shibpur and RUSA Scheme

of the Department of Higher Education, Government of West Bengal, for providing instrumental facilities to the Department of Chemistry, Bangabasi Morning College, Kolkata, India.

References

Almomani, F., Shawaqfah, M., & Alkasrawi, M. (2022). Solar-driven hydrogen production from a water-splitting cycle based on carbon-TiO_2 nano-tubes. *International Journal of Hydrogen Energy*, *47*(5), 3294-3305. https://doi.org/10.1016/j.ijhydene.2020.12.191

Banerjee, R., Pal, A., Ghosh, D., Ghosh, A. B., Nandi, M., & Biswas, P. (2021). Improved photocurrent response, photostability and photocatalytic hydrogen generation ability of CdS nanoparticles in presence of mesoporous carbon. *Materials Research Bulletin*, *134*, 111085. https://doi.org/10.1016/j.materresbull.2020.111085

Chatterjee, P., Ambati, M. S. K., Chakraborty, A. K., Chakrabortty, S., Biring, S., Ramakrishna, S., ... & Dalapati, G. K. (2022). Photovoltaic/photo-electrocatalysis integration for green hydrogen: A review. *Energy Conversion and Management*, *261*, 115648. https://doi.org/10.1016/j.enconman.2022.115648

da Silva, A. G., Fernandes, C. G., Hood, Z. D., Peng, R., Wu, Z., Dourado, A. H., ... & de Torresi, S. I. C. (2020). PdPt-TiO2 nanowires: correlating composition, electronic effects and O-vacancies with activities towards water splitting and oxygen reduction. *Applied Catalysis B: Environmental*, *277*, 119177. https://doi.org/10.1016/j.apcatb.2020.119177

Dutta, A. K., Maji, S. K., & Adhikary, B. (2014). γ-Fe_2O_3 nanoparticles: an easily recoverable effective photo-catalyst for the degradation of rose bengal and methylene blue dyes in the waste-water treatment plant. *Materials Research Bulletin*, *49*, 28-34. http://dx.doi.org/10.1016/j.materresbull.2013.08.024

Dutta, A. K., Maji, S. K., Srivastava, D. N., Mondal, A., Biswas, P., Paul, P., & Adhikary, B. (2012). Synthesis of FeS and FeSe nanoparticles from a single source precursor: a study of their photocatalytic activity, peroxidase-like behavior, and electrochemical sensing of H_2O_2. *ACS Applied Materials & Interfaces*, *4*(4), 1919-1927. https://doi.org/10.1021/am300408r

Fujishima, A., & Honda, K. (1972). Electrochemical photolysis of water at a semiconductor electrode. *Nature*, *238*(5358), 37-38. https://www.nature.com/articles/238037a0

Ge, J., Liu, Y., Jiang, D., Zhang, L., & Du, P. (2019). Integrating non-precious-metal cocatalyst Ni3N with g-C_3N_4 for enhanced photocatalytic H_2 production in water under visible-light irradiation. *Chinese Journal of Catalysis*, *40*(2), 160-167. https://doi.org/10.1016/S1872-2067(19)63283-3

Ghosh, A. B., Saha, N., Sarkar, A., Dutta, A. K., Satra, J., & Adhikary, B. (2018). Single source precursor driven phase selective synthesis of Au–$CuGaS_2$ heteronanostructures: an observation of plasmon enhanced photocurrent efficiency. *Dalton Transactions*, *47*(4), 1071-1081. https://doi.org/10.1039/C7DT04169A

Harichandan, S., Kar, S. K., & Rai, P. K. (2023). A systematic and critical review of green hydrogen economy in India. *International Journal of Hydrogen Energy*, *48*(81) 31425-31442. https://doi.org/10.1016/j.ijhydene.2023.04.316

Hoffmann, M. R., Martin, S. T., Choi, W., & Bahnemann, D. W. (1995). Environmental applications of semiconductor photocatalysis. *Chemical Reviews*, *95*(1), 69-96. https://doi.org/10.1021/cr00033a004

Holladay, J. D., Hu, J., King, D. L., & Wang, Y. (2009). An overview of hydrogen production technologies. *Catalysis Today*, *139*(4), 244-260. https://doi.org/10.1016/j.cattod.2008.08.039

Höök, M., & Tang, X. (2013). Depletion of fossil fuels and anthropogenic climate change—A review. *Energy Policy*, *52*, 797-809. https://doi.org/10.1016/j.enpol.2012.10.046

Jafari, T., Moharreri, E., Amin, A. S., Miao, R., Song, W., & Suib, S. L. (2016). Photocatalytic water splitting—the untamed dream: a review of recent advances. *Molecules*, *21*(7), 900. https://doi.org/10.3390/molecules21070900

Kim, J. H., Hansora, D., Sharma, P., Jang, J. W., & Lee, J. S. (2019). Toward practical solar hydrogen production–an artificial photosynthetic leaf-to-farm challenge. *Chemical Society Reviews*, *48*(7), 1908-1971. https://doi.org/10.1039/C8CS00699G

Kim, T. W., Ping, Y., Galli, G. A., & Choi, K. S. (2015). Simultaneous enhancements in photon absorption and charge transport of bismuth vanadate photoanodes for solar water splitting. *Nature Communications*, *6*(1), 8769. https://doi.org/10.1038/ncomms9769

Li, R., & Li, C. (2017). Photocatalytic water splitting on semiconductor-based photocatalysts. In *Advances in Catalysis* 60, 1-57. Academic Press. https://doi.org/10.1016/bs.acat.2017.09.001

Li, X., Wang, Z., & Wang, L. (2021). Metal–Organic Framework-Based Materials for Solar Water Splitting. *Small Science*, *1*(5), 2000074. https://doi.org/10.1002/smsc.202000074

Maji, S. K., Dutta, A. K., Srivastava, D. N., Paul, P., Mondal, A., & Adhikary, B. (2012). Peroxidase-like behavior, amperometric biosensing of hydrogen peroxide and photocatalytic activity by cadmium sulfide nanoparticles. *Journal of Molecular Catalysis A: Chemical*, *358*, 1-9. https://doi.org/10.1016/j.molcata.2012.03.007

Mondal, P., Satra, J., Srivastava, D. N., Bhadu, G. R., & Adhikary, B. (2021). Pdδ+-mediated surface engineering of AgMnO4 nanorods as advanced bifunctional electrocatalysts for highly efficient water electrolysis. *ACS Catalysis*, *11*(6), 3687-3703. https://doi.org/10.1021/acscatal.0c05638

Nakata, K., & Fujishima, A. (2012). TiO2 photocatalysis: Design and applications. *Journal of Photochemistry and Photobiology C: Photochemistry Reviews*, *13*(3), 169-189. https://doi.org/10.1016/j.jphotochemrev.2012.06.001

Nnabuife, S. G., Oko, E., Kuang, B., Bello, A., Onwualu, A. P., Oyagha, S., & Whidborne, J. (2023). The prospects of hydrogen in achieving net zero emissions by 2050: A critical review. *Sustainable Chemistry for Climate Action*, 100024. https://doi.org/10.1016/j.scca.2023.100024

Pihosh, Y., Turkevych, I., Mawatari, K., Uemura, J., Kazoe, Y., Kosar, S., ... & Kitamori, T. (2015). Photocatalytic generation of hydrogen by core-shell $WO_3/BiVO_4$ nanorods with ultimate water splitting efficiency. *Scientific Reports*, *5*(1), 1-10. https://doi.org/10.1038/srep11141

Qiao, M., Liu, J., Wang, Y., Li, Y., & Chen, Z. (2018). $PdSeO_3$ monolayer: promising inorganic 2D photocatalyst for direct overall water splitting without using sacrificial reagents and cocatalysts. *Journal of the American Chemical Society*, *140*(38), 12256-12262. https://doi.org/10.1021/jacs.8b07855

Sato, N. (1998). *Electrochemistry at Metal and Semiconductor Electrodes*. Elsevier. Netherlands

Shit, S., Chhetri, S., Jang, W., Murmu, N. C., Koo, H., Samanta, P., & Kuila, T. (2018). Cobalt sulfide/nickel sulfide heterostructure directly grown on nickel foam: an efficient and durable

electrocatalyst for overall water splitting application. *ACS Applied Materials & Interfaces*, *10*(33), 27712-27722. https://doi.org/10.1021/acsami.8b04223

Sun, M., Li, D., Li, W., Chen, Y., Chen, Z., He, Y., & Fu, X. (2008). New photocatalyst, Sb_2S_3, for degradation of methyl orange under visible-light irradiation. *The Journal of Physical Chemistry C*, *112*(46), 18076-18081. https://doi.org/10.1021/jp806496d

Teixeira, I. F., Barbosa, E. C., Tsang, S. C. E., & Camargo, P. H. (2018). Carbon nitrides and metal nanoparticles: from controlled synthesis to design principles for improved photocatalysis. *Chemical Society Reviews*, *47*(20), 7783-7817. https://doi.org/10.1039/C8CS00479J

Turoń, K. (2020). Hydrogen-powered vehicles in urban transport systems–current state and development. *Transportation Research Procedia*, *45*, 835-841. https://doi.org/10.1016/j.trpro.2020.02.086

Vardhan, R. V., Mahalakshmi, R., Anand, R., & Mohanty, A. (2022, April). A review on green hydrogen: Future of green hydrogen in india. In *2022 6th International Conference on Devices, Circuits and Systems (ICDCS)* (pp. 303-309). IEEE. https://doi.org/10.1109/ICDCS54290.2022.9780805

doi: 10.31674/book.2024ecc.013

Gold-Catalyzed Cycloisomerization of Ortho-Nitro-Alkynylbenzene: Mechanistic Developments

Biswajit Panda

Department of Chemistry, City College, Kolkata, West Bengal, India

Corresponding Author's Email: biswajitchem@gmail.com

Abstract

Gold catalysis has emerged as a pivotal area in modern organic synthesis, offering novel reactivity patterns and enabling the construction of intricate molecular architectures that were once considered challenging or inaccessible. While traditionally regarded as inert, the unique electronic properties of gold, particularly its propensity for π-acid activation and tolerance towards a wide range of functional groups, have propelled it to the forefront of modern catalysis. In recent decades, the exploration of gold catalysis has led to the development of a plethora of innovative synthetic methodologies, revolutionizing the way chemists' approach complex molecule synthesis. Historically, gold was perceived as a noble metal with limited reactivity in organic transformations. However, pioneering work by Toste, Hashmi, and others in the early 2000s demonstrated that gold complexes could catalyze a diverse array of organic reactions, including formation of carbon-carbon as well as carbon-heteroatom bonds, cycloisomerizations, and rearrangements. This paradigm shift challenged conventional wisdom and opened up new avenues for leveraging gold as a catalyst in organic synthesis. The exceptional reactivity exhibited by gold catalysts can be attributed to several key factors. Unlike transition metals such as palladium or platinum, which typically operate in high oxidation states, gold commonly operates in low oxidation states, facilitating π-acid activation of unsaturated substrates. Additionally, gold complexes exhibit a high degree of coordination flexibility, enabling them to adopt diverse coordination geometries and accommodate a wide range of substrates. Furthermore, gold complexes are often air- and moisture-stable, making them practical and user-friendly catalysts in synthetic laboratories.

Keywords: *Cycloisomerization; Gold-Catalysis; Hetero-Atom Transfer; 2-Nitro-Alkynylbenzene; Reaction Mechanism*

Introduction

Gold catalysis has gained significance in synthetic organic chemistry, offering a valuable technique to selectively modify carbon-carbon multiple bonds. One of the hallmark features of gold catalysis is its ability to activate alkynes, alkenes, and allenes, leading to the formation of C–C and C-hetero-atom bonds under mild reaction conditions

(Stylianakis & Kolocouris, 2023). The activation of unsaturated bonds by gold typically proceeds through a π- bond coordination followed by nucleophilic addition of carbon or heteroatom nucleophiles to form C-C and C-hetero-atom bonds (Kumar, Kaliya & Maurya, 2023). Co-ordination of gold with π-bond can stabilize the LUMO thus reducing the HOMO-LUMO energy barrier and facilitating the reaction. This unique reactivity has enabled the development of highly efficient and selective transformations that were previously inaccessible using traditional transition metal catalysts (Witzel, Hashmi & Xie, 2021). The broad scope of gold-catalyzed reactions encompasses a wide range of synthetic transformations, including cycloadditions (Zhang *et al*., 2020), cross-couplings (Panda & Sarkar, 2010, 2013; Nijamudheen & Datta, 2020), cycloisomerizations (Praveen, 2021; Tzouras *et al*., 2023), pericyclic reactions (He, Jana & Koenigs, 2020), cross-dehydrogenative coupling (oxidative coupling) (Panda, 2020; Zheng *et al*., 2021) and cascade reactions (Ghosh & Bhakta, 2023). These reactions have found applications in various areas of organic synthesis, including natural product synthesis (De *et al*., 2022), pharmaceutical chemistry (Soklou *et al*., 2022) and materials science (Hendrich *et al*., 2021). Furthermore, the ability of gold catalysts to operate under mild conditions and tolerate functional groups makes them valuable tools for late-stage functionalization and complex molecule synthesis.

Cycloisomerization reactions represent a class of transformations that hold significant importance in the synthesis of complex organic molecules (Panda, 2019). By efficiently constructing cyclic structures from simple starting materials, these reactions offer atom-economic pathways towards the synthesis of diverse structural motifs. The ability to access a wide array of cyclic compounds through cycloisomerization reactions has found applications in various fields, including natural product synthesis, pharmaceutical chemistry, and materials science. As such, understanding the mechanisms underlying these transformations is crucial for developing efficient synthetic methodologies and unlocking new avenues for chemical synthesis. Heterocyclic compounds are highly important classes of compounds due to their inherent biological activities. Gold catalysis was found to be efficient for the synthesis of various heterocyclic compounds (Kadiyala *et al*., 2024).

On the other hand, ortho-nitro-alkynylbenzenes have emerged as versatile substrates in metal-catalyzed cycloisomerization reactions due to their structural diversity and synthetic utility. These substrates possess an ortho-nitro group and an alkynyl functionality attached to a benzene ring, providing multiple handles for diversification and subsequent elaboration into complex cyclic structures. The cycloisomerization of ortho-nitro-alkynylbenzenes has garnered considerable attention in recent years, owing to its potential for accessing biologically active compounds and heterocyclic scaffolds with high efficiency and selectivity.

The primary intend of this chapter is to give a comprehensive overview of the mechanistic developments in gold-catalyzed cycloisomerization reactions of ortho-nitro-alkynylbenzenes. By elucidating the intricate mechanistic pathways involved in these transformations, this chapter aims to deepen the understanding of the reactivity patterns of gold catalysts and shed light on the factors governing their catalytic activity and selectivity. It is anticipated that this chapter will contribute to the advancement of gold catalysis and stimulate new avenues for chemical synthesis and discovery.

Results and Discussion

The cyclization reaction of o-alkynylnitrobenzenes represents one of the earliest documented redox processes in organic synthesis. In 1882, Baeyer reported the cycloisomerization of o-nitrophenylpropiolates 1 in cold concentrated sulfuric acid as part of the synthesis of indigo, resulting in the formation of 2-carboxy-3-oxo-3Hindole 1-oxide 2. This compound's central bicyclic core is commonly referred to as an isatogen (derived from "isatin" and "gen"), as it is isomeric to isatin. Subsequently, Pfeiffer (1916) and Ruggli, Caspar and Hegedüs (1937) systematically investigated this type of compound and made significant progress in o-nitroalkyne cycloisomerization. Their work included the utilization of pyridine-mediated internal redoxycyclization reactions under photochemical or thermal conditions (Scheme 1), as well as the application of nitrosobenzene as a promoter in the cycloisomerization process, which required several days for the formation of the isatogens.

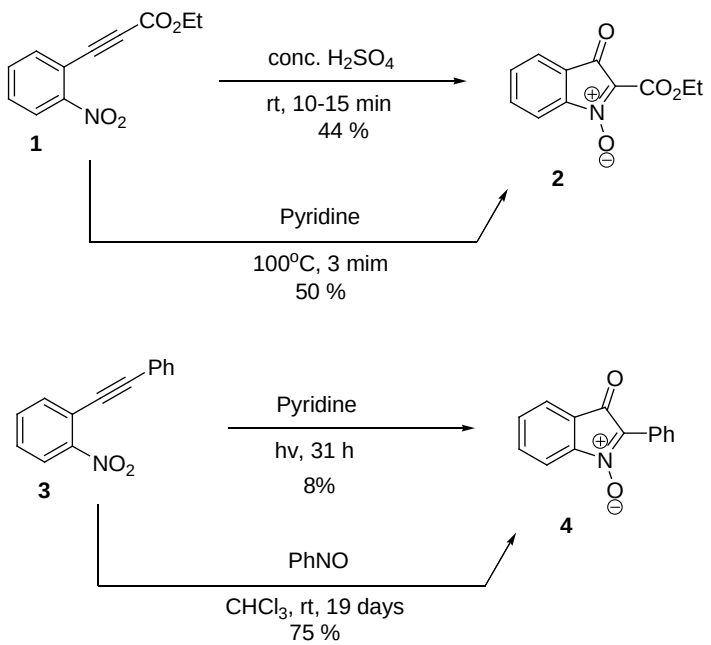

Scheme 1: Cycloisomerization of Nitroalkynes under various conditions

In 1969, Bond and Hooper made a significant observation while preparing unsymmetrical diaryl acetylenes using Cu(I) 2-nitrophenylacetylide 5 under Castro-Stephens coupling conditions. They found that in certain cases, heating of the reaction for long time in pyridine directly yielded the heterocyclic compound isatogens 7 (Scheme 2). In that case, the yields and reaction times varied depending on the substituents bearing on the aromatic ring. In a similar vein, Rosen and co-workers (2000) detailed a one-pot procedure involving the Sonogashira coupling of 2-iodonitrobenzene derivatives 8 with terminal alkyne 9a in neat triethylamine, followed by pursuing the reaction for 3–4 days at room temperature as shown in Scheme 3. This methodology has been effectively utilized for synthesizing various 2-hetero-aryl isatogens 10. It has been found that, when the terminal alkyne contains an alkyl group (e.g. methyl) on the alkyne terminus, the corresponding 2-methylisatogen was afforded in low yields. While the precise function of the actual Pd-catalyst in the cyclization remains somewhat ambiguous, the simplistic nitroalkyne cycloisomerization at room temperature suggests that the phosphine-free Pd(II)-salts formed after the initial Sonogashira coupling may play a significant role. Interestingly, a comparable protocol with 6-chloro-5-nitropyrimidine derivatives 11/13 necessitated separate heating in neat pyridine to facilitate the necessary nitroalkyne cycloisomerization (Susvilo, Brukstus & Tumkevicius, 2003; Cikotiene, Pudziuvelyte & Brukstus, 2008).

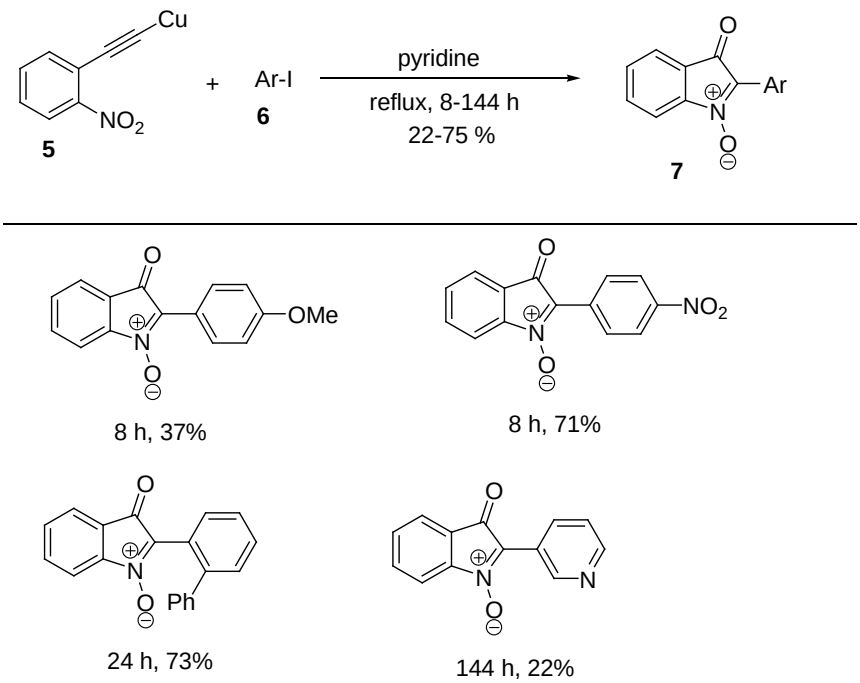

Scheme 2: Tandem Stephen-Castro coupling and cycloisomerization reaction

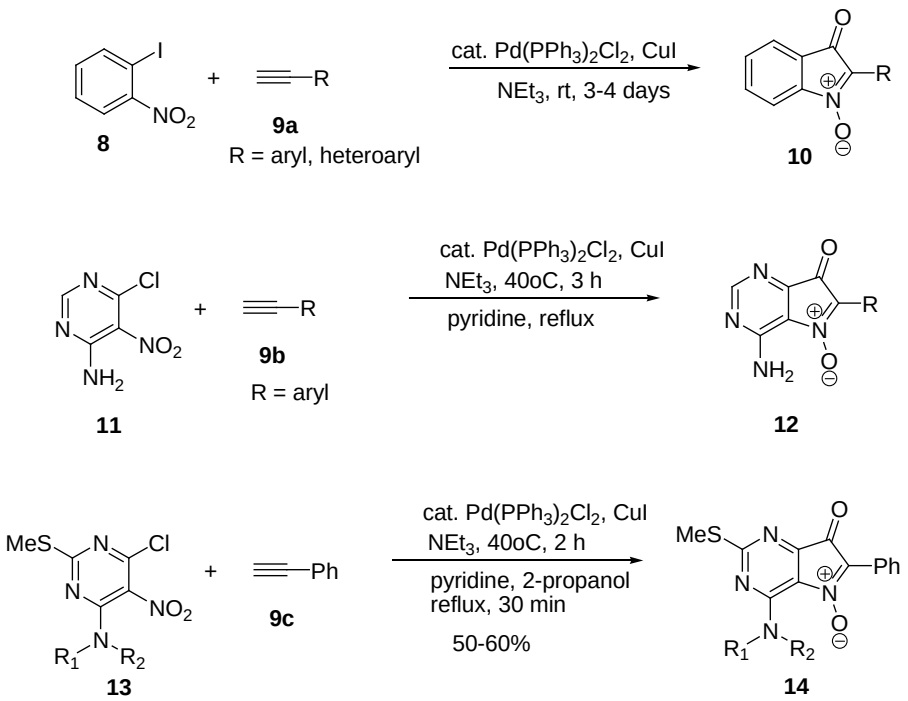

Scheme 3: One-pot tandem Sonogashira coupling –cycloisomerization reaction

In 2010, the team reported the first Sonogashira coupling of arenediazonium salts with terminal alkynes using a catalytic amount of both $PdCl_2$ and AuCl in the presence of an NHC ligand (Panda & Sarkar, 2010). This unique finding generates great attention to the chemical community and results in further development of more than ten protocols within ten years (Panda, 2021). During this work, the researchers found that when ortho-nitrobenzenediazonium salts were used in the Sonogashira coupling reaction, instead of forming the expected coupling product, the reaction underwent a tandem cyclization catalyzed by gold, leading to the formation of anthranils.

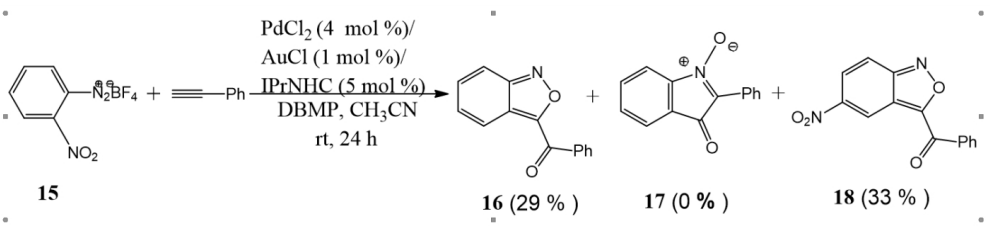

***Scheme 4**: Tandem Sonogashira coupling and cycloisomerization reaction*

The coupling of 2-nitrobenzenediazonium tetrafluroborate 15 with phenylacetylene gave the anthranil 16 in 29% yield, accompanied by nitro-anthranil 18 (33 %); however, no trace of the isatogen 17 could be detected in the crude reaction mixture (Scheme 4).

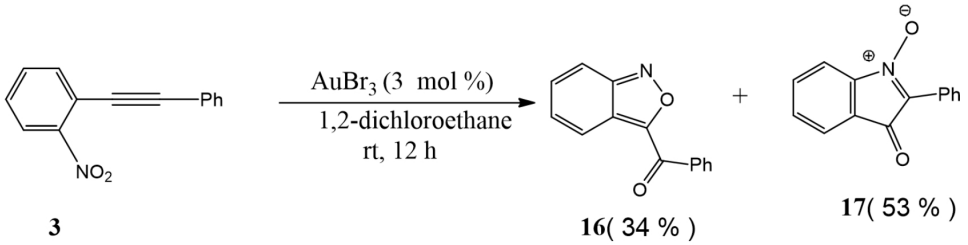

Scheme 5: Gold catalyzed cycloisomerization of 2-nitroalkyne

Table 1: *Summary of synthesis of isatogens*

Substrate(s)	Scheme	Reagent/ Catalyst(s), Temp.	Base/Additive	Ref.	Authors
Nitroalkynes	1	c. H_2SO_4, rt	Nil	19	Baeyer (1882)
Nitroalkynes	1	Pyridine, 100 ^oC	Nil	19	Baeyer (1882)
Nitroalkynes	1	Pyridine, hv	Nil	20	Pfeiffer (1916)
Nitroalkynes	1	PhNO, rt	Nil	21	Ruggli, Caspar and Hegedüs (1937)
Cu(I) 2-nitro-phenylacetylide and aryl iodides	2	Pyridine, reflux	Nil	22	Bond and Hooper (1969)
1-Iodo-2-nitrobenzene and aryl acetylenes	3	cat. $Pd(PPh_3)_2Cl_2$, CuI, rt	Et_3N	23	Rosen *et al*. (2000)
6-chloro-5-nitropyrimidine derivatives and aryl acetylenes	3	cat. $Pd(PPh_3)_2Cl_2$, CuI, 40 ^oC	Et_3N, Pyridine	24	Susvilo, Brukstus and Tumkevicius, (2003)
6-chloro-5-nitropyrimidine derivatives and phenylacetylene	3	cat. $Pd(PPh_3)_2Cl_2$, CuI, 40 ^oC	Et_3N, Pyridine, 2-propanol	25	Cikotiene, Pudziuvelyte and Brukstus
Nitroalkynes	5	cat. $AuBr_3$, rt	Nil	28	Asao, Sato and Yamamoto (2003)

The gold-catalyzed cycloisomerization of nitrotolans, as detailed by Asao and co-workers in 2003 (Scheme 5), marks a significant stride in the synthesis of 2-arylisatogens. It's noteworthy that when the pendant alkyne substituent is an alkyl group, an internal redox process takes place in a complementary manner, leading to the formation of benzo[c]isoxazole, commonly known as anthranil. On the other hand, when the pendant alkyne substituent is an aryl group, this cycloisomerization reaction yielded isatogen as major product. Table 1 summarizes the various methods used for the synthesis of isatogens through the cycloisomerization of 2-nitroalkynes.

Asao, Sato and Yamamoto (2003) suggested a mechanism for the gold catalyzed cycloisomerization of 2-nitroalkynes through the addition of the oxygen atom from the nitro group in a 6-endo-dig fashion as the pivotal step in the intramolecular redox process (Scheme 6). The coordination of the triple bond of compound 18 to $AuBr_3$ boosts the electrophilicity of the alkyne. This sets the stage for a nucleophilic attack by the oxygen atom of the nitro group onto the electron-deficient alkyne, resulting in the formation of an intermediate auric ate complex 20. Initially, it was proposed that the resulting gold-ate complex 20 undergoes protonolysis, followed by ring opening with water, leading to the formation of nitrosobenzene 23. In the reaction medium, even a trace amount of water can generate a proton due to the presence of $AuBr_3$. Subsequently, two potential pathways for the subsequent dehydrative cyclization have been suggested, leading either to isatogens (path a) or anthranil (path b). While this elucidates the potential pathways, it fails to explain why these pathways are dependent on the substituents present.

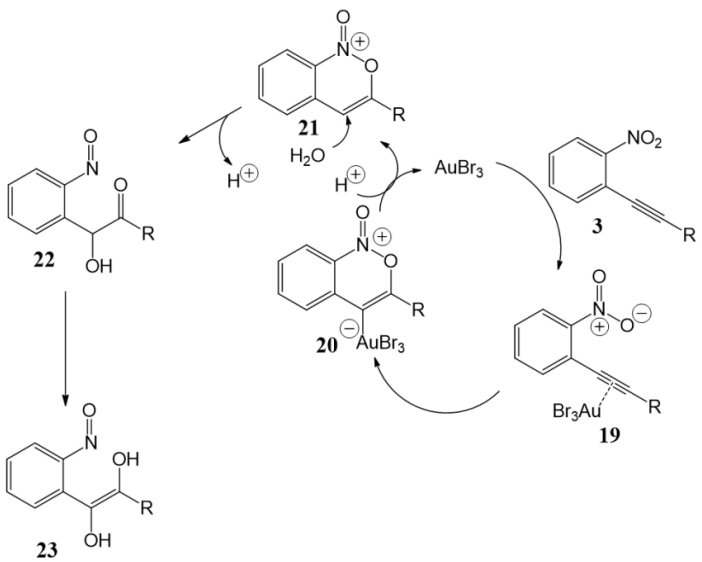

Scheme 6: *Yamamoto's postulated mechanism of gold catalyzed cycloisomerization of 2-nitroalkynes*

The formation of isatogen 17 involves a cyclization process of compound 24, followed by the elimination of water, as depicted in Scheme 7 (path a). Conversely, if the reaction progresses along path b, anthranil 16 is generated through the intramolecular nucleophilic addition of the enol oxygen, succeeded by water elimination.

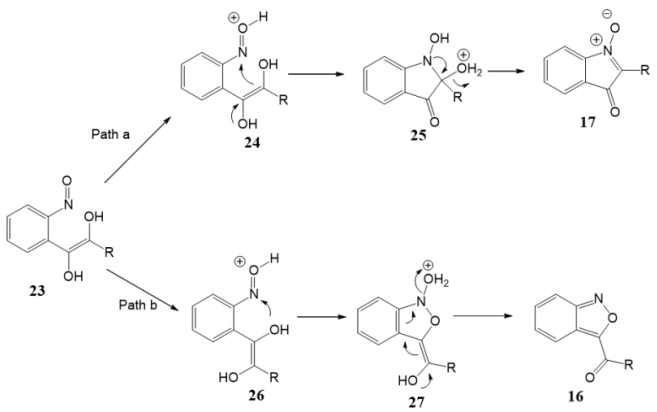

Scheme 7: Yamamoto's postulated mechanism for the formation of isatogens and anthranils

However, their proposal is notably different from those given by Asao, Sato, and Yamamoto (2003), as the reaction was carried out under strictly anhydrous conditions to furnish the desired products. A plausible mechanism for the formation of the anthranils 16 and isatogen 17 from 3 is given in Scheme 8 and 9; thus, the gold (I) coordinated triple bond of the Sonogashira product 3, that is 19, encourages nucleophilic attack by the neighbouring nitro group, thereby forming the auric ate complex 28; ring opening to gold carbenoid 29 followed by its capture by the nitroso group and elimination of the catalyst from 30 gives the anthranil 16. Similarly, addition of nitro-group to the coordinated alkyne intramolecularly via 5-exo-dig fashion provides complex 31, which then rearranged to gold carbene 32. Now addition of nitroso group to the gold carbene and subsequent rearrangement resulted in isatogen 17. This work was presented at the NOST conference on May 4, 2009, in Goa, India.

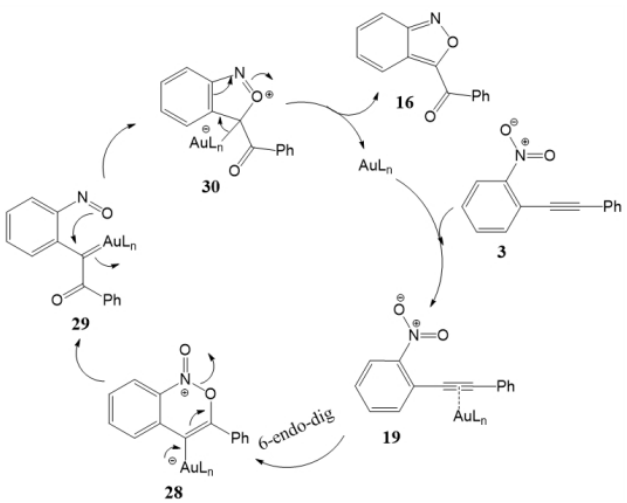

Scheme 8: Panda's postulated mechanism of gold catalyzed synthesis of anthranil

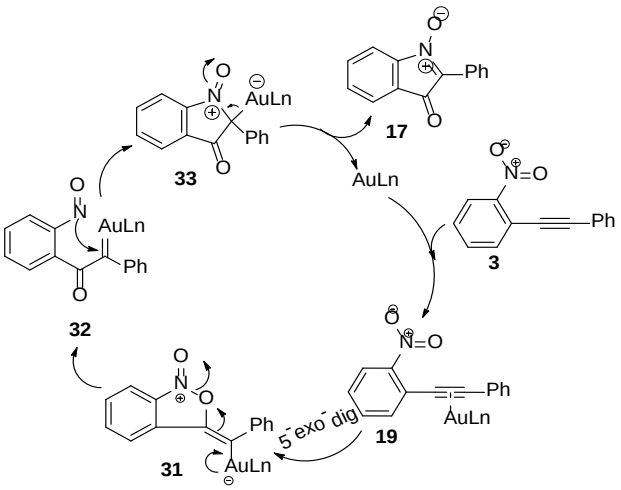

Scheme 9: Panda's postulated mechanism of gold catalyzed synthesis of isatogen

Later, density functional theory (DFT) calculations were conducted by Vipin Raj and co-workers (2021) to investigate the internal oxygen transfer in Au-catalyzed o-nitroalkyne cycloisomerization reactions, aiming to elucidate the relative energies associated with this process as well as the resulting α-oxo gold carbenes. These calculations provided clear insights into the thermodynamic stability of the α-oxo gold carbenes generated from the 6-endo dig addition of oxygen to the alkyne, in comparison to the alternative α-oxo gold carbene formed from the 5-exo dig addition. Additionally, their computational analysis suggests that substitutions on the o-nitroalkynes play a significant role in modulating the regio-selectivity of the reaction, thereby influencing the outcome of the cycloisomerization process. This study supports the researchers' speculation regarding the mechanism of gold-catalyzed cycloisomerization of o-nitroalkynes. Moreover, Dhote and Ramana (2021) successfully trapped the α-oxo gold carbenes intermediate using electron-rich anthranils, leading to the formation of highly functionalized 3-acyl-(2-formylphenyl)-2H-indazoles via sequential carbon-oxygen, carbon-nitrogen, and nitrogen-nitrogen bond formations. This observation provides indirect evidence supporting the existence of α-oxo gold carbenes in the [Au]-catalyzed internal redox processes of nitroalkynes (Dhote, Halnor & Ramana, 2021).

The preceding discussion highlights Yamamoto's report on Au-catalyzed nitroalkyne cycloisomerization, which has reignited interest in this field. This process leads to the synthesis of isatogens, offering a pathway for the facile functionalization of these compounds at the C2-position. This functionalization can occur through either nucleophilic addition or cycloaddition, yielding the synthetically valuable 2,2-disubstituted 1,2-dihydro-3H-indolin-3-one skeleton, commonly referred to as pseudoindoxyl—a subgroup within the indole group of alkaloids (Liu *et al.*, 2015). Researchers have been particularly inspired by the versatility of this skeleton, as

evidenced by the emergence of a variety of Pd, Cu, Ag, and Hg complexes aimed at developing regioselective nitroalkyne cycloisomerizations (Xie *et al*., 2021). However, the use of [Au]-complexes in these cyclizations holds particular appeal due to their facile operation at room temperature. Additionally, [Au]-complexes offer the advantage of Lewis acidity, which not only enables post-functionalization of the resulting isatogens but also opens avenues for employing other Lewis acids in tandem reactions, leading to the development of novel cascade and one-pot processes.

Conclusion

Understanding the reaction mechanism of a catalytic organic reaction is particularly crucial due to the pivotal role that catalysts play in these processes. Catalytic reactions occur with the assistance of a catalyst, which accelerates the reaction rate without being consumed in the process. By understanding the mechanism, chemists can optimize catalyst design and reaction conditions to enhance reaction efficiency and selectivity. Additionally, knowledge of the mechanism allows for the development of more sustainable and environmentally friendly catalytic processes by minimizing waste and energy consumption. Furthermore, understanding the intricacies of catalytic reactions facilitates the discovery of new catalytic systems and the improvement of existing ones, driving advancements in synthetic chemistry and catalysis research. In this chapter, we have shown that gold catalysed cycloisomerization reaction is feasible strictly in the absence of water, which is in contrary to Yamamoto's findings. The researchers have thoroughly discussed their previously proposed cycloisomerization reaction mechanism, which involves a gold carbenoid intermediate for the synthesis of anthranils and isatogens from 2-nitroaryl alkynes in the presence of a gold catalyst.

Acknowledgements

The author is grateful to the management of City College, Kolkata, India for giving necessary permission and Dr. Tarak Nath Podder Memorial Foundation, Kolkata, West Bengal, India, for necessary Financial support. The author also extends heartfelt thanks to Dr. Bhaskar Paul, Dr. Moumita Ganguli, Kirtika Dutta, Suban Kundu, Barnali Roy, Dr. Sujay Nandi, Dr. Totan Mondal, and Atanu Ghosh for their help.

References

Asao, N., Sato, K., & Yamamoto, Y. (2003). AuBr3-catalyzed cyclization of o-(alkynyl) nitrobenzenes. Efficient synthesis of isatogens and anthranils. *Tetrahedron Letters*, *44*(30), 5675-5677. https://doi.org/10.1016/S0040-4039(03)01357-1

Baeyer, A. (1882). Ueber die Verbindungen der Indigogruppe. *Berichte der deutschen chemischen Gesellschaft, 15*(1), 775-787. https://ia800708.us.archive.org/view_archive.php?archive=/22/items/crossref-pre-1909-scholarlyworks/10.1002%252Fcber.188201501110.zip&file=10.1002%252Fcber.188201501167.pdfCHECK

Bond, C. C., & Hooper, M. (1969). Isatogens. Part VI. Synthesis of isatogens via tolan (diphenylacetylene) intermediates. *Journal of the Chemical Society C: Organic*, (19), 2453-2460. https://doi.org/10.1039/J39690002453

Cikotiene, I., Pudziuvelyte, E., & Brukstus, A. (2008). Synthesis of 2, 4-disubstituted 6-phenyl-7H-pyrrolo [3, 2-d]-pyrimidin-7-one 5-oxides. *Journal of Heterocyclic Chemistry*, *45*(6), 1615-1620. https://doi.org/10.1002/jhet.5570450610

De, S., Dan, A. K., Sahu, R., Parida, S., & Das, D. (2022). Total synthesis of natural products using gold catalysis. *Chemistry–An Asian Journal*, *17*(24), e202200896. https://doi.org/10.1002/asia.202200896

Dhote, P. S., & Ramana, C. V. (2021). Interrupting the [Au]-catalyzed nitroalkyne cycloisomerization: trapping the putative α-oxo gold carbene with benzo [c] isoxazole. *Organic Letters*, *23*(7), 2632-2637. https://doi.org/10.1021/acs.orglett.1c00539
Dhote, P. S., Halnor, S. V., & Ramana, C. V. (2021). Gold-Catalysed Nitroalkyne Cycloisomerization–Synthetic Utility. *The Chemical Record*, *21*(12), 3546-3558. https://doi.org/10.1002/tcr.202100111

Ghosh, T., & Bhakta, S. (2023). Advancements in Gold-Catalyzed Cascade Reactions to Access Carbocycles and Heterocycles: An Overview. *The Chemical Record*, *23*(3), e202200225. https://doi.org/10.1002/tcr.202200225

He, F., Jana, S., & Koenigs, R. M. (2020). Gold-Catalyzed Sigmatropic Rearrangement Reactions via Carbene Transfer Reactions. *The Journal of Organic Chemistry*, *85*(18), 11882-11891. https://doi.org/10.1021/acs.joc.0c01678

Hendrich, C. M., Sekine, K., Koshikawa, T., Tanaka, K., & Hashmi, A. S. K. (2020). Homogeneous and heterogeneous gold catalysis for materials science. *Chemical Reviews*, *121*(14), 9113-9163. https://doi.org/10.1021/acs.chemrev.0c00824

Kadiyala, K. G., Goutham, K., Yamini, V., & Katari, N. K. (2024). Gold-catalyzed synthesis of small-sized carbo-and heterocyclic compounds: A review. *Heterocyclic Communications*, *30*(1), 20220172. https://doi.org/10.1515/hc-2022-0172

Kumar, M., Kaliya, K., & Maurya, S. K. (2023). Recent progress in the homogeneous gold-catalysed cycloisomerisation reactions. *Organic & Biomolecular Chemistry*, *21*(16), 3276-3295. https://doi.org/10.1039/D2OB02015G

Liu, R. R., Ye, S. C., Lu, C. J., Zhuang, G. L., Gao, J. R., & Jia, Y. X. (2015). Dual Catalysis for the Redox Annulation of Nitroalkynes with Indoles: Enantioselective Construction of Indolin-3-ones Bearing Quaternary Stereocenters. *Angewandte Chemie International Edition*, *54*(38), 11205-11208. https://doi.org/10.1002/anie.201504697

Nijamudheen, A., & Datta, A. (2020). Gold-catalyzed cross-coupling reactions: an overview of design strategies, mechanistic studies, and applications. *Chemistry–A European Journal*, *26*(7), 1442-1487. https://doi.org/10.1002/chem.201903377

Panda, B. (2019). Total synthesis of xyloketals and related natural product alboatrin: strategies and tactics. *ChemistrySelect*, *4*(31), 9143-9164. https://doi.org/10.1002/slct. 201900779

Panda, B. (2020). Joy and challenges of alkynylation of arenes and heteroarenes through double C− H functionalizations. *Asian Journal of Organic Chemistry*, *9*(4), 492-507. https://doi.org/10.1002/ajoc.201900733

Panda, B. (2021). Sonogashira coupling of arenediazonium salts: discovery and developments. *ARKIVOC*, *2021*, 177-199. https://doi.org/10.24820/ark.5550190.p011.559

Panda, B., & Sarkar, T. K. (2010). Gold and palladium combined for the Sonogashira-type cross-coupling of arenediazonium salts. *Chemical Communications*, *46*(18), 3131-3133. https://doi.org/10.1039/C001277G

Panda, B., & Sarkar, T. K. (2010). On the catalytic duo PdCl2 (PPh3) 2/AuCl (PPh3) that cannot effect a Sonogashira-type reaction: a correction. *Tetrahedron Letters*, *51*(2), 301-305. https://doi.org/10.1016/j.tetlet.2009.11.003

Panda, B., & Sarkar, T. K. (2013). Gold and palladium combined for the Sonogashira coupling of aryl and heteroaryl halides. *Synthesis*, 817-829. https://doi.org/10.1055/s-0032-1318119

Pfeiffer, P. (1916). Lichtchemische synthese von indolderivaten. *Justus Liebigs Annalen der Chemie*, *411*(1), 72-158. https://doi.org/10.1002/jlac.19164110105

Praveen, C. (2021). Cycloisomerization of π-Coupled Heteroatom Nucleophiles by Gold Catalysis: En Route to Regiochemically Defined Heterocycles, *The Chemical Record, 21*(7), 1697-1737. https://doi.org/10.1002/tcr.202100105

Rosen, G. M., Tsai, P., Barth, E. D., Dorey, G., Casara, P., Spedding, M., & Halpern, H. J. (2000). A one-step synthesis of 2-(2-pyridyl)-3H-indol-3-one N-oxide: is it an efficient spin trap for hydroxyl radical?. *The Journal of Organic Chemistry*, *65*(14), 4460-4463. https://doi.org/10.1021/jo0006122

Ruggli, P., Caspar, E., & Hegedüs, B. (1937). Zur Darstellung von 2-Phenyl-isatogen und 2-Phenyl-6-carbäthoxy-isatogen. *Helvetica Chimica Acta*, *20*(1), 250-263. https://doi.org/10.1002/hlca.19370200136

Soklou, K. E., Marzag, H., Vallée, B., Routier, S., & Plé, K. (2022). Synthesis of Heterospirocycles through Gold-(I) Catalysis: Useful Building Blocks for Medicinal Chemistry. *Advanced Synthesis & Catalysis*, *364*(1), 218-224. https://doi.org/10.1002/adsc.202101080

Stylianakis, I., & Kolocouris, A. (2023). Comprehensive Overview of Homogeneous Gold-Catalyzed Transformations of π-Systems for Application Scientists. *Catalysts*, *13*(6), 921. https://doi.org/10.3390/catal13060921

Susvilo, I., Brukstus, A., & Tumkevicius, S. (2003). The First Synthesis of Novel 7-Oxo-7H-pyrrolo [3, 2-d] pyrimidine 5-Oxides from 1-(5-Nitro-6-pyrimidinyl)-2-arylacetylenes. *Synlett*, *2003*(08), 1151-1152. https://doi.org/10.1055/s-2003-39883

Tzouras, N. V., Zorba, L. P., Kaplanai, E., Tsoureas, N., Nelson, D. J., Nolan, S. P., & Vougioukalakis, G. C. (2023). Hexafluoroisopropanol (HFIP) as a multifunctional agent in gold-catalyzed cycloisomerizations and sequential Transformations. *ACS Catalysis*, *13*(13), 8845-8860. https://doi.org/10.1021/acscatal.3c01660

Vipin Raj, K., Dhote, P. S., Vanka, K., & Ramana, C. V. (2021). Gold-catalyzed complementary nitroalkyne internal redox process: a DFT study. *Frontiers in Chemistry*, *9*, 689780. https://doi.org/10.3389/fchem.2021.689780

Witzel, S., Hashmi, A. S. K., & Xie, J. (2021). Light in gold catalysis. *Chemical Reviews*, *121*(14), 8868-8925. https://doi.org/10.1021/acs.chemrev.0c00841

Xie, L., Li, Y., Dong, S., Feng, X., & Liu, X. (2021). Catalytic asymmetric formal [3+ 2] cycloaddition of isatogens with azlactones to construct indolin-3-one derivatives. *Chemical Communications*, *57*(2), 239-242. https://doi.org/10.1039/D0CC06418A

Zhang, S., Tang, A., Chen, P., Zhao, Z., Miao, M., & Ren, H. (2020). Tunable gold (I)-catalyzed [4+ 3] cycloaddition for divergent synthesis of furan-fused N, O-heterocycles. *Organic Letters*, *22*(3), 848-853. https://doi.org/10.1021/acs.orglett.9b04312

Zheng, Z., Ma, X., Cheng, X., Zhao, K., Gutman, K., Li, T., & Zhang, L. (2021). Homogeneous gold-catalyzed oxidation reactions. *Chemical Reviews*, *121*(14), 8979-9038. https://doi.org/10.1021/acs.chemrev.0c00774

doi: 10.31674/book.2024ecc.014

Effect of Temperature on Dissociation Constant and Determination of Equivalent Conductance at Infinite Dilution (Λ°) of Two Weak Acids

Debashree Ganguly, Sugata Samanta*

Department of Chemistry, The Bhawanipur Education Society College, Kolkata, West Bengal, India

**Corresponding Author's Email: sugata.samanta@thebges.edu.in*

Abstract

Dissociation constants of Lactic Acid (2-hydroxy propionic acid) have been studied at four different temperatures (19°C, 25°C, 32°C, 38°C). The change in pKa of lactic acid with temperature has been investigated and found that it increases with the temperature rise. The relationship between temperature and dissociation constant is not linear. In the second section of the experiment, the equivalent conductance of propionic and lactic acids at infinite dilution (Λ°) has been studied using Kohlrausch's Law of independent ion migration. A Python program has been designed to estimate the equivalent conductance of two weak acids. Theoretical calculations support the observed results, providing valuable insights into the behaviour and chemical properties of two weak acids.

Keywords: *Dissociation Constant; Equivalent Conductance at Infinite Dilution (Λ°); Weak Acids*

Introduction

Dissociation of weak acids and bases is the constant that indicates the strength of that acid or base as well as the percentage of various ionic species that are present in the solution at a specific temperature. Temperature and solvent concentration have an impact on the dissociation constant (Albert, 2012). Since the physical and biological characteristics of ionic species vary, it is critical to understand biological substances' dissociation constants in preparative chemistry and spectroscopy (Martin Somer *et al*., 2019; Snyder, Harvey & Wysocki, 2021).

Comparing the pH-metric titration approach to other techniques like conductometric and spectrophotometric techniques, it is more precise and takes less time to determine the dissociation constants of weak acids and bases. It has long been known that one can accurately determine the strength of an acid or its dissociation constant by measuring the changes in pH that occur when a weak acid is neutralized with an alkali (Dasgupta & Nara, 1990; Poplewska, Zimoch & Antos, 2022).

One of the main transport characteristics of electrolyte solutions is conductance, which is important for both their inherent value and for use in technical and industrial settings like plating and batteries. When water samples are taken for chemical analysis, one of the properties of the water's quality that is frequently examined is electrical conductivity. Measurements in the field and the lab can be made quickly, easily, and reliably thanks to modern equipment. Electrical conductivity is frequently used to track the quality of water in streams (Hamid, Bhat & Jehangir, 2020), wastewater treatment plants (Yu *et al*., 2019), and industrial site effluent (Mortadi *et al*., 2020). Natural waters' salinity, ionic strength, main solute concentrations, and total dissolved solids concentrations have all been ascertained by electrical conductivity studies (Corwin & Yemoto, 2020).

Experimental sections

Materials

Propionic Acid (Fig. 1A) and Lactic Acid (2-hydroxy propionic acid) (Fig. 1B), Sodium hydroxide, Potassium hydroxide, Oxalic Acid, Potassium Chloride, and Hydrochloric Acid used in the study were all reagent-grade chemicals purchased from Merck PVT. LTD. Unless otherwise mentioned, these chemicals were used without purification.

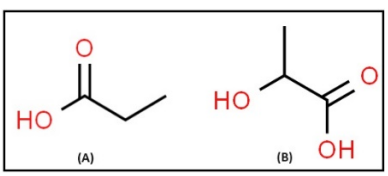

Figure 1: Structure of (A) Propionic Acid and (B) Lactic Acid (Source: Google Image)

Methods

Determination of dissociation constant pH-metrically

When a weak acid, HA, is dissociated in water, the following equilibrium is set up

$$\mathbf{HA\ (aq) \rightleftharpoons H^+\ (aq) + A^-\ (aq)} \qquad (1)$$

where the conjugated base is A^- (aq), the hydrogen ion is H^+ (aq), and the weak acid is HA (aq). The dissociation constant of the acid HA is the equilibrium constant Ka for this reaction.

$$\mathbf{Ka} = \frac{[\mathbf{H+}]\,[\mathbf{A-}]}{[\mathbf{HA}]} \qquad (2)$$

We need to know $[H^+]$, $[A^-]$, and [HA] to calculate Ka. By taking a pH reading, one can immediately determine the concentration of hydrogen ions $[H^+]$.

$$\mathbf{pH= -log[H^+]} \qquad (3)$$

Unfortunately, it is not that simple to calculate [HA] and [A^-]. A convenient way for determining K_a, is to determine the pH of the acid solution after a strong base has been added to half neutralize it. At that point, Ka equals to [H^+] as the ratio of [A^-]/[HA] becomes unity.

Determination of equivalent conductance at infinite dilution (Λ°)

The equivalent conductance of a strong electrolyte rises linearly with dilution. The linear relationship between Λ and √C can be extended to the Λ-axis, where the intercept corresponds to Λ°.

In the case of weak electrolytes, the equivalent conductance increases gradually initially and then rapidly when the concentration gets very low. This is due to (i) the larger degree of dissociation with dilution as per Ostwald's dilution law and (ii) growing distances between oppositely charged ions by increasing the volume of the solution. Therefore, extrapolation to have the Λ° value of a weak electrolyte is not feasible due to the slope's fluctuating nature.

The Λ° values of weak electrolytes can be effectively determined using Kohlrausch's law of independent migration of ions at infinite dilution. Three strong electrolytes are selected, and the algebraic combination of their Λ° values provides the required Λ° value (Picálek & Kolafa, 2007). For instance, the calculation of Λ° for CH_3COOH is:

$$\Lambda^\circ_{CH3COOH} = \Lambda^\circ_{CH3COOK} + \Lambda^\circ_{HCl} - \Lambda^\circ_{KCl} \quad (4)$$

All three electrolytes, viz., CH_3COOK, KCl, and HCl are strong electrolytes (the first two being salts), and their Λ° values are estimated by the extrapolation method. Thus Λ° of CH_3COOH is determined.

Instrumentations

The pH of all the solutions is recorded by Systronics Digital pH Meter 335, with 0 to 14 pH Range, 0 to +1999 mV Range, and 0.01 pH, 1 mV resolution. The temperature during the experiment was maintained by a thermostatic bath and monitored by the thermometer. The conductance of all the solutions was measured by Systronics Digital Conductivity Meter 304, with 0 µS to 200 mS range, 0.1µS resolution, 0^0C to 100^0C temperature range.

Theoretical confirmation for determination of equivalent conductance

A Python program has been devised to link to the graphs of λ_{eqv} vs √Concentration in cases of KCl, HCl, Potassium Lactate, and Potassium Propionate to cross-calculate the equivalent conductance λ at infinite dilution. Python software was created by Google Collaboratory, a Google Research offering. Anyone can write and run Python programs with it; installing various library packages is not a burden. It is simple to use and doesn't require setup, and the apps automatically save to Google Drive.

This Excel-linked application provides great results when calculating the equivalent conductance at infinite dilution using the Linear Regression approach. Because of its connectivity to the Excel sheet, the application uses the updated data whenever any changes are made to the sheet.

This software will help to cross-check our data and findings because Excel tends to store junk numbers and generate incorrect results. Additionally, this application uses LINEAR REGRESSION to provide findings after creating tables and graphs to calculate the equivalent conductance at infinite dilution.

Results and Discussion

Determination of dissociation constant at different temperatures pH-metrically

Results summarized in Table 1 show the effect of temperature on pKa values of Lactic acid using the pH-metric method. As temperature increases from 19°C to 38°C, pKa values increase from 3.63 to 4.11 and the total increase is 0.48 units. When weak acid dissociation occurs, a temperature rise gives the system more energy. In response, the system moves the equilibrium in the direction of the endothermic dissociation reaction, which absorbs the additional energy. Because of this, the weak acid's dissociation is encouraged, which increases the dissociation constant (pKa) as temperature rises.

Table 1: *Effect of temperature on pKa values of lactic Acid*

Temperature(°C)	pKa
19	3.63
25	3.87
32	3.98
38	4.11

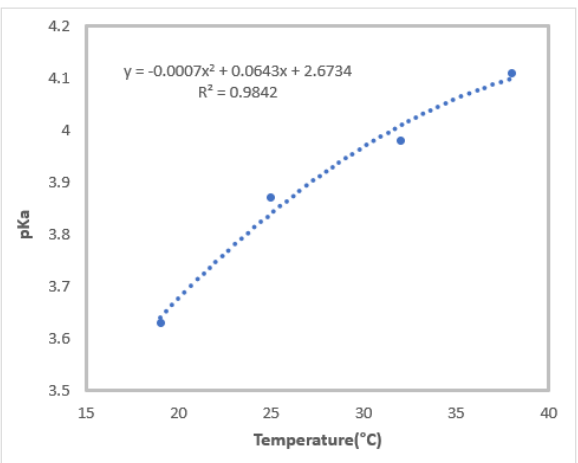

Figure 2: pKa vs Temperature plot of Lactic acid *(Source: Primary Source)*

It is important to note that the relationship between temperature and the dissociation constant (pKa) of Lactic acid is not linear. pKa of Lactic acid shows a parabolic curve (Figure 2, Equation 5) when the temperature increases. The equation is as follows:

$$\mathbf{y = -0.0007x^2 + 0.0643x + 2.6734} \quad (5)$$

Where y = pKa and x is the temperature in °C.

Determination of equivalent conductance at infinite dilution (Λ°)

Exact solutions of KCl, HCl, Lactic Acid, Propionic Acid, and KOH were prepared and conductance of KCl, and HCl were measured at (N/10), (N/20), (N/40), (N/80), (N/160) concentrations and that of Potassium lactate and Potassium Propionate were measured at (N/20), (N/40), (N/80), (N/160) concentrations. Graphs were plotted by λ_{eqv} vs √Concentration in each case (Figure 3).

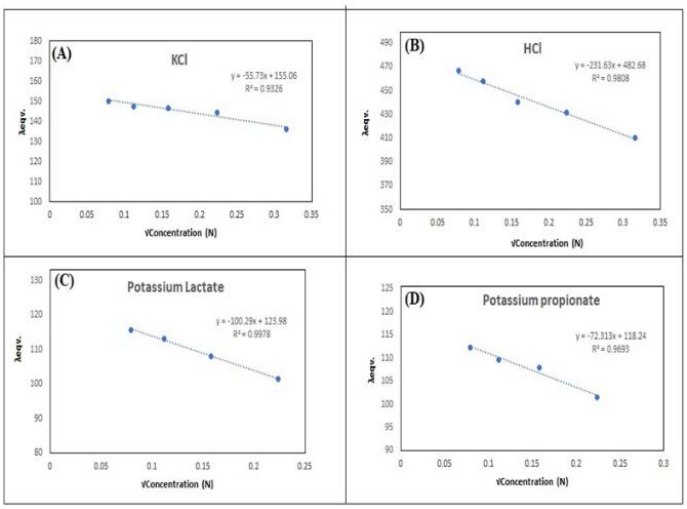

Figure 3: λeqv. Vs. √Concentration plots of (A) KCl (B) HCl (C) Potassium Lactate (D) Potassium Propionate at room temperature (*Source: Primary Source)*

Results summarized in Table 2 show equivalent conductance at infinite dilution of KCl, HCl, Potassium Lactate, and Potassium Propionate. The equivalent conductance at infinite dilution of Lactic acid and Propionic acid has been calculated using the Kohlrausch Law as follows:

$$\mathbf{\Lambda^\circ_{Lactic\ acid} = \Lambda^\circ_{Potassium\ Lactate} + \Lambda^\circ_{HCl} - \Lambda^\circ_{KCl}} \quad (6)$$

$$\mathbf{\Lambda^\circ_{Lactic\ acid}} = 123.98 + 482.68 - 155.06 = 451.6\ Ohm^{-1}Cm^2Eqv^{-1} \quad (7)$$

Similarly,

$\Lambda°_{\text{Propionic acid}}$ = 118.24 + 482.68 - 155.06 = 445.86 $Ohm^{-1}Cm^{2}Eqv^{-1}$ (8)

Table 2: *Equivalent conductance at infinite dilution of different electrolytes*

Electrolyte	$\Lambda°eqv.(Ohm^{-1}cm^{2}eqv^{-1})$
KCl	155.06
HCl	482.68
Potassium Lactate	123.98
Potassium Propionate	118.24
Lactic Acid	451.60
Propionic Acid	445.86

Theoretical Results for calculation of Equivalent Conductance at infinite dilution:

```
import pandas as pd
import numpy as np

# Read the Excel file into a DataFrame
df=pd.read_excel('/dissertation2.xls', sheet_name='KCL')

# Extract the concentration (c) and molar conductance (Λ) values from the DataFrame
c_values_KCl = df['Conc.(N)'].values
Λ_values_KCl = df['λ=1000k/Conc'].values

# Perform linear regression to obtain the slope and intercept
slope, intercept = np.polyfit(np.sqrt(c_values_KCl), Λ_values_KCl, 1)

# Calculate the equivalent conductance at infinite dilution (Λ0)
Λ_infinite_KCl = intercept

# Print the calculated Λ0 value
print("Equivalent Conductance at Infinite Dilution (Λ0) of KCl:",Λ_infinite_KCl,
"S/cm^2/mol")

# Read the Excel file into a DataFrame
df1=pd.read_excel('/dissertation2.xls', sheet_name='HCl')

# Extract the concentration (c) and molar conductance (Λ) values from the DataFrame
c_values_HCl = df1['Conc.(N)'].values
Λ_values_HCl = df1['λ=1000k/Conc'].values

# Perform linear regression to obtain the slope and intercept
slope, intercept = np.polyfit(np.sqrt(c_values_HCl), Λ_values_HCl, 1)

# Calculate the equivalent conductance at infinite dilution (Λ0)
Λ_infinite_HCl = intercept
```

```
# Print the calculated Λ0 value
print("Equivalent Conductance at Infinite Dilution (Λ0) of HCl:",Λ_infinite_HCl,
"S/cm^2/mol")

# Read the Excel file into a DataFrame
df1=pd.read_excel('/dissertation2.xls', sheet_name='LK')

# Extract the concentration (c) and molar conductance (Λ) values from the DataFrame
c_values_LK = df1['Conc.(N)'].values
Λ_values_LK = df1['λ=1000k/Conc'].values

# Perform linear regression to obtain the slope and intercept
slope, intercept = np.polyfit(np.sqrt(c_values_LK), Λ_values_LK, 1)

# Calculate the equivalent conductance at infinite dilution (Λ0)
Λ_infinite_LK = intercept

# Print the calculated Λ0 value
print("Equivalent Conductance at Infinite Dilution (Λ0) of POTASSIUM
LACTATE:",Λ_infinite_LK, "S/cm^2/mol")

# Read the Excel file into a DataFrame
df1=pd.read_excel('/dissertation2.xls', sheet_name='PA')

# Extract the concentration (c) and molar conductance (Λ) values from the DataFrame
c_values_PA = df1['Conc.(N)'].values
Λ_values_PA = df1['λ=1000k/Conc'].values

# Perform linear regression to obtain the slope and intercept
slope, intercept = np.polyfit(np.sqrt(c_values_PA), Λ_values_PA, 1)

# Calculate the equivalent conductance at infinite dilution (Λ0)
Λ_infinite_PA = intercept


# Print the calculated Λ0 value
print("Equivalent Conductance at Infinite Dilution (Λ0) of POTASSIUM
PROPIONATE:",Λ_infinite_PA, "S/cm^2/mol")
LA=(Λ_infinite_LK)+(Λ_infinite_HCl)-(Λ_infinite_KCl)
PA=(Λ_infinite_PA)+(Λ_infinite_HCl)-(Λ_infinite_KCl)
print("Equivalent Conductance at Infinite Dilution (Λ0) of LACTIC ACID:",LA,
"S/cm^2/mol")
print("Equivalent Conductance at Infinite Dilution (Λ0) of PROPIONIC ACID:",PA,
"S/cm^2/mol")
```

OUTPUT

Equivalent Conductance at Infinite Dilution (Λ_0) of KCl: 155.05871962722784 S/cm^2/mol

Equivalent Conductance at Infinite Dilution (Λ_0) of HCl: 482.6782230454404 S/cm^2/mol

Equivalent Conductance at Infinite Dilution (Λ_0) of POTASSIUM LACTATE: 123.97634009166136 S/cm^2/mol

Equivalent Conductance at Infinite Dilution (Λ_0) of POTASSIUM PROPIONATE: 118.24331067469753 S/cm^2/mol

Equivalent Conductance at Infinite Dilution (Λ_0) of LACTIC ACID: 451.5958435098739 S/cm^2/mol

Equivalent Conductance at Infinite Dilution (Λ_0) of PROPIONIC ACID: 445.8628140929101 S/cm^2/mol

Equivalent Conductance at infinite dilution (Λ_0) from the theoretical calculations of Lactic acid and Propionic acid is found to be 451.596 and 445.863 $Ohm^{-1}cm^2eqv^{-1}$ respectively. The output obtained from the theoretical calculations is almost similar to our experimental results. So, the theoretical calculation agrees well with the experimental values.

Conclusion

The pKa value of Lactic acid increases with an increase in temperature and the graph of pKa vs Temperature gives a parabolic curve. The equivalent conductance at infinite dilution for KCl, HCl, Potassium Lactate, and Potassium Propionate was determined and found to be 155.06, 482.68, 123.98, and 118.24 $Ohm^{-1}cm^2eqv^{-1}$ respectively. Using these values, the equivalent conductances of Lactic Acid and Propionic Acid were calculated and found to be 451.60 and 445.86 $Ohm^{-1}cm^2eqv^{-1}$ respectively. These data were well supported by the Python program.

Acknowledgment

The authors would like to express Warmest thanks to the supervisor Dr. Sanjib Ghosh and special thanks given to the Management, The Bhawanipur Education Society College, Kolkata, India for providing the research facilities.

References

Albert, A. (2012). *The Determination of Ionization Constants: A Laboratory Manual*. Springer Science & Business Media.

Corwin, D. L., & Yemoto, K. (2020). Salinity: Electrical conductivity and total dissolved solids. *Soil Science Society of America Journal*, *84*(5), 1442-1461. https://doi.org/10.1002/saj2.20154

Dasgupta, P. K., & Nara, O. (1990). Measurement of acid dissociation constants of weak acids by cation exchange and conductometry. *Analytical Chemistry*, *62*(11), 1117-1122. https://pubs.acs.org/doi/pdf/10.1021/ac00210a005

Hamid, A., Bhat, S. U., & Jehangir, A. (2020). Local determinants influencing stream water quality. *Applied Water Science*, *10*(1), 1-16. https://doi.org/10.1007/s13201-019-1043-4

Martin Somer, A., Macaluso, V., Barnes, G. L., Yang, L., Pratihar, S., Song, K., ... & Spezia, R. (2019). Role of chemical dynamics simulations in mass spectrometry studies of collision-induced dissociation and collisions of biological ions with organic surfaces. *Journal of the American Society for Mass Spectrometry*, *31*(1), 2-24.https://pubs.acs.org/doi/abs/10.1021/jasms.9b00062

Mortadi, A., Chahid, E. G., Elmelouky, A., Chahbi, M., Ghyati, N. E., Zaim, S., ... & El Moznine, R. (2020). Complex electrical conductivity as a new technique to monitor the coagulation-flocculation processes in the wastewater treatment of the textile Industry. *Water Resources and Industry*, *24*, 100130. https://doi.org/10.1016/j.wri.2020.100130

Picálek, J., & Kolafa, J. (2007). Molecular dynamics study of conductivity of ionic liquids: The Kohlrausch law. *Journal of Molecular Liquids*, *134*(1-3), 29-33. https://doi.org/10.1016/j.molliq.2006.12.015

Poplewska, I., Zimoch, P., & Antos, D. (2022). Dissociation events during processing of monoclonal antibodies on strong cation exchange resins. *Journal of Chromatography A*, *1670*, 462969. https://doi.org/10.1016/j.chroma.2022.462969

Snyder, D. T., Harvey, S. R., & Wysocki, V. H. (2021). Surface-induced dissociation mass spectrometry as a structural biology tool. *Chemical Reviews*, *122*(8), 7442-7487. https://doi.org/10.1021/acs.chemrev.1c00309

Yu, Q., Liu, R., Chen, J., & Chen, L. (2019). Electrical conductivity in rural domestic sewage: an indication for comprehensive concentrations of influent pollutants and the effectiveness of treatment facilities. *International Biodeterioration & Biodegradation*, *143*, 104719. https://doi.org/10.1016/j.ibiod.2019.104719

Subject Index

Published by:

Lincoln University College, Malaysia

e ISBN 978-967-2819-29-5

ISBN 978-967-2819-30-1